

Light harvesting, light adaptation
and photoprotection in aquatic
photosynthesis studied by time-
resolved fluorescence spectroscopy

Light harvesting, light adaptation and photoprotection in aquatic
photosynthesis studied by time-resolved fluorescence spectroscopy

V.U. Chukhutsina



2015

Volha U. Chukhutsina

The work described in this thesis was supported by the HARVEST Marie Curie Research Training Network (PITN-GA-2009-238017). Furthermore, it was carried out within the research program of BioSolar Cells, co-financed by the Dutch Ministry of Economic Affairs.

Cover illustration Chlorophyll concentration in Earth's waters in European winter (front cover, December 2014) and summer (back cover, August 2014).
Credits NASA Earth Observations (neo.sci.gsfc.nasa.gov)

Light harvesting, light adaptation
and photoprotection in aquatic
photosynthesis studied by time-
resolved fluorescence spectroscopy

Volha U. Chukhutsina

Thesis committee

Promotor

Prof. Dr H. van Amerongen
Professor of Biophysics
Wageningen University

Other members

Prof. Dr R.H. Wijffels, Wageningen University
Prof. Dr E.J. Boekema, University of Groningen
Prof. Dr A.R. Holzwarth, Max Planck Institute for Bioinorganic
Chemistry, Mülheim a.d. Ruhr, Germany
Dr D. Kirilovsky, Commissariat à l'Énergie Atomique, Institut de
Biologie et Technologies de Saclay, Gif-Sur-Yvette, France

This research was conducted under the auspices of the Graduate
School of Experimental Plant Sciences

Light harvesting, light adaptation and photoprotection in aquatic photosynthesis studied by time- resolved fluorescence spectroscopy

Volha U. Chukhutsina

Thesis

submitted in fulfilment of the requirements for the degree of doctor
at Wageningen University
by the authority of the Rector Magnificus
Prof. Dr M.J. Kropff,
in the presence of the
Thesis Committee appointed by the Academic Board
to be defended in public
on Wednesday 25 February 2015
at 1.30 p.m. in the Aula.

Volha U. Chukhutsina

Light harvesting, light adaptation and photoprotection in aquatic photosynthesis studied by time-resolved fluorescence spectroscopy, 190 pages.

PhD thesis, Wageningen University, Wageningen, NL (2015)
With references, with summaries in Dutch and English

ISBN 978-94-6257-245-4

*“Послушайте!
Ведь, если звезды зажигают -
значит - это кому-нибудь нужно?
Значит - кто-то хочет, чтобы они были?
Значит - кто-то называет эти плевочки
жемчужиной?”*

Владимир Маяковский, 1914

Contents

| | | |
|------------------|--|-----|
| | Abbreviations | iii |
| Chapter 1 | Introduction | 1 |
| Chapter 2 | Variations in the first steps of photosynthesis for the diatom <i>Cyclotella meneghiniana</i> grown under different light conditions | 33 |
| Chapter 3 | Disentangling two non-photochemical quenching processes in <i>Cyclotella meneghiniana</i> by spectrally-resolved picosecond fluorescence at 77 K | 63 |
| Chapter 4 | Disconnection of the light-harvesting antenna from Photosystem I restores the redox balance after dark-light transitions | 101 |
| Chapter 5 | Cyanobacterial <i>flv4-2</i> operon-encoded proteins optimize light harvesting and charge separation in photosystem II | 125 |
| Chapter 6 | General discussion | 165 |
| | Summary | 183 |
| | Samenvatting | 186 |
| | Acknowledgements | 189 |
| | Education Statement of the Graduate School Experimental Plant Sciences | 190 |

Abbreviations

| | |
|---------------|---|
| $\Delta flv4$ | a deletion mutant of the <i>flv4-2</i> operon |
| ADC | analogue-digital converter |
| ADP | adenosine diphosphate |
| APC | allophycocyanin |
| ATP | adenosine triphosphate |
| CFD | constant fraction discriminator |
| Car | carotenoid |
| Chl | chlorophyll |
| C-PC | phycocyanin |
| Cyt b_6f | Cytochrome b_6f |
| DAS | decay-associated spectrum/spectra |
| Ddx | diadinoxanthin |
| Dtx | diatoxanthin |
| EET | excitation energy transfer |
| F_o | fluorescence yield measured with all reaction centers open |
| F_m | fluorescence yield measured with all reaction centers closed |
| F_v/F_m | ratio of variable fluorescence to maximal fluorescence of dark-adapted sample with variable fluorescence being defined as $F_m - F_o$ |

| | |
|--------------------|---|
| F_m' | maximum fluorescence yield, measured in the presence of high light with all reaction centers closed |
| F_t | the initial (minimal) level of fluorescence in the presence of high light |
| FCP | fucoxanthin-chlorophyll <i>a/c</i> _{1,2} protein |
| FCPa | trimeric fucoxanthin-chlorophyll protein complex A |
| FCPb | oligomeric fucoxanthin-chlorophyll protein complex B |
| fx | fucoxanthin |
| fx _{blue} | blue-absorbing fucoxanthin |
| fx _{red} | red-absorbing fucoxanthin |
| FWHM | the full-width at half-maximum |
| HL | high light irradiance |
| ICT | intramolecular charge transfer |
| IRF | instrument response function |
| HPLC | high-performance liquid chromatography |
| LHC | light-harvesting complex |
| LHCI | light-harvesting complex I |
| LHCII | light-harvesting complex II |
| LL | low light irradiance |
| MCP | microchannel plate photomultiplier |
| ML | medium light irradiance |

| | |
|-------------------|---|
| NADP ⁺ | nicotinamide adenine dinucleotide phosphate (oxidized form) |
| NADPH | nicotinamide adenine dinucleotide phosphate (reduced form) |
| NPQ | non-photochemical quenching |
| OCP | Orange Carotenoid Protein |
| OD | optical density |
| OE | an overexpression mutant of the <i>flv4-2</i> operon |
| PQ | plastoquinon |
| PQH ₂ | plastoquinol |
| PC | plastocyanin |
| PBS | phycobilisome |
| PS | photosystem |
| PSU | photosynthetic unit |
| PSI | photosystem I |
| PSI-LHCI | photosystem I - Light Harvesting Complex I supercomplex |
| PSII | photosystem II |
| qE | the energy-dependent quenching |
| qI | the photoinhibitory quenching |
| qT | the state-transition quenching |

| | |
|-------|--|
| RC | reaction center |
| SVD | singular value decomposition |
| TAC | time-to-amplitude converter |
| TCSPC | time-correlated single photon counting |
| WT | wild type |
| XC | xanthophyll cycle |

Chapter 1

Introduction

Background and scope

Photosynthesis is the biological conversion of light energy to chemical bond energy that is stored in the form of organic carbon compounds. Photosynthetic organisms generate about 2×10^{11} tons of global biomass annually (Field et al., 1998). Extensive knowledge of this specific and highly efficient light energy conversion process is of fundamental interest.

Although plants deliver the major contribution to global carbon fixation, the contribution of aquatic photosynthetic organisms is sometimes overlooked: Approximately 45% of photosynthesis occurs in aquatic environments (Falkowski, 1994; Field et al., 1998). Aquatic photosynthetic organisms often live in turbulent waters, which leads to fluctuation light conditions as they move between different depths. Fluctuations in the incident light intensity and spectrum can pose major challenges to the photosynthetic apparatus. In particular, suddenly increasing light intensities can cause damage to the photosynthetic apparatus. Photosynthetic organisms have photoprotection and photo-acclimation mechanisms to respond to changes in light intensity on the short (minutes) and long (days to months) time scales, respectively. Aquatic photosynthetic organisms, thus, provide an excellent example of the capacity of the photosynthetic apparatus to adapt to fluctuating light conditions (Ruban et al., 2004). The scope of this thesis is to describe light-adaptation strategies of two aquatic model organisms: the diatom *Cyclotella meneghiniana* and the cyanobacterium *Synechocystis* (sp. PCC 6803). Diatoms, a group of algae, are among the most abundant of aquatic photosynthetic organisms (Mann, 1999; Yool and Tyrrell, 2003), whereas cyanobacteria or “blue green algae” are known for their capacity to survive extreme environmental conditions, from hypersaline bays up to Antarctic ice basins.

In this introduction, the general mechanism of photosynthesis is described first, together with an overview of unique characteristics of photosynthesis in aquatic organisms (section 1.1). Then some aspects of the physical process of light absorption common to all photosynthetic pigments are discussed (section 1.2). Sections 1.3 and 1.4 describe photosynthetic pigments and pigment-protein complexes present in the organisms discussed further on in this thesis. Various light adaptation strategies of the photosynthetic apparatus are summarized in section 1.5. Section 1.6 is devoted to relevant experimental techniques, followed by a thesis outline in section 1.7.

1. 1 Aquatic photosynthesis

In virtually all aquatic habitats, including oceans, lakes, rivers, and estuaries, photosynthesis provides the primary source of organic matter, supporting the growth and metabolic demands of all other organisms in the ecosystem (Carpenter et al., 2011; Ware and Thomson, 2005). Hence, the rate of photosynthesis places an upper bound on the overall biological flow of energy on our planet. Over two billion years ago, aquatic photosynthetic organisms permanently altered the Earth's atmosphere through the introduction of oxygen gas (Bekker et al., 2004; Farquhar et al., 2000). This phenomenon ultimately permitted multicellular animals, including humans, to evolve (Knoll, 2003). In oxygenic organisms (plants, algae, and cyanobacteria) two photosystems - photosystem (PS) I and PSII (Jordan et al., 2001; Kamiya and Shen, 2003), working in series, are involved in the light-dependent reactions of photosynthesis (Figure 1.1). Both photosystems contain a reaction center (RC), where excited-state energy induces primary charge separation and consequently drives linear electron transport between PSII and PSI (Duysens et al., 1961; Hill and Bendall, 1960). The RC contains several molecules of chlorophyll *a* (Chl *a*) (Ferreira et al., 2004). Chls in a RC are excited either upon direct light absorption or via excitation energy transfer (EET) from surrounding pigments. After charge separation in the PSII RC, the electron is transferred via an electron transfer chain to PSI. In the PSII RC, meanwhile, water is split into molecular oxygen and protons, while electrons are used to neutralize the Chl *a* cation (P_{680}^+) that remained after charge separation. The PSI RC is constantly being oxidized by light-driven charge separation in PSI, while the electrons from the linear electron transfer chain re-reduce PSI. The electrons that are produced via charge separation in PSI eventually go to the "final" electron acceptor nicotinamide adenine dinucleotide phosphate ($NADP^+$) and reduce it to the reducing equivalent NADPH. The proton motive force that is concomitantly generated across the thylakoid membrane is used for the synthesis of adenosine triphosphate (ATP) by the ATP synthase. ATP and NADPH formed in the so-called 'light reactions' in turn catalyze the 'dark reactions' (also called light-independent reactions) in which carbon dioxide is fixed and reduced (Calvin-Benson cycle) to build up carbohydrates (Bassham et al., 1954).

Although the principle of photosynthesis described above is similar for all oxygenic photosynthetic organisms, there are significant differences between terrestrial and aquatic environments due to a variety of adaptation and physiological acclimation phenomena of the photosynthetic apparatus in aquatic organisms that are without parallel in terrestrial plants. The most obvious adaptation is the evolutionary adjustment of the pigment content and, consequently, absorption cross-section of the

[INTRODUCTION]

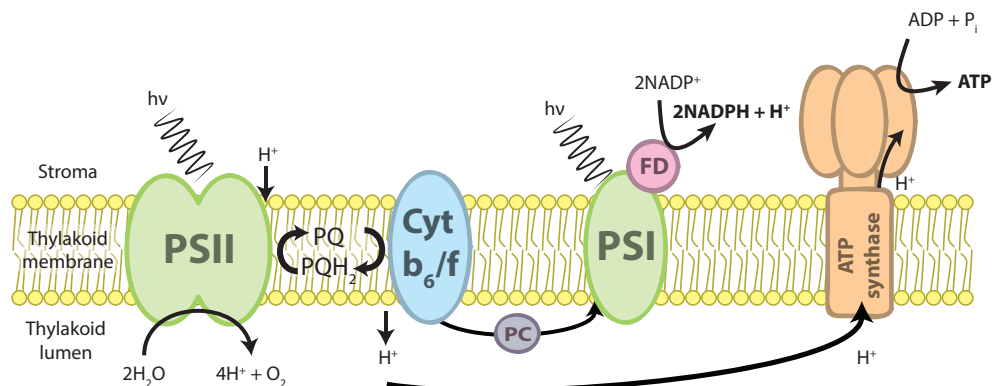


Figure 1.1. Simplified model of the light-dependent reactions of oxygenic photosynthesis, with the four main complexes PSII, Cyt b₆/f, PSI and ATP synthase. Electron and proton flows are indicated with lines.

light-harvesting complexes in aquatic organisms (Depauw et al., 2012). Living at different water depths and in different ecosystems, aquatic photosynthetic organisms stratify to absorb the available light spectrum. That explains why various aquatic photosynthetic organisms differ in color (Pierson et al., 1990). For example, diatoms are brown colored due to the presence of the fucoxanthin pigment. This carotenoid mainly absorbs green light, which is abundant in the lower layers of the photic zone, which they mostly occupy. Phycobiliproteins of cyanobacteria mostly harvest orange light, which is why they are more abundant in the top layers of the water column. Certain cyanobacteria that live underneath coral-reef invertebrates in a shaded niche enriched in near-infrared light contain Chl *d* as their principal light-harvesting pigment, which has its absorption maximum at 700–720 nm (Kühl et al., 2005). Even more recently Chl *f* was discovered. It absorbs up to 750 nm *in vivo*, in a cyanobacterium hosted by stromatolites (Chen et al., 2010), and thus also living in a near-infrared-rich environment.

Light quantity is a dynamic factor to which the organisms also have to adapt. Particularly in natural aquatic habitats, light quantity can vary substantially as a function of time and of the position of the organisms in the water. As a response to these variations, photosynthetic organisms apply various adaptation strategies to modulate the absorption cross section of PSs on a time scale from seconds to months (Croce and van Amerongen, 2014). Without these strategies, the photosynthetic machinery can be easily overexcited, causing photodamage or even death of the organism.

[INTRODUCTION]

This thesis is devoted to the study of various adaptation strategies in the diatom *Cyclotella meneghiniana*, hereafter *C. meneghiniana*, and the cyanobacterium *Synechocystis sp. PCC 6803* hereafter *Synechocystis*. Both of them, living in turbulent waters, are naturally exposed to fluctuating light regimes.

1.2 Absorption and fluorescence

Chls and other photosynthetic pigments absorb mainly visible and near-infrared light, roughly corresponding to the 350–1000 nm wavelength region of the electromagnetic spectrum. The energy E of a photon is expressed by $E = h \cdot \nu = \frac{h \cdot c}{\lambda}$, where h is Planck's constant, c the speed of light, ν the spectral frequency and λ the wavelength.

Electromagnetic energy can be absorbed because electrons can switch to a higher energy level. For this to happen, the energy of the photon, $h\nu$, must match the energy gap between the ground state and the excited state. Absorption of a photon leads to a transition from the singlet ground state (S_0) to an excited state. Electrons can only be excited into a singlet state (S_1, S_2, S_n) (Figure 1.2). The transition between singlet and triplet states is “forbidden”, because this implies switching of the orientation of

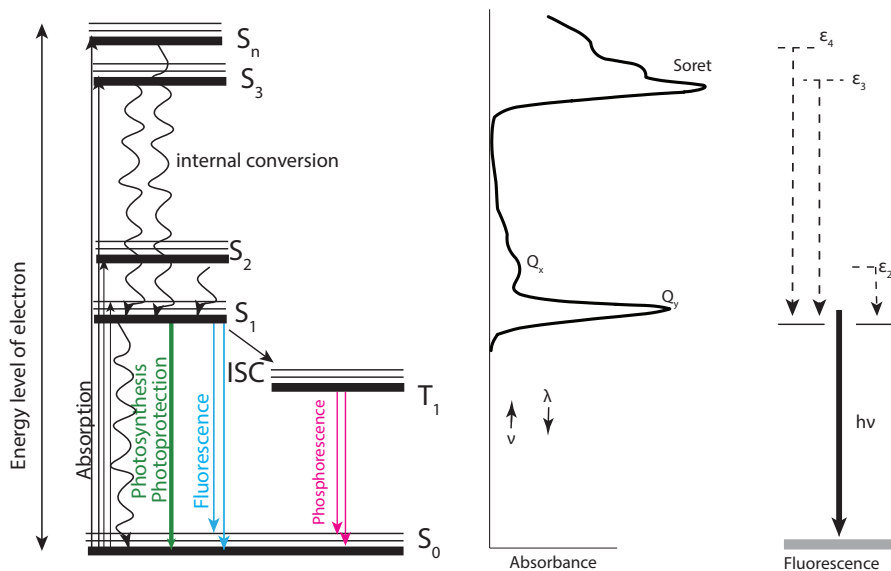


Figure 1.2. Energy levels and possible transitions of a photosynthetic pigment. Intersystem crossing (ISC), the singlet ground state (S_0), various excited states ($S_{1..n}$) and the lowest triplet state are indicated (T_1).

[INTRODUCTION]

electron spin during the transition, which is unlikely. After a molecule has been excited, fast ($\approx 10^{-12}$ s) relaxation to the first excited singlet state (S_1) takes place via a process called internal conversion. From there, the pigment can relax from S_1 back to S_0 through emission of a photon (fluorescence). Because of this kinetics, fluorescence spectra are typically independent of excitation wavelength. This observation is known as Kasha's rule (Kasha, 1950). The synonymous term "mirror image rule" refers to the emission spectrum usually being a red-shifted mirror image of the $S_0 \rightarrow S_1$ absorption. However, there are many exceptions to this rule. For example, molecules such as carotenoids (Cars) emit from their S_2 state, since the $S_1 \rightarrow S_0$ transition is symmetry forbidden whereas the $S_2 \rightarrow S_0$ transition is strongly allowed. Besides fluorescence, the energy of the excited state can be deactivated non-radiatively via internal conversion or through the formation of a triplet state (T) by spin-orbit coupling (intersystem crossing) (Figure 1.2), followed by relaxation to the ground state without or with (phosphorescence) emission of light.

Due to a proper arrangement of pigments in the pigment-protein complexes, the excitation energy can be transferred through the pigment network, via dipole-dipole interactions (Förster, 1955), until it finally reaches the RC. In the RC the energy is trapped and used to drive photochemistry (Figure 1.2). However, under excess light conditions more excitation energy is absorbed than can be utilized for photosynthesis. This would lead to longer lifetimes of Chl singlet excited states ($^1\text{Chl}^*$) and thus an increased probability for the formation of triplet excited states ($^3\text{Chl}^*$) (Vass et al., 1992). Chl triplet states in turn are responsible for the generation of highly reactive singlet oxygen ($^1\text{O}_2^*$). It can oxidate pigments, lipids and nucleic acids (Asada, 1996; Long et al., 1994). However, in photosynthetic organisms most of the excited-state energy in such conditions is safely dissipated as heat through non-photochemical quenching (Figure 1.2), so the formation of triplets is usually minimized (see sections 1.3.3 and 1.5).

The amount of absorbed light is given by law of Lambert-Beer according to $A(\lambda) = \log I_0/I = \varepsilon(\lambda) \cdot c \cdot d$, where A is the absorbance at a certain wavelength (λ), I_0 and I are the intensities of incident and transmitted light, respectively, c is the molar concentration of absorbing substance, d is the pathlength of light. The quantity ε is called the molar absorption coefficient or extinction coefficient. It is an intrinsic property of the investigated molecule and depends on the frequency of the incident photons. The product $\varepsilon(\lambda) \cdot c \cdot d$ is also known as the optical density OD and the ratio I/I_0 is termed transmittance T .

[INTRODUCTION]

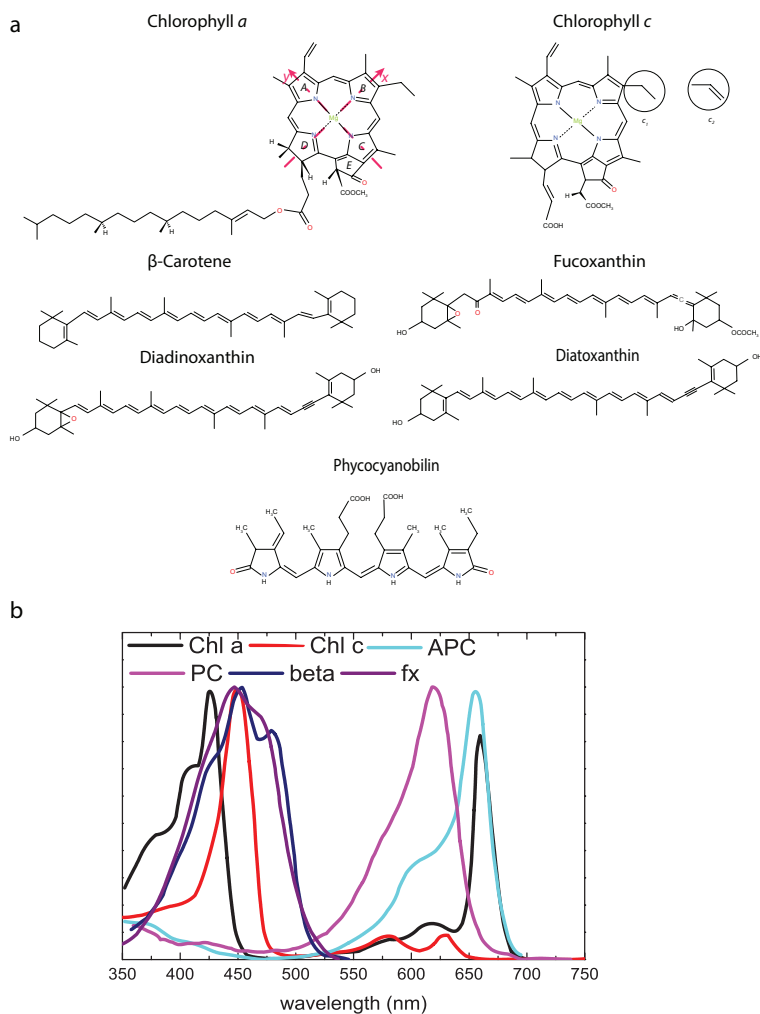


Figure 1.3. Photosynthetic pigments. (a) Molecular structures of pigments present in *C. meneghiniana* and *Synechocystis*. The orientations of the *x*- and *y*-axis in Chl are indicated. (b) Absorption spectra of chlorophylls, phycobilins and carotenoids. The spectra were normalized to their absorption maxima. Chl *a*- chlorophyll *a*; Chl *c*-chlorophyll *c*; APC, allophycocyanin; PC, phycocyanin; β -carotene; fx-fucoxanthin.

1.3 Photosynthetic pigments

There are three basic classes of photosynthetic pigments: chlorophylls, carotenoids, and phycobilins. All these pigments have multiple important functions in photosynthetic membrane, such as absorption of light, efficient energy transfer to the RCs, stabilization of the photosynthetic apparatus as well as the protection against excessive light. In this section pigments present in the *C. meneghiniana* diatom and *Synechocystis* cyanobacteria are described.

1.3.1 Chlorophylls

Chlorophyll is a cyclic tetrapyrrole with a central metal ion (Mg^{2+}), carrying a characteristic isocyclic five-membered ring. The five rings common to all Chls are conventionally designated with characters A through E (Figure 1.3). By convention, the molecular y -axis of all Chls is defined as passing through the N atoms of the A and C rings, while the x -axis passes through the N atoms of rings B and D. Most of the Chls have the ring D reduced. Chls show two main characteristic absorption bands in the visible region, which are called Soret (B) and Q bands (Figure 1.2). The structural asymmetry in Chls causes a further splitting of these two bands into x and y components (Thomas et al., 1990). The Q_x transition dipole moment is oriented perpendicular to the Q_y dipole moment and the former has a lower oscillator strength. The Soret band at higher energy has the strongest transition in the visible part of the light spectrum (Figure 1.2, Figure 1.3).

The most important Chl on the planet is Chl *a*. It can be found in all plants, algae and cyanobacteria, which photosynthesize. Chl *a* also possesses a long hydrophobic phytol chain (Figure 1.3), which facilitates binding in the hydrophobic inside of the light-harvesting proteins. A simplified energy level scheme of Chl *a* is shown in Figure 1.2 (Weiss, 1972). As mentioned before, Chl *a* in RCs acts as primary electron donor in the electron transport chain. While this function is unique for Chl *a* in oxygenic photosynthetic organisms, all Chls can act as light-harvesting pigments. In cyanobacteria, Chl *a* is the only type of Chl present. In case of diatoms and other brown-colored algae, the second Chl species present is Chl *c*. The structure of Chl *c* is shown in Figure 1.3: it lacks the phytol chain and also does not have the ring D reduced, explaining relatively weak Q_y transition and strong Soret band. The Chl *c* absorption spectrum is shifted as compared to that of Chl *a*, which helps to increase the light absorption of the diatom antenna in the 450-470 nm region (Figure 1.3). There are several structural variations of Chl *c* (Chl *c*₁, Chl *c*₂, Figure 1.3). In the

[INTRODUCTION]

diatom antenna, Chl c_2 is present (Durnford et al., 1996). Chl c_2 transfers excitation energy to Chl a on a 60 fs time scale (Songaila et al., 2013).

1.3.2 Phycobilins

In cyanobacteria, the major light-harvesting pigments, phycobilins, are linear tetrapyrroles that do not have an associated metal (Glazer, 1985). The two main classes of phycobilins are phycoerythrobilins, phycocyanobilins. Bilins are the only class of photosynthetic pigments that are covalently attached to proteins. Those proteins are known as biliproteins. Depending on the exact structure of the chromophore, these molecules absorb blue-green, green, yellow or orange light.

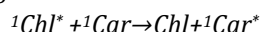
In *Synechocystis* cyanobacteria, used in the thesis, only phycocyanobilins (allophycocyanin and phycocyanin) are present (Zolla et al., 2002) (Figure 1.3).

1.3.3 Carotenoids

Carotenoids (Cars) represent an extremely large group of biological chromophores that demonstrate a remarkable range of spectral characteristics (Rowan, 1989). The basic structural element consist of two 6-carbon rings, joined by an 18-carbon, conjugated double-bond chain. There are two major groups of Cars: carotenes and xanthopylls. Xanthopylls contain oxygen, which is for instance bound to the rings, forming either hydroxyl groups and/or pairs with hydrogen atoms that are substituted by oxygen atoms acting as a bridge (epoxide) but it can also form keto groups. Carotenes have a hydrocarbon structure, and contain no oxygen. Major photosynthetic Cars that are present in cyanobacteria are β -carotenes, which are bound to the PSs, and various xanthophylls, like zeaxanthin, hydroechinenone, echinenone, canthaxanthine. Major carotenoids in diatoms are besides β -carotenes the xanthophylls fucoxanthin (fx), diadinoxanthin (Ddx), and diatoxanthin (Dtx). Spectrally all of these Cars display blue and/or blue-green absorption bands. They mostly serve as accessory light-harvesting pigments and transfer their energy to Chl a (Croce et al., 2003; Mimuro et al., 1992; Polivka and Sundstrom, 2004). In addition, Cars play an important role in protecting photosynthetic organisms from photodamage. One of the main photoprotective strategies is to dissipate a large part of harvested light as heat through a process called nonphotochemical quenching (NPQ). The intimate relationship between NPQ and the xanthophyll cycle (XC) has been known for decades (Demmig-Adams, 1990). The XC involves the enzymatic removal of epoxy groups from xanthophylls (e.g. violaxanthin, antheraxanthin) to create so-called de-epoxidised xanthophylls (e.g. zeaxanthin). The process is reversible and light

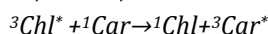
[INTRODUCTION]

dependent. In diatoms, the XC consists of the de-epoxidation of *Ddx* to *Dtx* in strong light and the epoxidation of *Dtx* to *Ddx* in low light (Goss and Jakob, 2010). However, the exact mechanism of *Dtx*-related NPQ is still not known. One possible scenario was suggested by Frank and coworkers: When the lowest excited Car singlet state lies below that of Chl, EET from Chl to Car can occur, followed by rapid internal conversion (Frank et al., 1996b):

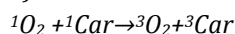


Other mechanisms, proposed to occur during NPQ in xanthophylls, involve either excitonic coupling (Bode et al., 2009) or electron transfer from Chl to Car (Ahn et al., 2008; Avenson et al., 2008).

In oxygenic photosynthetic organisms, Chl triplets are harmful excited states readily reacting with molecular oxygen to form singlet oxygen, which is a highly reactive oxygen species. Due to their low-lying triplet states, Cars can act as energy acceptors (quenchers) of Chl triplets, even if their singlet states are above those of Chls (Ballottari et al., 2013; Frank et al., 1996a; Peterman et al., 1995):



Furthermore, Cars also work as direct quenchers of reactive oxygen species (Edge and Truscott, 1999; Lepetit et al., 2012):



1.4 Pigment-protein complexes

1.4.1 Photosystems

Two large pigment-protein complexes, photosystems I and II, catalyze the first steps of photosynthesis, the light induced charge separation across the thylakoid membrane. Information concerning the structure of PSI is available from a variety of biochemical and biophysical studies as well as from the X-ray structure at 2.5 Å (Fromme et al., 2001; Grotjohann and Fromme, 2005; Jordan et al., 2001). The PSI core is highly conserved amongst plants, algae and cyanobacteria. In all these organisms the complex contains two subunits of around 83kDa (PsaA, PsaB) and at least eight small subunits (5-20 kDa) (Figure 1.4). PsaA and PsaB coordinate most of the components of the electron transport chain, including the primary donor. P700, the primary donor in PSI, from which the primary charge separation process starts, is composed of two Chl *a* molecules and is therefore referred to as a dimer. It is named P700 after Chl absorption maximum (700 nm). Additionally, the resolved X-ray structure of cyanobacterial PSI shows two small integral membrane proteins (PsaM,

[INTRODUCTION]

In total, 15 core proteins are known in PSI of higher plants and algae, ten of which are conserved. PSI of algae and plants also binds an outer light-harvesting antenna (LHCI). About 100 Chls in plants are bound to the core, the rest of the approximately 170 Chls is bound to LHCI or located between LHCI and the core. In green algae, LHCI-PSI complexes bind a larger number of antennas, which contain approximately 280 Chls in total (Bassi et al., 1992). All 15 assigned β -carotenes are found in the core of PSI, which exists as a monomer (Amunts et al., 2010; Ben-Shem et al., 2003). Like in higher plants, PSI of diatoms is a monomer. Studies on isolated FCP-PSI complexes show that they bind around 200 Chls in total, where around half should be assigned to the core and half to FCP complexes (Ikeda et al., 2008; Veith and Büchel, 2007).

The PSII core complex is organized as dimers, where each monomer is composed of an RC, two core antenna proteins CP47, CP43 and several proteins and inorganic cofactors involved in oxygen evolution (Figure 1.4). The PSII core X-ray structure reveals the positions and orientations of 35 Chls and 11 β -carotenes per monomer (Umena et al., 2011). The PSII RC, consisting of the primary donor, primary electron acceptor, the D1 and D2 polypeptides, primary and secondary quinone electron acceptors (Q_A and Q_B , respectively), cytochrome *b-559* and the *PsbI* gene product, binds six Chls, two pheophytins and 2 β -carotene molecules (Satoh, 1996). The primary donor in PSII is termed P680, due to the absorption maximum at 680 nm of the corresponding Chl *a* molecule. PSII in cyanobacteria is composed of the PSII core and receives excitations from the light-harvesting phycobilisomes, which are attached to the thylakoid membrane while in plants and algae the PSII core receives excitations from light-harvesting complexes in the thylakoid membrane (Boekema et al., 1999; Rowan, 1989; Van Amerongen and Dekker, 2003).

1.4.2 Light-harvesting complexes

1.4.2.1 Fucoxanthin-chlorophyll protein

Fucoxanthin-chlorophyll proteins (FCPs) are membrane-intrinsic antenna proteins of diatoms and brown algae. Belonging to the chlorophyll *a/b*-binding proteins (cab-family), FCPs show high sequence homology to plant light-harvesting complexes LHCII. Generally, FCPs are smaller in size (17–22kDa) (Bhaya and Grossman, 1993; Büchel, 2003; Green and Durnford, 1996) as compared to LHCII, mainly due to shorter loops and termini (Durnford et al., 1996). Until now a molecular structure for the

[INTRODUCTION]

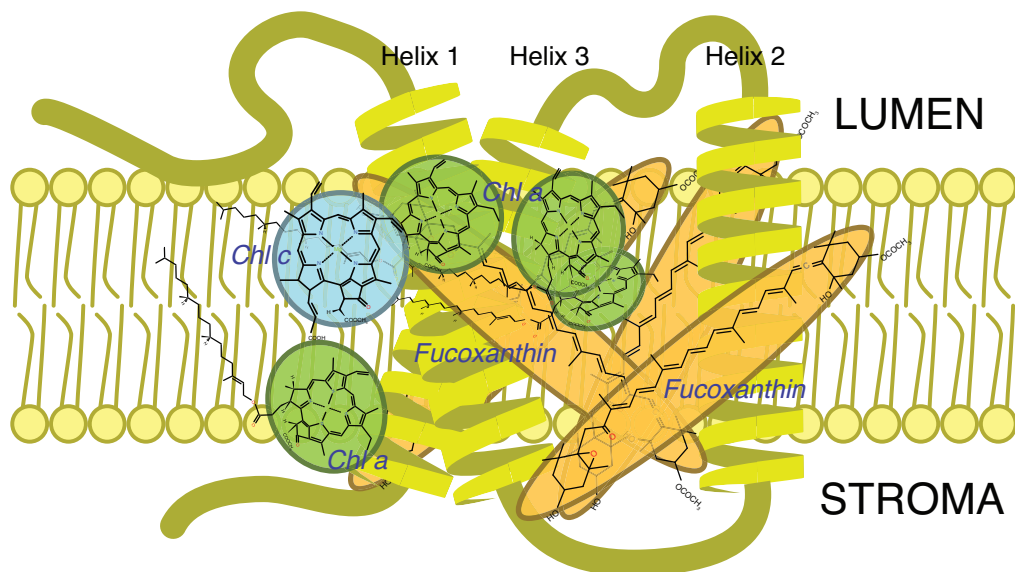


Figure 1.5. Model of the fucoxanthin-chlorophyll protein monomer including protein secondary structure and the pigments: Chl a (green), Chl c₂ (blue) and fucoxanthin (orange). Diadinoxanthin and diatoxanthin are not displayed since they are contained in substoichiometric amounts. Adapted from (Wilhelm et al., 2006).

FCPs is not available, but a preliminary model (Figure 1.5) has been developed (Wilhelm et al., 2006). It is based on the sequence analysis of the diatoms FCP in several diatom species and comparison to LHC proteins (Bhaya and Grossman, 1993; Eppard and Rhiel, 1998; Fromme et al., 2001; Grotjohann and Fromme, 2005; Jordan et al., 2001) as well as ultrafast transient absorption measurements (Papagiannakis et al., 2005). Three transmembrane α -helices are predicted from the sequence, where homology to LHC proteins is mainly found in helices 1 and 3 (Bhaya and Grossman, 1993; Eppard and Rhiel, 1998). Two different FCP complexes (trimeric FCPa and oligomeric FCPb) were isolated from *C. meneghiniana*, which differ in their polypeptide composition and oligomeric states (Büchel, 2003). Eppard and Rhiel analyzed the genes encoding FCPs in the diatom *C. cryptica*, which is related to *C. meneghiniana* (Eppard and Rhiel, 1998; Eppard and Rhiel, 2000). They found that the genes *fcp1*, *fcp2*, *fcp3*, and *fcp4* encode FCPs of about 18 kDa and *fcp5*, *fcp6*, and *fcp7* encode 19 kDa proteins. By means of gel filtration the two fractions of FCPs from *C. meneghiniana* were analyzed by (Beer et al., 2006). Beer and coworkers showed that the trimeric FCPa consists of mainly 18 kDa proteins (Fcp2 polypeptides) and only small amounts of 19 kDa subunits (Fcp6 polypeptides) whereas in case of FCPb

[INTRODUCTION]

exclusively 19 kDa proteins (Fcp5 polypeptides) assemble into higher oligomers (Beer et al., 2006; Büchel, 2003).

In general, FCPs function as light-harvesting complexes and most probably can also dissipate excess excitation energy as heat via NPQ (Bailleul et al., 2010; Miloslavina et al., 2009; Wilhelm et al., 2006). To date there is no hard evidence for distinct functions of the two FCP types, i.e. it is unclear if they function as a specific antenna for either PSI or PSII. Biochemical studies complemented with spectroscopic methods by Veith et al. suggested that the trimeric FCPa is associated with PSII whereas FCPb might be weakly bound to PSI (Veith et al., 2009). Fcp6 (Lhcx proteins in *C. meneghiniana*, encoded by *fcp6* genes) of the FCPa antenna complexes is known to be involved in photoprotection. In addition, Miloslavina and coworkers suggested two sites to be responsible for NPQ, which are located in two different FCP complexes, which is concluded on time-resolved spectroscopic studies on intact cells of *C. meneghiniana* and *Phaeodactylum. tricornutum* (Miloslavina et al., 2009). According to the authors' interpretation, one antenna (most likely FCPa) stays attached to PSII during NPQ. The other subpopulation is detached and forms aggregates comparable to FCPb. However, this assignment still needs validation.

1.4.1.2 Phycobilisome

Phycobilisomes (PBSs) are the major accessory light-harvesting complexes in red algae and in most cyanobacteria. They are complex, highly structured assemblies of brightly coloured phycobiliproteins and colourless linker polypeptides (Glazer and Clark, 1986; Grossman et al., 1993). These linker polypeptides are specifically responsible for each level of phycobiliprotein assembly and function to stabilize the PBS and optimize its absorption and energy transfer characteristics (Schirmer et al., 1986; Yu and Glazer, 1982). In contrast to most other light-harvesting complexes, phycobilisomes are composed of predominantly hydrophilic polypeptides. In cyanobacteria they are located in the cytoplasm and associated with the cytoplasmic surface of the thylakoid membrane. The structure of a hemidisoidal PBS consists of a set of rods radiating from the central core. Each of the rods consists of several phycobiliprotein units (Figure 1.6), while the number of the units per rod as well as the pigments that bind to the rods vary between different PBS-containing organisms. The core of the PBS, which attaches to the thylakoid membrane, consists of a variable number of allophycocyanin (APC) units. The structure of the APC core and number of APC units in it also depend on the type of organism (Ducret et al., 1996; Gantt, 1981; Glauser et al., 1992). In *Synechocystis* the core of the PBS antenna is built from three cylinders. Each cylinder consists of four APC trimers, where each APC is a light-harvesting entity. Rods of PBSs in *Synechocystis* are composed of phycocyanin (PC).

[INTRODUCTION]

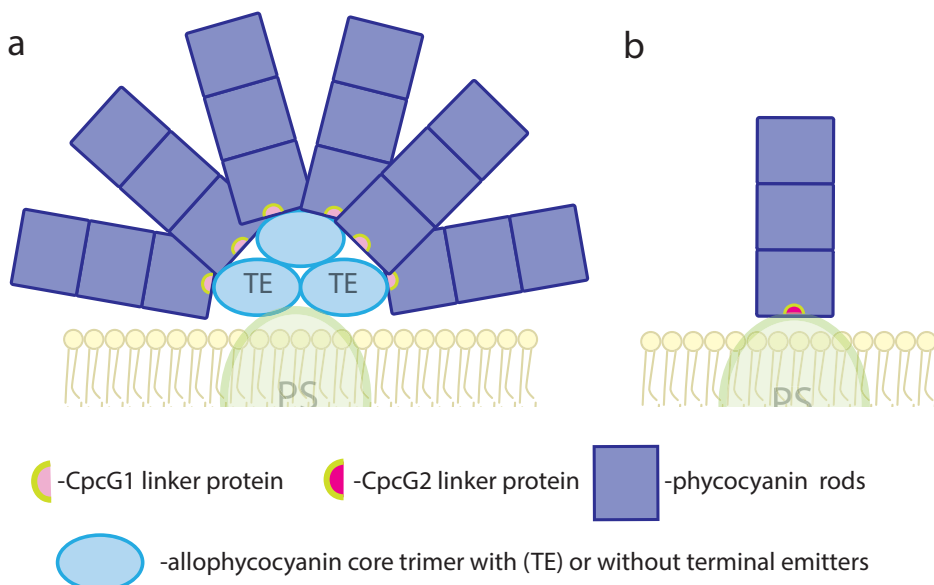


Figure 1.6. (a) Representation of a ‘conventional’ hemi-discoidal phycobilisome (PBS) and (b) CpcG2-PBS in *Synechocystis* as proposed by (Kondo et al., 2009).

Each rod consists of three hexameric PC discs (18 PC per hexamer). The APC core and the multiple peripheral PC rod complexes are connected via linker proteins (L_{RC} , or CpcG). CpcG has two copies encoded by two independent genes (CpcG1 and CpcG2).

PBSs are attached to the outer surface of the thylakoid membranes (Bhaya and Grossman, 1993; Eppard and Rhiel, 1998; Gantt and Conti, 1966a; Gantt and Conti, 1966b) via the large, chromophorylated, core membrane linker protein ApcE (Redlinger and Gantt, 1982), which also serves as terminal energy emitter. Two more terminal emitters –ApcD, ApcF– are also responsible for excitation energy transfer (EET) from PBS towards the photosystems (Mullineaux, 1992; Mullineaux and Holzwarth, 1991).

The entire PBS assembly typically has a molecular mass in the range from 7 to 15 MDa with diameter usually in the range of 32–70 nm. Thus PBSs are far larger than the reaction centres. According to multiple fluorescence studies PBSs can associate both with PSII and with PSI (for a review see (Mullineaux, 2008)).

Kondo and coworkers have recently reported that *Synechocystis* possesses two types of PBSs that differ in their interconnecting “rod-core linker” proteins (CpcG1 and CpcG2) (Kondo et al., 2005; Kondo et al., 2009). CpcG1-PBS was found to be equivalent to conventional PBS, whereas CpcG2-PBS retains phycocyanin rods but is devoid of the central core. These alternative PBSs consist of one PC rod with a

CpcG2 linker protein that allows its binding to the membrane (Figure 1.6). CpcG1-PBS seems to preferentially transfer excitation energy to PSI (Kondo et al., 2007; Veith et al., 2009; Watanabe et al., 2014).

1.5 Light adaptation of photosynthetic apparatus

All photosynthetic organisms must adapt to varying light conditions in order to balance between capturing a sufficient number of photons to run the photosynthetic machinery and avoiding the photons' damaging effects (Croce and van Amerongen, 2014; Eberhard et al., 2008; Kirilovsky, 2014).

Because PSs differ in their spectral properties, the change of the light quality might drastically decrease the photosynthetic efficiency due to induced imbalance between the two photosystems, in particular at low light intensities (Allen, 2003). Therefore, plants, green algae and cyanobacteria are able to change in the relative antenna size of PSI and PSII through the so-called state transition (Tikkanen et al., 2006; Ünlü et al., 2014; Wientjes et al., 2013). State transitions counterbalance the light-induced imbalance of energy distribution between the photosystems. In cyanobacteria, due to the high PSI/PSII ratio and respiration, such an imbalance can also be caused by changes in light quantity (Aoki and Katoh, 1982; Mullineaux and Allen, 1990). In these organisms, state transitions involve relative movements of PBSs and/or PSs, so they modify the energy flow between PBSs and each PS and/or between PSII and PSI (Kirilovsky, 2014). In diatoms, there is no evidence for state transitions so far (Owens, 1986).

Generally, upon fast increase of light intensity, the photosynthetic apparatus needs to be photoprotected, leading to excess energy being rapidly dissipated as heat through NPQ (Demmig-Adams and Adams, 1992; Horton and Hague, 1988). This response is rapid (minutes or less) and does not require changes in gene expression. Although, NPQ is present in both diatoms and cyanobacteria, the origin of heat dissipation is different for these two organisms. The orange carotenoid protein (OCP) is responsible for thermal dissipation of excess energy at the level of the PBSs in cyanobacteria. It is activated by intense blue-green light and converts from its inactive orange form to its active red form, after which it binds to a PBS (citation of Diana's work). Tian and coworkers demonstrated that the quenching site of NPQ is present at the level of APC₆₆₀ in PBSs and most probably occurs via charge transfer between hECN in OCP and APC₆₆₀ or EET from APC₆₆₀ to hECN (Tian et al., 2011). In diatoms, like in plants, the NPQ build-up is at least partly associated with the conversion of epoxidized to de-epoxidized forms of xanthophylls i.e. the conversion of Ddx into Dtx in diatoms (see Section 1.3.3). The quenching sites of NPQ in diatoms are still not

known. There is a debate whether the loss of heat occurs in PSs, FCP complexes or both (Eisenstadt et al., 2008; Gundermann and Büchel, 2012; Miloslavina et al., 2009). The mechanism of NPQ in diatoms as well as in higher plants is still under debate. It could occur through energy transfer from Chl to Dtx (see Section 1.3.3) or due to Chl-Dtx excitonic coupling, a mechanism that might also occur in LHCII (Van Amerongen and van Grondelle, 2001). Although a correlation between the Dtx concentration and the amount of NPQ was shown, part of the NPQ should be ΔpH related (Grouneva et al., 2008; Grouneva et al., 2009). Recently it was also demonstrated that *in vitro* aggregation of FCP leads to NPQ-like fluorescence quenching (Gundermann and Büchel, 2012), likely due to formation of a Chl-Chl charge transfer state, which is independent of Cars (Miloslavina et al., 2008). Unlike in FCPb, Dtx acts as an additional quencher of the fluorescence in FCPa complexes (both aggregated and solubilized) *in vitro* (Gundermann and Büchel, 2008; Gundermann and Büchel, 2012). To sum up, NPQ in diatoms has a multicomponent Dtx- and ΔpH -related origin, but the quenching sites of these components have not been revealed in diatoms yet.

If the exposure to high light continues, gene expression is activated to modify the photosynthetic apparatus and the photochemistry. In diatoms and cyanobacteria, it causes a decrease of the antenna size and affects PSI/PSII ratio (Hihara et al., 2001; Lepetit et al., 2012; Strzepak and Harrison, 2004). Details about the regulation of diatom structure in response to light acclimation will be presented in chapter 2.

1.6 Experimental. Time-resolved techniques

Time-resolved optical spectroscopy, as applied in this work, enables the observation of ultrafast dynamic events in photosynthetic systems *in vivo* on a ps scale, for example electron and energy transfer and photoprotection. To investigate fluorescence dynamics, both a time-correlated single photon counting and a streak-camera setup were used.

1.6.1 Time-correlated single photon counting

Time correlated single photon counting (TCSPC) relies on the determination of the time delay between the excitation pulse and the subsequent emission of a fluorescence photon from a sample (Figure 1.7). Single photons are detected repeatedly over many excitation cycles, and the time-dependent fluorescence signal can be reconstructed from a histogram of measured delay times (Karolczak et al., 2001; Lakowicz, 1988). The laser power used during TCSPC is low, to ensure that not

[INTRODUCTION]

more than a single photon is detected per excitation pulse. Under typical operation conditions, only one in a hundred excitation pulses will lead to the detection of an emitted photon.

We have used a TCSPC setup in “reverse” mode (Figure 1.7). This means that not the time between an excitation pulse and detection of a resulting photon is measured, but rather the time between the detection of a photon and the electronically delayed excitation laser pulse. After a short (<0.2 ps) laser light pulse excites the sample, emission of an individual photon of fluorescence is detected by a microchannel plate photomultiplier tube (MCP-PMT). One channel of a constant fraction discriminator (CFD) receives a single photon pulse from the MCP-PMT and generates an electronic pulse very accurately linked in time to the photon pulse arrival time. This electronic pulse successively starts a time-to-amplitude converter (TAC). The excitation pulses are fed via a photodiode into another channel of the CFD as well, which sends a stop signal to the TAC accurately upon arrival of the pulse. To allow the excitation pulse to be used as a stop signal, its arrival in the CFD has to be delayed, which is achieved in our setup through a suitable delay from a 50 Ω delay line. After a “start” signal due to photon detection, the “stop” signal will therefore arrive with a fixed delay after the original excitation pulse. After receiving a start signal, the TAC develops a voltage that increases linearly in time. After the stop signal, the TAC voltage is converted to a numerical value by an analogue-to-digital converter (ADC). The output of the ADC is gathered in 4096 channels of a multichannel analyzer (MCA), which sorts the voltage values according to counts at each voltage (\cong time). The channel time spacing was typically set to 2.0 or 5.0 ps.

During TCSPC measurements special care should be taken to keep the fluorescence signal low, so that the PMT detects only one photon per excitation pulse. Furthermore, detector and electronics have a finite recovery time before they are able to detect the next photon. When another fluorescence photon appears, after the TAC has been started, the timing information of that second photon will be wasted. That will lead to “pile-up distortion”. To avoid over-representation that the probability to detect more than one photon per excitation pulse the excitation pulse energy should be very low. As a rule of thumb the photon counting rate should not be more than 1 photon per 100 laser pulses. This criterion was achieved by reducing the energy of the excitation pulses with neutral density filters to the pJ level: the rate of detected fluorescence photons was set to about 30,000 per second (<1% of the number of excitation pulses per second, the repetition rate was 3.8 MHz) (Vos et al., 1987)). Also other instrumental sources for distortion of data such as TAC and ADC linearity, laser

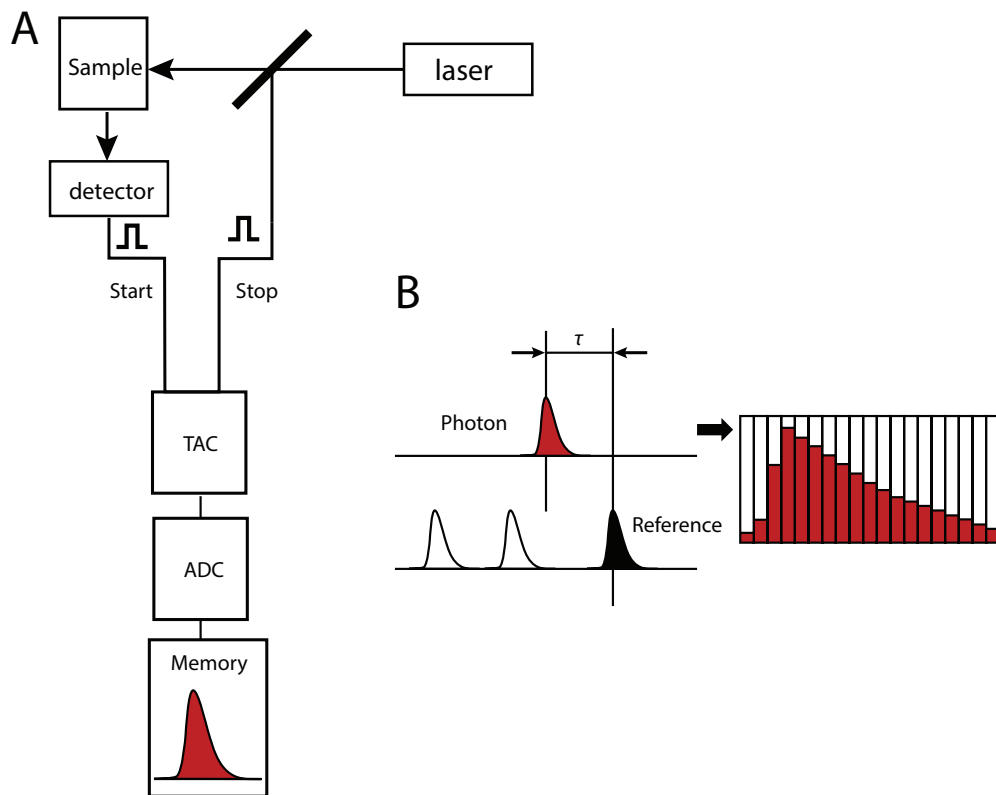


Figure 1.7. Principle of time-resolved fluorescence measurement with TCSPC. A- The time delay τ between the excitation pulse and single photon from the fluorescing sample is converted by a time-to-amplitude converter (TAC) to an output voltage signal. Then the Analog-to-Digital Converter (ADC) is used to resolve the signal from the TAC into thousands of time channels and write into the corresponding address of the memory. B- The histogram of photon arrivals per each time delay is constructed and yields a fluorescence decay curve.

mode locking were minimized (Van Hoek and Visser, 1985) to below the noise level of normal photon statistics.

The excitation sources for TCSPC were mode-locked continuous wave lasers. The pump laser was a CW diode-pumped, frequency-doubled Nd:YVO₄ laser. The mode-locked laser was a Ti:Sapphire laser, which was tuned to 800 nm. The laser repetition rate of 76 MHz was decreased to 3.8 MHz using a pulse picker. The output of the pulse picker was directed towards a second harmonic generation system to generate 400

[INTRODUCTION]

nm light. Alternatively, an Optical Parametric Oscillator (OPO) was used to provide wavelengths in the 525-665 nm range. For decreasing the pulse repetition rate after the OPO, a double pulse picker was used. The detection polarizer was placed under the magic angle with respect to the vertical direction of the polarization of the excitation light. To detect decay traces at various detection wavelengths various interference filters with bandwidths of about 12 nm were used. The samples were typically measured in a 3 mm flow cuvette, placed in a sample holder, which was temperature controlled.

1.6.2 Streak camera

Another time-resolved fluorescence method applied in the thesis uses detection with a synchroscan streak-camera system. The streak-camera system, used in this thesis, operates by dispersing photoelectrons across an imaging screen in wavelength and time, allowing monitoring the evolution of whole spectra on a ps-ns time scale instead of measuring fluorescence decay curves at individual wavelengths (Schiller, 1984). This method is extremely valuable when studying photosynthetic organisms *in vivo*, which usually contain fluorophores emitting at different wavelengths. Moreover, a streak camera has a better time resolution than TCSPC. The full-width-at-half-maximum (FWHM) of the IRF of the streak camera is typically 8 (for time-window 800 ps) and 20 ps (for time window 2 ns) in our measurements instead of 30-40 ps of the TCSPC setup with MCP PMT detection.

Figure 1.8 shows the operating principle of our streak camera. Emitted fluorescence photons induced by the laser excitation are focused by an objective on the input slit of a spectrograph, where they are wavelength dispersed in the horizontal direction by a grating. Then the photons strike the photocathode, where they lead to the emission of electrons. The photo-electrons first pass through an accelerating mesh. Then the accelerated photo-electrons pass between a pair of sweep electrodes; a high sweeping voltage is applied to the electrodes and the sweep frequency is synchronized to the frequency of excitation light pulses. During the high-speed sweep, the electrons that arrive at slightly different times, are deflected at different angles in the vertical direction, and enter the micro-channel plate (MCP) at different positions. As the

[INTRODUCTION]

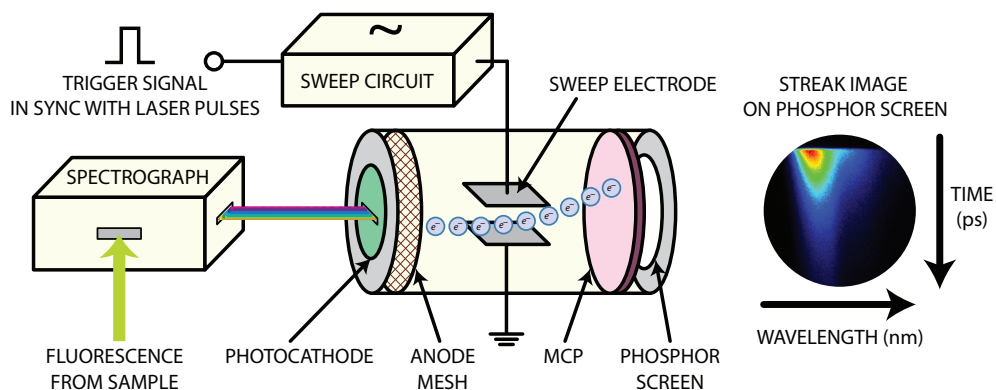


Figure 1.8. Operating principle of synchroscan streak-camera setup, consisting of a spectrograph, photocathode, accelerating mesh, fast sweeping electrodes and imaging part (micro-channel plate and phosphor screen). Sweep frequency is synchronized with laser pulses.

photo-electrons strike the MCP, they are multiplied several thousands of times, after which they reach a phosphor screen, where they are converted again into light. The photoelectrons generated at different times experience different deflection fields and therefore hit the phosphor screen at different vertical positions. The light of the phosphor screen is focused on a CCD detector and these data are stored for further processing.

For the experiments presented in this thesis, a mode-locked Ti:Sapphire laser was used to generate short light pulses of about 200 fs duration, 800 nm, at a repetition rate of 79.5 MHz. A few percent of the laser output was used for synchronization with the sweep field of the streak camera, while the major part was fed into a regenerative amplifier (RegA), where the energy of the pulses was increased and the repetition rate was decreased (down to 250 kHz). After the RegA the laser pulses were directed to an optical parameter amplifier (OPA), where the beam was split. Part of it was frequency doubled, while another part was used to generate white light. Mixing of these two beams was used in this thesis to produce excitation pulses of wavelengths longer than 470 nm; while the frequency-doubled part was used for 400-nm excitation. In all measurements, vertically polarized light was used.

1.6.3 Data analysis

In a time-resolved fluorescence experiment, the fluorescence kinetics reflect the decay of the excited-state population of contributing fluorophores as well as the excitation energy transfer between them. For a sample of identical fluorophores the decay can be described by an exponential function. In time-resolved measurements on photosynthetic samples, the fluorescence usually becomes non-exponential, and the fluorescence decay trace can adequately be approximated by a sum of exponentials:

$$f(t) = \sum_{1,2,\dots}^N \alpha_i \exp\left(-\frac{t}{\tau_i}\right) \quad (1)$$

In this expression τ_i are the fluorescence decay times, while α_i represent the corresponding amplitudes of the components whereas N is the total number of decay components.

When the width of the instrument response function (IRF) is not negligible, the exponential decay should be convoluted with the IRF and the fluorescence decay trace can be approximated as (Demas, 1983; O'Connor, 1984):

$$f(t) = \sum_{1,2,\dots}^N \alpha_i * \exp\left(-\frac{t}{\tau_i}\right) \oplus i(t) \quad (2)$$

where \oplus indicates convolution and the IRF is represented as $i(t)$.

The first application of global analysis was reported by Knorr and Harris in 1981 and soon after was applied in photosynthesis research (Knorr and Harris, 1981; Wendler et al., 1986). An advantage of global analysis is the improved resolution of closely spaced lifetimes (Beechem, 1992; Lakowicz and Masters, 2008). For that, data from more than one detection/excitation wavelength are combined.

Global analysis of decay traces measured at different detection wavelengths, yields decay associated spectra (DAS) (Holzwarth, 1996; Van Stokkum et al., 2004). In the analysis the fluorescence lifetimes τ_i are assumed to be identical at each emission wavelength. The total dataset is then fitted with function $f(t, \lambda)$, analogous to $f(t)$ in equation (2):

$$f(t, \lambda) = \sum_{1,2,\dots}^N DAS_i(\lambda) \left(\exp\left(-\frac{t}{\tau_i}\right) \oplus i(t) \right) \quad (3)$$

This equation relies on the superposition principle stating that the spectroscopic properties of the components are a superposition of the spectroscopic properties weighted by their concentration:

$$f(t, \lambda) = \sum_{i=1,2,\dots}^N \varepsilon_i(\lambda) c_i(t) \quad (4)$$

where $\varepsilon_i(\lambda)$ and $c_i(t)$ stand for spectrum and concentration of component i , respectively.

1.7 This thesis

This thesis concerns various light adaptation strategies of two common aquatic model organisms – the diatom *C. meneghiniana* and the cyanobacterium *Synechocystis*. We used mainly time-resolved fluorescence spectroscopy to study their responses to light attenuation to understand the changes in supra-molecular organization of the photosynthetic apparatus, charge separation, excitation energy transfer routes and lifetimes.

In chapter 2 we studied excitation energy transfer and trapping in intact *C. meneghiniana* cells grown at different light intensities. To discriminate between the kinetics of PSs cores and complexes, different excitation wavelengths were used. With this approach, we characterized excitation energy transfer from the outer antenna to the core of PSI and PSII. Previously, different antenna complexes were isolated from *C. meneghiniana* that vary in their composition and have slightly different spectral characteristics. Their role and primary association to one of the PSs, however, are still under debate. For this reason, one of the goals of this work was to determine spectral differences of PSI and PSII-associated antenna *in vivo*. To achieve this, a new method for the separation of excitation spectra of individual PSs *in vivo* was introduced.

Chapter 3 addresses the multistep process of NPQ (fast photoprotection mechanism) in the same diatom species. It is known that both ΔpH and Dtx contribute to NPQ build-up in *C. meneghiniana*. Dtx and ΔpH -related quenching mechanisms, however, have not been reported yet. In chapter 3, the picosecond fluorescence kinetics of *C. meneghiniana* cells at 77 K in three different states are described: (1) unquenched state (in the absence of NPQ); quenched state (in the presence of Dtx- and ΔpH -related NPQ); dark-adapted state directly following NPQ. In the third state, Dtx accumulated during the NPQ period and Dtx-related NPQ persisted, while ΔpH -related NPQ had relaxed. In this way, Dtx and ΔpH -related quenching sites were separated and the sequence of events that follows NPQ formation was revealed. Different excitation wavelengths were used to identify the location (site) of quenching. The results can be summarized in a multistep model of NPQ in *C. meneghiniana*.

Chapter 4 is devoted to changes in the photosynthetic apparatus of *Synechocystis* during state transitions. Unlike diatoms, cyanobacteria and higher plants adapt to changing light conditions through state transitions, which lead to a redistribution of light energy between PSI and PSII and can be observed as a change in the relative antenna size of PSI and PSII. In cyanobacteria, the cascade of microscopic events leading to state transitions is still not completely clear and different models have been proposed. These different models assume either PBS or PS mobility. The goal of this

[INTRODUCTION]

research was to unveil which mechanisms are involved in energy redistribution in *Synechocystis* during a naturally occurring light-darkness scheme. Previously, state transitions have always been studied by inducing changes that do not occur in nature: redox changes of the electron carriers were generated, for example, by chemicals or by applying illumination conditions with rather specific colors. Our conclusions conflict with all existing models of state transitions: we demonstrate that the main role of state transitions is to change the absorption cross-section of PSI, rather than that of PSII.

Other mechanisms of photoprotection involve the induction of alternative electron transfer routes, which dissipate the excess of electrons in the photosynthetic chain and result in decreased photodamage of PSs. Only very recently, *flv4-2* operon-encoded proteins were discovered to play a central role in safeguarding PSII activity in high light and in air-level CO₂ conditions. In chapter 5 various steady-state and time-resolved measurements were combined with thermoluminescence and biochemical methods to investigate the effect of *flv4-2* operon-encoded proteins 1) on the PSII charge separation kinetics 2) on excitation energy transfer kinetics from the antenna to RCs. For that, deletion and overexpression mutants of the entire *flv4-2* operon wild-type strain of *Synechocystis* were used and conclusions about the role of the *flv4-2* operon-encoded proteins on PBS association with the PSs and on PSII charge separation were drawn.

References

- Ahn, T.K., Avenson, T.J., Ballottari, M., Cheng, Y.C., Niyogi, K.K., Bassi, R., and Fleming, G.R. (2008). Architecture of a charge-transfer state regulating light harvesting in a plant antenna protein. *Science* 320:794-797.
- Allen, J.F. (2003). Botany. State transitions--a question of balance. *Science* 299:1530-1532.
- Amunts, A., Toporik, H., Borovikova, A., and Nelson, N. (2010). Structure determination and improved model of plant photosystem I. *The Journal of biological chemistry* 285:3478-3486.
- Aoki, M., and Katoh, S. (1982). Oxidation and Reduction of Plastoquinone by Photosynthetic and Respiratory Electron-Transport in a Cyanobacterium *Synechococcus* Sp. *Biochimica et biophysica acta* 682:307-314.
- Asada, K. (1996). Radical production and scavenging in the chloroplasts. In: *Photosynthesis and the Environment*: Springer. 123-150.
- Avenson, T.J., Ahn, T.K., Zigmantas, D., Niyogi, K.K., Li, Z., Ballottari, M., Bassi, R., and Fleming, G.R. (2008). Zeaxanthin radical cation formation in minor light-harvesting complexes of higher plant antenna. *The Journal of biological chemistry* 283:3550-3558.
- Bailleul, B., Rogato, A., de Martino, A., Coesel, S., Cardol, P., Bowler, C., Falcatore, A., and Finazzi, G. (2010). An atypical member of the light-harvesting complex stress-related protein family modulates diatom responses to light. *P Natl Acad Sci USA* 107:18214-18219.

[INTRODUCTION]

- Ballottari, M., Mozzo, M., Girardon, J., Hienerwadel, R., and Bassi, R. (2013). Chlorophyll triplet quenching and photoprotection in the higher plant monomeric antenna protein Lhcb5. *The journal of physical chemistry. B* 117:11337-11348.
- Bassham, J.A., Benson, A.A., Kay, L.D., Harris, A.Z., Wilson, A.T., and Calvin, M. (1954). The Path of Carbon in Photosynthesis. XXI. The Cyclic Regeneration of Carbon Dioxide Acceptor 1. *J Am Chem Soc* 76:1760-1770.
- Bassi, R., Soen, S.Y., Frank, G., Zuber, H., and Roach, J.D. (1992). Characterization of chlorophyll a/b proteins of photosystem I from *Chlamydomonas reinhardtii*. *The Journal of biological chemistry* 267:25714-25721.
- Beechem, J.M. (1992). Global analysis of biochemical and biophysical data. *Methods in enzymology* 210:37-54.
- Beer, A., Gundermann, K., Beckmann, J., and Büchel, C. (2006). Subunit composition and pigmentation of fucoxanthin-chlorophyll proteins in diatoms: evidence for a subunit involved in diadinoxanthin and diatoxanthin binding. *Biochemistry* 45:13046-13053.
- Bekker, A., Holland, H.D., Wang, P.L., Rumble, D., 3rd, Stein, H.J., Hannah, J.L., Coetzee, L.L., and Beukes, N.J. (2004). Dating the rise of atmospheric oxygen. *Nature* 427:117-120.
- Ben-Shem, A., Frolov, F., and Nelson, N. (2003). Crystal structure of plant photosystem I. *Nature* 426:630-635.
- Bhaya, D., and Grossman, A.R. (1993). Characterization of gene clusters encoding the fucoxanthin chlorophyll proteins of the diatom *Phaeodactylum tricoratum*. *Nucleic acids research* 21:4458-4466.
- Bode, S., Quentmeier, C.C., Liao, P.N., Hafi, N., Barros, T., Wilk, L., Bittner, F., and Walla, P.J. (2009). On the regulation of photosynthesis by excitonic interactions between carotenoids and chlorophylls. *P Natl Acad Sci USA* 106:12311-12316.
- Boekema, E.J., van Roon, H., van Breemen, J.F., and Dekker, J.P. (1999). Supramolecular organization of photosystem II and its light-harvesting antenna in partially solubilized photosystem II membranes. *Eur J Biochem* 266:444-452.
- Büchel, C. (2003). Fucoxanthin-chlorophyll proteins in diatoms: 18 and 19 kDa subunits assemble into different oligomeric states. *Biochemistry* 42:13027-13034.
- Carpenter, S.R., Cole, J.J., Pace, M.L., Batt, R., Brock, W.A., Cline, T., Coloso, J., Hodgson, J.R., Kitchell, J.F., Seekell, D.A., et al. (2011). Early Warnings of Regime Shifts: A Whole-Ecosystem Experiment. *Science* 332:1079-1082.
- Chen, M., Schliep, M., Willows, R.D., Cai, Z.-L., Neilan, B.A., and Scheer, H. (2010). A red-shifted chlorophyll. *Science* 329:1318-1319.
- Croce, R., Muller, M.G., Caffarri, S., Bassi, R., and Holzwarth, A.R. (2003). Energy transfer pathways in the minor antenna complex CP29 of photosystem II: a femtosecond study of carotenoid to chlorophyll transfer on mutant and WT complexes. *Biophysical journal* 84:2517-2532.
- Croce, R., and van Amerongen, H. (2014). Natural strategies for photosynthetic light harvesting. *Nature chemical biology* 10:492-501.
- Demas, J. (1983). *Excited state lifetime measurements*: Elsevier.
- Demmig-Adams, B. (1990). Carotenoids and Photoprotection in Plants - a Role for the Xanthophyll Zeaxanthin. *Biochimica et biophysica acta* 1020:1-24.
- Demmig-Adams, B., and Adams, W.W. (1992). Photoprotection and Other Responses of Plants to High Light Stress. *Annual review of plant physiology and plant molecular biology* 43:599-626.
- Depauw, F.A., Rogato, A., d'Alcalá, M.R., and Falciatore, A. (2012). Exploring the molecular basis of responses to light in marine diatoms. *Journal of experimental botany* 63:1575-1591.

[INTRODUCTION]

- Ducret, A., Sidler, W., Wehrli, E., Frank, G., and Zuber, H. (1996). Isolation, characterization and electron microscopy analysis of a hemidiscoidal phycobilisome type from the cyanobacterium *Anabaena* sp. PCC 7120. *European journal of biochemistry* 236:1010-1024.
- Durnford, D.G., Aebersold, R., and Green, B.R. (1996). The fucoxanthin-chlorophyll proteins from a chromophyte alga are part of a large multigene family: Structural and evolutionary relationships to other light harvesting antennae. *Mol Gen Genet* 253:377-386.
- Duysens, L.N., Ames, J., and Kamp, B.M. (1961). Two photochemical systems in photosynthesis. *Nature* 190:510-511.
- Eberhard, S., Finazzi, G., and Wollman, F.A. (2008). The dynamics of photosynthesis. *Annual review of genetics* 42:463-515.
- Edge, R., and Truscott, T.G. (1999). Carotenoid radicals and the interaction of carotenoids with active oxygen species. In: *The photochemistry of carotenoids*: Springer. 223-234.
- Eisenstadt, D., Ohad, I., Keren, N., and Kaplan, A. (2008). Changes in the photosynthetic reaction centre II in the diatom *Phaeodactylum tricornutum* result in non-photochemical fluorescence quenching. *Environmental microbiology* 10:1997-2007.
- Eppard, M., and Rhiel, E. (1998). The genes encoding light-harvesting subunits of *Cyclotella cryptica* (Bacillariophyceae) constitute a complex and heterogeneous family. *Mol Gen Genet* 260:335-345.
- Eppard, M., and Rhiel, E. (2000). Investigations on gene copy number, introns and chromosomal arrangement of genes encoding the fucoxanthin chlorophyll a/c-binding proteins of the centric diatom *Cyclotella cryptica*. *Protist* 151:27-39.
- Falkowski, P.G. (1994). The role of phytoplankton photosynthesis in global biogeochemical cycles. *Photosynthesis research* 39:235-258.
- Farquhar, J., Bao, H., and Thieme, M. (2000). Atmospheric influence of Earth's earliest sulfur cycle. *Science* 289:756-759.
- Ferreira, K.N., Iverson, T.M., Maghlaoui, K., Barber, J., and Iwata, S. (2004). Architecture of the photosynthetic oxygen-evolving center. *Science* 303:1831-1838.
- Field, C.B., Behrenfeld, M.J., Randerson, J.T., and Falkowski, P. (1998). Primary production of the biosphere: integrating terrestrial and oceanic components. *Science* 281:237-240.
- Förster, T. (1955). *Intermolecular energy transfer and fluorescence*: National Research Council of Canada.
- Frank, H.A., Chynwat, V., Posteraro, A., Hartwich, G., Simonin, I., and Scheer, H. (1996a). Triplet State Energy Transfer Between the Primary Donor and the Carotenoid in *Rhodobacter sphaeroides* R-26.1 Reaction Centers Exchanged with Modified Bacteriochlorophyll Pigments and Reconstituted with Spheroidene. *Photochemistry and photobiology* 64:823-831.
- Frank, H.A., Cua, A., Chynwat, V., Young, A., Gosztola, D., and Wasielewski, M.R. (1996b). The lifetimes and energies of the first excited singlet states of diadinoxanthin and diatoxanthin: The role of these molecules in excess energy dissipation in algae. *Bba-Bioenergetics* 1277:243-252.
- Fromme, P., Jordan, P., and Krauss, N. (2001). Structure of photosystem I. *Biochimica et biophysica acta* 1507:5-31.
- Gantt, E. (1981). Phycobilisomes. *Annual review of plant physiology and plant molecular biology* 32:327-347.
- Gantt, E., and Conti, S.F. (1966a). Granules associated with the chloroplast lamellae of *Porphyridium cruentum*. *The Journal of cell biology* 29:423-434.

[INTRODUCTION]

- Gantt, E., and Conti, S.F. (1966b). Phycobiliprotein localization in algae. Brookhaven symposia in biology 19:393-405.
- Glaser, M., Sidler, W.A., Graham, K.W., Bryant, D.A., Frank, G., Wehrli, E., and Zuber, H. (1992). Three C-phycoerythrin-associated linker polypeptides in the phycobilisome of green-light-grown *Calothrix* sp. PCC 7601 (cyanobacteria). Febs Lett 297:19-23.
- Glazer, A.N. (1985). Light harvesting by phycobilisomes. Annual review of biophysics and biophysical chemistry 14:47-77.
- Glazer, A.N., and Clark, J.H. (1986). Phycobilisomes: macromolecular structure and energy flow dynamics. Biophysical journal 49:115-116.
- Goss, R., and Jakob, T. (2010). Regulation and function of xanthophyll cycle-dependent photoprotection in algae. Photosynthesis research 106:103-122.
- Green, B.R., and Durnford, D.G. (1996). The Chlorophyll-Carotenoid Proteins of Oxygenic Photosynthesis. Annual review of plant physiology and plant molecular biology 47:685-714.
- Grossman, A.R., Schaefer, M.R., Chiang, G.G., and Collier, J.L. (1993). The phycobilisome, a light-harvesting complex responsive to environmental conditions. Microbiological reviews 57:725-749.
- Grotjohann, I., and Fromme, P. (2005). Structure of cyanobacterial photosystem I. Photosynthesis research 85:51-72.
- Grouneva, I., Jakob, T., Wilhelm, C., and Goss, R. (2008). A new multicomponent NPQ mechanism in the diatom *Cyclotella meneghiniana*. Plant & cell physiology 49:1217-1225.
- Grouneva, I., Jakob, T., Wilhelm, C., and Goss, R. (2009). The regulation of xanthophyll cycle activity and of non-photochemical fluorescence quenching by two alternative electron flows in the diatoms *Phaeodactylum tricornutum* and *Cyclotella meneghiniana*. Biochimica et biophysica acta 1787:929-938.
- Gundermann, K., and Büchel, C. (2008). The fluorescence yield of the trimeric fucoxanthin-chlorophyll-protein FCPa in the diatom *Cyclotella meneghiniana* is dependent on the amount of bound diatoxanthin. Photosynthesis research 95:229-235.
- Gundermann, K., and Büchel, C. (2012). Factors determining the fluorescence yield of fucoxanthin-chlorophyll complexes (FCP) involved in non-photochemical quenching in diatoms. Bba-Bioenergetics 1817:1044-1052.
- Hihara, Y., Kamei, A., Kanehisa, M., Kaplan, A., and Ikeuchi, M. (2001). DNA microarray analysis of cyanobacterial gene expression during acclimation to high light. The Plant cell 13:793-806.
- Hill, R., and Bendall, F. (1960). Function of the two cytochrome components in chloroplasts: a working hypothesis.
- Holzwarth, A.R. (1996). Data analysis of time-resolved measurements. In: Biophysical techniques in photosynthesis: Springer. 75-92.
- Horton, P., and Hague, A. (1988). Studies on the Induction of Chlorophyll Fluorescence in Isolated Barley Protoplasts .4. Resolution of Non-Photochemical Quenching. Biochimica et biophysica acta 932:107-115.
- Ikeda, Y., Komura, M., Watanabe, M., Minami, C., Koike, H., Itoh, S., Kashino, Y., and Satoh, K. (2008). Photosystem I complexes associated with fucoxanthin-chlorophyll-binding proteins from a marine centric diatom, *Chaetoceros gracilis*. Biochimica et Biophysica Acta (BBA)-Bioenergetics 1777:351-361.
- Jordan, P., Fromme, P., Witt, H.T., Klukas, O., Saenger, W., and Krauss, N. (2001). Three-dimensional structure of cyanobacterial photosystem I at 2.5 Å resolution. Nature 411:909-917.

[INTRODUCTION]

- Kamiya, N., and Shen, J.R. (2003). Crystal structure of oxygen-evolving photosystem II from *Thermosynechococcus vulcanus* at 3.7-Å resolution. *Proc Natl Acad Sci U S A* 100:98-103.
- Karolczak, J., Komar, D., Kubicki, J., Wróźowa, T., Dobek, K., Ciesielska, B., and Maciejewski, A. (2001). The measurements of picosecond fluorescence lifetimes with high accuracy and subpicosecond precision. *Chemical physics letters* 344:154-164.
- Kasha, M. (1950). Characterization of electronic transitions in complex molecules. *Discuss. Faraday Soc.* 9:14-19.
- Kirilovsky, D. (2014). Modulating energy arriving at photochemical reaction centers: orange carotenoid protein-related photoprotection and state transitions. *Photosynthesis research*.
- Knoll, A.H. (2003). *Life on a young planet: the first three billion years of evolution on earth*: Princeton University Press.
- Knorr, F.c., and Harris, J. (1981). Resolution of multicomponent fluorescence spectra by an emission wavelength-decay time data matrix. *Analytical Chemistry* 53:272-276.
- Kondo, K., Geng, X.X., Katayama, M., and Ikeuchi, M. (2005). Distinct roles of CpcG1 and CpcG2 in phycobilisome assembly in the cyanobacterium *Synechocystis* sp. PCC 6803. *Photosynthesis research* 84:269-273.
- Kondo, K., Mullineaux, C.W., and Ikeuchi, M. (2009). Distinct roles of CpcG1-phycobilisome and CpcG2-phycobilisome in state transitions in a cyanobacterium *Synechocystis* sp. PCC 6803. *Photosynthesis research* 99:217-225.
- Kondo, K., Ochiai, Y., Katayama, M., and Ikeuchi, M. (2007). The membrane-associated CpcG2-phycobilisome in *Synechocystis*: a new photosystem I antenna. *Plant physiology* 144:1200-1210.
- Kruij, J., Bald, D., Boekema, E., and Rogner, M. (1994). Evidence for the existence of trimeric and monomeric Photosystem I complexes in thylakoid membranes from cyanobacteria. *Photosynthesis research* 40:279-286.
- Kühl, M., Chen, M., Ralph, P.J., Schreiber, U., and Larkum, A.W.D. (2005). Ecology: A niche for cyanobacteria containing chlorophyll d. *Nature* 433:820-820.
- Lakowicz, J.R. (1988). Principles of frequency-domain fluorescence spectroscopy and applications to cell membranes. *Sub-cellular biochemistry* 13:89-126.
- Lakowicz, J.R., and Masters, B.R. (2008). Principles of fluorescence spectroscopy. *Journal of Biomedical Optics* 13:9901.
- Lepetit, B., Goss, R., Jakob, T., and Wilhelm, C. (2012). Molecular dynamics of the diatom thylakoid membrane under different light conditions. *Photosynthesis research* 111:245-257.
- Long, S., Humphries, S., and Falkowski, P.G. (1994). Photoinhibition of photosynthesis in nature. *Annual review of plant biology* 45:633-662.
- Mann, D.G. (1999). The species concept in diatoms. *Phycologia* 38:437-495.
- Miloslavina, Y., Grouneva, I., Lambrev, P.H., Lepetit, B., Goss, R., Wilhelm, C., and Holzwarth, A.R. (2009). Ultrafast fluorescence study on the location and mechanism of non-photochemical quenching in diatoms. *Biochimica et biophysica acta* 1787:1189-1197.
- Miloslavina, Y., Wehner, A., Lambrev, P.H., Wientjes, E., Reus, M., Garab, G., Croce, R., and Holzwarth, A.R. (2008). Far-red fluorescence: A direct spectroscopic marker for LHCII oligomer formation in non-photochemical quenching. *Febs Lett* 582:3625-3631.
- Mimuro, M., Nagashima, U., Takaichi, S., Nishimura, Y., Yamazaki, I., and Katoh, T. (1992). Molecular-Structure and Optical-Properties of Carotenoids for the In vivo Energy-Transfer Function in the Algal Photosynthetic Pigment System. *Biochimica et biophysica acta* 1098:271-274.

[INTRODUCTION]

- Mullineaux, C.W. (1992). Excitation-Energy Transfer from Phycobilisomes to Photosystem-I in a Cyanobacterium. *Biochimica et biophysica acta* 1100:285-292.
- Mullineaux, C.W. (2008). Phycobilisome-reaction centre interaction in cyanobacteria. *Photosynthesis research* 95:175-182.
- Mullineaux, C.W., and Allen, J.F. (1990). State-1-State-2 Transitions in the Cyanobacterium *Synechococcus* 6301 Are Controlled by the Redox State of Electron Carriers between Photosystem-I and Photosystem-II. *Photosynthesis research* 23:297-311.
- Mullineaux, C.W., and Holzwarth, A.R. (1991). Kinetics of Excitation-Energy Transfer in the Cyanobacterial Phycobilisome-Photosystem-II Complex. *Biochimica et biophysica acta* 1098:68-78.
- O'Connor, D. (1984). Time-correlated single photon counting: Academic Press.
- Owens, T.G. (1986). Light-Harvesting Function in the Diatom *Phaeodactylum tricornutum*: II. Distribution of Excitation Energy between the Photosystems. *Plant physiology* 80:739-746.
- Papagiannakis, E., I, H.M.v.S., Fey, H., Buchel, C., and van Grondelle, R. (2005). Spectroscopic characterization of the excitation energy transfer in the fucoxanthin-chlorophyll protein of diatoms. *Photosynthesis research* 86:241-250.
- Peterman, E.J., Dukker, F.M., van Grondelle, R., and van Amerongen, H. (1995). Chlorophyll a and carotenoid triplet states in light-harvesting complex II of higher plants. *Biophysical journal* 69:2670-2678.
- Pierson, B.K., Sands, V.M., and Frederick, J.L. (1990). Spectral Irradiance and Distribution of Pigments in a Highly Layered Marine Microbial Mat. *Applied and environmental microbiology* 56:2327-2340.
- Polivka, T., and Sundstrom, V. (2004). Ultrafast dynamics of carotenoid excited States-from solution to natural and artificial systems. *Chemical reviews* 104:2021-2071.
- Redlinger, T., and Gantt, E. (1982). A M(r) 95,000 polypeptide in *Porphyridium cruentum* phycobilisomes and thylakoids: Possible function in linkage of phycobilisomes to thylakoids and in energy transfer. *Proc Natl Acad Sci U S A* 79:5542-5546.
- Rowan, K.S. (1989). Photosynthetic pigments of algae: CUP Archive.
- Ruban, A.V., Lavaud, J., Rousseau, B., Guglielmi, G., Horton, P., and Etienne, A.L. (2004). The super-excess energy dissipation in diatom algae: comparative analysis with higher plants. *Photosynthesis research* 82:165-175.
- Satoh, K. (1996). Introduction to the Photosystem II reaction center-isolation and biochemical and biophysical characterization. In: *Oxygenic photosynthesis: the light reactions*: Springer. 193-211.
- Schiller, N. (1984). Picosecond streak camera photonics. *Semiconductors probed by ultrafast laser spectroscopy* 2:441-458.
- Schirmer, T., Huber, R., Schneider, M., Bode, W., Miller, M., and Hackert, M.L. (1986). Crystal-Structure Analysis and Refinement at 2.5-Å of Hexameric C-Phycocyanin from the Cyanobacterium *Agmenellum-Quadruplicatum* - the Molecular-Model and Its Implications for Light-Harvesting. *J Mol Biol* 188:651-676.
- Shubin, V.V., Bezsmertnaya, I.N., and Karapetyan, N.V. (1992). Isolation from *Spirulina* Membranes of 2 Photosystem I-Type Complexes, One of Which Contains Chlorophyll Responsible for the 77-K Fluorescence Band at 760 Nm. *Febs Lett* 309:340-342.
- Songaila, E., Augulis, R., Gelzinis, A., Butkus, V., Gall, A., Büchel, C., Robert, B., Zigmantas, D., Abramavicius, D., and Valkunas, L. (2013). Ultrafast Energy Transfer from Chlorophyll c(2) to Chlorophyll a in Fucoxanthin-Chlorophyll Protein Complex. *J Phys Chem Lett* 4:3590-3595.

[INTRODUCTION]

- Strzpepek, R.F., and Harrison, P.J. (2004). Photosynthetic architecture differs in coastal and oceanic diatoms. *Nature* 431:689-692.
- Thomas, L.L., Kim, J.H., and Cotton, T.M. (1990). Comparative-Study of Resonance Raman and Surface-Enhanced Resonance Raman Chlorophyll-a Spectra Using Soret and Red Excitation. *J Am Chem Soc* 112:9378-9386.
- Tian, L., van Stokkum, I.H., Koehorst, R.B., Jongerius, A., Kirilovsky, D., and van Amerongen, H. (2011). Site, rate, and mechanism of photoprotective quenching in cyanobacteria. *J Am Chem Soc* 133:18304-18311.
- Tikkanen, M., Piippo, M., Suorsa, M., Sirpio, S., Mulo, P., Vainonen, J., Vener, A.V., Allahverdiyeva, Y., and Aro, E.M. (2006). State transitions revisited-a buffering system for dynamic low light acclimation of Arabidopsis. *Plant molecular biology* 62:779-793.
- Umena, Y., Kawakami, K., Shen, J.R., and Kamiya, N. (2011). Crystal structure of oxygen-evolving photosystem II at a resolution of 1.9 angstrom. *Nature* 473:55-U65.
- Ünlü, C., Drop, B., Croce, R., and van Amerongen, H. (2014). State transitions in *Chlamydomonas reinhardtii* strongly modulate the functional size of photosystem II but not of photosystem I. *Proc Natl Acad Sci U S A* 111:3460-3465.
- Van Amerongen, H., and Dekker, J.P. (2003). Light-harvesting in photosystem II. In: *Light-harvesting antennas in photosynthesis*: Springer. 219-251.
- Van Amerongen, H., and van Grondelle, R. (2001). Understanding the energy transfer function of LHCII, the major light-harvesting complex of green plants. *The Journal of Physical Chemistry B* 105:604-617.
- Van Hoek, A., and Visser, A.J.W.G. (1985). Artifact and Distortion Sources in Time Correlated Single Photon-Counting. *Anal Instrum* 14:359-378.
- Van Stokkum, I.H., Larsen, D.S., and van Grondelle, R. (2004). Global and target analysis of time-resolved spectra. *Biochimica et Biophysica Acta (BBA)-Bioenergetics* 1657:82-104.
- Vass, I., Styring, S., Hundal, T., Koivuniemi, A., Aro, E.M., and Andersson, B. (1992). Reversible and Irreversible Intermediates during Photoinhibition of Photosystem .2. Stable Reduced Qa Species Promote Chlorophyll Triplet Formation. *P Natl Acad Sci USA* 89:1408-1412.
- Veith, T., Brauns, J., Weisheit, W., Mittag, M., and Büchel, C. (2009). Identification of a specific fucoxanthin-chlorophyll protein in the light harvesting complex of photosystem I in the diatom *Cyclotella meneghiniana*. *Biochimica Et Biophysica Acta-Bioenergetics* 1787:905-912.
- Veith, T., and Büchel, C. (2007). The monomeric photosystem I-complex of the diatom *Phaeodactylum tricorutum* binds specific fucoxanthin chlorophyll proteins (FCPs) as light-harvesting complexes. *Biochimica et Biophysica Acta (BBA)-Bioenergetics* 1767:1428-1435.
- Vos, K., van Hoek, A., and Visser, A.J.W.G. (1987). Application of a Reference Convolution Method to Tryptophan Fluorescence in Proteins - a Refined Description of Rotational-Dynamics. *Eur J Biochem* 165:55-63.
- Ware, D.M., and Thomson, R.E. (2005). Bottom-up ecosystem trophic dynamics determine fish production in the northeast Pacific. *Science* 308:1280-1284.
- Watanabe, M., Semchonok, D.A., Webber-Birungi, M.T., Ehira, S., Kondo, K., Narikawa, R., Ohmori, M., Boekema, E.J., and Ikeuchi, M. (2014). Attachment of phycobilisomes in an antenna-photosystem I supercomplex of cyanobacteria. *Proc Natl Acad Sci U S A* 111:2512-2517.
- Weiss, C. (1972). Pi-Electron Structure and Absorption-Spectra of Chlorophylls in Solution. *J Mol Spectrosc* 44:37-&.

[INTRODUCTION]

- Wendler, J., John, W., Scheer, H., and Holzwarth, A. (1986). Energy transfer in trimeric C-phycoyanin studied by picosecond fluorescence kinetics. *Photochemistry and photobiology* 44:79-85.
- Wientjes, E., Drop, B., Kouřil, R., Boekema, E.J., and Croce, R. (2013). During State 1 to State 2 Transition in *Arabidopsis thaliana*, the Photosystem II Supercomplex Gets Phosphorylated but Does Not Disassemble. *Journal of Biological Chemistry* 288:32821-32826.
- Wilhelm, C., Büchel, C., Fisahn, J., Goss, R., Jakob, T., Laroche, J., Lavaud, J., Lohr, M., Riebesell, U., Stehfest, K., et al. (2006). The regulation of carbon and nutrient assimilation in diatoms is significantly different from green algae. *Protist* 157:91-124.
- Yool, A., and Tyrrell, T. (2003). Role of diatoms in regulating the ocean's silicon cycle. *Global Biogeochemical Cycles* 17:1103.
- Yu, M.H., and Glazer, A.N. (1982). Cyanobacterial phycobilisomes. Role of the linker polypeptides in the assembly of phycocyanin. *The Journal of biological chemistry* 257:3429-3433.
- Zolla, L., Bianchetti, M., and Rinalducci, S. (2002). Functional studies of the *Synechocystis* phycobilisomes organization by high performance liquid chromatography on line with a mass spectrometer. *Eur J Biochem* 269:1534-1542.

[INTRODUCTION]

Chapter 2

Variations in the first steps of photosynthesis for the diatom *Cyclotella meneghiniana* grown under different light conditions

V. U. Chukhutsina[‡], C. Büchel[†], H. van Amerongen^{*§‡}

[‡]Laboratory of Biophysics and [§]MicroSpectroscopy Centre, Wageningen University, Wageningen, The Netherlands; [†]Institute for Molecular Bio Sciences, Johann Wolfgang Goethe-University, Frankfurt am Main, Germany

published in Biochimica et Biophysica Acta (BBA)-Bioenergetics, 2013
1827 (1), 10-18

Abstract

In this work we have applied picosecond and steady-state fluorescence measurements to study excitation energy transfer and trapping in intact *Cyclotella meneghiniana* diatom cells grown at different light intensities. Different excitation and detection wavelengths were used to discriminate between Photosystem I and II (PSI and PSII) kinetics and to study excitation energy transfer from the outer antenna to the core of PSI and PSII. It is found that the light-harvesting fucoxanthin chlorophyll proteins (FCPs) transfer their excitation energy predominantly to PSII. It is also observed that the PSII antenna is slightly richer in red-absorbing fucoxanthin than the FCPs associated with PSI. The average excitation trapping time in PSI is around 75 ps whereas this time is around 450 ps for PSII in cells grown in 20 μmol of photons per m^2 per s. The latter time decreases to 425 ps for 50 μmol of photons and 360 ps for 140 μmol of photons. It is concluded that cells grown under higher photon flux densities have a smaller antenna size than the ones grown in low light. At the same time, the increase of growth light intensity leads to a decrease of the relative amount of PSI. This effect is accompanied by a substantial increase in the amount of chlorophyll *a* that is not active in excitation energy transfer and most probably attached to inactivated/disassembled PSII units.

2.1 Introduction

Diatoms, unicellular eukaryotes, capable of performing oxygenic photosynthesis, are ecologically important in both fresh water and marine ecosystems with their key role in the biochemical cycles of carbon, nitrogen, phosphorus and silica (Falkowski et al., 1998). In contrast to higher plants, their thylakoid membranes are not segregated into stromal and granal regions. However, like in plants, their antenna complexes, the so-called fucoxanthin-chlorophyll *a/c* proteins (FCPs), are also membrane-intrinsic (for reviews, see (Wilhelm et al., 2006), (Lavaud, 2007)).

Since recently various research groups have studied the photosynthesis apparatus of diatoms. In many cases they perform *in vitro* studies on the FCPs (see e.g. (Beer et al., 2006; Gildenhoff et al., 2010; Papagiannakis et al., 2005; Premvardhan et al., 2010)), but also research has been performed on intact cells (Miloslavina et al., 2009; Su et al., 2012; Szabo et al., 2010).

Although the antenna complexes in this alga belong to the light-harvesting chlorophyll (Chl) protein (LHC) superfamily (Durnford et al., 1996), their pigment content differs from that of LHCI in higher plants. FCPs do not possess Chl *b* but use Chl *c* as an accessory pigment, and they contain fucoxanthin (fx) as the major light-

harvesting xanthophyll. Also the chlorophyll:carotenoid stoichiometry of the light-harvesting antennae of diatoms differs from that of higher plants, with the Chl *a*: carotenoid ratio being 1:1 (Gildenhoff et al., 2010; Liu et al., 2004; Papagiannakis et al., 2005)], much lower than for plants where it is around 3 (see e.g. (Liu et al., 2004)).

Two major fractions of FCPs were observed in *Cyclotella meneghiniana*, differing both in their polypeptide composition and oligomeric state: one fraction contains trimeric FCPa, consisting of mainly 18kDa proteins and only small amounts of 19kDa subunits whereas FCPb in another fraction is associated into higher oligomeric states and contains only 19kDa polypeptides (Beer et al., 2006; Büchel, 2003). In *C. meneghiniana* FCPs are mainly found in the trimeric FCPa state, irrespective of the growth light regime (Beer et al., 2006).

So far not many studies have addressed the processes of excitation energy transfer and charge separation in diatoms. The first femtosecond absorption studies of FCPs showed that energy transfer from Chl *c* to Chl *a* occurs on a time scale of ~100 fs with nearly 100% efficiency. Target analysis on isolated FCPs also revealed that the EET efficiency from fx, which was excited at 530 nm, to Chl *a* reaches around 80 % (Papagiannakis et al., 2005), while FCPa samples show a somewhat higher energy transfer efficiency than oligomeric FCPb forms, irrespective of the excitation wavelength (Gildenhoff et al., 2010). Some structural differences between the complexes were observed as well: trimeric FCP binds relatively more fx than higher oligomers (Beer et al., 2006; Gildenhoff et al., 2010; Premvardhan et al., 2010). Stark and resonance Raman spectroscopy data were the first to show the existence of different fx forms in FCPs (Premvardhan et al., 2009; Premvardhan et al., 2008). From the excitation and absorption spectra of different FCPs populations it can be observed that oligomeric FCPb shows slightly less absorption around 490 nm and increased values around 540 nm as compared to FCPa trimers (Beer et al., 2006; Gildenhoff et al., 2010; Premvardhan et al., 2010), implying that trimers might bind more blue-shifted fx as compared to FCPb.

For a long time it was believed that the two types of FCP are associated with both photosystem (PS) I and PSII, but this topic is still under debate (Brakemann et al., 2006; Ikeda et al., 2008; Nagao et al., 2007). Veith et al., for instance, found that the Fcp5 polypeptide that is part of FCPb, is loosely bound to PSI complexes (Beer et al., 2006; Büchel, 2003; Veith et al., 2009). On the other hand, Szabo et al. provided experimental evidence that inside intact diatom cells fx_{red} (presumably FCPb, see above) binds to PSII in a slightly greater amount than to PSI (Szabo et al., 2010).

Recently, the first ps fluorescence study of intact diatoms was performed (Miloslavina et al., 2009). The fluorescence kinetics of two diatom species were analyzed with the use of global target analysis. Six components were used to describe

[LIGHT ACCLIMATION OF DIATOMS]

the kinetics of both PSI and PSII in the open state (three for PSI and three for PSII). The average lifetime of the overall PSI kinetics was found to be ~51 ps for *C. meneghiniana* and 100 ps for *P. tricornutum*, while the total contribution of PSII was described by an average lifetime of ~395 ps for *C. meneghiniana* and ~432 ps for *P. tricornutum*. A detailed model was proposed as well to describe the occurrence of nonphotochemical quenching (NPQ) at two independent quenching sites. One was thought to be located in FCP that detaches from PSII during NPQ while the second one is located in the PSII-associated antenna.

The investigation of the long-time response of diatoms to different light conditions is another topic of growing scientific interest. Diatoms are known to have interesting acclimation mechanisms, responding to alterations in growth irradiance. One of them includes the adjustment of the ratio between PSII and PSI. The PSII:PSI ratio increases when the light intensity decreases in *Thalassiosira weissflogii*, a species closely related to *C. meneghiniana*, (LL - 2.2:1, HL - 4.4:1) (Strzepek and Harrison, 2004) and in *Skeletonema costatum* from LL 0.4 to HL 1 (Falkowski et al 1981). On the other hand, Smith and Melis found exactly the opposite in *Cylindrotheca fusiformis* (HL - 1.3:1 ; LL -3.9:1)(Smith et al., 1988).

A change in the photon flux density also leads to a change in the size of the photosynthetic units (PSU). Gallagher et al. were the first to report a decrease in size of PSI and PSII units in diatom species under high-light conditions (Gallagher et al., 1984). It was concluded that the amount of FCPb is not highly affected by the differences in light intensity but that the amount of FCPa decreases in high-light conditions (Beer et al., 2006).

In the present work we have studied *C. meneghiniana* with picosecond fluorescence spectroscopy using different excitation and detection wavelengths, linking the resolved spectroscopic features to the various processes taking place, with special attention for the response of the diatoms to different light conditions. A new method is introduced to separate the PSI and PSII excitation spectra of diatoms *in vivo* and it is found that the light-harvesting systems of PSI and PSII have different spectroscopic properties in agreement with recent experimental data (Szabo et al., 2010).

2.2 Materials and methods

2.2.1 Cell culture

The diatom *C. meneghiniana* (Culture Collection Göttingen, strain 1020-1a) was grown in batch cultures at 18^o C with constant shaking at 120 rpm in low light (LL, 20 $\mu\text{mol photons m}^{-2}\text{s}^{-1}$), medium light (ML, 50 $\mu\text{mol photons m}^{-2}\text{s}^{-1}$) and high light (HL, 140 $\mu\text{mol photons m}^{-2}\text{s}^{-1}$) in the silica-enriched ASP medium according to (Provasoli et al., 1957). A 16 h light: 8 h dark cycle was used in all cases.

Cells were adapted to these light conditions for months, and they were always harvested in the logarithmic growth phase.

2.2.2 Steady-state fluorescence measurements

Steady-state emission spectra

Steady-state fluorescence spectra were recorded with a Jobin Yvon Fluorolog FL3A22 spectrofluorimeter at 77 K and corrected for wavelength-dependent sensitivity of the detection and fluctuations in the lamp output. The samples were diluted with 60% glycerol (v/v). Two excitation wavelengths were used: 400 nm and 535 nm; a bandwidth of 3 nm was used both for the excitation and the emission branch. Fluorescence emission spectra were recorded using a step size of 0.5 nm. To minimize re-absorption the samples were adjusted to an absorbance of 0.04/cm in the Q_y band of Chl *a*.

Different wavelengths were used in order to modulate the relative amount of excitations in the core and the outer antenna complexes by using either 400 nm (mainly Chl *a*) and 535 nm (fx) as excitation wavelength. It was shown that Chl *a* dominates the absorption intensity of isolated FCPs in the 400-415 nm region (Chl *a* ~ 56%, Chl *c* ~36%)(Premvardhan et al., 2009; Premvardhan et al., 2010; Premvardhan et al., 2008). In case of whole cells, Chl *a* excitation at 400 nm is even more selective because the pigment concentration of Chl *a*, being the major pigment of PSI and PSII cores, rises by ~10 % in intact cells (from 40 % to 50 %), while the Chl *c* concentration decreases from 10 % to 5 % (Lepetit et al., 2010). The second wavelength (535 nm) was chosen for fx excitation. This antenna-specific carotenoid is responsible for 90% of the absorption for isolated FCPs at this wavelength. This value will not change much in the case of whole cells because both Chl *a/c* and Ddx hardly absorb at 535 nm (Premvardhan et al., 2009; Premvardhan et al., 2010; Premvardhan et al., 2008).

Steady-state excitation spectra

For steady-state fluorescence excitation spectra the same Jobin Yvon Fluorolog FL3A22 spectrofluorimeter was used. The fluorescence excitation spectra were recorded between 420 and 650 nm with excitation and emission bandwidths of 2 and 10 nm, respectively. The emission was collected at 680 and 690 nm. An integration time of 0.4 s was used to reduce the noise level. Each spectrum was measured 20 times in a run and then averaged. The sample was measured in two states: an “open” state and a “closed” state. For keeping reaction centers (RCs) open (“open” state), the cells were dark-adapted for 5 min and then kept at 287 K in a flow cuvette and a sample reservoir (5 ml). The sample was flowing from the reservoir to the cuvette and back in darkness, with a flow speed of ~ 2.5 ml/sec. To (partly) close the RCs (“closed” state), 100 μ M DCMU was added to the sample and it was preilluminated with relatively strong light (~ 100 μ mol photons $m^{-2}s^{-1}$). After measuring for 10 min the sample was refreshed. The experiment was repeated two times on cells from different generations.

2.2.3 Time-resolved fluorescence measurements

Time-correlated single photon counting

Time-correlated single photon counting (TCSPC) measurements were performed at magic angle (54.7°) polarization as described previously (Somsen et al., 2005). High detection sensitivity and time accuracy are the main advantages of this setup.

In brief, excitation was carried out by ~ 0.2 ps vertically polarized excitation pulses at a repetition rate of 3.8 MHz. The excitation wavelength was either 400 nm or 535 nm. The sample was kept at 287 K in a flow cuvette and a sample reservoir (5 ml). It was flowing from the reservoir to the cuvette and back, with a speed of ~ 2.5 ml/sec. The optical path length of the cuvette was 3 mm. For each measurement the *C. meneghiniana* sample was diluted to an optical density (OD) of 0.06 per cm at the excitation wavelength (for 400 nm: $OD_{680} \approx 0.04$, for 535 nm: $OD_{680} \approx 0.08$). The size of the excitation spot was 2 mm. In combination with the low laser power (0.5-4 μ W), this guaranteed that nearly 100% of the RCs stayed open and a significant buildup of triplet states was avoided (see Supplementary material). Moreover, the 8 ns time window used for the TCSPC measurements makes it possible to determine “long-lifetime” components that are hard to estimate with alternative techniques. For each run of measurements the following interference filters were used for detection: 671,

679, 693, 701, 712, and 724 nm (15 nm bandwidth) (Balzers, Liechtenstein model B40). The final experiment of a measuring series was always a repetition of the first experiment. The resulting decay curves were indistinguishable (Figure S2 A in Supplementary material).

Each experiment was repeated 3-5 times for different generations of the cell culture. The decay curves measured for different generations grown under the same light intensities were found to be very reproducible (Figure S2 B in Supplementary material).

The full-width at half-maximum (FWHM) of the system response function was 35 ps when a resolution of 2 ps per channel was used, as obtained with the 6 ps decay of pinacyanol iodide in methanol (Van Oort et al., 2008). Data analysis was performed using a home-built computer program (Digris et al., 1999; Novikov et al., 1999). The data were fitted to multi-exponential decay functions with amplitudes a_i and fluorescence decay times τ_i . For the global analysis the decay lifetimes were forced to be equal for each run of measurements on a sample at a certain excitation wavelength but the amplitudes were allowed to differ. The fit quality was judged from the Poissonian maximum likelihood estimator, the residuals, and the autocorrelation of the residuals (Brakemann et al., 2006).

The amplitude-weighted average lifetime was calculated via

$$\tau_{avg} = \sum_{i=1}^n a_i * \tau_i (1),$$

where $\sum_{i=1}^n a_i = 1$ and τ_i is the lifetime of the i -th component.

Measurements using streak-camera setup

The streak camera allows simultaneous recording of the fluorescence intensity as a function of time and wavelength. This means the output provides entire spectra with a high spectral (few nm) and temporal (~5 ps) resolution. For the fluorescence measurements on the streak-camera setup the sample was diluted to an optical density of 0.09/cm at the excitation wavelength (for 400nm: $OD_{680} \approx 0.06$, for 535 nm: $OD_{680} \approx 0.13$) and a cuvette with 1 mm optical path was used. Time-resolved emission spectra were recorded using a synchroscan streak-camera system as described in (Van Oort et al., 2008; Van Oort et al., 2009; Van Stokkum et al., 2008). Before analysis the images were corrected for the background signal and detector sensitivity and sliced up into traces of 5 nm. An average of 100 images, all measured for 10 s, was used. Each sample was measured with two time windows: 800 ps and 2000 ps. The laser power was typically 15 μ W for the 2 ns time window measurements and 35 μ W for the 800 ps time window. The spot size was 100 μ m while the repetition rate of excitation pulses was 250 kHz. The sample was constantly

[LIGHT ACCLIMATION OF DIATOMS]

flowing with a speed of 2.5 ml/sec as described in the subsection about time-correlated single photon counting setup (see above).

The streak images were analyzed using the TIMP package for R language (Mullen and van Stokkum, 2007) and Glotaran, a graphical user interface for the R-package TIMP (Snellenburg et al., 2012). A Gaussian-shaped instrument response function was used for the analysis and its width was a free fitting parameter. Typical fwhm values obtained from the fitting procedure are: ~ 10 ps for the 800 ps time window, ~ 23 ps for the 2 ns time window. The synchroscan period (13.17 ns) results in the back and forth sweeping of long-lived components and leads to some signal before time zero in the streak-camera images (Van Stokkum et al., 2006). This is used for long-lived-component estimation. The fit quality was judged by singular value decomposition of the residuals matrix (Mullen and van Stokkum, 2007).

All experiments were performed at room temperature (293K).

Extraction of PSII and PSI excitation spectra from steady-state measurements

When it is assumed that the amount of detached antenna complexes is negligible then the fluorescence excitation spectrum $F(\lambda_{exc})$ is a linear combination of the excitation spectra $PSI(\lambda_{exc})$ and $PSII(\lambda_{exc})$ of PSI and PSII, respectively:

$$F_{open}(\lambda_{exc}) = q_1 * PSI(\lambda_{exc}) + q_2^{open} * PSII(\lambda_{exc}) \quad (2).$$

The subscript “open” indicates that the PSII RCs are open in this case. When the RCs are partly closed the excitation spectrum becomes:

$$F_{closed}(\lambda_{exc}) = q_1 * PSI(\lambda_{exc}) + q_2^{closed} * PSII(\lambda_{exc}) \quad (3),$$

and due to the increased fluorescence lifetime of closed PSII, its contribution q_2^{closed} to the fluorescence excitation spectrum increases substantially. Note that the contribution of PSI is independent of the fact whether its RC is open or closed (Wientjes and Croce, 2012). Therefore, by taking the difference between these two excitation spectra (3) and (2), one obtains the PSII excitation spectrum multiplied by a constant, i.e.:

$$PSII(\lambda_{exc}) = (1/(q_2^{closed} - q_2^{open})) * (F_{closed}(\lambda_{exc}) - F_{open}(\lambda_{exc})) \quad (4).$$

The excitation spectrum of PSI can now be obtained by subtracting $PSII(\lambda_{exc})$ from $F_{open}(\lambda_{exc})$ after proper scaling of the spectra to each other. Detection wavelength

for the excitation spectra was 679 nm. Fluorescence emission at 679 nm among other wavelengths was detected with time-resolved fluorescence measurements, while 400 nm wavelength was used for excitation. The relative or fractional contribution of PSII to the fluorescence can then be estimated according to:

$$E_{PSII^{ex/det}} = \alpha_2 * \tau_2 / (\alpha_1 * \tau_1 + \alpha_2 * \tau_2) \quad (5)$$

where α_1 , α_2 are the amplitudes and τ_1 and τ_2 are the (average) fluorescence lifetimes of PSI and PSII, respectively. In other words

$$PSII(400nm) = E_{PSII^{ex/det}} * F_{open}(400nm) \quad (6)$$

and this allows proper scaling of the excitation spectra at 400 nm, which of course also fixes the relative values at all other excitation wavelengths. Therefore, the PSI excitation spectrum can be estimated according to:

$$PSI(\lambda_{exc}) = F_{open}(\lambda_{exc}) - k^{PSII(400nm)} * PSII(\lambda_{exc}) \quad (7),$$

where $k^{PSII(400nm)}$ is a scaling parameter obtained according to (6) and $PSII(\lambda_{exc})$ is the PSII excitation spectrum from eq (4).

The procedure was also performed at detection wavelength 693 nm in order to check the consistency of the outcome.

2.3 Results

2.3.1 Picosecond kinetics and steady-state fluorescence of *C. menegheniana* LL cells

Both PSs in diatoms are composed of a core with FCPs attached to them. It is not possible to excite the cores entirely selectively, because of the strong spectral overlap of outer antenna and core but here we used two excitation wavelengths: 400 nm (the major contribution of Chl *a* absorption) and 535 nm (fx absorption) to modulate the relative amount of excitations in the outer antenna complexes. In this way the corresponding variation in fluorescence kinetics makes it possible to study EET from FCPs to both PSs *in vivo*.

Global analysis of streak-camera data, obtained after 400 nm and 535 nm excitation leads to the decay-associated spectra (DAS) in Figure 2.1. Three components are sufficient to fit the data in both cases. The quality of the fits was judged by left and right vectors of singular value decomposition of the residuals matrix (for more information about parameter estimation in Glotaran read (Mullen and van Stokkum, 2007); (Snellenburg et al., 2012)).

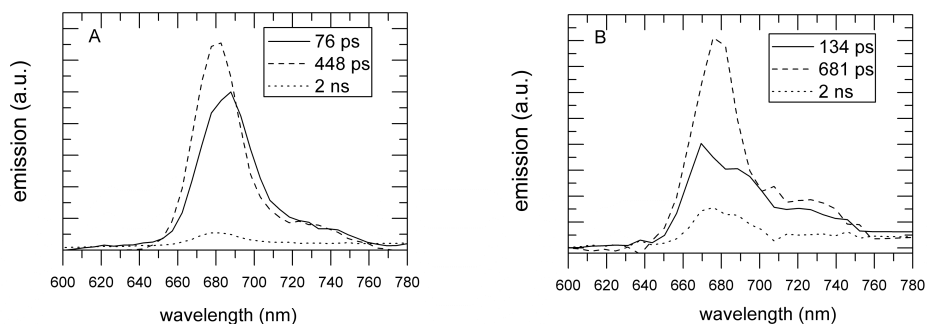


Figure 2.1. DAS of *C. meneghiniana* LL, obtained after global analysis of streak-camera data. The corresponding lifetimes are given in the inset. Excitation wavelengths are 400 nm (A) and 535 nm (B). The time window is 2 ns.

Upon 400-nm excitation the kinetics is dominated by 76 ps and 448 ps components, whereas a minor contribution stems from a 2-ns component (Figure 2.1A). The latter time constant is not very accurately determined with the streak setup. The DAS of the 76 ps component peaks at ~690 nm, indicating that it contains a large contribution from PSI (Miloslavina et al., 2009). The two slowest components resolved from the streak-camera data (448 and 2 ns) are assigned to PSII according to their 680 nm peak (Miloslavina et al., 2009). The minor contribution with the relatively long lifetime of 2 ns probably originates from a small fraction of closed RCs and/or detached FCPs. In order to study the origin of the resolved components in more detail, additional streak-camera measurements were performed in the presence of 100 μ M DCMU to close the PSII reaction centers (RCs) (Supplementary material), thereby increasing the corresponding PSII lifetimes, while the lifetimes of PSI are hardly affected (Byrdin et al., 2000; Wientjes and Croce, 2012). The results show that in the presence of DCMU a very similar short component (76 ps) is observed (Figure S3). Its lifetime, spectral shape and relative contribution are nearly identical to those observed for open RCs, demonstrating that this compartment is mainly due to PSI.

Global analysis of the streak-camera data obtained upon 535 nm excitation resolves three lifetimes: 134 ps, 681 ps and 2 ns. The components are characterized by rather complicated DAS shapes: both the 681-ps and 2-ns components have a peak at ~680 nm, indicating that they are mainly due to PSII. Moreover, a “red” shoulder around 700-750 nm can also be observed in both cases. It is reminiscent of a broad plateau in the long-wavelength range, observed by Miloslavina et al. in case of NPQ measurements and it was assigned to a fluorescence antenna compartment, functionally disconnected

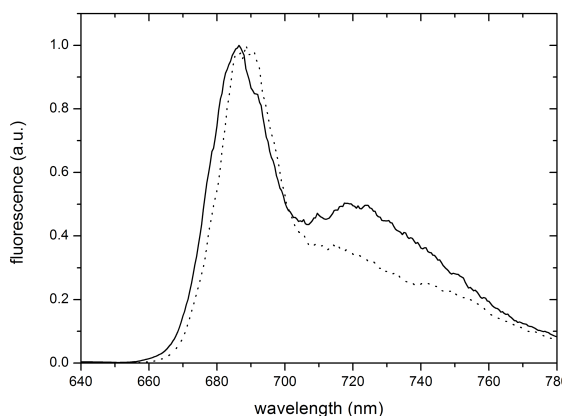


Figure 2.2. *Normalized 77K Fluorescence emission spectra obtained upon 400 nm excitation (solid line) and 535 nm excitation (dotted line), indicating that 535-nm excitation leads to significantly less long-wavelength PSI fluorescence.*

from both PSI and PSII (Miloslavina et al., 2009). It was proposed that the FCPs that contribute to this red wing are in an aggregated state similar to oligomerized trimeric LHCII in higher plants (Miloslavina et al., 2008). The shortest component resolved by the streak setup, in case of 535-nm excitation, has a lifetime of 134 ps and a peak at 670 nm.

Most importantly, upon 535-nm excitation, hardly any PSI spectral characteristics can be observed in the global analysis of the data, although the shoulder in the 690 nm region indicates that there is still some PSI contribution to the 134 ps component. However it is significantly smaller than in case of Chl *a* excitation, demonstrating that the FCPs that are preferentially excited at 535 nm transfer their excitation energy mainly to PSII. Additional measurements were done in the presence of DCMU, which leads to the closure of PSII RCs and, thus, to longer fluorescence lifetimes. From the global analysis of the data measured on closed RCs we found that all resolved components had longer lifetimes than in the case of open PSII RCs (results not shown) in contrast to the measurements at 400 nm excitation, where the PSI contribution remained unchanged (Figure S3 in Supplementary material). Therefore, it is concluded that the PSII contribution is dominating when the cells are excited at 535 nm excitation (Figure 2.1B).

In order to obtain better estimates of the fluorescence lifetimes for LL cells, the samples were also measured using the TCSPC technique. The excitation wavelength was either 400 nm or 535 nm and fluorescence was detected in the 671-724 nm region. The decay curves were fitted globally to a sum of exponential decay functions, except the longest component, that was left as a free parameter. In case of 400-nm excitation, four components were needed to obtain a satisfactory fit for all wavelength

[LIGHT ACCLIMATION OF DIATOMS]

combinations, as was judged from the Poissonian maximum likelihood estimator, and from the residuals and the autocorrelation function of the residuals. The lifetimes of the resolved components are 75 ps, 300 ps, 687 ps and 1.2-6 ns. For 535-nm excitation, only three components are enough to get a satisfactory fit: 198 ps, 600 ps and 2.0-2.4 ns. The fitting results are summarized in Table 1.

Table 1. *C. meneghiniana* LL results of global fitting of the TCSPC decay curves upon 400 nm and 535 nm excitation.

| λ_{det} | 670 nm | 679 nm | 693 nm | 701 nm | 712 nm | 724 nm | *avg |
|--------------------------|--------|--------|--------|--------|--------|--------|------------|
| τ | | | | | | | |
| 400 nm excitation | | | | | | | |
| 75 ps | 13% | 19% | 37% | 44% | 43% | 41% | |
| 300 ps | 63% | 53% | 36% | 30% | 33% | 31% | |
| 687 ps | 21% | 26% | 26% | 24% | 21% | 26% | |
| 1.2-6 ns | 3% | 2% | 1% | 2% | 3% | 2% | |
| * τ_{avg} , ps | 391 | 372 | 330 | 325 | 326 | 328 | 345 |
| * τ'_{avg} , ps | 354 | 359 | 317 | 294 | 284 | 308 | 319 |
| * τ_{PSII} , ps | 397 | 427 | 462 | 472 | 450 | 476 | 447 |
| 535 nm excitation | | | | | | | |
| 198 ps | 32% | 31% | 34% | 36% | 38% | 37% | 35% |
| 600 ps | 67% | 68% | 63% | 63% | 61% | 61% | 64% |
| 2.0-2.4 ns | 1% | 1% | 3% | 1% | 1% | 2% | 1% |
| * τ_{avg} , ps | 504 | 528 | 448 | 475 | 518 | 485 | 493 |
| * τ'_{avg} , ps | 470 | 469 | 459 | 454 | 446 | 462 | 460 |

The longest component was not fitted globally and was a free parameter in the analysis. Confidence intervals of fluorescence lifetimes were calculated by an exhaustive search algorithm and were <7% for the entire detection interval. Standard errors of amplitudes were estimated from 3-5 repetitions and were not higher than 5%. The 75 ps component is very similar to the 76 ps component obtained from the streak-camera data (400 nm excitation case). Its lifetime, spectral shape and relative contribution are all nearly identical to its counterpart for the streak measurements. It was demonstrated that this component is entirely due to PSI (Supplementary material), whereas the 300 ps and 687 ps compartments are assigned to the PSII kinetics in the TCSPC measurements upon 400 nm excitation.

avg, mean value of an amplitude/average lifetime over the whole detection region. In case of the amplitude, only the rows that do not show strong deviations throughout the detection region were averaged.

τ_{avg} , total average lifetime of the fluorescence decay;

τ'_{avg} , average lifetime of the fluorescence decays when the contribution of the longest component was omitted from the calculations. Its amplitude is very small and probably it originates from closed RCs of PSII or/and small fraction of detached FCPs, so for most of the estimations it is not of interest;

τ_{PSII} , overall charge separation time that was calculated as a weighted average lifetime of the 300 ps and 687 ps components.

[CHAPTER 2]

The results obtained with the TCSPC setup upon 400-nm excitation are very similar to the streak-camera results. Again the shortest component (75 ps) has PSI characteristics with the amplitude peaking around 701 nm, while the rest of the lifetimes should be assigned to open PSII (except for the 1.2-6 ns component that is due to closed RCs and/or detached FCPs). The main difference is the fact that the 448 ps component observed with the streak-camera setup is further resolved into a 300 ps and a 687 ps compartment in case of the TCSPC data. The average lifetime of these two components was calculated for each detection wavelength (Table 1, row τ_{PSII}) and turned out to be ~ 447 ps on average ($\tau_{PSII, avg}$), which is virtually identical to the 448 ps lifetime as obtained from the streak-camera data and it is attributed to the average overall trapping time of excitations in PSII due to charge separation.

The average lifetime resolved from the TCSPC data in case of 535 nm excitation (~ 500 ps) is very close to the one obtained from the streak-camera measurements (~ 520 ps). But the resolved components, in case of different techniques, are somewhat different (198 ps, 600 ps for TCSPC vs. 134 ps and 681 ps for streak camera), while the amplitudes of the corresponding components are close to each other (the shortest component contributes ~ 60 %, while the second one ~ 35 % of the 670-690 nm emission for both TCSPC and streak camera).

As can be judged from the average TCSPC lifetimes (τ_{avg} , τ'_{avg} Table 1), the fluorescence decay times after fx excitation are somewhat longer than for 400 nm excitation where Chl *a* is excited to a large extent. The contribution of the longest component is equally small in both cases, and it is not responsible for the observed difference (if it is excluded: τ'_{avg} (535 nm) - τ'_{avg} (400 nm) ≈ 140 ps; if included: τ_{avg} (535 nm) - τ_{avg} (400 nm) ≈ 150 ps, Table 1).

Like in the case of the streak-camera measurements, the presence of a compartment mainly due to PSI is also not observed upon fx excitation in the TCSPC data. This is in agreement with the finding above that the FCP complexes that are excited at 535 nm, mainly transfer their excitation energy to PSII. The shortest component resolved by TCSPC is 198 ps with an amplitude of ~ 35 % that shows only a few percent of variation for the different detection wavelengths.

To obtain further evidence that excitation energy is preferably transferred to PSII, in case of selective antenna excitation at 535 nm, steady-state low-temperature spectra were recorded using 400 nm and 535 nm excitation at 77 K. Indeed, Figure 2.2 shows that the relative amount of PSI fluorescence is smaller upon 535 nm excitation.

From the two shortest components resolved by TCSPC at 535 nm the weighted average lifetime was determined at each detection wavelength and it is presented in the row τ'_{avg} of Table 1 (535 nm excitation part). Because both lifetimes are mainly due to PSII, τ'_{avg} can be considered as the overall average PSII trapping

time ($\tau'_{avg} = \tau_{PSII}$). Its mean value for the whole detection region is 460 ps ($\tau'_{avg, avg}$), which is ~ 13 ps longer than it was observed upon Chl *a* excitation (447 ps). The lengthening of the lifetime attributed to PSII is expected because the excitation at 535 nm leads to relatively more excitations in the antennas and, thus, to a longer migration time (Broess et al., 2008). This finding is reminiscent of the earlier data obtained for thylakoid membranes from *Arabidopsis thaliana*, where a difference in migration time led to a difference in the average lifetime of 13 ps after excitation at 484 and 412 nm (Van Oort et al., 2010). Note, that in that case the estimated migration time, i.e. the average time it takes for an excitation to reach the reaction center or primary electron donor for the first time, was around 150 ps.

2.3.2 PSI and PSII excitation spectra of *C. meneghiniana*

In order to obtain the PSI and PSII excitation spectra for intact *C. meneghiniana* cells use was made of the procedure described in Materials and Methods. For obtaining the PSII excitation spectrum *in vivo*, steady-state measurements with and without DCMU were performed, while for obtaining the PSI excitation spectrum a scaling parameter was needed and it was calculated from the time-resolved measurements (Eq. 5, 6). Use was made of the time-resolved streak-camera data obtained with “open” RCs upon 400 nm excitation (Figure 2.1A). It was shown above that the 76-ps component is mainly due to PSI, while the 448-ps compartment can be considered as the overall trapping time of PSII. The contribution of PSII to the 76ps DAS is very small, but the exact value is not known. Therefore, in order to estimate the PSI excitation spectrum, we considered two rather extreme cases: 1) the 76 ps component is entirely due to PSI; 2) 20 % of its amplitude is due to PSII (which is clearly an overestimation). The final shape of PSI excitation spectrum was very similar in both cases (data not shown). The origin of the longest component is not completely clear (most probably it originates from a small fraction of closed RCs or/and detached FCPs), and the scaling value was calculated by both including and excluding its contribution from the PSII estimations. This resulted only in a small variation of the $E_{PSI}^{ex/det}$ value (<4%), and the resulting PSI excitation spectra were nearly indistinguishable (data not shown). To verify these results the procedure was done for two detection wavelengths: 679 nm and 693 nm. From the DAS presented in Figure 2.1 A the following estimations of the PSI contribution to $Q^{ex/det}$ were obtained:

$$679 \text{ nm} \pm 5 \text{ nm}: E_{PSI}^{400/679} = 0.07;$$

$$693 \text{ nm} \pm 5 \text{ nm}: E_{PSI}^{400/693} = 0.11.$$

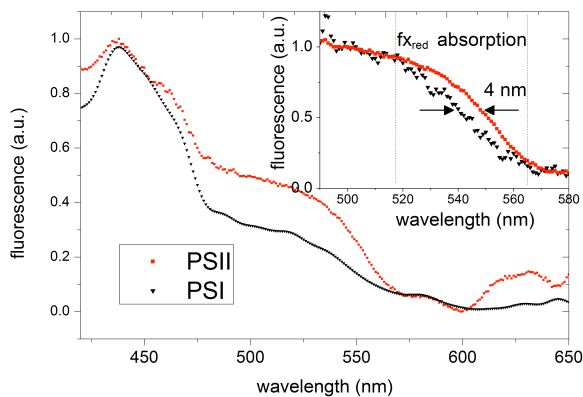


Figure 2.3. Normalized fluorescence excitation spectra of PSI (black) and PSII (red) from *C. meneghiniana* LL cells extracted by the procedure described in the Materials and Methods subsection. Insert: fluorescence excitation spectra normalized at 500 nm.

The extracted excitation spectra appeared to be independent of the detection wavelength, also confirming that the PSI and PSII kinetics were nicely separated in the time-resolved data. In Figure 2.3 the obtained PSI and PSII excitation spectra are presented. As compared to the PSII spectrum, the PSI spectrum exhibits less contribution in the absorption region of the accessory antenna pigments (Chl *c* and fx_{red}) indicating again that FCPs transfer their excitation energy preferably to PSII. Using the obtained spectra, we also tried to estimate whether the proportion of fx_{blue} and fx_{red} is different in case of FCPs bound to the different PSs. There are some indications derived from *in vivo* measurements that fx_{red} is bound to PSII in a slightly higher amount than to PSI (Szabo et al., 2010). In order to compare the shape of the PSI and PSII excitation spectra, they were normalized at 500 nm and the spectral shoulders were compared in the fx absorption region (Figure 2.3: Insert). Both spectra appear to be very similar but the PSII excitation spectrum is red-shifted by 4 nm as compared to the PSI excitation spectrum. This is in qualitative agreement with results published earlier by Szabo et al. (Szabo et al., 2010), although the effect observed in the present study is less pronounced.

2.3.3 Fluorescence kinetics of LL-, ML- and HL-grown *C. meneghiniana* cells upon 535 nm excitation

C. meneghiniana cells grown in different light intensities (LL, ML, HL) were studied by time-resolved fluorescence using 535 nm and 400 nm excitation wavelengths. From the measurements reported in the previous section it was concluded that most of the excitation energy is transferred from FCPs to PSII RCs. In

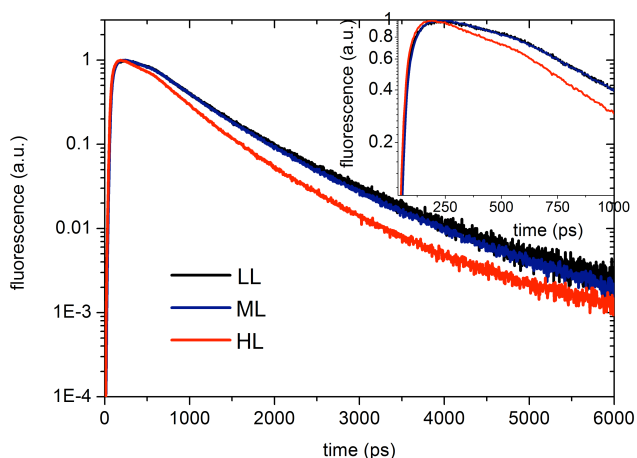


Figure 2.4. TCSPC results for LL (black line), ML (blue line) and HL (red line) *C. meneghiniana* cells upon 535 nm excitation and 679 nm detection. Insert: initial part of the decay curves.

this subsection we monitor the difference in the fluorescence kinetics of *C. meneghiniana* cells grown in different light conditions (LL, ML, HL) after using the 535 nm excitation wavelength in the TCSPC measurements. In Figure 2.4 679 nm TCSPC decay curves are presented of *C. meneghiniana* cells grown in different photon flux densities. Whereas there is no strong difference between the decay kinetics of the LL and ML samples, the decay curve of the HL cells is considerably faster.

The global fitting results for the LL sample are given in Table 1. In case of ML and HL cultures, three decay components were needed to get satisfactory fits for all detection wavelengths (Table 2). The longest component (2.3-3.6 ns) was not fitted globally. Its contribution is very small (<3%) and it is assumed to be due to a small fraction of closed RCs or/and detached FCPs. Therefore, in Table 2 only τ'_{avg} is presented, which does not include the longest component. The value of τ'_{avg} for the HL culture is substantially smaller than for LL and ML cells. Although the lifetimes of the resolved components do not differ much for all three samples (165 and 619 ps for HL as compared to 189 ps and 641 ps for ML and 196 and 600 ps for LL), the relative contributions of the resolved components vary strongly: going from LL to HL the amplitude of the shortest component increases from ~35% to 56%, while the contribution of the second component decreases from 64% to 43%. Comparison of the fitting results of LL and ML samples shows that the ML average lifetimes are on average 35 ps shorter. The difference between HL and LL samples is even more striking: the LL average decay time is ~100 ps slower than that of the HL cells. As stated before, the kinetics upon 535 nm excitation is dominated by PSII. That is why

the calculated average lifetime upon fx excitation (τ'_{avg}) can be considered as the overall average trapping time of PSII ($\tau'_{avg} = \tau_{PSII}$). Then the 100 ps decrease of the τ_{PSII} value for the HL cells as compared to the LL cells reflects a difference in the antenna size. In higher plants it has been established that the LHCII/RC ratio strongly affects the overall average PSII decay lifetime. In case of PSII membranes (BBY preparations) from spinach (Berthold et al., 1981), where this ratio was 2.35—2.55, a lifetime of ~150 ps was found by Broess et al. (Broess et al., 2006), while van Oort and coworkers observed an increase of the average PSII lifetime up to ~330 ps for thylakoid membranes with an LHCII/PSII ratio of 4.0 (Van Oort et al., 2010).

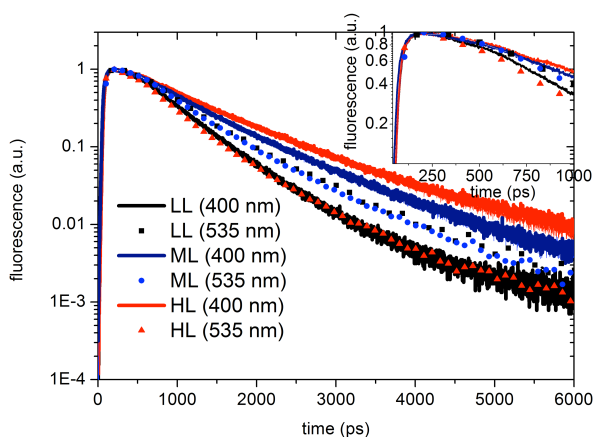


Figure 2.5. Time-resolved (TCSPC) fluorescence kinetics of *C. meneghiniana* LL (black), ML (blue) and HL (red) cells detected at 679 nm using 400 nm (lines) and 535 nm excitation (dots). Insert: initial part of the decay curves.

2.3.4 Fluorescence kinetics of LL-, ML- and HL- *C. meneghiniana* cells upon 400 nm excitation

In Figure 2.5 a comparison is made between *C. meneghiniana* LL, ML, HL decay curves upon 400 nm excitation and 535 nm excitation. As was already explained above, 535 nm excitation leads to a longer average PSII trapping time for LL cells than for HL cells upon fx excitation, due to the difference in antenna size.

However, for ML and HL cells the fluorescence kinetics upon 400 nm excitation are considerably slower than upon 535 nm excitation, meaning that apart from a reduction in the antenna size, also some other changes take place upon increasing the light intensity during growth. The global analysis of TCSPC ML and HL

[LIGHT ACCLIMATION OF DIATOMS]

Table 2. Results of global fitting of the fluorescence decay curves of *C. meneghiniana* upon 535 nm excitation.

| λ_{det} | 670 nm | 679 nm | 693 nm | 701 nm | 712 nm | 724 nm | *avg |
|----------------------------------|--------|--------|--------|--------|--------|--------|------------|
| τ | | | | | | | |
| <i>C. meneghiniana</i> ML | | | | | | | |
| 189 ps | 51% | 47% | 45% | 45% | 46% | 46% | 47% |
| 641 ps | 47% | 52% | 52% | 54% | 51% | 51% | 51% |
| 2.3-3.6ns | 2% | 1% | 3% | 1% | 3% | 3% | 2% |
| * τ'_{avg} , ps | 406 | 426 | 431 | 436 | 426 | 426 | 425 |
| <i>C. meneghiniana</i> HL | | | | | | | |
| 165 ps | 58% | 56% | 53% | 55% | 60% | 53% | 56% |
| 619 ps | 41% | 43% | 45% | 44% | 40% | 45% | 43% |
| 2.7-3.6 ns | 1% | 1% | 2% | 1% | <1% | 2% | 1% |
| * τ'_{avg} , ps | 353 | 364 | 373 | 367 | 347 | 373 | 363 |

The longest component was not fitted globally and was a free parameter in the analysis. Confidence intervals of fluorescence lifetimes were calculated by exhaustive search algorithm and were <4% through all detection interval. Standard errors of amplitudes were calculated from 3-5 repeats and were not more than 3%.

avg, mean value of an amplitude/average lifetime over the whole detection region;

τ'_{avg} , average lifetime of the fluorescence decays when the contribution of the longest component was omitted from the calculations. Its amplitude is very small and probably it originates from closed RCs of PSII or/and small fraction of detached FCPs.

data is presented in Table 3. The value of τ_{avg} increases by ~100 ps for ML cells as compared to LL cells (~391 ps for LL, ~488 ps for ML). This difference is remarkable because the growth irradiance for ML is only 30 $\mu\text{mol photons m}^{-2}\text{s}^{-1}$ higher than in case of the culture grown in low light. For HL cells the average lifetime increases even further up to ~520 ps. From the global analysis of the ML data (Table 3) the PSI component is found to be 68 ps. Its amplitude varies a lot at different wavelengths and peaks at 701 nm. This result is around the same as for LL cells, where a PSI 75-ps component was observed (Table 1). The main difference between the LL and ML results stems from the longest component (LL: 1.2-6 ns; ML: 1.5 -1.9 ns), which has a far higher amplitude for ML cells, even up to 8%, which is almost 3 times higher as was observed for LL cells. It can neither be assigned to detached FCPs nor to closed RCs attached to FCPs because the component does not have a counterpart upon 535 nm excitation (Table 2). Therefore, it most probably originates either from non-functioning PSII (inactivated/disassembled PSII units) or PSII with closed RCs that are disconnected from the antenna complexes.

[CHAPTER 2]

HL results show that the kinetics of PSI cannot be completely resolved anymore from the TCSPC data. The shortest component that was resolved for the HL cells upon 400 nm excitation is 122 ps. Its amplitude contribution varies between 49-54% over the entire detection window without showing any specific peaks. This provides direct evidence for a significant decrease of functional PSI for cultures grown in high-light intensities. This result is in agreement with the results of Strzepek and Harrison, who detected a strong decrease of the PSI concentration with an increase of the growth irradiance for the diatom *Thalassiosira weissflogii* (Strzepek and Harrison, 2004).

Table 3. Global fitting results of the *C. meneghiniana* (ML and HL) decay curves upon 400 nm excitation.

| λ_{det} | 670 nm | 679 nm | 693 nm | 701 nm | 712 nm | 724 nm | *avg |
|----------------------------------|--------|--------|--------|--------|--------|--------|------------|
| τ | | | | | | | |
| <i>C. meneghiniana</i> ML | | | | | | | |
| 68 ps | 8% | 23% | 36% | 48% | 46% | 47% | |
| 241 ps | 43% | 25% | 22% | 13% | 14% | 12% | |
| 764 ps | 46% | 45% | 38% | 33% | 32% | 33% | |
| 1.5-1.9 ns | 3% | 7% | 4% | 6% | 8% | 7% | |
| τ_{avg} , ps | 500 | 516 | 480 | 470 | 470 | 493 | 488 |
| <i>C. meneghiniana</i> HL | | | | | | | |
| 122 ps | 53% | 55% | 50% | 54% | 54% | 49% | 53% |
| 803 ps | 40% | 40% | 44% | 40% | 40% | 42% | 41% |
| 1.7-2.4 ns | 7% | 5% | 6% | 6% | ~6% | ~8% | 6% |
| τ_{avg} , ps | 507 | 544 | 517 | 516 | 529 | 527 | 523 |

The longest component was not fitted globally and was left as a free parameter in the analysis. Confidence intervals of fluorescence lifetimes were calculated by exhaustive search algorithm and were <6% through all detection interval. Standard errors of amplitudes were calculated from 3-5 repeats and were not larger than 3%.

avg, mean value of an amplitude/average lifetime over the whole detection region. In case of the amplitude, only the rows that do not show strong deviations throughout the detection region were averaged.

It is also in line with Beer et al, who measured a slower PSII reoxidation in HL cells of *C. meneghiniana* (Beer et al., 2011). The second component resolved in HL is 803 ps with a contribution of ~41% throughout the whole detection region, and this lifetime is somewhat longer than in case of LL and ML samples, where 687 ps (LL) and 764 ps (ML) lifetimes were obtained.

Another aspect that contributes to the increase of the average lifetime is similar as for the ML culture: a strong increase of the amplitude of the slowest

[LIGHT ACCLIMATION OF DIATOMS]

component (1.7-2.4 ns) up to 8%. Again, this rise is not observed upon 535 nm excitation.

To summarize, upon relatively selective Chl *a* excitation a strong increase of the average fluorescence lifetime was observed for ML and HL cultures, which is due to two main effects: a decrease in the relative amount of PSI and an increase of Chl *a* that is not active in excitation energy transfer and most probably attached to inactivated/disassembled PSII units as a result of photoinhibition (Wu et al., 2011). This hypothesis is in agreement with the observation that the maximum quantum yield of PSII photochemistry (F_v/F_m) decreases substantially under HL growing conditions as compared to LL (Beer et al., 2011)(Strzepak and Harrison, 2004). Interestingly this effect is already substantial for the ML culture, where the growth irradiance was (only) 50 $\mu\text{mol photons m}^{-2}\text{s}^{-1}$.

2.4 Discussion

In this work we have investigated and interpreted the variation in fluorescence kinetics of the diatom *C. meneghiniana in vivo* grown in different light conditions. Use was made of different excitation wavelengths to preferentially excite antenna or core complexes and different detection wavelengths were used to discriminate between PSI and PSII. The combination of steady-state and time-resolved fluorescence allowed us to distinguish between the excitation spectra of PSI and PSII.

400 nm excitation of low-light cultures leads to a 75 ps lifetime that mainly corresponds to excitation trapping in PSI, which is close to the lifetime of PSI in higher plants (Van Oort et al., 2008; Wientjes et al., 2009; Wientjes et al., 2011). For PSII an average lifetime of 448 ps is found. These results are reminiscent of those obtained for thylakoid membranes from *Arabidopsis thaliana* (Van Oort et al., 2010), where the average fluorescence lifetime of PSII was reported to be ~ 333 ps and a 73 ps lifetime was found that was predominantly due to PSI. The longer lifetime for PSII in *C. meneghiniana* LL cells may be due to a larger antenna size (the *Arabidopsis* thylakoids contained ~ 300 pigments/RC (Croce and van Amerongen, 2011; Sandonà et al., 1998; Van Oort et al., 2010)) although it should be realized that the antenna composition differs and the same is true for its organization. A larger antenna size allows more effective light harvesting in LL growing conditions as shown by Smith and Melis in diatoms (Smith et al., 1988), while high photon flux densities cause a decrease of the antenna size that is also reflected in the average lifetimes (see below). It is worth mentioning that the DAS for our PSI and PSII components are very similar in shape as those reported by Miloslavina et al. with the same peak positions (~ 680 nm for PSII and ~ 690 nm for PSI)(Miloslavina et al., 2009). In that study three components for

both PSI and PSII were observed by performing target model fitting (*C. meneghiniana*: 2.6 ps, 12 ps, 66 ps for PSI and 159 ps, 300 ps and 580 ps for PSII). A rough average lifetime estimation for their results leads to ~51 ps for PSI and ~395 ps for PSII (*C. meneghiniana*). These values are slightly shorter than in our case but, as was shown above, the growth conditions can influence the average lifetimes. We conclude that the antenna size for the samples used by Miloslavina et al. were smaller, probably as a result of different illumination conditions used during growth (reported intensity was 40 $\mu\text{mol photons m}^{-2}\text{s}^{-1}$).

In case of selective antenna excitation at 535 nm, we observed that PSI was excited rather poorly and no PSI can be distinguished by the global analysis of the data. Furthermore the PSII-associated antenna seems to be enriched in $f_{x_{\text{red}}}$ (Figure 2.3: Insert), indicating that the FCPb oligomeric form can be not only connected to PSI (Veith et al., 2009) but also to PSII.

The decrease of the PSI contribution upon f_x excitation at 535 nm results in the fact that the kinetics starts to be dominated by two components, both of which are predominantly attributed to PSII and the lifetimes are around 460 ps on average (Table 1, τ'_{avg}). This value is ~13 ps longer than the average PSII lifetime observed upon Chl *a* excitation (449 ps), due to an increase of the migration time when there are relatively more excitations in the outer antenna. We cannot estimate the difference in migration time very accurately because it is not possible yet to completely correct for the PSI kinetics both at 400 nm and at 535 nm and moreover the ratio of PSII core and antenna excitations at 400 nm is not known.

We have observed a strong effect of growth light conditions on the PSII fluorescence kinetics. In case of selective antenna excitation, the average lifetime decreased from 460 ps for LL- to 363 ps in case of HL-cultures. The ~ 100 ps shortening reflects a decrease of the FCP antenna size connected to the RC of PSII. In this respect our results agree with those of Gallagher et al. (Gallagher et al., 1984). On the other hand our findings are in disagreement with those of Lepetit and co-workers, who claimed that the number of antenna complexes per RC is relatively constant in different light regimes (Lepetit et al., 2010).

In case of higher plants, it was shown that the size of the PSII antenna influences the fluorescence lifetimes substantially (Caffarri et al., 2011; Croce and van Amerongen, 2011). For membranes that contain 2.0-2.5 LHCII trimers per PSII RC, the fluorescence lifetime was reported to be around 150 ps upon Chl *a* excitation (Broess et al., 2006; Broess et al., 2008) whereas for thylakoid membranes with 4.0 trimers per PSII RC, the lifetime goes up to around 330 ps (Caffarri et al., 2011; Croce and van Amerongen, 2011; Van Oort et al., 2010), partly because the extra trimers are connected less well with the RC. Although significant sequence similarity exists

[LIGHT ACCLIMATION OF DIATOMS]

between FCP and LHCII proteins the antenna composition and organization differs. In diatoms, special FCP proteins (Lhcr) are bound to PSI only (Grouneva et al., 2011; Veith et al., 2009; Veith and Büchel, 2007), whereas no data about the precise organization of the PSII antenna composition exists. Both FCPa and FCPb complexes were isolated separately from the PSs and consist of Lhcf proteins, whereby FCPa contain Lhcx polypeptides in addition (Beer et al., 2006). As mentioned above, only hints exist about the attribution of FCP complexes to either PS. The enrichment of the PSII antenna with $f_{x_{red}}$ points at least to FCPa being associated with PSII. Thus we tentatively assume that losing one FCPa trimer from the PSII antenna might be responsible for the difference in PSII lifetime for LL and HL cells. Such a change in PSU size would not result in a detectable change in the relative pigment concentrations, making these values less good indicators for the antenna size change in contrast to what was assumed in (Lepetit et al., 2010).

The results obtained for the light-treated cells upon 400-nm excitation demonstrate that apart from the PSII antenna size also other changes occur. Increasing the growth irradiance leads to a relative decrease of the amount of PSI as compared to PSII, which is reflected by the fact that the ~ 70 ps PSI lifetime cannot be resolved anymore in case of HL cells. Moreover, the samples grown in ML- and HL-conditions start to experience strong photoinhibition. This effect manifests itself by a substantial increase of the contribution of long lifetime components. This is reminiscent of results obtained by Wu et al. (Wu et al., 2011), who observed large pools of inactive or disassembled PSII centers in *Thalassiosira pseudonana* in case of a sudden increase of irradiance.

Acknowledgments

The authors thank Rob Koehorst and Arie van Hoek for technical help with the measurements, Cor Wolfs for initial help with growing cells and Sergey Laptinok, Joris Snellenburg and Ivo van Stokkum for seminal support in the usage of the Glotaran software analysis toolkit. This work was supported by HARVEST Marie Curie Research Training Network (PITN-GA-2009-238017) to VUC.

References

- Beer, A., Gundermann, K., Beckmann, J., and Büchel, C. (2006). Subunit composition and pigmentation of fucoxanthin-chlorophyll proteins in diatoms: evidence for a subunit involved in diadinoxanthin and diatoxanthin binding. *Biochemistry* 45:13046-13053.
- Beer, A., Juhas, M., and Büchel, C. (2011). Influence of Different Light Intensities and Different Iron Nutrition on the Photosynthetic Apparatus in the Diatom *Cyclotella meneghiniana* (Bacillariophyceae). *Journal of Phycology* 47:1266-1273.

[CHAPTER 2]

- Berthold, D.A., Babcock, G.T., and Yocum, C.F. (1981). A Highly Resolved, Oxygen-Evolving Photosystem-Ii Preparation from Spinach Thylakoid Membranes - Electron-Paramagnetic-Res and Electron-Transport Properties. *Febs Letters* 134:231-234.
- Brakemann, T., Schlormann, W., Marquardt, J., Nolte, M., and Rhiel, E. (2006). Association of fucoxanthin chlorophyll a/c-binding polypeptides with photosystems and phosphorylation in the centric diatom *Cyclotella cryptica*. *Protist* 157:463-475.
- Broess, K., Trinkunas, G., van der Weij-de Wit, C.D., Dekker, J.P., van Hoek, A., and van Amerongen, H. (2006). Excitation energy transfer and charge separation in photosystem II membranes revisited. *Biophysical journal* 91:3776-3786.
- Broess, K., Trinkunas, G., van Hoek, A., Croce, R., and van Amerongen, H. (2008). Determination of the excitation migration time in Photosystem II consequences for the membrane organization and charge separation parameters. *Biochimica et biophysica acta* 1777:404-409.
- Büchel, C. (2003). Fucoxanthin-chlorophyll proteins in diatoms: 18 and 19 kDa subunits assemble into different oligomeric states. *Biochemistry* 42:13027-13034.
- Byrdin, M., Rimke, I., Schlodder, E., Stehlik, D., and Roelofs, T.A. (2000). Decay kinetics and quantum yields of fluorescence in photosystem I from *Synechococcus elongatus* with P700 in the reduced and oxidized state: are the kinetics of excited state decay trap-limited or transfer-limited? *Biophys J* 79:992-1007.
- Caffarri, S., Broess, K., Croce, R., and van Amerongen, H. (2011). Excitation energy transfer and trapping in higher plant Photosystem II complexes with different antenna sizes. *Biophys J* 100:2094-2103.
- Croce, R., and van Amerongen, H. (2011). Light-harvesting and structural organization of Photosystem II: from individual complexes to thylakoid membrane. *J Photochem Photobiol B* 104:142-153.
- Digris, A.V., Skakoun, V.V., Novikov, E.G., van Hoek, A., Claiborne, A., and Visser, A.J.W.G. (1999). Thermal stability of a flavoprotein assessed from associative analysis of polarized time-resolved fluorescence spectroscopy. *Eur Biophys J Biophys* 28:526-531.
- Durnford, D.G., Aebersold, R., and Green, B.R. (1996). The fucoxanthin-chlorophyll proteins from a chromophyte alga are part of a large multigene family: structural and evolutionary relationships to other light harvesting antennae. *Mol Gen Genet* 253:377-386.
- Falkowski, P.G., Barber, R.T., and Smetacek, V. (1998). Biogeochemical controls and feedbacks on ocean primary production. *Science* 281:200-206.
- Falkowski, P.G., Owens, T.G., Ley, A.C., and Mauzerall, D.C. (1981). Effects of growth irradiance levels on the ratio of reaction centers in two species of marine phytoplankton. *Plant Physiol* 68:969-973.
- Gallagher, J.C., Wood, A.M., and Alberte, R.S. (1984). Ecotypic Differentiation in the Marine Diatom *Skeletonema-Costatum* - Influence of Light-Intensity on the Photosynthetic Apparatus. *Mar Biol* 82:121-134.
- Gildenhoff, N., Amarie, S., Gundermann, K., Beer, A., Büchel, C., and Wachtveitl, J. (2010). Oligomerization and pigmentation dependent excitation energy transfer in fucoxanthin-chlorophyll proteins. *Biochimica et biophysica acta* 1797:543-549.
- Grouneva, I., Rokka, A., and Aro, E.M. (2011). The Thylakoid Membrane Proteome of Two Marine Diatoms Outlines Both Diatom-Specific and Species-Specific Features of the Photosynthetic Machinery. *J Proteome Res* 10:5338-5353.
- Ikeda, Y., Komura, M., Watanabe, M., Minami, C., Koike, H., Itoh, S., Kashino, Y., and Satoh, K. (2008). Photosystem I complexes associated with fucoxanthin-chlorophyll-binding

[LIGHT ACCLIMATION OF DIATOMS]

- proteins from a marine centric diatom, *Chaetoceros gracilis*. *Biochimica et biophysica acta* 1777:351-361.
- Lavaud, F. (2007). Fast Regulation of Photosynthesis in Diatoms: Mechanisms, Evolution and Ecophysiology. *Func Plant Sci Biotech* 1:267-287.
- Lepetit, B., Volke, D., Gilbert, M., Wilhelm, C., and Goss, R. (2010). Evidence for the Existence of One Antenna-Associated, Lipid-Dissolved and Two Protein-Bound Pools of Diadinoxanthin Cycle Pigments in Diatoms. *Plant physiology* 154:1905-1920.
- Liu, Z., Yan, H., Wang, K., Kuang, T., Zhang, J., Gui, L., An, X., and Chang, W. (2004). Crystal structure of spinach major light-harvesting complex at 2.72 Å resolution. *Nature* 428:287-292.
- Miloslavina, Y., Grouneva, I., Lambrev, P.H., Lepetit, B., Goss, R., Wilhelm, C., and Holzwarth, A.R. (2009). Ultrafast fluorescence study on the location and mechanism of non-photochemical quenching in diatoms. *Biochimica et biophysica acta* 1787:1189-1197.
- Miloslavina, Y., Wehner, A., Lambrev, P.H., Wientjes, E., Reus, M., Garab, G., Croce, R., and Holzwarth, A.R. (2008). Far-red fluorescence: A direct spectroscopic marker for LHCII oligomer formation in non-photochemical quenching. *Febs Letters* 582:3625-3631.
- Mullen, K.M., and van Stokkum, I.H.M. (2007). TIMP: An R package for modeling multi-way spectroscopic measurements. *J Stat Softw* 18.
- Nagao, R., Ishii, A., Tada, O., Suzuki, T., Dohmae, N., Okumura, A., Iwai, M., Takahashi, T., Kashino, Y., and Enami, I. (2007). Isolation and characterization of oxygen-evolving thylakoid membranes and photosystem II particles from a marine diatom *Chaetoceros gracilis*. *Biochim Biophys Acta* 1767:1353-1362.
- Novikov, E.G., van Hoek, A., Visser, A.J.W.G., and Hofstraat, J.W. (1999). Linear algorithms for stretched exponential decay analysis. *Opt Commun* 166:189-198.
- Papagiannakis, E., I, H.M.v.S., Fey, H., Buchel, C., and van Grondelle, R. (2005). Spectroscopic characterization of the excitation energy transfer in the fucoxanthin-chlorophyll protein of diatoms. *Photosynth Res* 86:241-250.
- Premvardhan, L., Bordes, L., Beer, A., Buchel, C., and Robert, B. (2009). Carotenoid Structures and Environments in Trimeric and Oligomeric Fucoxanthin Chlorophyll a/c(2) Proteins from Resonance Raman Spectroscopy. *Journal of Physical Chemistry B* 113:12565-12574.
- Premvardhan, L., Robert, B., Beer, A., and Buchel, C. (2010). Pigment organization in fucoxanthin chlorophyll a/c(2) proteins (FCP) based on resonance Raman spectroscopy and sequence analysis. *Bba-Bioenergetics* 1797:1647-1656.
- Premvardhan, L., Sandberg, D.J., Fey, H., Birge, R.R., Buchel, C., and van Grondelle, R. (2008). The charge-transfer properties of the S-2 state of fucoxanthin in solution and in fucoxanthin chlorophyll-a/c(2) protein (FCP) based on stark spectroscopy and molecular-orbital theory. *Journal of Physical Chemistry B* 112:11838-11853.
- Provasoli, L., Mclaughlin, J.J.A., and Droop, M.R. (1957). The Development of Artificial Media for Marine Algae. *Arch Mikrobiol* 25:392-428.
- Sandonà, D., Croce, R., Pagano, A., Crimi, M., and Bassi, R. (1998). Higher plants light harvesting proteins. Structure and function as revealed by mutation analysis of either protein or chromophore moieties. *Biochimica et Biophysica Acta (BBA) - Bioenergetics* 1365:207-214.
- Smith, M., B., Melis, and A. (1988). Photochemical apparatus organization in the diatom *Cylindrotheca fusiformis*: photosystem stoichiometry and excitation distribution in cells grown under high and low irradiance. Oxford, ROYAUME-UNI: Oxford University Press.

[CHAPTER 2]

- Snellenburg, J.J., Laptенок, S., Seger, R., Mullen, K.M., and van Stokkum, I.H.M. (2012). Glotaran: a Java-based Graphical User Interface for the R-package TIMP. *J Stat Softw* 49:1-23.
- Somsen, O.J., Keukens, L.B., de Keijzer, M.N., van Hoek, A., and van Amerongen, H. (2005). Structural heterogeneity in DNA: temperature dependence of 2-aminopurine fluorescence in dinucleotides. *Chemphyschem* 6:1622-1627.
- Strzepek, R.F., and Harrison, P.J. (2004). Photosynthetic architecture differs in coastal and oceanic diatoms. *Nature* 431:689-692.
- Su, W.W., Jakob, T., and Wilhelm, C. (2012). The Impact of Nonphotochemical Quenching of Fluorescence on the Photon Balance in Diatoms under Dynamic Light Conditions. *J Phycol* 48:336-346.
- Szabo, M., Premvardhan, L., Lepetit, B., Goss, R., Wilhelm, C., and Garab, G. (2010). Functional heterogeneity of the fucoxanthins and fucoxanthin-chlorophyll proteins in diatom cells revealed by their electrochromic response and fluorescence and linear dichroism spectra. *Chem Phys* 373:110-114.
- Van Oort, B., Alberts, M., de Bianchi, S., Dall'Osto, L., Bassi, R., Trinkunas, G., Croce, R., and van Amerongen, H. (2010). Effect of antenna-depletion in Photosystem II on excitation energy transfer in *Arabidopsis thaliana*. *Biophysical journal* 98:922-931.
- Van Oort, B., Amunts, A., Borst, J.W., van Hoek, A., Nelson, N., van Amerongen, H., and Croce, R. (2008). Picosecond fluorescence of intact and dissolved PSI-LHCI crystals. *Biophys J* 95:5851-5861.
- Van Oort, B., Murali, S., Wientjes, E., Koehorst, R.B.M., Spruijt, R.B., van Hoek, A., Croce, R., and van Amerongen, H. (2009). Ultrafast resonance energy transfer from a site-specifically attached fluorescent chromophore reveals the folding of the N-terminal domain of CP29. *Chem Phys* 357:113-119.
- Van Stokkum, I.H., van Oort, B., van Mourik, F., Gobets, B., and van Amerongen, H. (2008). (Sub)-Picosecond Spectral Evolution of Fluorescence Studied with a Synchroscan Streak-Camera System and Target Analysis. In: *Biophysical Techniques in Photosynthesis* Dordrecht: Springer. 223-240.
- Van Stokkum, I.H.M., Gobets, B., Gensch, T., van Mourik, F., Hellingwerf, K.J., van Grondelle, R., and Kennis, J.T.M. (2006). (Sub)-picosecond spectral evolution of fluorescence in photoactive proteins studied with a synchroscan streak camera system. *Photochemistry and photobiology* 82:380-388.
- Veith, T., Brauns, J., Weisheit, W., Mittag, M., and Buchel, C. (2009). Identification of a specific fucoxanthin-chlorophyll protein in the light harvesting complex of photosystem I in the diatom *Cyclotella meneghiniana*. *Bba-Bioenergetics* 1787:905-912.
- Veith, T., and Buchel, C. (2007). The monomeric photosystem I-complex of the diatom *Phaeodactylum tricornutum* binds specific fucoxanthin chlorophyll proteins (FCPs) as light-harvesting complexes. *Photosynthesis Research* 91:164-165.
- Wientjes, E., and Croce, R. (2012). PMS: Photosystem I electron donor or fluorescence quencher. *Photosynthesis Research* 111:185-191.
- Wientjes, E., Oostergetel, G.T., Jansson, S., Boekema, E.J., and Croce, R. (2009). The role of Lhca complexes in the supramolecular organization of higher plant photosystem I. *J Biol Chem* 284:7803-7810.
- Wientjes, E., van Stokkum, I.H., van Amerongen, H., and Croce, R. (2011). The role of the individual Lhcas in photosystem I excitation energy trapping. *Biophys J* 101:745-754.
- Wilhelm, C., Büchel, C., Fisahn, J., Goss, R., Jakob, T., Laroche, J., Lavaud, J., Lohr, M., Riebesell, U., Stehfest, K., et al. (2006). The regulation of carbon and nutrient assimilation in diatoms is significantly different from green algae. *Protist* 157:91-124.

[LIGHT ACCLIMATION OF DIATOMS]

Wu, H., Cockshutt, A.M., McCarthy, A., and Campbell, D.A. (2011). Distinctive photosystem II photoinactivation and protein dynamics in marine diatoms. *Plant Physiol* 156:2184-2195.

Supplementary material

This supplementary material contains two sections:

- (i) details about experimental conditions
- (ii) comparison of streak-camera DAS obtained from *C. meneghiniana* in open and closed state upon 400 nm excitation

(i) Experimental conditions

Measurements using streak-camera setup

For streak-camera measurements, the sample was kept at 287 K in a flow cuvette and a sample reservoir (3-4 ml). In order to minimize the contribution of closed reaction centers and of annihilation, the cells were flowing from the reservoir to the cuvette and back, with a flow speed of ~ 2.5 ml/sec. Excitation light was vertically polarized, the spot size diameter was typically ~ 100 μm , and the laser repetition rate was 250 kHz while the excitation power was 15-35 μW . The detector polarizer was set at magic angle orientation. For the experiments we used a cuvette with optical path length of 1 mm. To avoid significant self-absorption the OD at the excitation wavelength was set to $\sim 0.1/\text{cm}$ (for 400nm: $\text{OD}_{680} \approx 0.06$, for 535 nm: $\text{OD}_{680} \approx 0.13$). In this way during the time (~ 3 μs) needed to travel through the excitation spot 1 out of ~ 900 to 2200 pigments is excited. Supposing equal excitation of PSI and PSII, and a PSII antenna size of ~ 300 pigments/RC (for the estimations the number of pigments in PSII supercomplex of higher plants was used (Van Oort et al., 2010), it follows that 20 ± 10 % of the RCs are excited while passing through the excitation beam.

In order to be able to resolve the components in the region from ~ 5 ps to ~ 2 ns two time windows were used: 800 ps and 2 ns. Each experiment was repeated 3 times on different generations. The streak-images of different samples grown in the same light conditions are very similar in case of the independent cultivation and are shown in Figure S1.

TCSPC measurements

For the TCSPC measurements the pumping system as well as temperature conditions were kept the same as for the streak-camera measurements (see above). But in case of the TCSPC setup the spot size diameter was typically 3mm, and the laser repetition rate was 3.8MHz, while the excitation power was 0.1-5 μW , which is up to 350 times lower than in case of streak camera. The optical path length of the cuvette used for the TCSPC experiments was 3 mm; to avoid significant self-absorption the OD

[LIGHT ACCLIMATION OF DIATOMS]

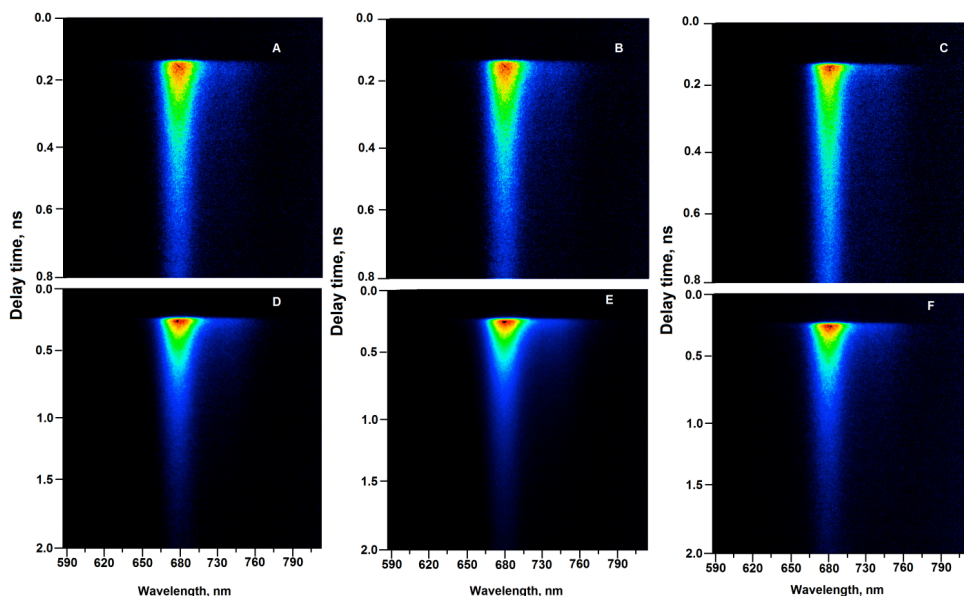


Figure S1. Fluorescence 2D images obtained for 3 different generations of *C. meneghiniana* LL as measured with the streak-camera setup upon 400nm excitation. The time window was 0.8 ns (A, B, C) and 2.0 ns (D, E, F). False colors reflect the fluorescence intensity.

at the excitation wavelength was set to $\sim 0.06/\text{cm}$ (for 400nm: $\text{OD}_{680} \approx 0.04$, for 535 nm: $\text{OD}_{680} \approx 0.08$). In this way each laser pulse excites 1 out of $\sim 5 \cdot 10^7$ to $2 \cdot 10^9$ Chls. In the time (~ 4 ms) to travel through the excitation spot $\sim 1 \cdot 10^4$ pulses hit the sample, exciting 1 out of $\sim 4 \cdot 10^3$ to $1 \cdot 10^5$ pigments. Supposing equal excitation of PSI and PSII, and a PSII antenna size of ~ 300 pigments/ RC, it follows that while passing through the excitation beam, pigments associated with $\sim 0.2\%$ - 7.0% of the RCs are excited. So the probability to have an excitation on a RC in case of TCSPC measurements is on average 5 times lower than in case of streak-camera measurements. In order to be sure that the laser power as well as the measuring procedure did not introduce any changes in the results, the final experiment of a measuring series was always a repetition of the first experiment. The resulting decay curves were indistinguishable. Each sample was measured 3-5 times for different generations of cells. The fluorescence decay curves for every sample appeared to be very similar in case of independent generations. Figure S2 shows the *C. meneghiniana* LL fluorescence kinetics excited at 400 nm, and detected at 689 nm in the beginning and in the end of measuring series (Figure S2 A) and cells grown in different generations (Figure S2 B).

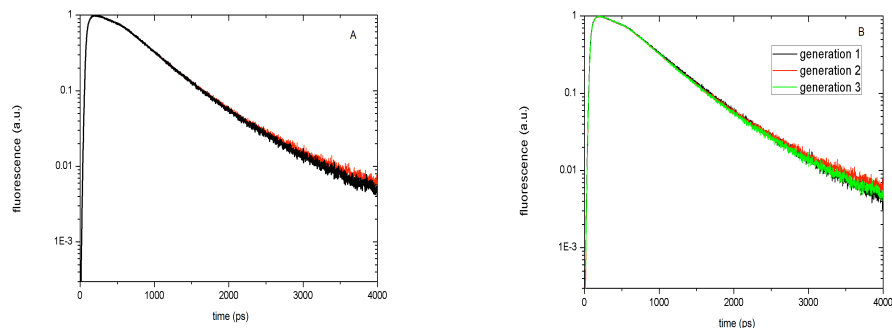


Figure S2. Fluorescence kinetics of *C. meneghiniana* excited at 400 nm and detected at 679 nm, measured on the same sample in the beginning (black line) and in the end (red line) of the measuring series (A) and for three independent generations (B)

(ii) Comparison of streak-camera DAS obtained from *C. meneghiniana* LL under 400 nm excitation without and in the presence of DCMU

A rough estimate of the relative PSI contribution to the 76 ps component resolved in streak-camera measurements of *C. meneghiniana* LL cells upon 400 nm excitation (Figure 1A) was performed in the following way: streak-camera measurements of the sample grown in the same light conditions were performed in the presence of 100 μ M DCMU. In this case a substantial increase of “closed” PSII reaction centers should be observed, thereby increasing the corresponding PSII lifetimes, while the lifetimes of PSI are hardly affected (Byrdin et al., 2000; Wientjes and Croce, 2012). Streak-camera data of *C. meneghiniana* LL cells in the presence of DCMU was fitted globally and compared with the results obtained for the open state (Figure 1A). The 76 ps component was also resolved in case of closed RCs with the spectral properties similar to the “open” state case (Figure S3). Generally the area under a positive DAS scales linearly with the number of pigments contributing to the component. Because the closing of RC should not affect the proportion of pigments attached to the PSs, the relative contribution of the area assigned to the PSI component should not experience significant changes as well. Indeed the calculated relative contribution of the 76 ps DAS to the total area (the sum of the DAS areas of all components) stayed \sim 40% in both cases, while the total contribution of two longest components was evidently \sim 60 %. As expected the PSII average lifetime increased

[LIGHT ACCLIMATION OF DIATOMS]

substantially from ~ 0.5 ns to 1.0 ns. These numbers are not very accurate because of the limited time window of the setup.

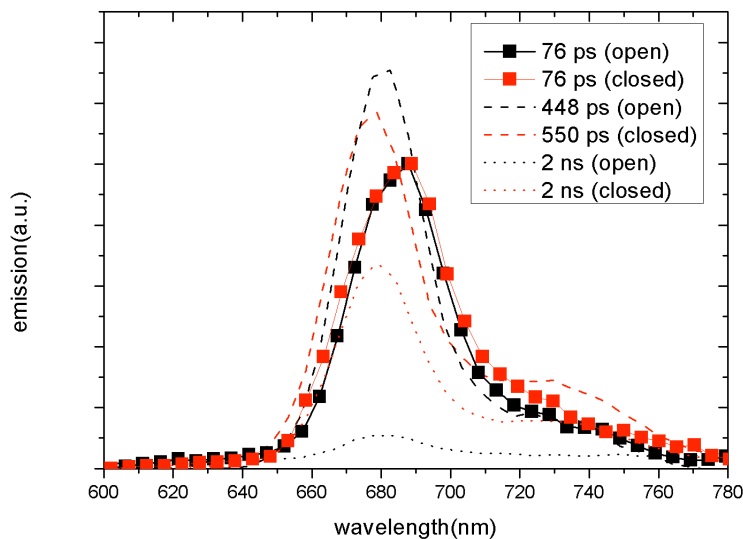


Figure S3. Comparison of the results obtained from *C. meneghiniana* LL by streak-camera measurements in the presence of DCMU (“closed” state) (red lines) and in the open state (black lines). The DAS in both cases were normalized to the 76 ps component.

- Byrdin, M., Rimke, I., Schlodder, E., Stehlik, D., and Roelofs, T.A. (2000). Decay kinetics and quantum yields of fluorescence in photosystem I from *Synechococcus elongatus* with P700 in the reduced and oxidized state: are the kinetics of excited state decay trap-limited or transfer-limited? *Biophys J* 79:992-1007.
- Van Oort, B., Alberts, M., de Bianchi, S., Dall’Osto, L., Bassi, R., Trinkunas, G., Croce, R., and van Amerongen, H. (2010). Effect of antenna-depletion in Photosystem II on excitation energy transfer in *Arabidopsis thaliana*. *Biophysical journal* 98:922-931.
- Wientjes, E., and Croce, R. (2012). PMS: Photosystem I electron donor or fluorescence quencher. *Photosynthesis Research* 111:185-191.

Chapter 3

Disentangling two non-photochemical quenching processes in *Cyclotella meneghiniana* by spectrally-resolved picosecond fluorescence at 77 K

Volha U. Chukhutsina^{ab}, Claudia Büchel^c, Herbert van Amerongen^{abd}

^aLaboratory of Biophysics, Wageningen University, 6703 HA Wageningen, The Netherlands;

^bBioSolar Cells, P.O. Box 98, 6700 AB Wageningen, The Netherlands

^cInstitute for Molecular Bio Sciences, Johann Wolfgang Goethe-University, 60438 Frankfurt am Main, Germany

^dMicroSpectroscopy Centre, Wageningen University, 6703 HA Wageningen, The Netherlands

published in *Biochimica et Biophysica Acta (BBA)-Bioenergetics*, 2014
1837 (6), 899-907

Abstract

Diatoms, which are primary producers in the oceans, can rapidly switch on/off efficient photoprotection to respond to fast light-intensity changes in moving waters. The corresponding thermal dissipation of excess-absorbed-light energy can be observed as non-photochemical quenching (NPQ) of chlorophyll *a* fluorescence. Fluorescence-induction measurements on *Cyclotella meneghiniana* diatoms show two NPQ processes: qE_1 relaxes rapidly in the dark while qE_2 remains present upon switching to darkness and is related to the presence of the xanthophyll-cycle pigment diatoxanthin (Dtx). We performed picosecond fluorescence measurements on cells locked in different (quenching) states, revealing the following sequence of events during full development of NPQ. At first, trimers of light-harvesting complexes (fucoxanthin-chlorophyll *a/c* proteins), or FCPa, become quenched, while being part of photosystem II (PSII), due to the induced pH gradient across the thylakoid membrane. This is followed by (partial) detachment of FCPa from PSII after which quenching persists. The pH gradient also causes the formation of Dtx, which leads to further quenching of isolated PSII cores and some aggregated FCPa. In subsequent darkness, the pH gradient disappears but Dtx remains present and quenching partly pertains. Only in the presence of some light the system completely recovers to the unquenched state.

3.1 Introduction

Diatoms are unicellular photosynthetic eukaryotes that are very abundant in water bodies and have a key role in the biochemical cycles of carbon, nitrogen, phosphorus and silica. They are thought to contribute ~20% to the global primary productivity, producing perhaps 20 Pg of carbon per year, and providing more oxygen than all tropical rainforests together (Falkowski et al., 1998; Field et al., 1998). Thriving in turbulent waters, diatoms have to cope with light-intensity fluctuations that can vary over several orders of magnitude on a timescale of seconds to minutes. In case of high-light stress the diatoms activate alternative energy sinks and dissipate excessively absorbed light through non-photochemical quenching (NPQ) in order to maintain an optimal photosynthetic activity.

Most of the photosynthesis processes take place in and around the thylakoid membranes, which in contrast to those of higher plants, are not segregated into stromal and granal regions. However, like in plants, their antenna complexes, the so-called fucoxanthin-chlorophyll *a/c* proteins (FCPs), are membrane-intrinsic (for reviews, see (Falkowski et al., 1998; Lavaud, 2007)). Although these antenna

[CHAPTER 3]

complexes belong to the light-harvesting chlorophyll (Chl) protein (LHC) superfamily (Durnford et al., 1996), their pigment content differs considerably from that of light-harvesting complex (LHC) II in higher plants. FCPs do not possess Chl *b* but use Chl *c* as an accessory pigment, and they contain fucoxanthin (fx) as the major light-harvesting xanthophyll, which is not present in plants. Several studies have shown that red-absorbing fx forms (fx_{red}) are predominantly connected to PSII (photosystem II), whereas PSI receives relatively more excitation energy from the more blue-absorbing fx forms (fx_{blue}) (Chukhutsina et al., 2013; Szabo et al., 2010). The Chl *a* to carotenoid ratio is ~1 for diatom antenna complexes (Gildenhoff et al., 2010; Papagiannakis et al., 2005), whereas this number is ~3 for plants (see e.g. (Liu et al., 2004)). Two different major FCP complexes can be isolated from *Cyclotella meneghiniana*, the organism under investigation in the present study: trimeric FCPa and oligomeric FCPb, that have similar spectroscopic properties but consist of different polypeptides, with only FCPa complexes containing the light-harvesting complex stress-related protein subunits, denoted as Lhcx, needed for photoprotection (Baillleul et al., 2010; Beer et al., 2006; Büchel, 2003; Gildenhoff et al., 2009; Gildenhoff et al., 2010; Premvardhan et al., 2009).

In general, thermal energy dissipation via NPQ comprises a high-energy-state (qE), a state-transition (qT), and a photoinhibitory (qI) component (see e.g. (Niyogi, 1999)). In diatoms, NPQ is dominated by qE, whereas qT is missing (Owens, 1986) and qI is strongly reduced (Ting and Owens, 1994). Diatoms have in common with vascular plants and green algae that the qE component is modulated by the conversion of xanthophyll cycle (XC) pigments. In diatoms, this comprises the de-epoxidation of diadinoxanthin (Ddx) to diatoxanthin (Dtx) (for a recent review see (Goss and Jakob, 2010)). This conversion correlates with the build-up of NPQ, which is far more pronounced than in higher plants (Ruban et al., 2004). The quenching involves several components. One of them depends most probably directly on the light-driven proton gradient across the thylakoid membrane and it relaxes/disappears relatively fast upon switching to darkness (Grouneva et al., 2008) as can be observed by fluorescence induction measurements. Another one is thought to be directly related to the de-epoxidation of Ddx to Dtx (Goss et al., 2006; Grouneva et al., 2008).

In vitro, quenching of excitations can be induced via the aggregation of light-harvesting complexes, reducing excited-state lifetime and fluorescence yield (Van Oort et al., 2007), and this aggregation has often been implied to be responsible for NPQ in higher plants and algae, at least partly (Ballottari et al., 2010; Horton and Ruban, 2005; Ruban et al., 2007; Wentworth et al., 2001). Based on picosecond spectroscopic studies NPQ in *C. meneghiniana* was also partly ascribed to aggregation

of peripheral FCP complexes (Miloslavina et al., 2009), whereas a second quenching process was postulated to be Dtx-dependent and to occur in an FCP complex close to the reaction centre (RC) of PSII. It was suggested more recently (Gundermann and Büchel, 2012) that the FCPa antenna might aggregate in *C. meneghiniana* upon lumen acidification, thereby leading to excited-state quenching. Furthermore, it was shown that the fluorescence yield of FCPa depends on the Dtx content *in vitro*, which is not the case for FCPb (Gundermann and Büchel, 2008).

Although both fluorescence induction and picosecond spectroscopic measurements point at the presence of two different quenching mechanisms in *C. meneghiniana*, it has not been possible to correlate these to each other and to the *in vitro* results on isolated (quenched and unquenched) antenna complexes. In the present study we prepare cells in different quenching states according to the fluorescence induction (PAM) measurements, stabilize these states by rapid cooling to 77 K and study the corresponding ultrafast kinetic and spectroscopic characteristics. By comparing our decomposed *in vivo* spectra with earlier reported *in vitro* spectra, a detailed model is proposed that reflects spectral and temporal characteristics of the various NPQ mechanisms in *C. meneghiniana* and pinpoints the locations where quenching takes place.

3.2 Materials and methods

3.2.1 Cell culture

The diatom *C. meneghiniana* (Culture Collection Göttingen, strain 1020-1a) was grown in batch cultures in Erlenmeyer flasks of 40 ml culture volume at 18 °C during constant shaking at 120 rpm at 20 $\mu\text{mol photons m}^{-2}\text{s}^{-1}$ in the silica-enriched ASP medium according to (Provasoli et al., 1957). A 16 h light: 8 h dark cycle was used. Cells were harvested in the logarithmic growth phase. For all measurements 10 mM KHCO_3 was added to the algal cultures to ensure sufficient CO_2 -supply during the periods of actinic high-light illumination.

3.2.2 Pigment preparation and analysis

Pigment stoichiometries of the cells were determined by analytical HPLC (Merck Elite LaChrom, L-2130 / L-2450, Darmstadt, Germany). The cells were broken in 90% methanol buffered with 1mM Tris pH 7.5 with 0.45 mm glass beads in a Bead Beater (Biospec Products, Bartlesville, OK) for 9 min. Samples were centrifuged shortly at maximal speed in an Eppendorf centrifuge (Thermo Scientific,

Langenselbold, Germany), and the supernatants were loaded onto the column. Pigments were separated and quantified using a RP18 column and a photodiode array detector as described previously (Papagiannakis et al., 2005).

3.2.3 PAM setup

Fluorescence induction kinetics of variable Chl fluorescence and the development of NPQ were monitored with a PAM fluorimeter (Walz GmbH, Effeltrich) on cells adjusted to a Chl *a* content of 2 $\mu\text{g ml}^{-1}$ (Jeffrey and Humphrey, 1975). Saturating light flashes ($3500 \mu\text{mol photons m}^{-2} \text{s}^{-1}$) of 800 ms were applied every 2 min. The cells were dark adapted for 2 min before F_m was determined. Then the illumination protocol consisted of 10 min high-light illumination ($\sim 750 \mu\text{mol photons m}^{-2} \text{s}^{-1}$), followed by 30 min of complete darkness (“relaxed” cells). The complete recovery of NPQ (“recovered” cells) was obtained when 30 min of low light ($\sim 10 \mu\text{mol photons m}^{-2} \text{s}^{-1}$) followed 10 min of high-light illumination.

3.2.4 Measurements using the streak-camera setup

Time-resolved fluorescence experiments were performed at 77 K with a streak-camera setup (Broess et al., 2006; van Oort et al., 2008; Van Oort et al., 2009; van Stokkum et al., 2008), measuring fluorescence intensity as a function of wavelength and time. Three excitation wavelengths were used: 400 nm, 490 nm and 550 nm. The resulting images were corrected for background signal and detector sensitivity and sliced up into traces of 2 nm. The average was taken of 100 images, each measured for 10 s. The laser power was in the range of 40-70 μW , the spot size was 100 μm , and the repetition rate 250 kHz. Each sample was measured in 3 different states: original (“unquenched”) state (taken directly from the growing chamber, followed by ~ 2 min of dark adaptation); “quenched” state (~ 10 min of white light preillumination at $\sim 750 \mu\text{mol photons m}^{-2} \text{s}^{-1}$); “relaxed” (~ 30 min of darkness after 10 min of actinic light). Each measurement was repeated 3 times on different generations of the diatoms. Each generation was measured using two time windows: 800 ps and 2 ns. The streak images were analyzed using the TIMP package for R language (Mullen and van Stokkum, 2007) and Glotaran, a graphical user interface for the R-package TIMP (glotaran.org). To get an equal good estimation of long (>700 ps) and short components, streak images obtained with different time windows were linked during the analysis. For the unquenched and relaxed state, datasets of different generations were linked. In the quenched situation, the datasets were analyzed independently, because of small variations in the amount of quenching between the measurements, but all trends and conclusions are fully consistent. A

Gaussian-shaped instrument response function was used for the analysis and its width was a free fitting parameter. FWHM values obtained from the fitting procedure are in the range of 10-13 ps for the 800 ps time window and ~ 25-28 ps for the 2 ns time window. The synchroscan period (13.17 ns) results in a back and forth sweeping of long-lived components and leads to some signal “before time zero” in the streak-camera images (van Stokkum et al., 2006). This is used for the estimation of long lifetimes (many ns). The slowest component was always fixed to 3.7 ns. This lifetime was obtained independently for many datasets, but due to the limited time window of our setup, it was not possible to resolve it in a reliable way. The fit quality was judged by singular value decomposition of the residuals matrix (see also Supplemental Figure 1) (Mullen and van Stokkum, 2007). In Supplemental Materials and Methods it is described how the obtained DAS are decomposed into different components, like those of PSII and various antenna complexes.

Table 1. Pigment content of *C. meneghiniana* cells locked in four different states: unquenched, quenched, relaxed (in dark) and recovered (in low light). Pigment concentrations are presented as mM pigment M⁻¹ Chl *a*. The table shows mean values with standard deviations of at least 3 measurements.

| Sample | Pigment content (mM pigment M ⁻¹ Chl <i>a</i>) | | | | |
|--------------------------|--|--------|--------|------|------------|
| | Chl <i>c</i> | fx | Ddx | Dtx | β-carotene |
| unquenched | 178±10 | 692±22 | 190±18 | 28±4 | 8±2 |
| quenched | 176±4 | 658±33 | 128±12 | 82±3 | 11±5 |
| relaxed | 172±6 | 691±17 | 123±7 | 81±5 | 11±10 |
| recovered (in low light) | 181±16 | 686±37 | 189±20 | 30±6 | 13±7 |

3.3 Results and discussion

3.3.1 PAM measurements

First, we confirmed the presence of two different quenching processes using fluorescence induction measurements. Fluorescence and NPQ induction of *C.*

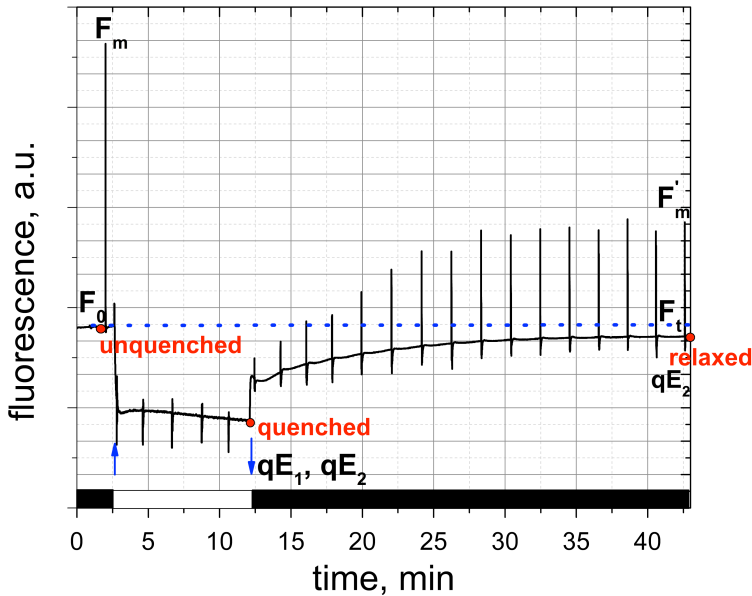


Figure 3.1. *Chl a* fluorescence induction kinetics of *C. meneghiniana* cells. Samples were adjusted to 2 $\mu\text{g/ml}$. The Figure depicts the transition from darkness to high light and to darkness again. High-light switch on/off is indicated by up/down arrows. The first saturating pulse was applied after 2 min of dark adaptation just before high light was switched on and the obtained F_v/F_m value is 0.60. *C. meneghiniana* was measured in complete darkness for 30 min after 10 min of high-light illumination. After 30 min of recovery in the dark, F_t and especially F_m' do not come back to the original level and stay quenched (original level of F_0 is indicated by dotted line).

meneghiniana cells were recorded with the PAM setup and different quenched and unquenched states of the culture were characterized. The average F_v/F_m value for cells in growth conditions (before further measurements) was 0.60, which is close to values obtained previously for *C. meneghiniana*, grown in similar conditions ($F_v/F_m = 0.65$ (Miloslavina et al., 2009), $F_v/F_m = 0.52$ (Beer et al., 2011)).

After determining F_v/F_m , high light of 760 $\mu\text{mol photons m}^{-2} \text{s}^{-1}$ was applied for 10 min. Within a few seconds strong fluorescence quenching was observed (Figure 3.1), which is believed to be partly triggered by a ΔpH across the photosynthetic

membrane, that rapidly activates conversion of XC pigments (Goss et al., 2006; Grouneva et al., 2008). The maximum fluorescence yield, measured in the presence of high light with all RCs closed (F_m') reached its highest amount of quenching during the first minute of illumination while the minimal fluorescence level in the presence of high light (F_t) continued to decrease during the whole illumination period and the dynamic control of this slower phase is achieved by the regulatory role of the XC carotenoids (Ddx and Dtx) (Goss et al., 2006; Grouneva et al., 2008; Lavaud et al., 2002; Ruban et al., 2004). Then the actinic light was switched off and cells were kept in complete darkness for 30 min. An immediate drop in NPQ was observed. This rapidly disappearing quenching is termed qE_1 (Figure 3.1) and is thought to be directly linked to the drop in the pH gradient. Then both F_t and F_m' continued to increase but did not recover to the original level during these 30 mins. So around 5% of F_t remained quenched while for F_m' this was ~40%. It should be noted that NPQ remains present in complete darkness (qE_2) whereas it disappears in the presence of $\sim 10 \mu\text{mol photons m}^{-2} \text{s}^{-1}$ (results not shown, see also (Grouneva et al., 2009)). qE_2 is supposedly regulated by Dtx (Goss et al., 2006; Grouneva et al., 2009), which is confirmed by pigment analysis (Table 1) of the cells measured in four different states: unquenched, quenched, relaxed (30 min. in darkness) and recovered (in low light). Relaxed cells have almost identical Ddx and Dtx concentrations as quenched cells, confirming that indeed Dtx epoxidation is inhibited in complete darkness (see also (Goss et al., 2006)) whereas cells that recovered in low light have very similar amounts of Ddx and Dtx as cells in the unquenched state.

3.3.2 Picosecond kinetics of unquenched *C. meneghiniana* cells

In order to test the involvement of PSII and antenna complexes in NPQ, different pigment pools were selectively excited. Three excitation wavelengths were used: with 550 nm light fx_{red} is preferably excited (antenna) while 490 nm light excites both fx_{blue} and fx_{red} (antenna) (Premvardhan et al., 2009; Premvardhan et al., 2008). At 400 nm mainly Chl *a* is excited (Premvardhan et al., 2009; Premvardhan et al., 2008) which is present in both photosystems as well as in FCPs (Lepetit et al., 2010)).

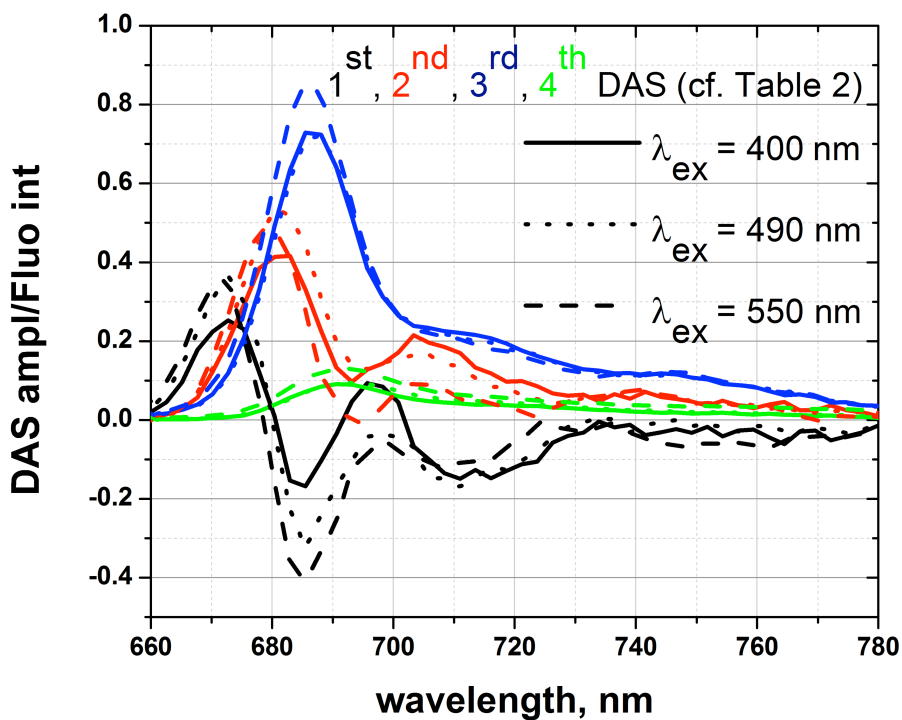


Figure 3.2. DAS obtained from global analysis of streak-camera data measured at 77 K using unquenched cells for different excitation wavelengths: 400 nm (solid line), 490 nm (dotted line) and 550 nm (dashed line). For comparison, the total fluorescence spectra at $t=0$ (which equals the sum of all DAS for a particular excitation wavelength) are normalized to their maximum (see Supplemental Figure S2). The lifetimes of the corresponding DAS are presented in Table 2.

Four decay components are sufficient to fit the fluorescence kinetics for all wavelengths. The resulting decay-associated spectra (DAS) for unquenched cells are shown in Figure 3.2. The lifetimes are rather similar for all excitation wavelengths (Table 2). The total fluorescence spectra at $t=0$ (sum of the corresponding DAS) were normalized to each other. They slightly differ in peak wavelength and amplitude for different λ_{ex} (Supplemental Figure S2) and the corresponding DAS cannot be compared in absolute terms but their relative contributions can be judged. The

shortest component has a DAS with positive peaks at 673 nm and 695 nm and negative peaks at 685 nm and 710 nm-720 nm. The corresponding excitation energy transfer (EET) from Chls with fluorescence peaking around 673 nm (Chl₆₇₃) to Chl₆₈₅ is observed for all excitation wavelengths (positive/negative peaks at 673/685 nm) and is most pronounced for $\lambda_{\text{ex}} = 550$ nm, followed by $\lambda_{\text{ex}} = 490$ nm. Therefore, it largely represents EET within/between FCP's and from FCP towards PSII cores, because more energy is transferred to PSII from fx_{red} than from fx_{blue} (Chukhutsina et al., 2013; Szabo et al., 2010). EET from Chls₆₉₅ to Chls₇₁₀₋₇₂₀ reflects excitation equilibration within PSI and the negative 710-720 nm peak corresponds to the 717 nm peak of PSI that is observed in steady-state fluorescence emission measurements at 77 K (Veith and Buchel, 2007). This process is most pronounced for 400 nm excitation. The shape of the 2nd DAS (130-150 ps) indicates some EET from Chl₆₈₂ to Chl₆₉₂. The area underneath the 680-682 nm band is higher for both fx excitation wavelengths, indicating that this corresponds largely to EET from FCP to PSII cores (Chukhutsina et al., 2013; Szabo et al., 2010). Apparently, there is heterogeneity in the transfer kinetics towards the core complexes, since the shape and amplitude of the 680-682 band differs for different fx excitation wavelengths. The "red" shoulder above 700 nm is largely due to PSI and its contribution decreases for excitation at longer wavelengths because fx_{blue} transfers more energy to PSI than fx_{red} (Chukhutsina et al., 2013; Szabo et al., 2010) whereas fx_{red} excitation mainly leads to transfer to PSII (Chukhutsina et al., 2013). The 3rd DAS component is to a large extent due to PSII. It peaks at ~685 nm which is close to the fluorescence emission bands of the PSII components at RT (Chukhutsina et al., 2013; Miloslavina et al., 2009). The 3.7 ns component has the smallest amplitude. The spectral shape with the peak near 690 nm and enhanced fluorescence above 720 nm very much resembles that of aggregated FCP antenna *in vitro* at 77 K (Gundermann and Büchel, 2012).

It should be mentioned that no ns component with PSI characteristic was observed, in contrast to what was reported for native membranes of higher plants, where DAS with 2.3 ns and 7.4 ns lifetimes represent slow PSI trapping from red pigments (van der Weij-de Wit et al., 2007). It agrees however with previously reported steady-state 77 K measurements where the contribution of the PSI band is much smaller for diatoms than for plants (Chukhutsina et al., 2013; Tikkanen et al., 2008).

In summary, in unquenched cells the fastest DAS reflects EET between the pigments of FCPs and into both photosystems, the second DAS is mainly due to EET into PSII together with some charge separation in PSI, PSII dominates the 3rd DAS and the 4th DAS mainly reflects aggregated FCP complexes.

Table 2. Results of global fitting of the streak-camera data upon 400 nm, 490 nm and 550 nm excitation in unquenched, quenched and relaxed state.

| Lifetimes, ps | λ_{ex} , nm | τ_1 (ps) black DAS | τ_2 (ps) red DAS | τ_3 (ps) blue DAS | τ_4 (ns) green DAS | τ_{avg} (ns) $\lambda_{\text{det}}=685$ nm | τ_{avg} (ns) $\lambda_{\text{det}}=700$ nm |
|---------------|----------------------------|----------------------------------|--------------------------|------------------------------|----------------------------------|--|--|
| unquenched | 400nm | 27 | 128 | 579 | 3.7 | 0.75 | 0.75 |
| | 490nm | 26 | 149 | 601 | 3.7 | 0.83 | 1.0 |
| | 550nm | 30 | 139 | 596 | 3.7 | 1.12 | 1.62 |
| quenched | 400nm | 27 | 132 | 520 | 3.7 | 0.40 | 0.56 |
| | 490nm | 26 | 124 | 518 | 3.7 | 0.57 | 0.86 |
| | 550nm | 27 | 140 | 552 | 3.7 | 0.79 | 1.17 |
| relaxed | 400nm | 25 | 128 | 580 | 3.7 | 0.63 | 0.75 |
| | 490nm | 28 | 145 | 600 | 3.7 | 0.83 | 1.02 |
| | 550nm | 30 | 143 | 604 | 3.7 | 1.12 | 1.62 |

Lifetimes estimated from global analysis of the fluorescence data obtained for the *C. meneghiniana* cells in different states. The DAS colors specified in the lifetimes rows correspond to the colors of the DAS in Figs 2 and 4. Typical standard errors are 2.0-3.0 % for τ_1 , 0.5-1.0 % for τ_2 and ~ 0.5 % for τ_3 for all analyzed datasets. The slowest component is at the limit of the setup resolution and was always fixed to 3.7 ns. Average lifetimes of the total fluorescence decays were calculated at two detection wavelengths: 685 nm and 700 nm.

3.3.3 Picosecond kinetics of *C. meneghiniana* cells measured in different states

To discriminate between qE_1 and qE_2 *C. meneghiniana* cells were locked in three different states at 77 K: unquenched, quenched and relaxed. Typical streak-camera measurements are presented in Figure 3.3 for the same 3 excitation wavelengths as used above. At all excitation wavelengths the fluorescence of unquenched cells (Figure 3.3 a, d, h) is longer-lived than for quenched cells (Figure 3.3 b, e, i) as expected, but when comparing unquenched and relaxed cells the situation is different. Upon exciting the outer antenna at either 490 or 550 nm the unquenched

and relaxed cells show nearly identical kinetics, whereas $\lambda_{\text{ex}} = 400$ nm leads to clear differences. This immediately indicates that qE_2 is not related to the outer antenna FCP but must be related to PSII cores that are not or hardly connected to FCP.

3.3.3.1 Upon fx excitation only qE_1 is observed

First we analyzed streak-camera data measured upon fx excitation (490 and 550 nm) in different states to confirm that qE_2 is not monitored upon antenna excitation. So the resulting decay-associated spectra (DAS) for unquenched, quenched and relaxed cells are compared in Figs 4A B. Four components are sufficient to fit the data in all cases. Most lifetimes are similar for the different conditions except for τ_3 (blue DAS, Table 2), which is obviously shorter for quenched cells. However, the amplitudes of all four DAS differ substantially for the quenched and unquenched state, thereby strongly changing the average lifetime (Table 2) and fluorescence quantum yield (Supplemental Figure S3). In agreement with Figure 3.3, relaxed cells show nearly identical results as unquenched cells for 490 nm and 550 nm excitation. The results for 490 nm excitation show a decrease in intensity upon quenching for the 3rd and 4th component leading to an increase of the shorter-lived 2nd component that peaks around 685 nm. The decrease of the 3rd DAS and corresponding increase of the 2nd one are even larger for $\lambda_{\text{ex}}=550$ nm excitation. The effect of qE_1 on the longest component is more or less the same for both fx excitation wavelengths and leads to a decrease of fluorescence peaking at around 690 nm. Summarizing, upon exciting the outer antenna complexes no effect of qE_2 is observed whereas qE_1 leads to a decrease of the relative amplitudes in the long-lived 3rd and 4th DAS and an amplitude increase of the short-lived 2nd DAS, thereby decreasing the total fluorescence quantum yield. The effect is largest upon 550 nm excitation where more PSII antenna is excited than at 490 nm (Chukhutsina et al., 2013).

3.3.3.2 Monitoring qE_1 and qE_2 upon Chl a (400 nm) excitation

The DAS for unquenched, quenched and relaxed cells upon 400 nm excitation are depicted in Figure 3.4C. Most notably, the DAS of relaxed cells substantially differ from those of unquenched cells due to the effect of qE_2 . Since this is not observed upon fx excitation (Figure 3.3) it is concluded that PSII (core) complexes that are largely disconnected from FCPs are responsible for it. Upon going from the unquenched to the quenched state there is a strong decrease of the amplitude of the 3rd DAS whereas the corresponding lifetime is reduced by 60 ps (Table 2), which is also seen for fx excitation but to a lesser extent upon fx_{red} (550 nm) excitation. In darkness after high light illumination the amplitude of this component does not recover completely due to the remaining qE_2 .

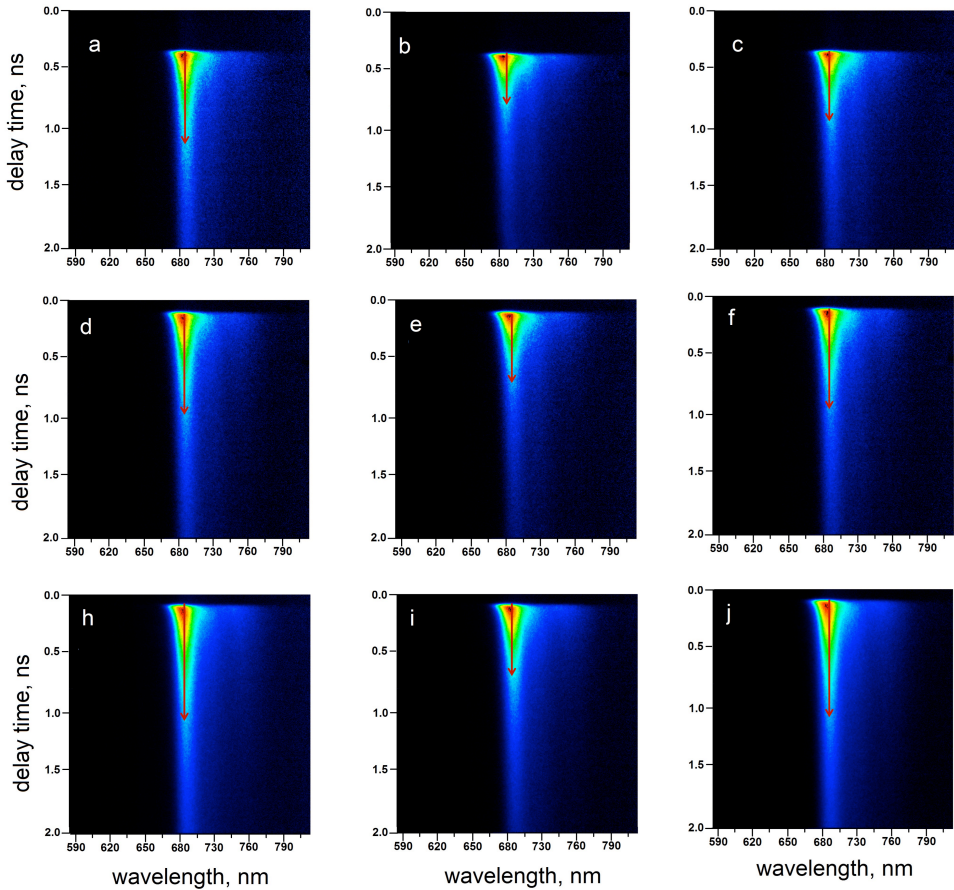


Figure 3.3. Streak-camera images of unquenched (a, d, h), quenched (b, e, i) and relaxed cells (c, f, j). In panels a, b, c Chl a was preferentially excited at 400 nm, in panels d, e, f $f_{x_{blue}}$ and $f_{x_{red}}$ was excited at 490 nm while in panels h, i, j results for $\lambda_{ex}=550$ nm ($f_{x_{red}}$) are presented. The lengths of the arrows correspond to the average lifetime detected at 685 nm.

Also the longest component is influenced by both qE_1 and qE_2 since its contribution drops by 55% upon quenching and its area recovers in complete darkness to only 85 % of the original value. Upon quenching the main band of the 2nd component increases in intensity while the PSI shoulder hardly changes in amplitude. In darkness the amplitude of the main peak does not recover completely to the original state, demonstrating that not only qE_1 but also qE_2 lead to an increased

contribution of the 2nd DAS. So upon exciting at 400 nm qE₁ is again observed but in addition qE₂ is now present that apparently occurs in PSII cores with little or no outer antenna connected. Because also Dtx remains present in the dark we conclude that it is involved in the quenching of these cores.

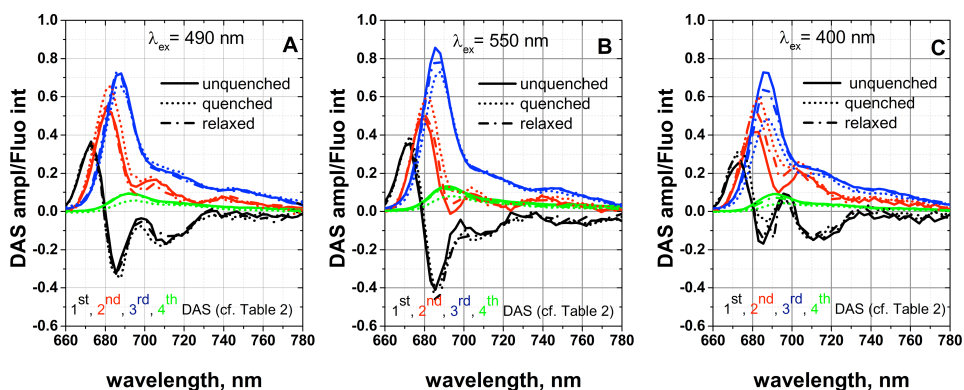


Figure 3.4. DAS for unquenched (solid line), quenched (dotted line), relaxed (dash dotted line) states obtained from global analysis of streak-camera data measured at 77 K upon 490 nm (A), 550 nm (B) and 400 nm (C) excitation. The lifetimes of the corresponding DAS are presented in Table 2 with the corresponding colors. The overall fluorescence spectra at t=0 were normalized to each other.

3.3.4 Spectral reconstruction upon antenna excitation describes qE₁

3.3.4.1 Evidence for PSII quenching

In order to attribute the different effects described above to certain photosynthetic protein complexes, we reconstructed spectra of separate emitting Chl *a* species from the obtained DAS, starting with that of PSII. The DAS with a clear PSII contribution is the 3rd component and upon quenching it shows a substantial decrease in amplitude for all excitation wavelengths. After subtracting the quenched 3rd DAS from the unquenched one (Figure 3.5), we obtain a spectrum with the shape of that of PSII, peaking at 685 nm with a vibronic band around 750 nm. Similar 77 K spectra were reported before for PSII preparations from higher plants (Andrizhievskaya et al., 2005; Van Dorssen et al., 1987a; Van Dorssen et al., 1987b) and the diatom *Chaetoceros gracilis* (Nagao et al., 2010). However, a pronounced 695-nm

fluorescence maximum from red-absorbing Chls of CP47 is missing but such a peak is only observed for PSII-RC and some BBY preparations where the antenna/RC ratio is lower than in native thylakoid membranes (Broess et al., 2008; Croce and van Amerongen, 2011; Van Oort et al., 2010). For whole thylakoid membranes this band tends to disappear and only the 685 nm PSII band is observed (Bennett et al., 1980). The absence of the 695 nm peak is also typical for crude PSII preparations of *Chaetoceros gracilis*, confirming that the difference spectrum represents PSII complexes with additional antenna rather than pure PSII cores (Nagao et al., 2010).

After having estimated an ‘*in vivo*’ fluorescence emission spectrum of PSII complexes, this spectrum was used to determine the influence of PSII and the antenna on qE_1 by decomposing the 3rd DAS for the unquenched and quenched datasets as described in Supplemental Materials (Supplemental Figure S4). The results for 490 nm excitation are given in Figure 6A (for 550 nm results, see Supplemental Figure S5). As was already found above, the PSII contribution decreases in case of NPQ while the residual spectra obtained after PSII subtraction (we term this *antenna 1* spectrum) look very similar for the unquenched and quenched datasets with a peak at 690 nm and a broad fluorescence feature between 690 nm and 720 nm. The *antenna 1* spectrum is also given in Figure 3.6C and it was obtained by averaging four spectra from the 3rd DAS in the unquenched/quenched state for 490/550 nm excitation. It resembles the fluorescence emission spectrum of aggregated FCPb at 77 K as obtained

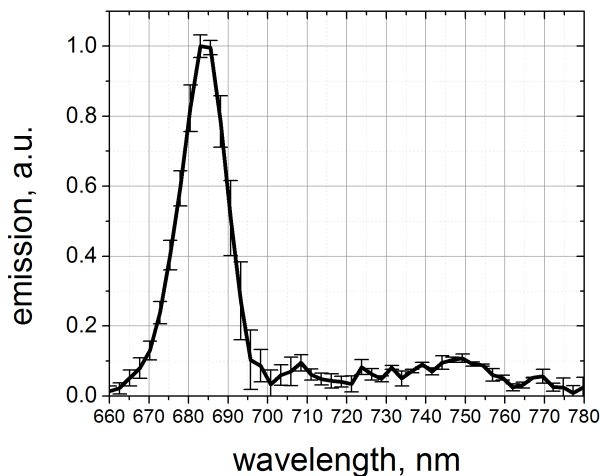


Figure 3.5. Fluorescence emission spectrum of PSII complexes obtained by subtracting the 3rd (blue) DAS of quenched cells from that of unquenched cells. The procedure was repeated for all three excitation wavelengths, after which the resulting spectra were averaged. The black line represents the average spectrum and error bars reflect standard deviations.

in (Gundermann and Büchel, 2012) (see Figure 3.6C and Supplemental Figure S4 E, F). *In vivo* there is apparently a fraction of aggregated FCPs that is not influenced by NPQ, at least not at 77 K. In this respect it is interesting to note that both oligomeric FCPbs and FCPa trimers show strong reduction of fluorescence yield when being artificially aggregated by detergent removal but only FCPa trimers show ΔpH and Dtx - dependent quenching (Gundermann and Büchel, 2008; Gundermann and Büchel, 2012).

Thus the effect of quenching on the 3rd DAS is solely due to a reduction of PSII fluorescence, whereas FCPb is not influenced by quenching and contributes equally in both states.

3.3.4.2 Evidence for FCPa aggregation and quenching

The shape of the 4th component differs considerably for unquenched and quenched cells (Figure 3.6B). Again the fact that PSII becomes quenched is obvious: its contribution to the area of the unquenched DAS is 20% while it is at most 8% for the quenched state. Interestingly the shape of the residual spectrum after PSII subtraction from the 4th DAS (*antenna 2*) differs substantially for the various states. For quenched cells the relative fluorescence increases in the 700-730 nm region, while the total area decreases strongly, which is characteristic for aggregation of FCP. Also this residual spectrum is reminiscent of the 77 K fluorescence spectrum of aggregated FCPs (Gundermann and Büchel, 2012). In Figure 3.6C also the residual spectra obtained from the 4th (*antenna 2*, unquenched, quenched) DAS are shown (see the legend for details). In contrast to *antenna 1* (presumably FCPb), *antenna 2* is strongly involved in qE_1 , i.e. its contribution to the 4th DAS decreases substantially upon quenching. Since *in vitro* the ΔpH -dependent quenching is only observed for FCPa trimers but not for FCPb oligomers (Gundermann and Büchel, 2008; Gundermann and Büchel, 2012), and since only FCPa contains Lhcx proteins known to be involved in NPQ (Bailleul et al., 2010) this suggests that mostly FCPa contributes to the *antenna 2* decrease as part of qE_1 . Upon 550 nm excitation, the decomposition of the longest DAS gives (somewhat) similar results (Supplemental Figure S5). Finally, it appears that upon 490 nm excitation the decrease of the 4th DAS in the quenched state is for 35% due to the decrease of the PSII fluorescence and for 65% to the decrease of *antenna 2* fluorescence while upon 550 nm excitation these percentages are 25% (for PSII) and 75% (for *antenna 2*).

Figure 3.4 shows that the amplitude of the 2nd DAS increases upon quenching. The increase corresponds largely to a decrease in amplitude of the 3rd DAS, and to a lesser extent to that of the 4th DAS. These results are consistent with the fact that the

contribution of PSII to the 3rd and 4th DAS and the contribution of *antenna 2* (presumably mostly FCPa) to the 4th DAS decrease upon quenching.

In summary, qE_1 is due to PSII complexes and aggregated FCPa complexes, whilst FCPb does not contribute.

3.3.5 Describing qE_2 using spectral reconstruction

3.3.5.1 qE_2 observed for *Chl a* excitation

qE_1 is observed for all excitation wavelengths while qE_2 is detected for Chl *a* excitation (400 nm) and hardly observable for fx (antenna) excitation, suggesting that qE_2 occurs in PSII cores that are not connected to the outer antenna. To confirm this, the 400 nm DAS of quenched, unquenched and relaxed cells were decomposed and the results of the 3rd component decomposition are presented in Supplemental Figure S6A. They confirm that the difference between the quenched and relaxed state is mostly due to the contribution of PSII and not of the outer antenna. The PSII spectrum does not recover to its original unquenched state in darkness, but stays partly quenched after strong light illumination. The contribution of aggregated antenna to the 3rd DAS (*antenna 1*) remains more or less the same in all three states and it does not participate in any of the two quenching processes.

The decomposition of the 4th component is in agreement with the observations described before (Supplemental Figure S6B). The amplitude of the residual (*antenna 2*) spectrum decreases strongly upon quenching as compared with the unquenched state, but largely recovers in darkness, reflecting again FCPa quenching as part of qE_1 but not qE_2 . The PSII contribution accounts for around 25% of the total area in the case of unquenched cells, while for the quenched state its contribution is almost negligible. 'Relaxed' data show that the PSII fluorescence does not recover to its original unquenched state in the dark, confirming the PSII origin of qE_2 . It can be concluded that qE_2 accounts for 35% of the total decrease of the PSII area of the 3rd and 4th DAS while qE_1 accounts for the remaining 65%. It should be realized that the latter percentage refers to PSII complexes that are connected to the outer antenna, so qE_1 in PSII reflects quenching of both cores and the connected antenna, whereas the 35% refers to largely disconnected PSII cores (qE_2), which does not relax in the dark and is correlated with the persistence of Dtx. Therefore, it might be that qE_2 protects even a larger amount of PSII cores, although the fluorescence quenching might at first sight suggest that qE_1 represents the dominant protection mechanism.

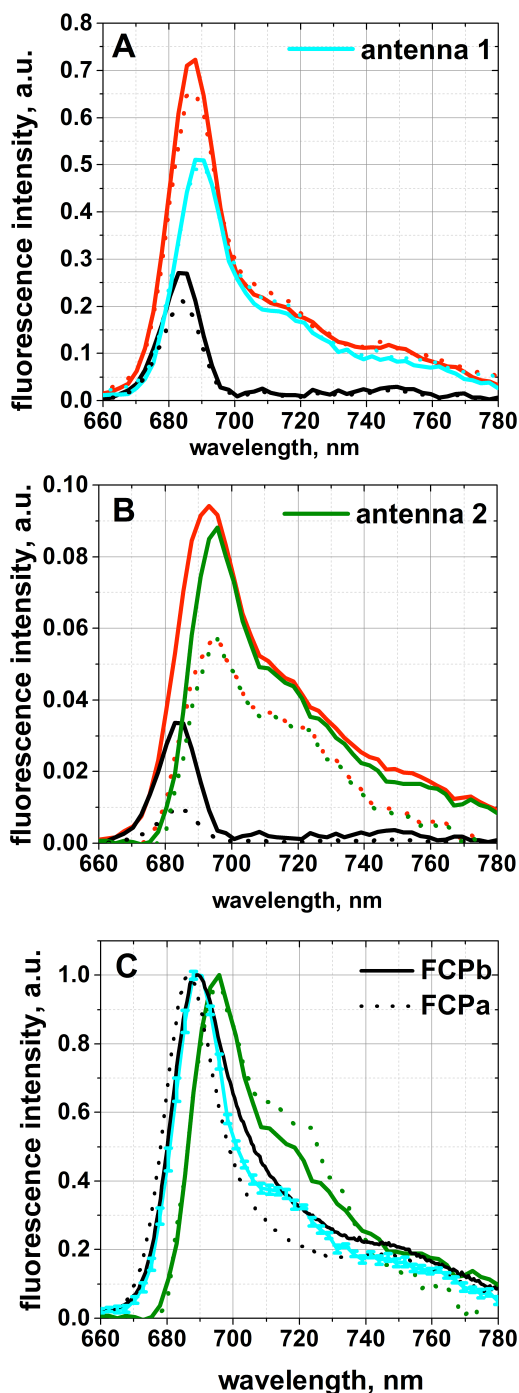


Figure 3.6. Decomposition of the 3rd (A) and 4th (B) components (red lines) obtained from global analysis of unquenched (solid), quenched (dotted) datasets upon 490 nm excitation using PSII fluorescence emission spectrum (black lines). The residual spectra in cyan and green represent different subpopulations of aggregated antenna (called antenna 1 and antenna 2 from the 3rd and 4th DAS, respectively). In Figure 3.6C averaged and normalized antenna 1 and 2 spectra (see text) are compared with aggregated forms of FCPb (black solid) and FCPa (black dotted) from (Gundermann and Büchel, 2012). The antenna 2 spectra (unquenched and quenched) in Figure 3.6C were obtained by averaging corresponding spectra from 490 nm and 550 nm data, since they are virtually identical for two excitation wavelengths. The antenna 1 spectrum is an average of four spectra from the 3rd DAS in the unquenched/quenched state for 490/550 nm excitation. The error bars reflect standard deviations (Figure 3.6C).

3.3.5.2 Minor effect of qE₂ for $\lambda_{ex}=550$ nm

Although the spectra of relaxed cells closely resemble those of unquenched cells in case of antenna excitation, a small difference between unquenched and relaxed data was still present when exciting at 550 nm ($f_{x_{red}}$), but not at 490 nm (Figure 3.4). Around 4% of the PSII area in the 3rd DAS is not recovered in the relaxed state upon selective $f_{x_{red}}$ excitation (Supplemental Figure S7). This indicates that a small fraction of “PSII cores” is excited at 550 nm, either because it is energetically connected to very small amounts of FCPs binding preferentially $f_{x_{red}}$, or because there is a small amount of Chl *a* absorption at 550 nm (Premvardhan et al., 2008). The 4th DAS in the relaxed state has a slightly lower amplitude while the fluorescence intensity in the PSII region (below 690 nm) hardly changes when compared to the unquenched state, implying the presence of quenching of *antenna 2*, previously attributed to FCPa. Because this is also part of the qE₂ type quenching, it is again Dtx-dependent. This quenching does not contribute more than 10% to the total quenching of the FCPa pool. This is in agreement with PAM measurements, where ~5% of the F_t amplitude (exclusively attributed to antenna NPQ (Demmig-Adams et al., 1990)) remains quenched in the qE₂ state.

In summary, the qE₂ process appears to act on PSII RCs that are functionally disconnected from all or most of the antenna complexes since it is hardly observed upon f_x excitation. Considering that qE₂ is observed in the relaxed state where Dtx is still present, we suggest that Dtx is responsible for this quenching and it might even be responsible for antenna detachment that leads to photoprotection of RCs (less excitations are captured) like in plants (Johnson et al., 2011; Miloslavina et al., 2008; Ruban et al., 2012). Although our $f_{x_{red}}$ excitation data indicate that those ‘PSII cores’ might still bind at least one antenna complex that works as a quencher, direct Dtx-related quenching of PSII cores cannot be excluded, since the presence of lipid-dissolved Dtx-cycle pigments that are not bound to FCPs has been reported (Lepetit et al., 2010). Furthermore, there are some indications of direct PSII core quenching in *Phaeodactylum tricornutum*, although it was excluded that Dtx was causing that quenching (Eisenstadt et al., 2008). From our $f_{x_{red}}$ excitation measurements, we also conclude that some antenna (presumably FCPa) detachment occurs during the qE₂ process, which should correspond to not more than 10% of the total fraction of FCPa.

[NPQ IN DIATOMS]

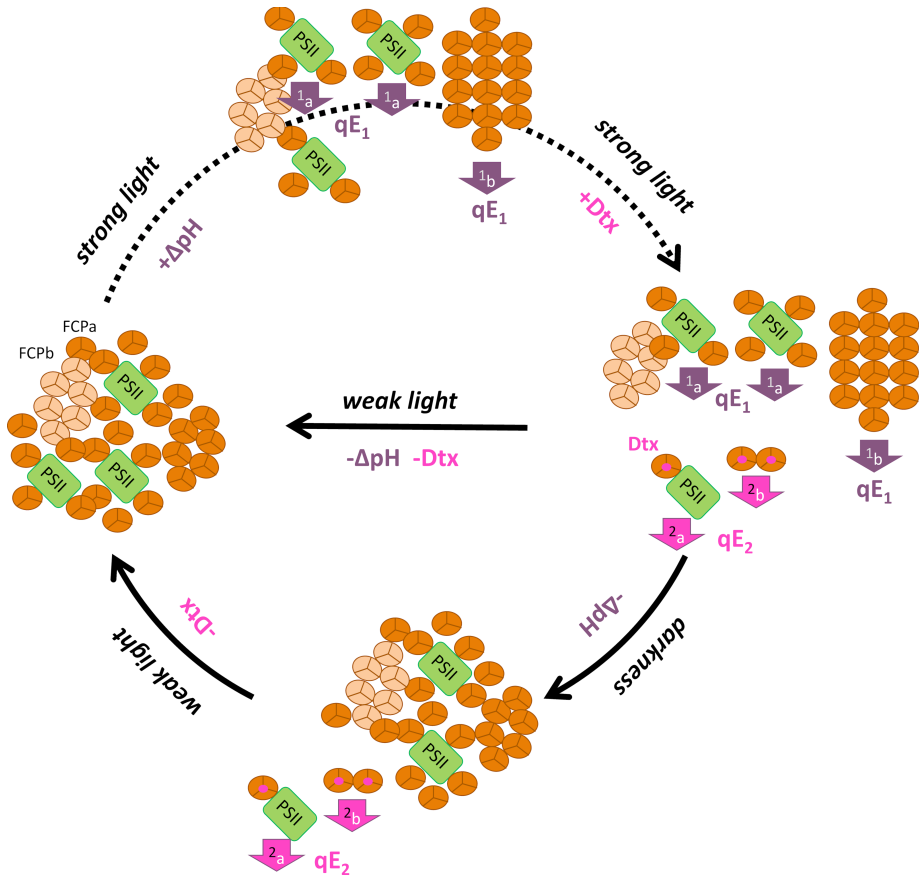


Figure 3.7. Model for non-photochemical quenching in *C. meneghiniana*. In strong light two quenching mechanisms independent of diatoxanthin (Dtx) are present. The first (upper part of Figure) represents quenching (qE_1) of the whole PSII complex (1_a) and the second is quenching of FCPa antenna that is aggregated due to ΔpH formation (1_b). With the rapid accumulation of a Dtx pool (middle right), Dtx-related quenching appears (qE_2). It is manifested by quenching of PSII that almost lack FCPs (2_a). Most probably the quenching site is located at an FCPa antenna attached to the core, although direct quenching of PSII cores cannot be excluded. This effect is accompanied with Dtx-dependent quenching of FCPa that has been disconnected from PSII complexes: 2_b (not more than 10% of the total FCPa pool). All qE_2 quenching is persistent in the darkness (lower part of Figure), but not under weak light.

3.4 Conclusions

Non-photochemical quenching in the diatom *C. meneghiniana* shows two distinct contributions: qE_1 and qE_2 (Figure 3.1, Figure 3.7). qE_1 is rapidly induced in strong light and also rapidly disappears again in darkness and supposedly it is directly coupled to the pH gradient across the thylakoid membrane. qE_2 is induced directly after pH gradient formation, it remains present in subsequent darkness and only disappears again in the presence of a low amount of light. Its presence is directly related to the conversion of Ddx to Dtx (Grouneva et al., 2008). The amount of Dtx increases in the presence of strong light but remains present after switching to darkness. qE_1 takes place in PSII with a substantial amount of antenna connected (qE_{1a} , Figure 3.7) whereas also aggregated FCPa antenna complexes appear to be quenched (qE_{1b}). qE_2 takes place in PSII cores that are detached from almost all the FCP antenna although it cannot be completely ruled out that there is still a very small amount of FCP bound to these cores (qE_{2a}), accompanied by very minor further quenching of aggregated FCPa complexes due to Dt (qE_{2b}). FCPb antenna complexes on the other hand remain unquenched during both qE_1 and qE_2 . Therefore, it seems that upon the induction of NPQ at first FCPa aggregates in PSII become quenched, after which they partly detach from PSII cores while the quenching persists. Then the continued formation of Dtx leads to the additional quenching of isolated PSII cores and to a minor extent of aggregated FCPa complexes. Although the amount of quenching during qE_2 is smaller than during qE_1 it might be more effective because it corresponds to selective quenching of the PSII cores. In subsequent darkness the quenching of FCPa disappears while qE_2 remains present and only in the presence of some light does recovery to the fully unquenched state occur.

Acknowledgements

This work was supported by HARVEST Marie Curie Research Training Network [PITN-GA-2009-238017 to VUC, CB and HvA]. This project was also carried out within the research programme of BioSolar Cells, co-financed by the Dutch Ministry of Economic Affairs (to VUC and HvA). We thank R.B.M. Koehorst (Wageningen UR), A. van Hoek (Wageningen UR), and Dr. A. Bader (Wageningen UR) for technical help with the measurements, C. Wolfs (Wageningen UR) for initial help with growing cells and Dr. S. Liptenok (University of East Anglia), J. Snellenburg (VU Amsterdam University) for help with the usage of the Glotaran software analysis toolkit. Dr. R. Croce and D. de Kort are acknowledged for critical reading of the manuscript and for many helpful suggestions.

References

- Andrizhiyevskaya, E.G., Chojnicka, A., Bautista, J.A., Diner, B.A., van Grondelle, R., and Dekker, J.P. (2005). Origin of the F685 and F695 fluorescence in Photosystem II. *Photosynthesis Research* 84:173-180.
- Bailleul, B., Rogato, A., de Martino, A., Coesel, S., Cardol, P., Bowler, C., Falciatore, A., and Finazzi, G. (2010). An atypical member of the light-harvesting complex stress-related protein family modulates diatom responses to light. *P Natl Acad Sci USA* 107:18214-18219.
- Ballottari, M., Girardon, J., Betterle, N., Morosinotto, T., and Bassi, R. (2010). Identification of the chromophores involved in aggregation-dependent energy quenching of the monomeric photosystem II antenna protein Lhcb5. *Journal of Biological Chemistry* 285:28309-28321.s
- Beer, A., Gundermann, K., Beckmann, J., and Büchel, C. (2006). Subunit composition and pigmentation of fucoxanthin-chlorophyll proteins in diatoms: evidence for a subunit involved in diadinoxanthin and diatoxanthin binding. *Biochemistry* 45:13046-13053.
- Beer, A., Juhas, M., and Büchel, C. (2011). Influence of Different Light Intensities and Different Iron Nutrition on the Photosynthetic Apparatus in the Diatom *Cyclotella meneghiniana* (Bacillariophyceae). *Journal of Phycology* 47:1266-1273.
- Bennett, J., Steinback, K.E., and Arntzen, C.J. (1980). Chloroplast phosphoproteins: regulation of excitation energy transfer by phosphorylation of thylakoid membrane polypeptides. *Proc Natl Acad Sci U S A* 77:5253-5257.
- Broess, K., Trinkunas, G., van der Weij-de Wit, C.D., Dekker, J.P., van Hoek, A., and van Amerongen, H. (2006). Excitation energy transfer and charge separation in photosystem II membranes revisited. *Biophysical journal* 91:3776-3786.
- Broess, K., Trinkunas, G., van Hoek, A., Croce, R., and van Amerongen, H. (2008). Determination of the excitation migration time in Photosystem II consequences for the membrane organization and charge separation parameters. *Biochimica et biophysica acta* 1777:404-409.
- Büchel, C. (2003). Fucoxanthin-chlorophyll proteins in diatoms: 18 and 19 kDa subunits assemble into different oligomeric states. *Biochemistry* 42:13027-13034.
- Chukhutsina, V.U., Buchel, C., and van Amerongen, H. (2013). Variations in the first steps of photosynthesis for the diatom *Cyclotella meneghiniana* grown under different light conditions. *Biochim Biophys Acta* 1827:10-18.
- Croce, R., and van Amerongen, H. (2011). Light-harvesting and structural organization of Photosystem II: from individual complexes to thylakoid membrane. *J Photochem Photobiol B* 104:142-153.
- Demmig-Adams, B., Adams, W.W., Heber, U., Neimanis, S., Winter, K., Kruger, A., Czygan, F.C., Bilger, W., and Bjorkman, O. (1990). Inhibition of zeaxanthin formation and of rapid changes in radiationless energy dissipation by dithiothreitol in spinach leaves and chloroplasts. *Plant Physiol* 92:293-301.
- Durnford, D.G., Aebersold, R., and Green, B.R. (1996). The fucoxanthin-chlorophyll proteins from a chromophyte alga are part of a large multigene family: structural and

[CHAPTER 3]

- evolutionary relationships to other light harvesting antennae. *Mol Gen Genet* 253:377-386.
- Eisenstadt, D., Ohad, I., Keren, N., and Kaplan, A. (2008). Changes in the photosynthetic reaction centre II in the diatom *Phaeodactylum tricornutum* result in non-photochemical fluorescence quenching. *Environmental microbiology* 10:1997-2007.
- Falkowski, P.G., Barber, R.T., and Smetacek, V. (1998). Biogeochemical controls and feedbacks on ocean primary production. *Science* 281:200-206.
- Field, C.B., Behrenfeld, M.J., Randerson, J.T., and Falkowski, P. (1998). Primary production of the biosphere: integrating terrestrial and oceanic components. *Science* 281:237-240.
- Gildenhoff, N., Amarie, S., Beer, A., Gundermann, K., Büchel, C., and Wachtveitl, J. (2009). Light Harvesting, Energy Transfer and Photoprotection in the Fucoxanthin-Chlorophyll Proteins of *Cyclotella meneghiniana*. *Springer Series Chem* 92:577-579.
- Gildenhoff, N., Amarie, S., Gundermann, K., Beer, A., Büchel, C., and Wachtveitl, J. (2010). Oligomerization and pigmentation dependent excitation energy transfer in fucoxanthin-chlorophyll proteins. *Biochimica et biophysica acta* 1797:543-549.
- Goss, R., Ann Pinto, E., Wilhelm, C., and Richter, M. (2006). The importance of a highly active and DeltapH-regulated diatoxanthin epoxidase for the regulation of the PS II antenna function in diadinoxanthin cycle containing algae. *Journal of plant physiology* 163:1008-1021.
- Goss, R., and Jakob, T. (2010). Regulation and function of xanthophyll cycle-dependent photoprotection in algae. *Photosynthesis research* 106:103-122.
- Grouneva, I., Jakob, T., Wilhelm, C., and Goss, R. (2008). A new multicomponent NPQ mechanism in the diatom *Cyclotella meneghiniana*. *Plant and Cell Physiology* 49:1217-1225.
- Grouneva, I., Jakob, T., Wilhelm, C., and Goss, R. (2009). The regulation of xanthophyll cycle activity and of non-photochemical fluorescence quenching by two alternative electron flows in the diatoms *Phaeodactylum tricornutum* and *Cyclotella meneghiniana*. *Bba-Bioenergetics* 1787:929-938.
- Gundermann, K., and Büchel, C. (2008). The fluorescence yield of the trimeric fucoxanthin-chlorophyll-protein FCPa in the diatom *Cyclotella meneghiniana* is dependent on the amount of bound diatoxanthin. *Photosynthesis research* 95:229-235.
- Gundermann, K., and Büchel, C. (2012). Factors determining the fluorescence yield of fucoxanthin-chlorophyll complexes (FCP) involved in non-photochemical quenching in diatoms. *Bba-Bioenergetics* 1817:1044-1052.
- Horton, P., and Ruban, A. (2005). Molecular design of the photosystem II light-harvesting antenna: photosynthesis and photoprotection. *Journal of Experimental Botany* 56:365-373.
- Ikeda, Y., Komura, M., Watanabe, M., Minami, C., Koike, H., Itoh, S., Kashino, Y., and Satoh, K. (2008). Photosystem I complexes associated with fucoxanthin-chlorophyll-binding proteins from a marine centric diatom, *Chaetoceros gracilis*. *Biochimica et biophysica acta* 1777:351-361.

[NPQ IN DIATOMS]

- Jeffrey, S.t., and Humphrey, G. (1975). New spectrophotometric equations for determining chlorophylls a, b, c1 and c2 in higher plants, algae and natural phytoplankton. *Biochem. Physiol. Pflanz* 167:1-194.
- Johnson, M.P., Goral, T.K., Duffy, C.D., Brain, A.P., Mullineaux, C.W., and Ruban, A.V. (2011). Photoprotective energy dissipation involves the reorganization of photosystem II light-harvesting complexes in the grana membranes of spinach chloroplasts. *Plant Cell* 23:1468-1479.
- Lavaud, F. (2007). Fast Regulation of Photosynthesis in Diatoms: Mechanisms, Evolution and Ecophysiology. *Func Plant Sci Biotech* 1:267-287.
- Lavaud, J., Rousseau, B., and Etienne, A.-L. (2002). In diatoms, a transthylakoid proton gradient alone is not sufficient to induce a non-photochemical fluorescence quenching. *Febs Letters* 523:163-166.
- Lepetit, B., Volke, D., Gilbert, M., Wilhelm, C., and Goss, R. (2010). Evidence for the Existence of One Antenna-Associated, Lipid-Dissolved and Two Protein-Bound Pools of Diadinoxanthin Cycle Pigments in Diatoms. *Plant physiology* 154:1905-1920.
- Liu, Z.F., Yan, H.C., Wang, K.B., Kuang, T.Y., Zhang, J.P., Gui, L.L., An, X.M., and Chang, W.R. (2004). Crystal structure of spinach major light-harvesting complex at 2.72 angstrom resolution. *Nature* 428:287-292.
- Miloslavina, Y., Grouneva, I., Lambrev, P.H., Lepetit, B., Goss, R., Wilhelm, C., and Holzwarth, A.R. (2009). Ultrafast fluorescence study on the location and mechanism of non-photochemical quenching in diatoms. *Biochimica et biophysica acta* 1787:1189-1197.
- Miloslavina, Y., Wehner, A., Lambrev, P.H., Wientjes, E., Reus, M., Garab, G., Croce, R., and Holzwarth, A.R. (2008). Far-red fluorescence: A direct spectroscopic marker for LHCII oligomer formation in non-photochemical quenching. *Febs Letters* 582:3625-3631.
- Mullen, K.M., and van Stokkum, I.H.M. (2007). TIMP: An R package for modeling multi-way spectroscopic measurements. *J Stat Softw* 18.
- Nagao, R., Tomo, T., Noguchi, E., Nakajima, S., Suzuki, T., Okumura, A., Kashino, Y., Mimuro, M., Ikeuchi, M., and Enami, I. (2010). Purification and characterization of a stable oxygen-evolving Photosystem II complex from a marine centric diatom, *Chaetoceros gracilis*. *Bba-Bioenergetics* 1797:160-166.
- Niyogi, K.K. (1999). Photoprotection revisited: Genetic and molecular approaches. *Annu Rev Plant Phys* 50:333-359.
- Owens, T.G. (1986). Light-Harvesting Function in the Diatom *Phaeodactylum-Tricornutum* .2. Distribution of Excitation-Energy between the Photosystems. *Plant Physiology* 80:739-746.
- Papagiannakis, E., I, H.M.v.S., Fey, H., Buchel, C., and van Grondelle, R. (2005). Spectroscopic characterization of the excitation energy transfer in the fucoxanthin-chlorophyll protein of diatoms. *Photosynth Res* 86:241-250.
- Premvardhan, L., Bordes, L., Beer, A., Buchel, C., and Robert, B. (2009). Carotenoid Structures and Environments in Trimeric and Oligomeric Fucoxanthin Chlorophyll a/c(2) Proteins from Resonance Raman Spectroscopy. *Journal of Physical Chemistry B* 113:12565-12574.

[CHAPTER 3]

- Premvardhan, L., Sandberg, D.J., Fey, H., Birge, R.R., Buchel, C., and van Grondelle, R. (2008). The charge-transfer properties of the S-2 state of fucoxanthin in solution and in fucoxanthin chlorophyll-a/c(2) protein (FCP) based on stark spectroscopy and molecular-orbital theory. *Journal of Physical Chemistry B* 112:11838-11853.
- Provasoli, L., McLaughlin, J.J.A., and Droop, M.R. (1957). The Development of Artificial Media for Marine Algae. *Arch Mikrobiol* 25:392-428.
- Ruban, A., Lavaud, J., Rousseau, B., Guglielmi, G., Horton, P., and Etienne, A.-L. (2004). The super-excess energy dissipation in diatom algae: comparative analysis with higher plants. *Photosynthesis Research* 82:165-175.
- Ruban, A.V., Berera, R., Ilioaia, C., van Stokkum, I.H.M., Kennis, J.T.M., Pascal, A.A., van Amerongen, H., Robert, B., Horton, P., and van Grondelle, R. (2007). Identification of a mechanism of photoprotective energy dissipation in higher plants. *Nature* 450:575-U522.
- Ruban, A.V., Johnson, M.P., and Duffy, C.D.P. (2012). The photoprotective molecular switch in the photosystem II antenna. *Bba-Bioenergetics* 1817:167-181.
- Szabo, M., Premvardhan, L., Lepetit, B., Goss, R., Wilhelm, C., and Garab, G. (2010). Functional heterogeneity of the fucoxanthins and fucoxanthin-chlorophyll proteins in diatom cells revealed by their electrochromic response and fluorescence and linear dichroism spectra. *Chem Phys* 373:110-114.
- Tikkanen, M., Nurmi, M., Suorsa, M., Danielsson, R., Mamedov, F., Styring, S., and Aro, E.M. (2008). Phosphorylation-dependent regulation of excitation energy distribution between the two photosystems in higher plants. *Biochim Biophys Acta* 1777:425-432.
- Ting, C.S., and Owens, T.G. (1994). The Effects of Excess Irradiance on Photosynthesis in the Marine Diatom *Phaeodactylum-Tricornutum*. *Plant Physiology* 106:763-770.
- van der Weij-de Wit, C.D., Ihalainen, J.A., van Grondelle, R., and Dekker, J.P. (2007). Excitation energy transfer in native and unstacked thylakoid membranes studied by low temperature and ultrafast fluorescence spectroscopy. *Photosynth Res* 93:173-182.
- Van Dorssen, R., Breton, J., Plijter, J., Satoh, K., Van Gorkom, H., and Amesz, J. (1987a). Spectroscopic properties of the reaction center and of the 47 kDa chlorophyll protein of photosystem II. *Biochimica et Biophysica Acta (BBA)-Bioenergetics* 893:267-274.
- Van Dorssen, R., Plijter, J., Dekker, J., Den Ouden, A., Amesz, J., and Van Gorkom, H. (1987b). Spectroscopic properties of chloroplast grana membranes and of the core of photosystem II. *Biochimica et Biophysica Acta (BBA)-Bioenergetics* 890:134-143.
- Van Oort, B., Alberts, M., de Bianchi, S., Dall'Osto, L., Bassi, R., Trinkunas, G., Croce, R., and van Amerongen, H. (2010). Effect of antenna-depletion in Photosystem II on excitation energy transfer in *Arabidopsis thaliana*. *Biophysical journal* 98:922-931.
- van Oort, B., Amunts, A., Borst, J.W., van Hoek, A., Nelson, N., van Amerongen, H., and Croce, R. (2008). Picosecond fluorescence of intact and dissolved PSI-LHCI crystals. *Biophys J* 95:5851-5861.
- Van Oort, B., Murali, S., Wientjes, E., Koehorst, R.B.M., Spruijt, R.B., van Hoek, A., Croce, R., and van Amerongen, H. (2009). Ultrafast resonance energy transfer from a site-specifically

- attached fluorescent chromophore reveals the folding of the N-terminal domain of CP29. *Chem Phys* 357:113-119.
- Van Oort, B., van Hoek, A., Ruban, A.V., and van Amerongen, H. (2007). Aggregation of Light-Harvesting Complex II leads to formation of efficient excitation energy traps in monomeric and trimeric complexes. *Febs Lett* 581:3528-3532.
- van Stokkum, I.H., van Oort, B., van Mourik, F., Gobets, B., and van Amerongen, H. (2008). (Sub)-Picosecond Spectral Evolution of Fluorescence Studied with a Synchroscan Streak-Camera System and Target Analysis. In: *Biophysical Techniques in Photosynthesis* Dordrecht: Springer. 223-240.
- van Stokkum, I.H.M., Gobets, B., Gensch, T., van Mourik, F., Hellingwerf, K.J., van Grondelle, R., and Kennis, J.T.M. (2006). (Sub)-picosecond spectral evolution of fluorescence in photoactive proteins studied with a synchroscan streak camera system. *Photochemistry and photobiology* 82:380-388.
- Veith, T., and Buchel, C. (2007). The monomeric photosystem I-complex of the diatom *Phaeodactylum tricornutum* binds specific fucoxanthin chlorophyll proteins (FCPs) as light-harvesting complexes. *Bba-Bioenergetics* 1767:1428-1435.
- Wentworth, M., Ruban, A.V., and Horton, P. (2001). Kinetic analysis of nonphotochemical quenching of chlorophyll fluorescence. 2. Isolated light-harvesting complexes. *Biochemistry* 40:9902-9908.
- Yamagishi, A., Ikeda, Y., Komura, M., Koike, H., Satoh, K., Itoh, S., and Shibata, Y. (2010). Shallow sink in an antenna pigment system of photosystem I of a marine centric diatom, *Chaetoceros gracilis*, revealed by ultrafast fluorescence spectroscopy at 17 K. *J Phys Chem B* 114:9031-9038.

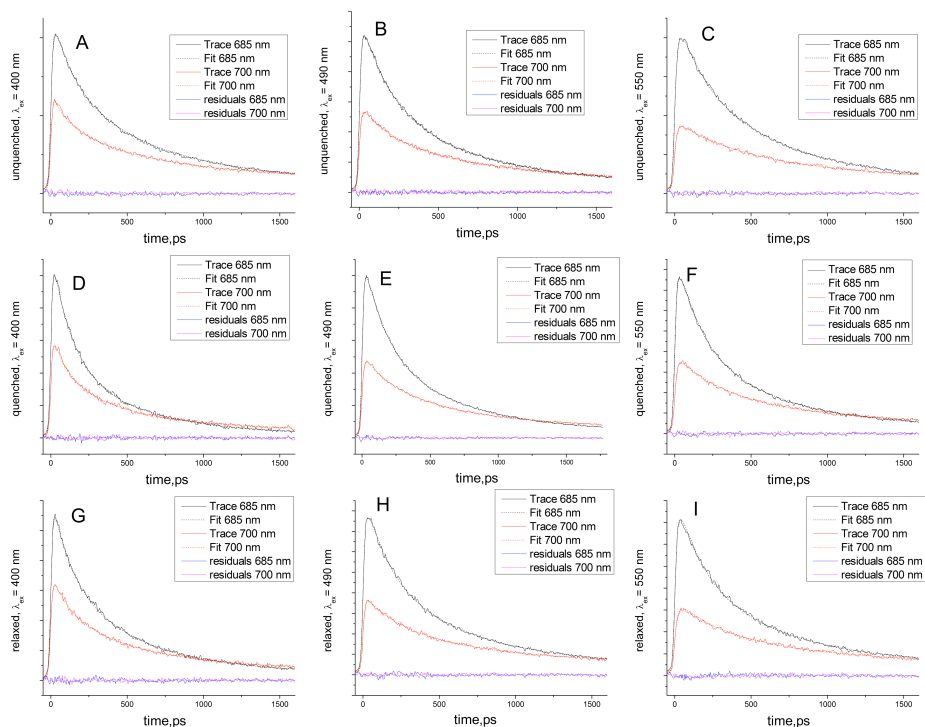
Supplementary material

This supplementary data contains seven sections:

- (i) Quality of the fit
- (ii) Comparison of $t=0$ spectra obtained at different excitation wavelengths
- (iii) Reconstructed steady-state fluorescence spectra of *C. meneghiniana* cells, measured in three states for different excitation wavelengths
- (iv) Estimation of the PSII contribution used in decomposition procedure
- (v) Decomposition of the 3rd and 4th DAS obtained from global analysis of unquenched and quenched datasets for 550 nm excitation
- (vi) Spectral decomposition of global analysis data for 400 nm excitation
- (vii) Comparison of data from unquenched and relaxed cells for 550 nm excitation

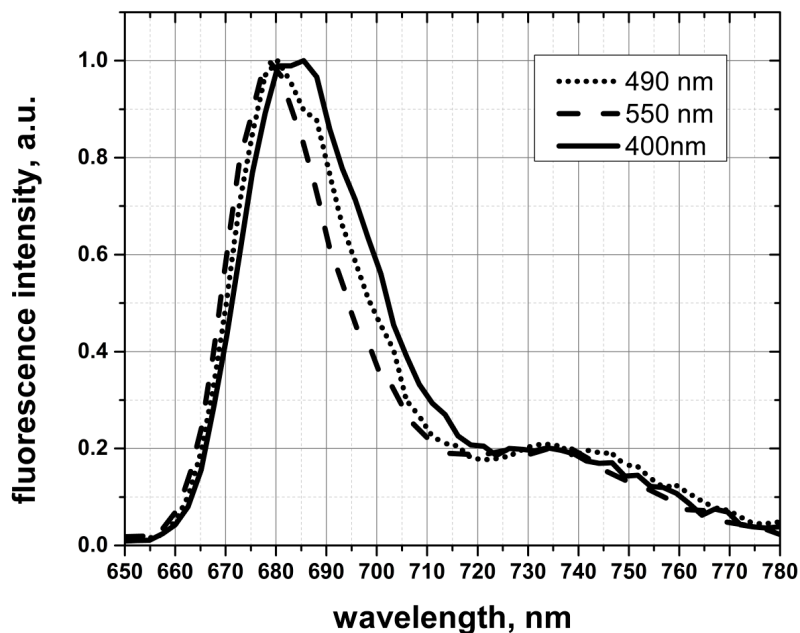
(i) Quality of the fit

The high fitting quality is clearly visualized by a high overlap between the fitted curves and the measured traces. In Supplemental Figure S1 typical measured traces are shown together with the corresponding fitting results obtained at two detection wavelengths (685 nm and 700 nm) and the residuals.



Supplemental Figure S1. Representative kinetic traces of unquenched (A, B, C), quenched (D, E, F) and relaxed (G, H, I) samples recorded at two detection wavelengths: 685 nm (black lines) and 700 nm (red lines). Solid lines represent measured traces while dashed lines indicate the curves obtained from the global analysis fit. Blue and magenta lines correspond to the residuals at 685 nm and 700 nm, respectively.

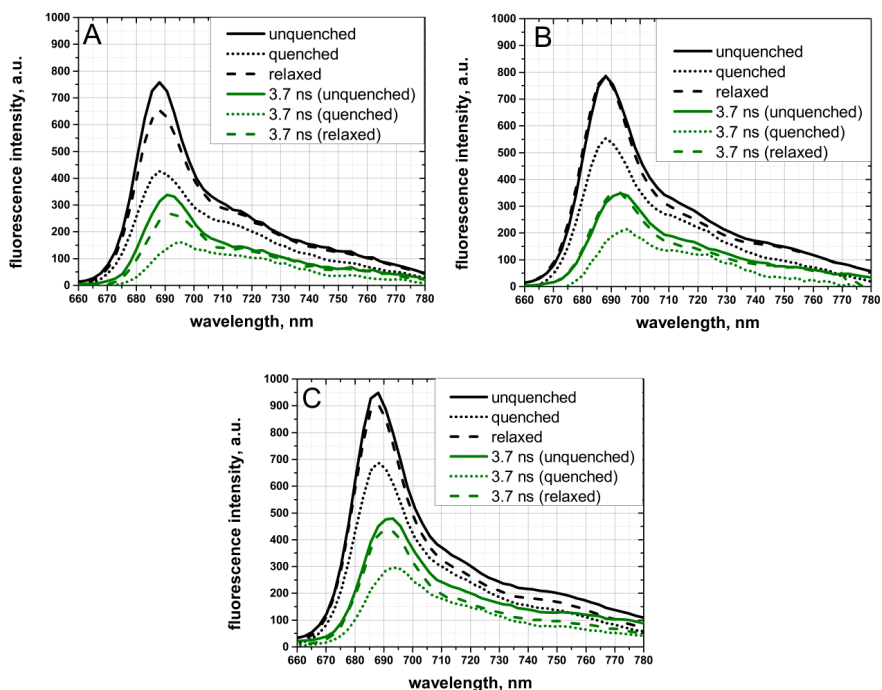
(ii) Comparison of $t=0$ spectra obtained at different excitation wavelengths



Supplemental Figure S2. Comparison of $t=0$ spectra obtained at 400 nm (solid line), 490 nm (dots), 550 nm (dashes) excitation.

The total spectra at $t=0$ are equal to the sum of the various corresponding DAS for a particular excitation wavelength. So to obtain each spectrum, all DAS obtained from global analysis of datasets for a particular (un)quenched state one of the three excitation wavelengths were summed and normalized in the maximum. The resulting spectra are different for different excitation wavelengths but do not depend on the state of the cells (unquenched/quenched/relaxed). The latter is in agreement with the fact that most Ddx cycle pigments do not excitonically interact with *Chl a* (Lepetit et al., 2010).

(iii) Reconstructed steady-state fluorescence spectra of *C. meneghiniana* cells, measured in three states for different excitation wavelengths



Supplemental Figure S3. Reconstructed steady-state fluorescence spectra (black lines) in unquenched (solid lines), quenched (dotted lines) and relaxed (dashed lines) state obtained from global analysis of the fluorescence data with 400 nm (A), 490 nm (B) and 550 nm (C) excitation. The green lines represent the spectral contribution of the slowest (3.7 ns) component.

The total steady-state fluorescence spectrum can be reconstructed from the global analysis results as the sum of each resolved DAS amplitude multiplied by the corresponding lifetime. As expected, the spectral contribution of the 3.7 ns DAS, which is mostly represented by FCP antenna, is essential for the total amount of fluorescence, especially at 550 nm excitation.

The 490 nm and 550 nm spectra show a smaller amount of quenching than the 400 nm spectrum (area decrease of ~30 % vs. ~35%). It is also worth mentioning

[CHAPTER 3]

that upon 550 nm excitation the quenching of the longest DAS is dominating the overall fluorescence decrease.

(iv) Supplemental Materials and Methods. Estimation of the PSII contribution used in decomposition procedure

The PSII contribution to a particular DAS is approximated by taking the average of the estimated maximum and minimum amounts. Both for relaxed and unquenched cells for all excitation wavelengths the intensities of the 3rd DAS are higher when comparing them with quenched results due to the higher PSII contribution (see “3.3.3.1. Upon fx excitation only qE₁ is observed” and “3.3.3.2. Monitoring qE₁ and qE₂ upon Chl *a* (400 nm) excitation” subsections). Therefore, the minimum amount of PSII area contributing to the 3rd unquenched (and relaxed) DAS is the difference between unquenched (and relaxed) and quenched DAS (Supplemental Figure S4A, 400 nm excitation data were used as an example).

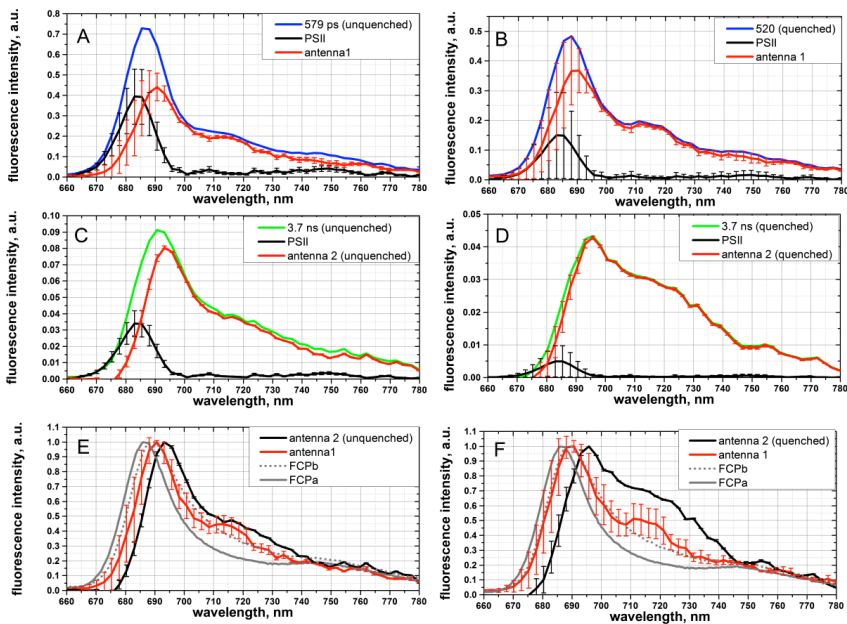
The shape of the 4th DAS suggests a strong contribution of the antenna spectrum (Results and Discussion, “3.3.3.1. Upon fx excitation only qE₁ is observed” and “3.3.3.2. Monitoring qE₁ and qE₂ upon Chl *a* (400 nm) excitation” subsections). However, there are also some indications of PSII contribution: decrease of fluorescence intensity is observed in the 670-685 nm region for the quenched state in comparison with the unquenched state at all excitation wavelengths. When the difference between the unquenched (or relaxed) and the quenched 4th DAS at 685 nm was used to estimate the minimal PSII amplitude (like for the 3rd DAS case), it showed a clear overestimation of the PSII contribution (data not shown). So, it can be concluded that there is a strong overlap of PSII and antenna spectra contributing to the 4th DAS. This is the reason why an average difference between the unquenched (or relaxed) and quenched spectra was used in the region where the antenna should have its minimal contribution (670-680 nm) in order to estimate the minimal PSII amplitude for the 4th DAS.

The maximum PSII contribution to all 3rd and 4th DAS was estimated by subtracting the maximum amount of PSII from these DAS such that the remaining difference spectrum was non-negative everywhere. The PSII spectra used in the final decomposition routine were taken as the average of the maximum and minimum PSII spectra, and are indicated in Supplemental Figure S4 with black solid lines. The final *antenna 1* and *antenna 2* spectra were obtained by subtracting the estimated PSII contribution from the original 3rd. and 4th DAS, respectively. Error margins of antenna spectra (Supplemental Figure S4E, F) show how their shapes differ when using either maximum or minimum PSII contributions. The *antenna 1* peak/shape might vary slightly while the estimated *antenna 2* spectrum is almost identical when using the

[CHAPTER 3]

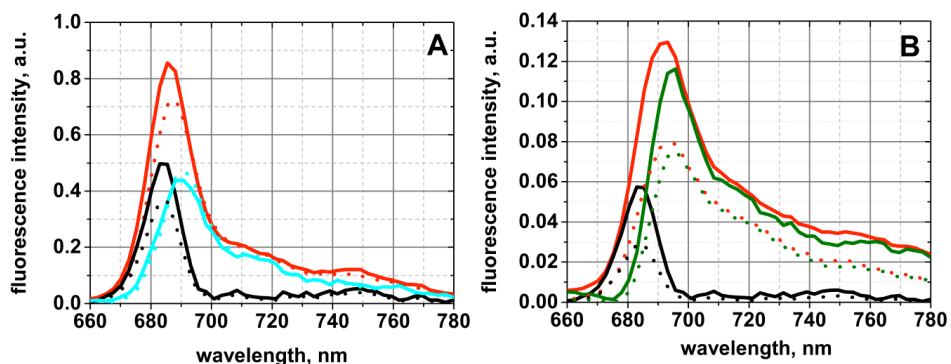
maximum and minimum PSII amounts (Supplemental Figure S4E). Therefore, the choice of the approximated contribution of PSII will not strongly influence the quantitative conclusions whereas the qualitative conclusions are unambiguous.

In case of quenched cells, the minimal PSII contribution was set to 0 for the 3rd and 4th DAS since it decreases substantially for quenched cells as compared with other states (Supplemental Figure S4A, C and Supplemental Figure S4B, D).

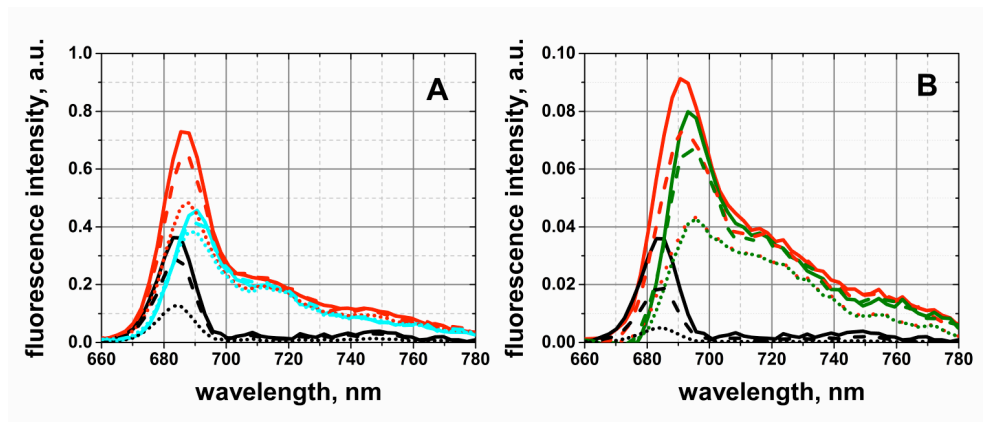


Supplemental Figure S4. Estimation of maximum and minimum PSII area (indicated by black error margins) contributions to the 3rd (A, B) and 4th (C, D) DAS for the unquenched (A, C) and quenched (B, D) state upon 400 nm excitation. For the final decomposition procedure the average of the estimated maximum and minimum PSII contributions were used (indicated in Supplemental Figure S4 A-D with black solid lines). Supplemental Figure S4 E, F represent normalized antenna 1,2 spectra together with obtained error margins in the unquenched (E) and quenched (F) state.

(v) Decomposition of the 3rd and 4th DAS obtained from global analysis at 550 nm excitation

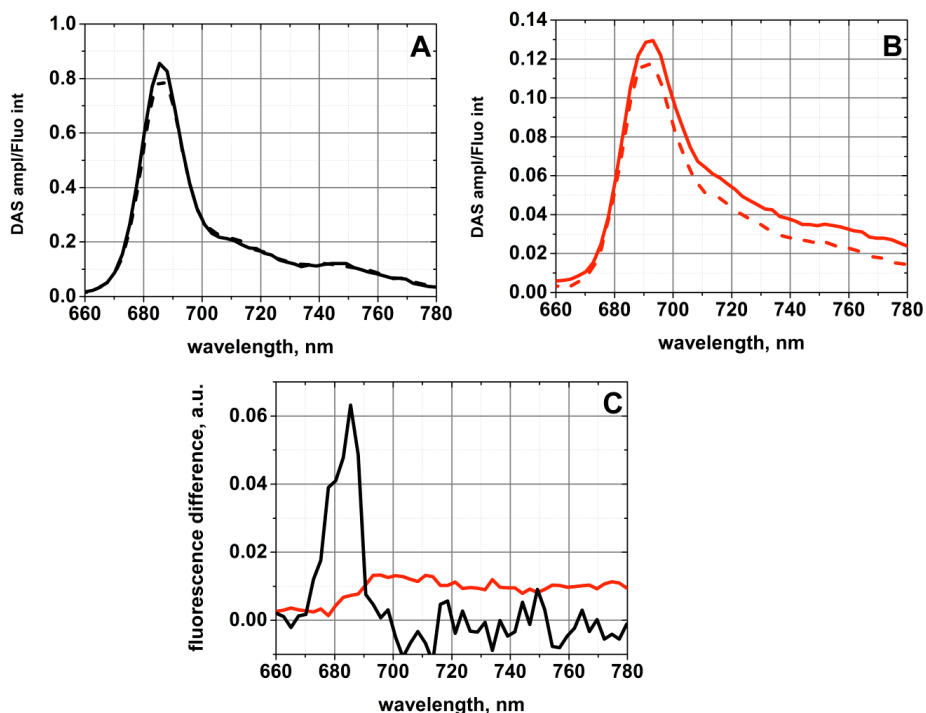


Supplemental Figure S5. Decomposition of the 3rd (A) and 4th (B) DAS (red lines) obtained from global analysis of unquenched (solid lines), quenched (dots) datasets upon 550 nm excitation. The residual spectra are shown in cyan (A) and green (B) and represent different antenna subpopulations.

(vi) Spectral decomposition of global analysis data for 400 nm excitation

Supplemental Figure S6. Decomposition of the 3rd (A) and 4th (B) components obtained from global analysis of unquenched (solid), quenched (dot) and relaxed (dash) datasets at 400 nm excitation using the PSII fluorescence spectrum (black lines). The residuals are shown in cyan (A) and green (B) and represent different antenna subpopulations.

(vii) Comparison of data from unquenched and relaxed cells for 550 nm excitation



Supplemental Figure S7. Comparison of the 3rd (A) and 4th (B) DAS of cells in unquenched (solid line) and relaxed (dotted line) state obtained from global analysis upon 550 nm excitation. The difference DAS corresponding to qE_2 (unquenched minus relaxed) for 550 nm excitation are presented on Supplemental Figure S7 C. The difference spectra were plotted for the 3rd (black line) and 4th (red line) component.

Comparison of the 3rd DAS for unquenched and relaxed state upon 550 nm excitation shows that there is a small contribution of qE_2 detected in the relaxed data (Supplemental Figure S7 A) in contrast to 490 nm excitation (Figure 4), where no difference is observed.

Since decomposition analyses show that there is only PSII quenching contributing to the DAS decrease while the *antenna 1* spectrum stays unchanged (see “2.4.1. Evidence for PSII quenching” subsection, Supplemental Figure S5 A), the

[CHAPTER 3]

decrease of the aforementioned DAS (~4% of PSII contribution) must be ascribed to PSII quenching selectively. The difference spectrum of the 3rd DAS shows PSII spectrum characteristics confirming the PSII origin of the 3rd DAS decrease in the relaxed state (Supplemental Figure S7 C, black line).

The small decrease of the 4th DAS in the relaxed state shows clear *antenna 2* characteristics since it affects only the fluorescence above 690 nm (Supplemental Figure S7 C, red line), indicating that part of the antenna is quenched in the relaxed state. Since the antenna pool involved in quenching (presumably FCPa) is preferably presented by the 4th spectrum we can conclude that not more than 10% of Dtx-dependent FCPa antenna quenching from the total FCPa pool is present.

Lepetit, B., Volke, D., Gilbert, M., Wilhelm, C., and Goss, R. (2010). Evidence for the Existence of One Antenna-Associated, Lipid-Dissolved and Two Protein-Bound Pools of Diadinoxanthin Cycle Pigments in Diatoms. *Plant Physiology* 154:1905-1920.

Chapter 4

Disconnection of the light-harvesting antenna from Photosystem I restores the redox balance after dark-light transitions

Volha Chukhutsina^{123*}, Luca Bersanini^{4*}, Eva-Mari Aro⁴, Herbert van Amerongen^{123#}

¹Laboratory of Biophysics, Wageningen University, P.O. Box 8128, 6700 ET, Wageningen, The Netherlands

²MicroSpectroscopy Centre, Wageningen University, 6703 HA Wageningen, The Netherlands

³BioSolarCells, P.O. Box 98, 6700 AB Wageningen, The Netherlands

⁴Department of Biochemistry, Molecular Plant Biology, University of Turku, FI-20014 Turku, Finland

submitted

Abstract

Photosynthetic organisms cope with changing light conditions by actively balancing the distribution of light-induced excitation energy between photosystems I (PSI) and II (PSII) in a process, often called state transitions. In cyanobacteria the molecular events during state transitions have not been fully clarified yet. Energy redistribution has been suggested to be achieved by movement of the light-harvesting phycobilisome complexes between PSI and PSII [Mullineaux CW, Tobin MJ, Jones GR (1997) *Nature* 390(6658): 421-424], or by nanometer scale rearrangements of the complexes constituting the recently discovered PBS-PSII-PSI megacomplexes [Liu H, Zhang H, Niedzwiedzki DM, Prado M, He G, Gross ML, Blankenship RE (2013) *Science* 342(6162): 1104-1107]. The alternative 'spillover' model, on the other hand, states that energy redistribution is achieved by mutual association/dissociation of PSI and PSII. State transitions have either been studied by changing the redox state of the electron carriers using electron transfer inhibitors, by applying illumination conditions with rather specific colors, or by changing between dark and light conditions. Here we investigated changes in excitation energy transfer from the phycobilisomes to the photosystems, which were induced by dark-light transitions, making use of picosecond fluorescence spectroscopy. It appears that megacomplexes are not involved in these changes, and also spillover does not play a role. Instead, it is found that the phycobilisomes partly detach from PSI but hardly reattach to PSII. In this way the redox balance, which is disturbed by dark-light transitions, is restored.

4.1 Introduction

To optimize their light-harvesting capacity, photosynthetic organisms adapt rapidly to changing light conditions and/or metabolic demands by regulating the distribution of absorbed light energy between photosystems I and II (PSI, PSII) in a process called state transitions (Allen, 2003; Allen and Forsberg, 2001; Croce and van Amerongen, 2014). State transitions can be defined as a change in the relative antenna size of PSI and PSII as a response to a change of the redox status of intersystem electron carriers. State 1 is induced by oxidation of intersystem electron carriers, usually upon excess excitation of PSI as compared to PSII. State 2 is induced by reduction of intersystem electron carriers, either through excess excitation of PSII or by dark respiratory pathways (Mullineaux and Allen, 1990).

In higher plants, all major light-harvesting antennas are attached to PSII in state I, whereas part of the antennas are attached to PSI in state II (Allen and

Forsberg, 2001). Isolation of a functional antenna-PSII megacomplex (Chereskin et al., 1985) as well as multiple fluorescence studies suggest that phycobilisomes (PBSs), the light-harvesting antennas of cyanobacteria, can associate with PSII and with PSI (for review, (Mullineaux, 2008)). However, the PBS interactions with PSs as well as PSs macro-organization are not well understood at the microscopic level (Chereskin et al., 1985).

The “spillover” model of state transitions was first proposed based on freeze-fracture analysis. Olive and coworkers found that in the cyanobacterial membrane in state 1, PSII complexes are arranged in row-like superstructures, while in state 2 the organization of PSII was more random (Olive et al., 1986). Based on this observation, the state transition model was proposed, which assumes that in state 2, excess energy absorbed by pigments associated with PSII “spills over” to PSI, because in this state PSI and PSII have moved sufficiently close to each other (Bruce et al., 1989; Vernotte et al., 1990). The spillover model therefore implies that PBSs, or their movement, play no role in state transitions.

More recently, Joshua and Mullineaux correlated the presence of PBS mobility in cyanobacteria with state transitions. They fixed cyanobacteria in either state 1 or 2 by immersing the cells in a buffer of high osmotic strength, which strongly inhibited PBS diffusion (Joshua and Mullineaux, 2004). Substantial differences could be observed in steady-state fluorescence emission spectra at 77K. The suggestion that PBS detaches from PSI and attaches to PSII during the transition from state 2 to state 1 was based on enhanced fluorescence emission from PSII in the 680-695 nm spectral region at 77K, after normalizing the spectra for state 1 and 2 to their PBS-related peak at 665 nm or to the PSI peak at 720 nm (Joshua and Mullineaux, 2004; Kana et al., 2014). PBS migration between PSs in this study was also supported by fluorescence recovery after photobleaching (FRAP) measurements, which showed that PBSs diffuse quite rapidly in the cells while PSII is immobile on the time scale of the measurements. From these steady-state fluorescence and FRAP observations, the model of physical redistribution (diffusion) of PBS during state transitions was suggested. The suggested movement of PBS from one photosystem towards the other was, however, never explicitly demonstrated: The 695-nm emission peak as observed by Joshua and Mullineaux is indeed characteristic for the PSII antenna CP47, but the 685-nm peak can contain contributions from both PSII and allophycocyanin (APC₆₈₀) in PBSs (Jallet et al., 2012; Tian et al., 2013). Furthermore, APC₆₈₀ fluorescence dominates the PBS steady-state spectra both in intact cells and in isolated PBSs (Jallet et al., 2012; Scott et al., 2006), which makes it difficult to distinguish between PBS migration from PSI to PSII and simple detachment of PBS from PSI with the use of steady-state fluorescence emission measurements only. To summarize, PBS mobility

[DARK-LIGHT TRANSITIONS IN CYANOBACTERIA]

seems to play a role during state transitions; however, the PBS migration between the photosystems is still questionable.

It has been proposed that both PBS mobility and spillover effects contribute to state transitions, but the major contribution comes from PBS mobility (Emlyn-Jones et al., 1999; McConnell et al., 2002). Based on x-ray structures of PSII, PSI, and allophycocyanin and 77K steady-state fluorescence measurements, it was hypothesized that the major part of energy redistribution comes from only slight movements of PBSs and that a single PBS might feed energy to PSI and PSII simultaneously (McConnell et al., 2002). This theory was supported recently by the isolation and characterization of a fully functional cyanobacterial megacomplex, composed of PBS, PS I and II (Liu et al., 2013). Although the megacomplexes were obtained through chemical cross-linking, Liu and coworkers showed that a single PBS feeds excitations to both PSs within the megacomplex (Liu et al., 2013). If such megacomplexes would occur *in vivo*, PBSs would not have to move in order to induce a change in excitation flow from PBS to PSI or PSII. In the isolated PBS-PSII-PSI megacomplex, the rate of excitation energy transfer (EET) to PSI was found to be slower than to PSII, which provides the opportunity to check whether such a PBS-PSII-PSI megacomplex is also present *in vivo*: Slower EET to PSI than to PSII would indeed be a signature of the presence of PSII-PSI-PBS megacomplexes. For that reason we have compared rates of EET to PSII and PSI in *Synechocystis* cells *in vivo*.

Experimentally, low-intensity blue or far-red light is commonly used to induce state 1, while a short period of pre-illumination with low-intensity orange light or of darkness is used to put cells into state 2 (Ashby and Mullineaux, 1999; El Bissati et al., 2000). As an alternative to the selective illumination scheme, state 1 can be induced by any color of white light after a period of darkness (Mullineaux and Allen, 1990). Darkness will subsequently bring cells back to state 2 (Aoki and Katoh, 1982; Mullineaux and Allen, 1986). When using selective light regimes instead of the white light/darkness scheme, the fluorescence emission intensity differences between states 1 and 2 at 680-690 and 720 nm are generally more pronounced, but of the same order of magnitude. Here, we studied “dark” and “light” states of the cyanobacterium *Synechocystis* sp. PCC 6803 (hereafter *Synechocystis*) using steady-state as well as time-resolved fluorescence methods. We first followed dark/light transitions by steady-state fluorescence measurements at 77K in order to confirm the occurrence of two distinct states. But instead of the commonly used normalization to one of the emission peaks, we used an external fluorescent calibration probe and normalized the spectra to their fluorescence emission. This allowed us to monitor absolute changes in fluorescence emission at all bands. Additionally, we used picosecond fluorescence spectroscopy (Tian et al., 2011; Ünlü et al., 2014) to explicitly

address the questions (1) whether antenna move between photosystems, (2) whether cyanobacterial megacomplexes occur *in vivo* and (3) to assess the contribution of spillover to dark/light transitions.

4.2 Materials and Methods

4.2.1 Strains and Growth Conditions

Synechocystis sp. PCC 6803 cells were grown at 30°C in BG-11 (Allen, 1968) buffered with 20 mM HEPES-NaOH (pH 7.5) and sodium carbonate was omitted from the culture ingredients. White light was used for illumination at 50 $\mu\text{mol photons m}^{-2} \text{ s}^{-1}$. The cultures were grown in 100-ml flasks with a culture volume of 20 ml. The flasks were shaken at 100 rpm. Supplemental Figure 1 shows the profile of the light that was used for cultivation.

4.2.2 Sample preparation

The *Synechocystis* sp. PCC 6803 cells were harvested during the logarithmic phase (optical density at 750 nm (OD_{750}) between 0.6 and 1.1 for a pathlength of 1 cm), resuspended in fresh BG-11 medium, and adjusted to $\text{OD}_{670} = 0.2\text{-}0.3$ (again for 1 cm), using a spectrophotometer with integrating sphere. The cells were either taken directly from the growth chamber (light state) or after keeping them in the dark for 10 min (dark state). For the fluorescence measurements samples in both states were collected in glass Pasteur pipettes with ~ 1 mm diameter to avoid reabsorption effects and then frozen by immersion in liquid nitrogen. The reversibility of the light-dark transition was checked by recording 77 K steady-state fluorescence spectrum of light-adapted cells (10 min light adaptation, Supplemental Figure 4, light 2) after a 10 min dark-adaptation period. The obtained spectrum was identical to the spectrum of the cells in the light state.

4.2.3 Steady-State Fluorescence

Steady-state fluorescence spectra were recorded with a Fluorolog FL3-22 spectrofluorimeter (Horiba Jobin Yvon, Edison, NJ) and corrected for wavelength-dependent sensitivity of the detection and fluctuations in lamp output. The excitation wavelength was 580 nm; a band-pass of 2 nm was used for both the excitation and emission monochromator. Instead of the commonly used normalization to the emission peaks, Rhodamin B was used as an internal standard to independently check

the fluorescence emission changes in the whole range of steady-state spectra. The standard was added to the culture just before freezing in liquid nitrogen. Fluorescence emission spectra were recorded using an integration time of 0.2 s. Each measurement was repeated three times and the results were averaged.

4.2.4 Time-resolved fluorescence measurements

Time-resolved emission spectra were recorded using a synchroscan streak-camera system as described in (van Oort et al., 2009; van Stokkum et al., 2006). An excitation wavelength of 580 nm was used to excite preferentially the PBSs, while 400 nm was used to preferentially excite Chl *a* in the PSs. The laser power was 60 μ W, the time-window 800 ps, the spot size 100 μ m, and the repetition rate 250 kHz. An average of 100 images, all measured for 10 s, was used to achieve high signal/noise ratio. Before analysis, the images were corrected for background signal and detector sensitivity and sliced up into traces of 5 nm.

The streak-camera images were analyzed using the TIMP package for the R language (Mullen and van Stokkum, 2007) and Glotaran, a graphical user interface for TIMP (Snellenburg et al., 2012). A Gaussian-shaped instrument response function was used as input for the analysis with the width as a free fitting parameter. FWHM values obtained from the fitting procedure were in the range of 12 ± 1 ps. To estimate long lifetimes (longer than 1 ns), a sum of exponential decays, characterizing forward and backward sweeps of the synchroscan (period of 13.17 ns) in the streak camera, was included in the fit (Van Stokkum et al., 2008). The fit quality was judged by singular value decomposition of the residuals matrix (Mullen and van Stokkum, 2007).

4.3 Results and discussion

4.3.1 Changes in antenna excitation-energy distribution observed by 77K steady-state fluorescence emission

First we recorded fluorescence emission spectra upon 580 nm excitation (PBS) at 77 K. The steady-state fluorescence emission spectra of the dark and the light state were normalized to the fluorescence signal of Rhodamin B (see Fig. 1). The broad fluorescence emission in the 630-670 region originates from phycocyanin (630-665 nm, PC) (Debrecezeny et al., 1993) and allophycocyanin (660-670 nm, APC₆₆₀) (Glazer, 1985) of the PBSs. The maximum at 685 nm corresponds to emission from both PBS terminal emitter (APC₆₈₀) and PSII (Scott et al., 2006; Tian et al., 2013),

while the maximum at 695 nm is due to red-shifted Chl *a* emission of CP47 in PSII (Andrizhiyevskaya et al., 2005). The fluorescence emission at 720 nm is due to PSI (Liu et al., 2013).

In the light state, the fluorescence spectrum shows less PSI emission at 720 nm, but increased emission at 685-695 nm as compared to the dark state. Such differences in the 685-695/720 nm fluorescence ratio are typical for states 1 and 2, and are thought to indicate increased energy transfer from PBSs to PSII in state 1 and to PSI in state 2. However, in the light state, we also observed increased fluorescence in the 630-670 nm region, which can entirely be attributed to PC and APC₆₆₀ in PBSs. Therefore, the spectral differences cannot only be explained by PBS migration from PSI to PSII. To clarify whether PBS detachment could contribute to the observed spectral changes and/or whether some other processes could be involved, we performed time-resolved measurements.

4.3.2 The two states characterized by time-resolved measurements

Synechocystis cells, locked in two different states, were monitored by recording their time-resolved fluorescence emission spectra upon 580 nm excitation. The obtained streak-camera images are presented in Figure 4.2 together with several representative fluorescence decay traces and several fluorescence spectra at various delay times. The spectral resolution of time-resolved data is 5 nm (as opposed to 2 nm for steady state data). Like in the steady-state fluorescence emission spectra, three distinct emission bands are observed in the streak-camera data with maxima at 665, 685, and 720 nm. Again, these peaks are associated with PC and APC₆₆₀ in PBS, APC₆₈₀ and PSII, and PSI, respectively. In Figure 4.3 fluorescence at the three emission maxima is compared for the two states. We additionally plotted the difference at 678 nm to specifically illustrate the difference of APC₆₈₀-fluorescence (Figure 4.3 B). The above-given suggestion that the higher intensity in the 650-670 nm region for the light state (Figure 4.1) is due to PBS detachment in the light is confirmed by comparison of the fluorescence decay kinetics of two PBS-related emission wavelengths (665 and 678 nm) for the two states (Figure 4.2 and Figure 4.3 A and B). The final parts of the fluorescence traces (0.2 - 0.7 ns) at 665 nm (PC and APC₆₆₀, Figure 4.3 A) and at 678 nm (APC₆₈₀, Figure 4.3 B) in the light state decay slower than in the dark state, which indicates a higher contribution of long-living components in the light state. This effect leads to the observed increase of steady-state fluorescence in the PC (630-655 nm) and APC (660-670 nm, ~685 nm) wavelength regions.

Subsequently, we looked at the differences between the fluorescence kinetics in the light and dark states, measured at PS-related wavelengths (PSII: 685 nm (Figure

[DARK-LIGHT TRANSITIONS IN CYANOBACTERIA]

3 C), PSI: 720 nm (Figure 4.3 D)). We found that both for the dark and the light state the PSI fluorescence reaches its maximum intensity in ~ 35 ps (Figure 4.3 D). However, the rise in PSII/APC₆₈₀-related fluorescence takes ~ 40 ps in the dark state and ~ 55 ps in the light state. Due to the APC₆₈₀ fluorescence contribution at 685 nm, the effect of PBS detachment, as discussed in the previous paragraph, is also observed at 685 nm, namely an overall lengthening of the fluorescence decay.

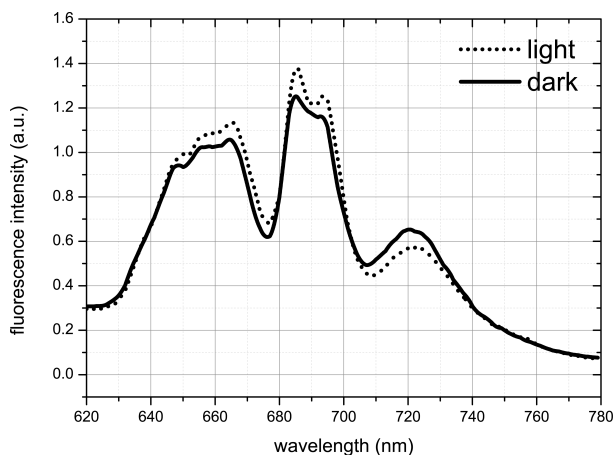


Figure 4.1. Fluorescence spectra of *Synechocystis* sp. PCC 6803 cells measured at 77K upon 580 nm excitation. The spectra are normalized to the fluorescence emission of the external fluorescent probe Rhodamin B that was added to the sample just before freezing.

To check whether the observed delay in the rise of fluorescence intensity from ~ 40 to ~ 55 ps in the PSII/APC₆₈₀-related emission band upon 580 nm excitation is PBS- or PSII-related, we also performed streak-camera measurements using 400-nm excitation (Supplemental Figure 4.3). At this excitation wavelength, mainly the PSs are excited. In this case the fluorescence decay traces do not differ for the dark and light states, leading to the conclusion that all the observed changes in fluorescence rise and decay kinetics upon 580 nm excitation must be PBS-related. Decay traces at the PSI emission maximum (720 nm) of dark and light states upon 400 nm excitation also do not show any differences (Supplemental Figure 4.3 D). Our results obtained upon 400 nm excitation also show that spillover does not play a role in dark-light transitions. The spillover model assumes reorganization of PSs in such a way that EET between PSII and PSI changes, which would affect PSI and PSII fluorescence kinetics. However, in our measurements the fluorescence decay traces of PSII and PSI do not differ for the two states.

To summarize, EET from PBS towards PSI occurs equally fast for both states (~ 35 ps) (Figure 4.3), while the initial part of the 685-nm fluorescence trace is clearly slower in the light state (dark: ~ 40 ps; light ~ 55 ps), reflecting slower EET from PBS towards PSII. Interestingly, the fact that the rate of EET from PBS to PSII is not faster than to

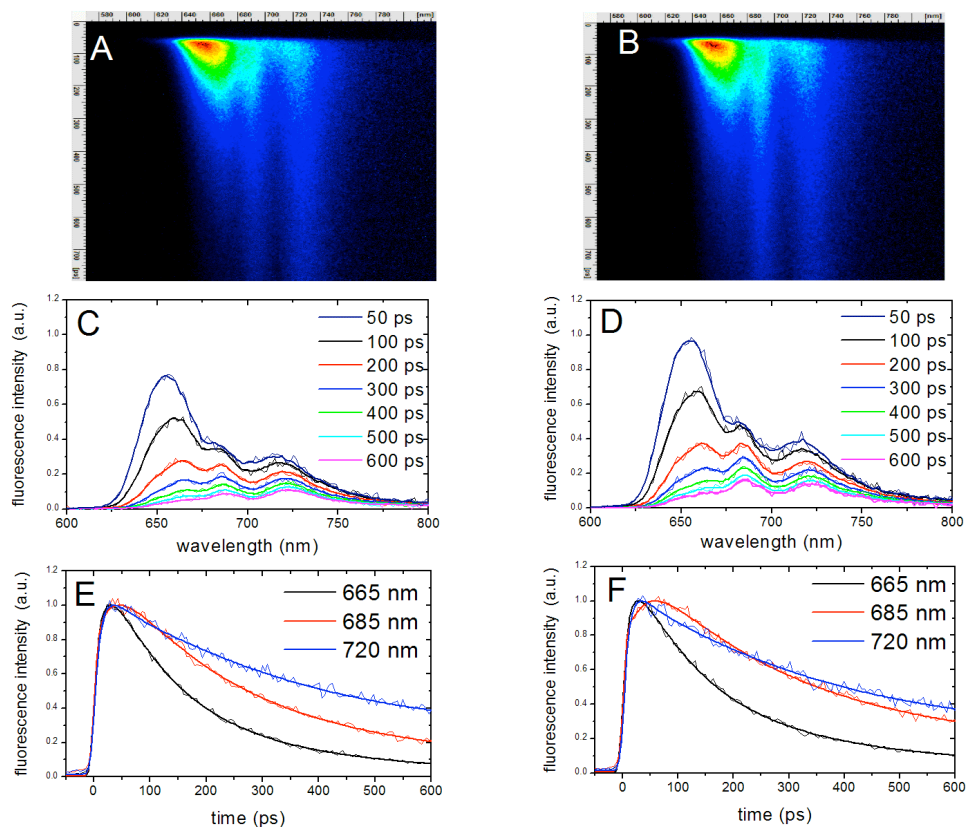


Figure 4.2. Time-resolved fluorescence of *Synechocystis* sp. PCC 6803 measured in dark (state 2) (A, C, E) and light-adapted states (state 1) (B, D, F) at 77K upon 580 nm excitation. (A, B) Streak-camera images. False colors indicate the fluorescence intensity. (C, D) Representative fluorescence spectra measured at various delay times after the excitation pulse. (E, F) Representative decay traces were taken at three characteristic emission wavelengths: 665 nm (PBS), 685 nm (APC680, PSII) and 720 nm (PSI). For better comparison the traces were normalized at their maxima

PSI differs from recent *in vitro* results on the PBS-PSII-PSI megacomplex (Liu et al., 2013), which showed that EET from PBS towards PSI is slower than towards PSII. Apparently, PBS-PSII-PSI megacomplexes do not dominate fluorescence kinetics *in vivo* neither in the dark nor in the light.

[DARK-LIGHT TRANSITIONS IN CYANOBACTERIA]

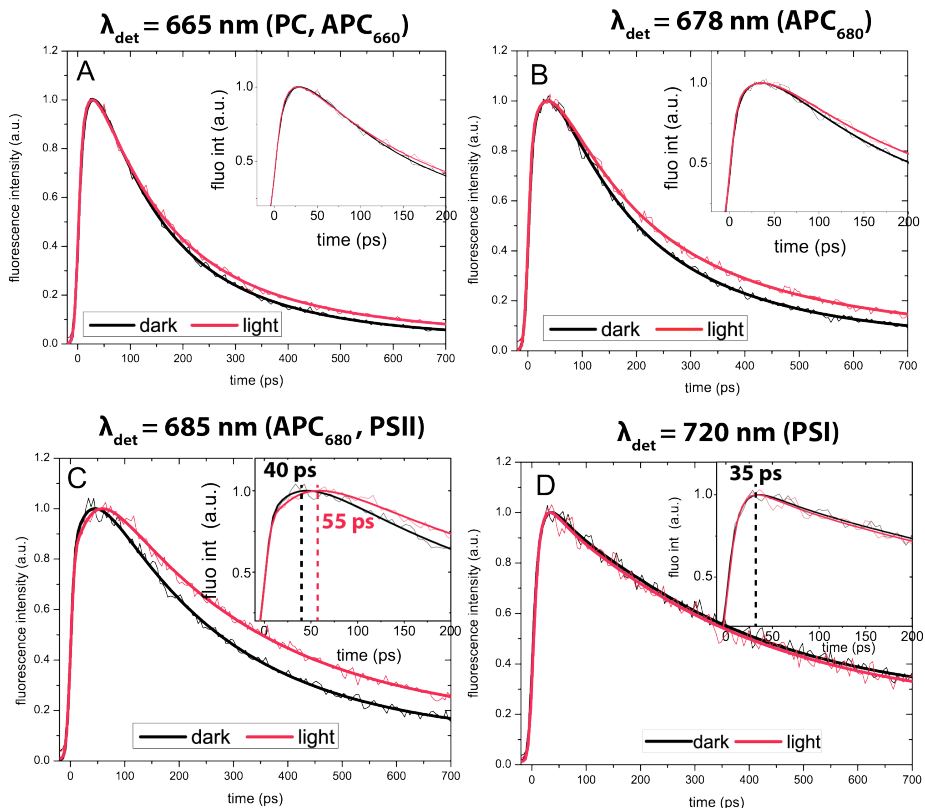


Figure 4.3. Comparison of kinetic traces in dark (black line) and light (gray line) states, taken at four emission bands: 665 nm (PBS), 678 nm (APC₆₈₀), 685 nm (APC₆₈₀, PSII) and 720 nm (PSI). The insets zoom in on the first part of the kinetics. Each experiment was repeated at least 3 times for different generations of the cell culture. All differences for the two states, measured for different generations, were found to be very reproducible (Supplemental Figure. 2).

4.3.3 Global analysis of streak-camera data

In order to study PBS mobility between PSs, we performed global analysis of the streak-camera data obtained upon 580 nm excitation at 77K. The resulting decay-associated spectra (DAS) are presented in Figure 4.4 A. Five components were sufficient to describe the data for both the dark and the light state. The 1st DAS (11 ps) has a positive and a negative peak at 630 and 650 nm, respectively, representing EET

in the PC rods together with a positive and a negative peak respectively at 690 nm and 720 nm, representing EET within PSI (Krumova et al., 2010; Tian et al., 2011). The 2nd DAS carries the typical signature of EET from PC towards APC₆₆₀ with a positive peak at 640 nm and a negative one at ~665 nm (Krumova et al., 2010; Tian et al., 2011). For dark-state cells it also has a positive and a negative band in the 700-760 nm region, representing PSI fluorescence kinetics, which is lacking for light-state cells. The 3rd component represents EET from APC₆₆₀ to APC₆₈₀ /Chls with a 100±10 ps time constant. The 4th component, decaying with a ~250 ps in the dark and ~275 ps in the light, reflects the sum of several decay processes with peaks at 665 nm, 682 nm, and 715 nm. The 665-nm peak is characteristic for PBSs (Liu et al., 2013). The 682-nm peak of the 4th DAS, due to its lifetime, was previously assigned to PSII, while the 715 nm peak is characteristic for PSI (Tian et al., 2013). The 5th DAS (2 ns) represents the decay of both PSII at ~695 nm and PSI at ~725 nm, while a small contribution from PC and APC₆₆₀ results in the 650-660 nm band. The 686-nm maximum of the 5th DAS should be dominated by APC₆₈₀, since no PSII-related components, with ~ns lifetimes and 686-nm peak position, have been resolved before, neither *in vivo* nor *in vitro* (Liu et al., 2013; Tian et al., 2013). We note that 360 ps and 1.3 ns lifetimes have previously been reported for APC₆₈₀ *in vivo* at RT (Scott et al., 2006), while at 77K APC₆₈₀ fluorescence decays with a 2 ns lifetime *in vitro*; thus APC₆₈₀ emission contributes to the 5th DAS and hardly to the 4th DAS in the 685 nm region (Figure 4.3).

Next we compare the individual DAS for dark and light states, as presented in Figure 4.4 B-E. The 1st DAS (not shown) does not differ for the dark and the light state. The 2nd DAS (Figure 4 B) shows higher amplitudes for the positive 640-nm and negative 665-nm peaks in the dark state than in the light state. In the dark state, it also carries a positive and a negative band in the PSI-related region (700-760 nm) that is absent in the light state. The first difference might be caused by a lower number of pigments participating in EET from PC towards APC₆₆₀ in PBSs in the light. In case there would indeed be a lower number of pigments, we would expect the energy transfer rate from PBS rods to PBS cores to be faster (Tian et al., 2012). However, the rising parts of the APC-associated traces detected at 665 nm and 678 nm (Figure 4.3, inserts) do not differ. Alternatively, the decrease in amplitude of the positive 640-nm and negative 665-nm peaks in combination with the disappearance of the positive and negative PSI-related bands in light most probably indicates that less energy is transferred from PC and/or APC₆₆₀ to PSI. Also in the 3rd DAS (Figure 4.4 C), the intensity of the negative PSI-related band is lower in the light state than in the dark state, again indicating that less energy is

[DARK-LIGHT TRANSITIONS IN CYANOBACTERIA]

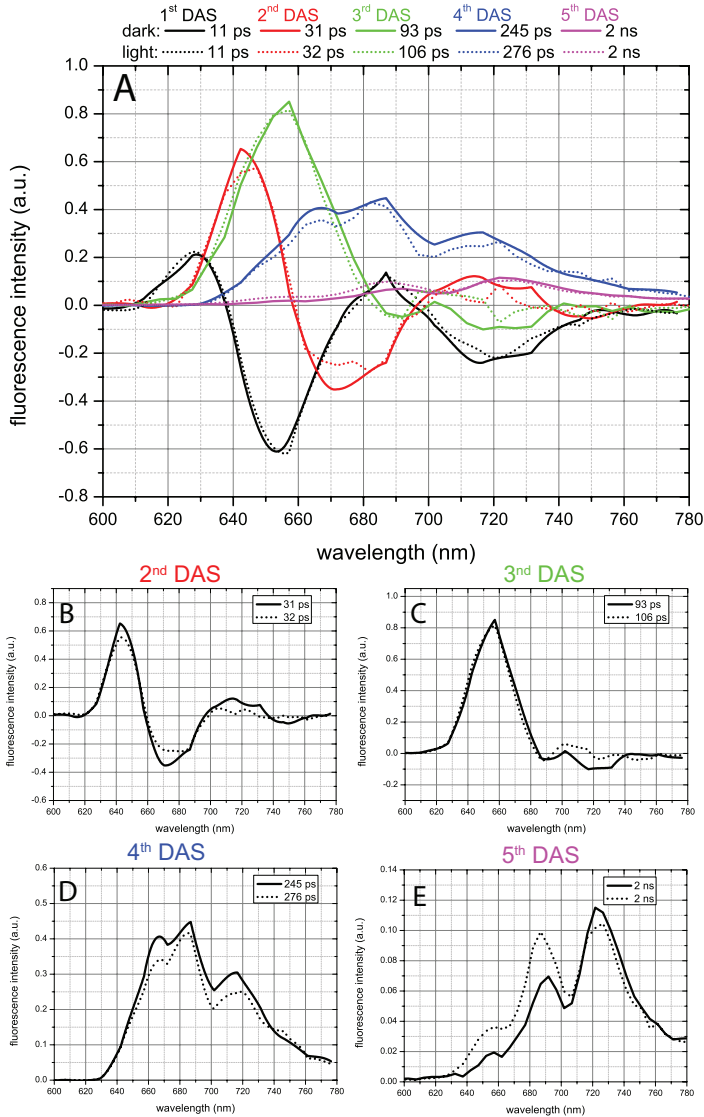


Figure 4.4. DAS for dark (solid line) and light (dotted line) states obtained from global analysis of streak-camera data measured at 77 K upon 580 nm excitation. A—The lifetimes of the corresponding DAS are presented in the legend with the corresponding colors. The slowest component was always fixed to 2 ns. This lifetime was obtained independently for many datasets, but due to the limited time window of our setup (800 ps), it was not possible to resolve it in a reliable way. The shape of both fluorescence spectra at $t = 0$ were identical and they were normalized to each other. B–E—Comparison of individual DAS as presented in A. The first DAS (11 ps) was identical for both measurements and is not presented here

transferred from PBSs to PSI. In the light state, this DAS shows EET from APC₆₆₀ towards APC₆₈₀ pigments of PBSs and Chls of PSII, both emitting at ~685 nm. However, the amplitude of the negative APC₆₈₀/PSII-related 680-685-nm band is not

higher in the light state than in the dark state, suggesting that (most of the) PBSs that detach from PSI in the light, do not migrate to PSII. In the light state, we also observe a 15 ps longer lifetime for the 3rd DAS, which reflects a decrease of the rate of EET from PBS to PSII, as discussed in the previous section. PBS detachment from PSI should not significantly contribute to the changes of the 3rd DAS lifetime, since it was demonstrated that energy transfer rates in isolated cyanobacterial phycobilisomes are nearly identical to those obtained for intact cells (Tian et al., 2012; Tian et al., 2011).

In the 4th DAS, the main differences between dark and light states are the lower PBS-related 665-nm fluorescence and PSI-related 715-nm fluorescence in the light state. The PSII-related 685-nm fluorescence does not seem to differ for the two states, again suggesting that PBSs do not attach to PSII in the light. In the 5th DAS we see a fluorescence increase by 50 % in the PC/APC₆₆₀-related region (640-660 nm), and by 40 % in the APC₆₈₀/CP47-related region (685-695 nm), and again a small decrease of PSI emission. The higher long-lived PBS-related fluorescence of the 5th DAS for the light state indicates PBS detachment (an increase in long-time (~ns) DAS amplitudes always points at inefficient EET), and the decrease of PSI-related emission in the 4th and 5th DAS shows that the PBSs detach from PSI (Figure 4.4 E). From the analysis of the cells in different states presented above, we conclude that a fraction of the population of PBSs is detached from PSI in the light state. It appears that this detachment is not generally followed by antenna attachment to PSII, as can be judged from the 3rd-5th DAS.

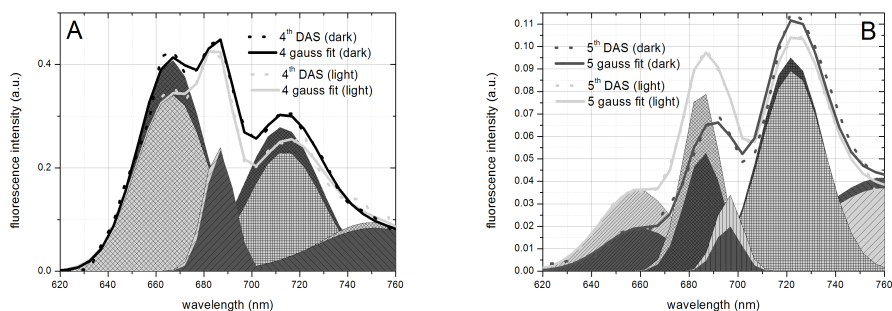


Figure 4.5. Gaussian decomposition of 4th (A) and 5th (B) DAS obtained from global analysis of time-resolved data in dark (black lines) and light (gray lines) states. The solid lines represent the original DAS, while the dotted lines show the spectrum fitted with the Gaussians. Dark and light gray shaded areas represent (dark and light) Gaussian bands. The corresponding parameters can be found in Supplemental Table 1.

4.3.4 Gaussian decomposition of the 4th and 5th DAS

The 680-690 nm region of the 4th and 5th DAS is contributed to by APC₆₈₀, PSII, CP47 in PSII, which are spectrally all very close. Therefore, it is difficult to separate their individual contributions directly by visual inspection. In order to answer the question whether more PBSs are attached to PSII in the light state than in the dark state, we performed a Gaussian decomposition of the 4th and 5th DAS (Figure 4.5). Four Gaussians were needed to decompose the 4th DAS for both states, while five Gaussians were needed for the 5th DAS (Figure 4.5, Supplemental Table 1).

First we checked the amplitude differences for the PSII-related Gaussians of the dark and light states. The area of the PSII-related Gaussian of the 4th DAS (maximum at 685 nm) is the same for the dark and the light state. If more PBSs would attach to PSII in the light, we would expect this area to be higher. However, the area of the CP47-related Gaussian in the 5th DAS, centered at 695-nm, is higher in the light state by 25 %. This increase suggests that PBSs attach to PSII only at the side of the red CP47 Chls. This is in agreement with earlier claims by Bittersmann and Vermaas (Bittersmann and Vermaas, 1991), who suggested the involvement of CP47 in EET between PBS and PSII. In that study, EET from PBS towards PSII in several PSII mutants of *Synechocystis* was measured by time-resolved fluorescence spectroscopy, and it was found that, in the absence of CP47, hardly any excitation energy is transferred to PSII.

Secondly, we looked into the differences of the PBS- and PSI-related Gaussians for the two states. The area of the 665-nm PBS-related Gaussian in the 4th DAS, decreased by 13% in the light. This is almost identical to the total decrease of two PSI-related Gaussians in the 4th and 5th DAS (12 %). In the 5th DAS, the areas of two PBS-related Gaussians, centered at 656 and 685 nm, increase substantially. The increase of the 695-nm Gaussian area constitutes around 2 % of the PBS-related Gaussian area in the 4th DAS. Altogether, this indicates that 13 % of the PBSs of the total PBS pool remain detached from both PSs after they have left PSI, while the amount of PBSs that attaches to the CP47 side in the light state is only minor (2%) (Figure 4.6). By comparing the total area decrease of the PSI-related Gaussians and the increase of the 695-nm Gaussian, we conclude that around 15% of those PBSs that detach from PSI in the light (13% of the total PBS pool) attach to PSII at 695-nm side, while 85% of them remain detached in the light.

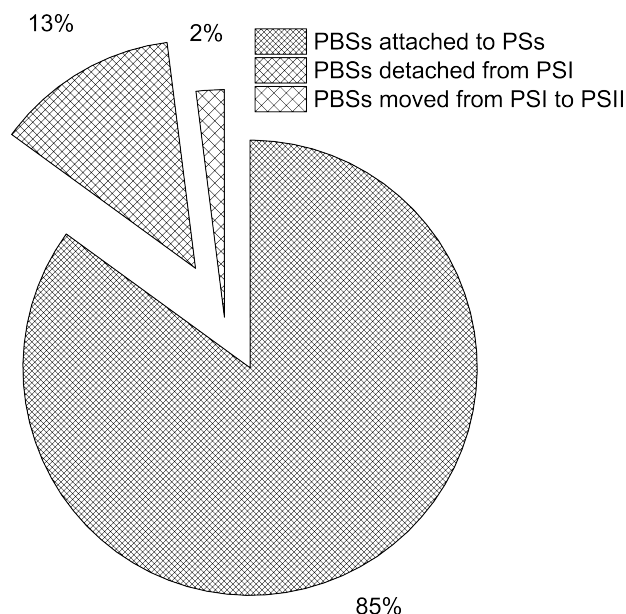


Figure 4.6. Pie graph representing changes in PBS-PS association during dark-light transition. 85% of the PBSs do not change their associations with the PSs during this transition and remain attached to the photosystems; 15% detaches from PSI, while only 2% moves from PSI to PSII.

Due to the fact that the increase of the area of the PC-related band is 50% higher than that of the APC₆₈₀-related Gaussian, the detached PBSs should contain more PC as compared to ‘conventional’ PBSs (Jallet et al., 2012). For this reason, the 2nd DAS shows that fewer PC pigments transfer energy to PSI in the light than in the dark state, while there is no change in the total amount of APC₆₆₀ pigments transferring their excitation energy to APC₆₈₀ and to PSs.

We visualized the steady-state fluorescence spectrum of the detached PBS pool by plotting the intensity difference for the light and dark states in the 5th DAS, after the spectra were normalized to the PSI emission (Figure 4.7). The ratio of the 650-660/685 nm emission bands of the difference spectrum, namely 0.5:1.0, departs substantially from the reported ratios for isolated PBSs, namely 0.15: 1.0 (Jallet et al., 2012). Kondo et al recently reported the existence of ‘alternative’ PBSs consisting of only PC rods that seem to preferentially transfer energy to PSI (Kondo et al., 2007). Such enhanced emission in the 650-660 nm of our difference spectrum as compared to APC₆₈₀, indicates that the detached PBS pool might be mainly represented by this type of PBSs. In (Kondo et al., 2009), it was concluded that such PBSs were not involved in state transitions, but we demonstrate their involvement in dark/light transitions through detachment from PSI in the light state. We suggest that PBSs stay attached to PSI during darkness, because the PQ pool (pool of electron carriers connecting PSI with PSII) is reduced in the dark due to respiration and residual cyclic

[DARK-LIGHT TRANSITIONS IN CYANOBACTERIA]

electron transport. Therefore, once light is introduced again, the primary task of the cell is to achieve a redox balance. A larger PSI antenna in this situation will increase the rate of plastoquinone re-oxidation by PSI. In this way PSII has sufficient electron acceptors to re-reduce. Once sufficient reducing power is achieved, a fraction of PBSs detach from PSI. In this way, over-oxidation of the electron transport chain is avoided.

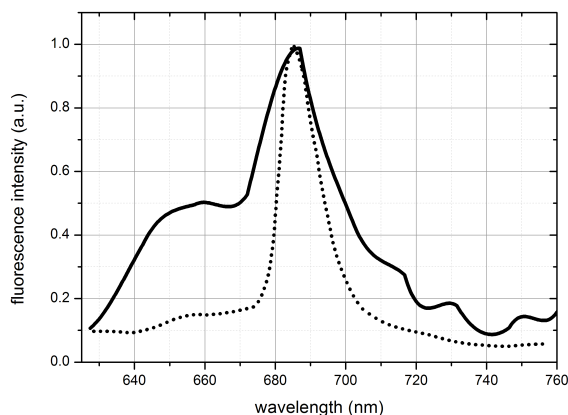


Figure 4.7. Difference spectrum (solid line) obtained by subtracting the 5th DAS for the dark state from that for the light state. Before subtraction, both DAS were normalized to their 722-nm bands. The difference spectrum is compared with the spectrum of isolated PBSs measured at 77K (dotted line, from (Jallet et al., 2012) , red-shifted 5 nm because a different medium was used).

4.4 Concluding Remarks

The rearrangement of photosynthetic apparatus during dark-light transitions is mainly related to PBS coupling/uncoupling to the PSs and it is not affected by PS rearrangements (spillover). We have demonstrated that during dark-light transitions, around 13 % of the total pool of PBSs detaches from PSI. PBS detachment from PSI is generally not followed by attachment to PSII, except for about 2% of the PBSs, which attach to PSII at the CP47 side. We also conclude that the *in vitro* signature of the PBS-PSII-PSI megacomplex, i.e. a slower EET rate from PBS to PSI than to PSII, is not present *in vivo*, neither in darkness nor in light. Therefore, PBS-PSII-PSI megacomplexes do not dominate the fluorescence kinetics and, therefore, if present, they have a very transient role *in vivo*.

Acknowledgments

This project was carried out within the research program of BioSolar Cells, co-financed by the Dutch Ministry of Economic Affairs (to VUC and HvA), and by the

FinSynBio2013 project (N° 272424 to LB and EMA). This work was supported financially by the HARVEST Marie Curie Research Training Network (PITN-GA-2009-238017 to VUC, LB, EMA and HvA) and by the Academy of Finland Projects (N° 271832 to LB and EMA, and N° 273870 to EMA).

References

- Allen, J.F. (2003). Botany. State transitions--a question of balance. *Science* 299:1530-1532.
- Allen, J.F., and Forsberg, J. (2001). Molecular recognition in thylakoid structure and function. *Trends in plant science* 6:317-326.
- Allen, M.M. (1968). Simple Conditions for Growth of Unicellular Blue-Green Algae on Plates. *J Phycol* 4:1-4.
- Andrizhiyevskaya, E.G., Chojnicka, A., Bautista, J.A., Diner, B.A., van Grondelle, R., and Dekker, J.P. (2005). Origin of the F685 and F695 fluorescence in photosystem II. *Photosynth Res* 84:173-180.
- Aoki, M., and Katoh, S. (1982). Oxidation and Reduction of Plastoquinone by Photosynthetic and Respiratory Electron-Transport in a Cyanobacterium *Synechococcus* Sp. *Biochimica et biophysica acta* 682:307-314.
- Ashby, M.K., and Mullineaux, C.W. (1999). The role of ApcD and ApcF in energy transfer from phycobilisomes to PSI and PSII in a cyanobacterium. *Photosynth Res* 61:169-179.
- Bittersmann, E., and Vermaas, W. (1991). Fluorescence Lifetime Studies of Cyanobacterial Photosystem-II Mutants. *Biochimica et biophysica acta* 1098:105-116.
- Bruce, D., Brimble, S., and Bryant, D.A. (1989). State transitions in a phycobilisome-less mutant of the cyanobacterium *Synechococcus* sp. PCC 7002. *Biochimica et biophysica acta* 974:66-73.
- Chereskin, B.M., Clement-Metral, J.D., and Gantt, E. (1985). Characterization of a Purified Photosystem II-Phycobilisome Particle Preparation from *Porphyridium cruentum*. *Plant physiology* 77:626-629.
- Croce, R., and van Amerongen, H. (2014). Natural strategies for photosynthetic light harvesting. *Nature chemical biology* 10:492-501.
- Debreczeny, M.P., Sauer, K., Zhou, J.H., and Bryant, D.A. (1993). Monomeric C-Phycocyanin at Room-Temperature and 77-K - Resolution of the Absorption and Fluorescence-Spectra of the Individual Chromophores and the Energy-Transfer Rate Constants. *J Phys Chem-U*s 97:9852-9862.
- El Bissati, K., Delphin, E., Murata, N., Etienne, A., and Kirilovsky, D. (2000). Photosystem II fluorescence quenching in the cyanobacterium *Synechocystis* PCC 6803: involvement of two different mechanisms. *Biochimica et biophysica acta* 1457:229-242.
- Emlyn-Jones, D., Ashby, M.K., and Mullineaux, C.W. (1999). A gene required for the regulation of photosynthetic light harvesting in the cyanobacterium *Synechocystis* 6803. *Molecular microbiology* 33:1050-1058.
- Glazer, A.N. (1985). Light harvesting by phycobilisomes. *Annual review of biophysics and biophysical chemistry* 14:47-77.
- Jallet, D., Gwizdala, M., and Kirilovsky, D. (2012). ApcD, ApcF and ApcE are not required for the Orange Carotenoid Protein related phycobilisome fluorescence quenching in the cyanobacterium *Synechocystis* PCC 6803. *Bba-Bioenergetics* 1817:1418-1427.
- Joshua, S., and Mullineaux, C.W. (2004). Phycobilisome diffusion is required for light-state transitions in cyanobacteria. *Plant physiology* 135:2112-2119.

[DARK-LIGHT TRANSITIONS IN CYANOBACTERIA]

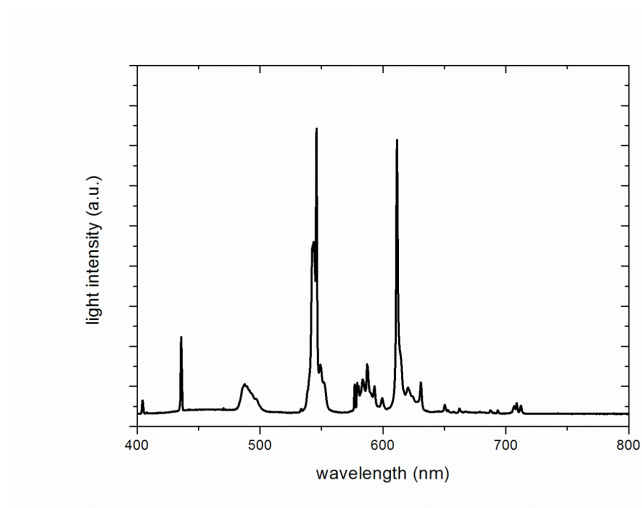
- Kana, R., Kotabova, E., Lukes, M., Papacek, S., Matonoha, C., Liu, L.N., Prasil, O., and Mullineaux, C.W. (2014). Phycobilisome Mobility and Its Role in the Regulation of Light Harvesting in Red Algae. *Plant physiology* 165:1618-1631.
- Kondo, K., Mullineaux, C.W., and Ikeuchi, M. (2009). Distinct roles of CpcG1-phycobilisome and CpcG2-phycobilisome in state transitions in a cyanobacterium *Synechocystis* sp. PCC 6803. *Photosynth Res* 99:217-225.
- Kondo, K., Ochiai, Y., Katayama, M., and Ikeuchi, M. (2007). The membrane-associated CpcG2-phycobilisome in *Synechocystis*: a new photosystem I antenna. *Plant physiology* 144:1200-1210.
- Krumova, S.B., Laptенок, S.P., Borst, J.W., Ughy, B., Gombos, Z., Ajlani, G., and van Amerongen, H. (2010). Monitoring photosynthesis in individual cells of *Synechocystis* sp. PCC 6803 on a picosecond timescale. *Biophysical journal* 99:2006-2015.
- Liu, H.J., Zhang, H., Niedzwiedzki, D.M., Prado, M., He, G.N., Gross, M.L., and Blankenship, R.E. (2013). Phycobilisomes Supply Excitations to Both Photosystems in a Megacomplex in Cyanobacteria. *Science* 342:1104-1107.
- McConnell, M.D., Koop, R., Vasil'ev, S., and Bruce, D. (2002). Regulation of the distribution of chlorophyll and phycobilin-absorbed excitation energy in cyanobacteria. A structure-based model for the light state transition. *Plant physiology* 130:1201-1212.
- Mullen, K.M., and van Stokkum, I.H. (2007). TIMP: an R package for modeling multi-way spectroscopic measurements. *Journal of Statistical Software* 18:1-46.
- Mullineaux, C.W. (2008). Phycobilisome-reaction centre interaction in cyanobacteria. *Photosynth Res* 95:175-182.
- Mullineaux, C.W., and Allen, J.F. (1986). The State-2 Transition in the Cyanobacterium *Synechococcus*-6301 Can Be Driven by Respiratory Electron Flow into the Plastoquinone Pool. *Febs Lett* 205:155-160.
- Mullineaux, C.W., and Allen, J.F. (1990). State-1-State-2 Transitions in the Cyanobacterium *Synechococcus* 6301 Are Controlled by the Redox State of Electron Carriers between Photosystem-I and Photosystem-II. *Photosynth Res* 23:297-311.
- Olive, J., M'Bina, I., Vernotte, C., Astier, C., and Wollman, F.A. (1986). Randomization of the EF particles in thylakoid membranes of *synechocystis* 6714 upon transition from state I to state II. *Febs Lett* 208:308-312.
- Scott, M., McCollum, C., Vasil'ev, S., Crozier, C., Espie, G.S., Krol, M., Huner, N.P., and Bruce, D. (2006). Mechanism of the down regulation of photosynthesis by blue light in the Cyanobacterium *synechocystis* sp. PCC 6803. *Biochemistry* 45:8952-8958.
- Snellenburg, J.J., Laptенок, S.P., Seger, R., Mullen, K.M., and van Stokkum, I.H.M. (2012). Glotaran: A Java-Based Graphical User Interface for the R Package TIMP. *Journal of Statistical Software* 49:1-22.
- Tian, L., Farooq, S., and van Amerongen, H. (2013). Probing the picosecond kinetics of the photosystem II core complex in vivo. *Phys Chem Chem Phys* 15:3146-3154.
- Tian, L., Gwizdala, M., van Stokkum, I.H., Koehorst, R.B., Kirilovsky, D., and van Amerongen, H. (2012). Picosecond kinetics of light harvesting and photoprotective quenching in wild-type and mutant phycobilisomes isolated from the cyanobacterium *Synechocystis* PCC 6803. *Biophysical journal* 102:1692-1700.
- Tian, L., van Stokkum, I.H., Koehorst, R.B., Jongerius, A., Kirilovsky, D., and van Amerongen, H. (2011). Site, rate, and mechanism of photoprotective quenching in cyanobacteria. *Journal of the American Chemical Society* 133:18304-18311.
- Ünlü, C., Drop, B., Croce, R., and van Amerongen, H. (2014). State transitions in *Chlamydomonas reinhardtii* strongly modulate the functional size of photosystem II but not of

[CHAPTER 4]

- photosystem I. *Proceedings of the National Academy of Sciences of the United States of America* 111:3460-3465.
- Van Oort, B., Murali, S., Wientjes, E., Koehorst, R.B.M., Spruijt, R.B., van Hoek, A., Croce, R., and van Amerongen, H. (2009). Ultrafast resonance energy transfer from a site-specifically attached fluorescent chromophore reveals the folding of the N-terminal domain of CP29. *Chem Phys* 357:113-119.
- Van Stokkum, I.H., Van Oort, B., Van Mourik, F., Gobets, B., and Van Amerongen, H. (2008). (Sub)-picosecond spectral evolution of fluorescence studied with a synchroscan streak-camera system and target analysis. In: *Biophysical techniques in photosynthesis: Springer*. 223-240.
- Van Stokkum, I.H.M., Gobets, B., Gensch, T., van Mourik, F., Hellingwerf, K.J., van Grondelle, R., and Kennis, J.T.M. (2006). (Sub)-picosecond spectral evolution of fluorescence in photoactive proteins studied with a synchroscan streak camera system. *Photochem Photobiol* 82:380-388.
- Vernotte, C., Astier, C., and Olive, J. (1990). State 1-state 2 adaptation in the cyanobacteria *Synechocystis* PCC 6714 wild type and *Synechocystis* PCC 6803 wild type and phycocyanin-less mutant. *Photosynth Res* 26:203-212.

SUPPLEMENTARY MATERIAL

1. Spectral profile of the growth light



Supplemental Figure 1.
Spectral profile of the light used for cultivation.

2. Gaussian decomposition of 4th and 5th DAS

The 4th DAS in both states were described by four Gaussians centered at 666 nm, 686 nm, 713-714 nm and 750 nm, respectively (Figure 4.6, Supplemental Table 1). The 666/667-nm Gaussians represent emission from PC and APC pigments in PBSs, while the 686-nm band should be assigned to PSII and maybe (partly) to APC₆₈₀. The last two Gaussians should be mostly attributed to PSI, while some small contribution from PSII and PBS vibration bands is also present. Steady-state fluorescence spectrum of PSII is well known and has two fluorescence emission peaks (685 nm and 695 nm) of around equal amplitudes, arising from CP43 as well as CP47 and from low-energy Chls in CP47, respectively (Andrizhiyevskaya et al., 2005). Both *in vivo* and *in vitro* time-resolved studies demonstrated that Chls emitting at around 685 nm in PSII contributes to the fastest part of PSII fluorescence decay (200-400 ps lifetime) at 77K, while red-absorbing Chls in CP47 decays with around 1 ns lifetime (Liu et al., 2013; Tian et al., 2013). The 5th DAS were decomposed with five Gaussians centered at 656 nm, 686 nm, 696 nm, 722 nm and 760 nm, respectively. Again two the most red-shifted Gaussians should be mostly attributed to PSI. The 656-nm Gaussian

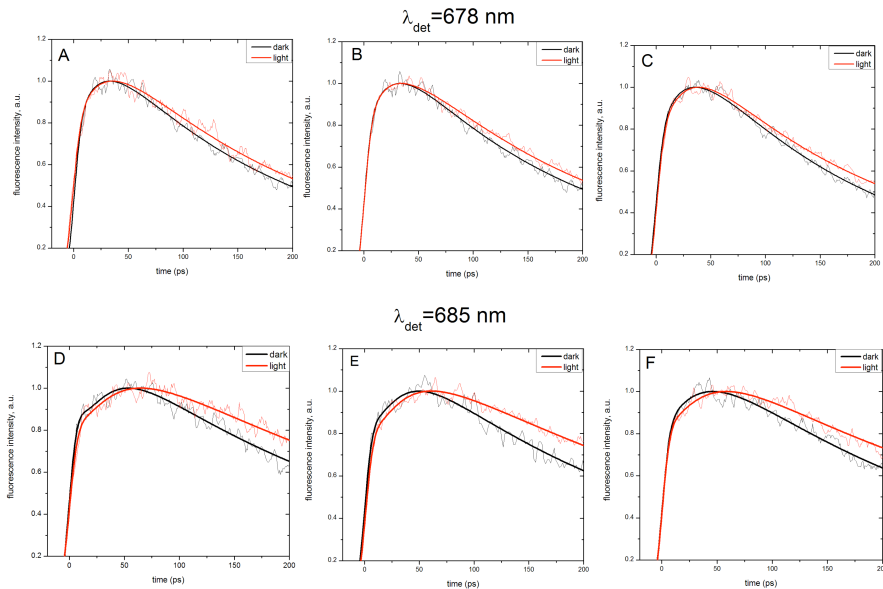
[CHAPTER 4]

mostly represents emission from PC rather than from APC because of its peak position. The 696-nm Gaussian should be mostly constituted by CP47 fluorescence emission in PSII, although the emission from APC₆₈₀ of PBSs in this region cannot be completely excluded. The 686-nm Gaussian of the 5th DAS, due to its lifetime, should be mostly constituted by APC₆₈₀ (Liu et al., 2013). Although its peak position is quite close to the 1 ns component, previously assigned to radical pair formation in PSII, some PSII contribution can not be completely excluded (van der Weij-de Wit et al., 2011).

Supplemental Table 1. *Decomposition of 4th and 5th DAS into Gaussians for dark and light states.*

| | Gauss 1 | Gauss 2 | Gauss 3 | Gauss 4 | Gauss 5 |
|---------------------------|---------|---------|---------|---------|---------|
| WT_{Dark} | | | | | |
| 4th DAS | | | | | |
| Ampl. *100, a.u. | 41 | 23 | | 28 | 8 |
| Peak, nm | 666 | 687 | | 713 | 751 |
| FWHM, nm | 19.5 | 8.5 | | 22 | 34 |
| 5th DAS | | | | | |
| Ampl. *100, a.u. | 1.9 | 5.2 | 2.0 | 9.4 | 4.2 |
| Peak, nm | 656 | 686 | 696 | 722 | 760 |
| FWHM, nm | 21 | 11 | 7.5 | 18 | 40 |
| WT_{Light} | | | | | |
| 4th DAS | | | | | |
| Ampl. *100, a.u. | 34 | 24 | | 23 | 9 |
| Peak, nm | 667 | 686 | | 714 | 750 |
| FWHM, nm | 21 | 8.5 | | 21 | 30 |
| 5th DAS | | | | | |
| Ampl. *100, a.u. | 3.6 | 7.8 | 3.4 | 8.9 | 3.7 |
| Peak, nm | 656 | 685 | 696 | 722 | 760 |
| FWHM, nm | 21.5 | 11 | 7.7 | 19 | 40 |

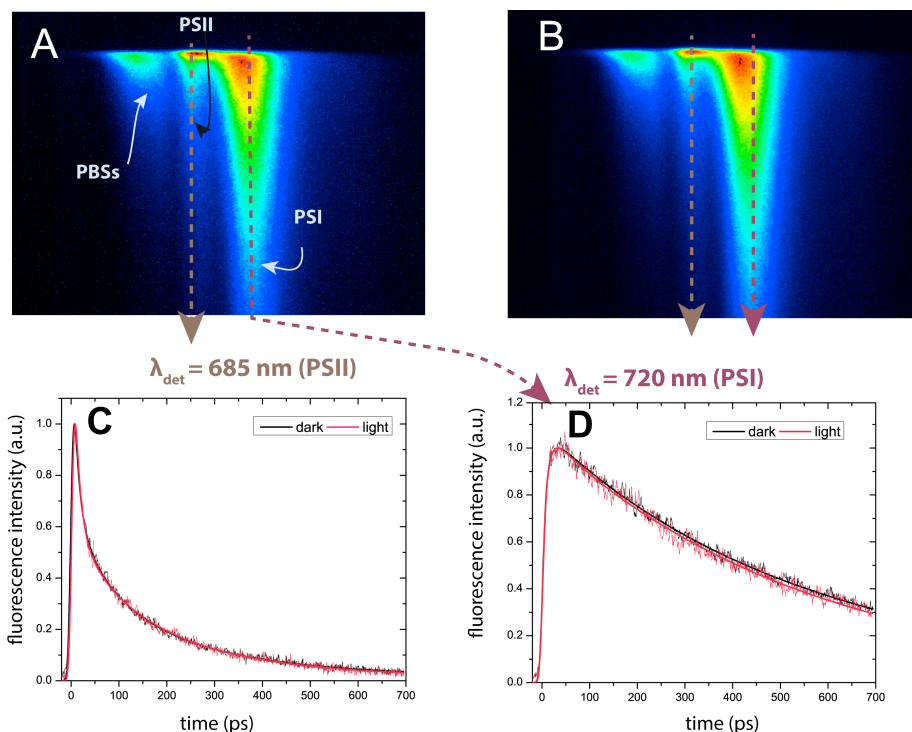
3. Data reproducibility



Supplemental Figure 2. Fluorescence kinetics of excited at 580 nm and detected at 678 nm (A, B, C) and 685 nm (D, E, F) measured for three independent generations.

Each experiment was repeated at least 3 times for different generations of cells. The streak-camera images as well as fluorescence decay curves for every measurement appeared to be very similar in case of independent generations and the difference between 'light' and 'dark' states were consistent. Supplemental Figure 2 shows the initial part of fluorescence kinetics in light/'state 1' and dark/state 2 measured on different generations of the cells detected at 678 nm and at 685 nm. As we see the differences between EET rates between light and dark states are always present at 685 nm and are not observable at 678 nm.

4. Time-resolved measurements upon 400 nm excitation

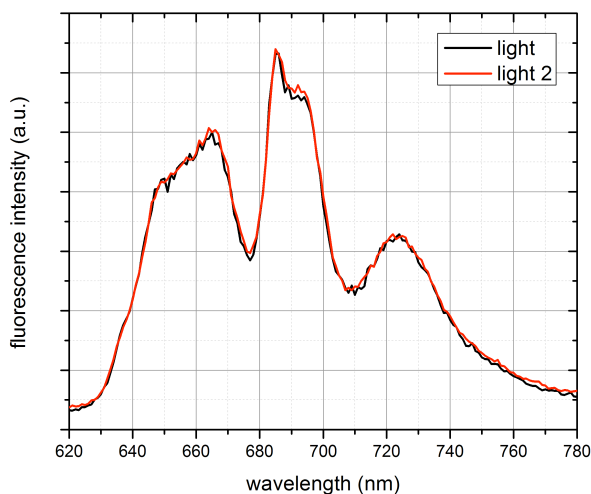


Supplemental Figure 3. Time-resolved fluorescence of *Synechocystis* sp. PCC 6803 measured in dark- (A) and light-adapted states (B) at 77K upon 400 nm excitation. (A, B) Streak-camera images. False colors indicate the fluorescence intensity. (C, D) Representative decay traces were taken at PSII (C) and PSI (D) emission maxima: 685 nm and 720 nm, respectively. For better comparability, the traces in light (red lines) and dark (black lines) states were normalized to their maxima.

5. Reversibility of light-dark transitions

We checked the reversibility of light-dark transition by recording 77 K steady-state fluorescence spectrum on the cells that were adapted for 10 min to light after reaching dark state (10 min of dark-adaptation) (Supplemental Figure 4, light 2). The obtained spectrum was similar to light state.

[DARK-LIGHT TRANSITIONS IN CYANOBACTERIA]



Supplemental Figure 4. Comparison of steady-state fluorescence spectra in light and light 2 (10 min of light-adaptation after dark state) states measured at 77K upon 580 nm excitation.

- Andrizhiyevskaya, E.G., Chojnicka, A., Bautista, J.A., Diner, B.A., van Grondelle, R., and Dekker, J.P. (2005). Origin of the F685 and F695 fluorescence in photosystem II. *Photosynth Res* 84:173-180.
- Liu, H.J., Zhang, H., Niedzwiedzki, D.M., Prado, M., He, G.N., Gross, M.L., and Blankenship, R.E. (2013). Phycobilisomes Supply Excitations to Both Photosystems in a Megacomplex in Cyanobacteria. *Science* 342:1104-1107.
- Tian, L., Farooq, S., and van Amerongen, H. (2013). Probing the picosecond kinetics of the photosystem II core complex in vivo. *Phys Chem Chem Phys* 15:3146-3154.
- Van der Weij-de Wit, C.D., Dekker, J.P., van Grondelle, R., and van Stokkum, I.H. (2011). Charge separation is virtually irreversible in photosystem II core complexes with oxidized primary quinone acceptor. *The journal of physical chemistry. A* 115:3947-3956.

Chapter 5

Cyanobacterial *flv4-2* operon-encoded proteins optimize light harvesting and charge separation in photosystem II

Volha Chukhutsina^{123*}, Luca Bersanini^{4*}, Eva-Mari Aro⁴, Herbert van Amerongen^{123#}

¹Laboratory of Biophysics, Wageningen University, P.O. Box 8128, 6700 ET, Wageningen, The Netherlands

²MicroSpectroscopy Centre, Wageningen University, 6703 HA Wageningen, The Netherlands

³BioSolarCells, P.O. Box 98, 6700AB Wageningen, The Netherlands

⁴Department of Biochemistry, Molecular Plant Biology, University of Turku, FI-20014 Turku, Finland

* V.C. and L.B. contributed equally to this work

accepted in *Molecular Plant*,
<http://dx.doi.org/10.1016/j.molp.2014.12.016>.

Abstract

Photosystem II (PSII) complexes drive the water splitting reaction necessary to transform sunlight into chemical energy. However, too much light can damage and disrupt PSII. In cyanobacteria, the *flv4-2* operon encodes three proteins (Flv2, Flv4 and Sll0218), which safeguard PSII activity under air-level CO₂ and in high-light conditions. However, the exact mechanism of action of these proteins has not been clarified yet. We demonstrate that the PSII electron transfer properties are influenced by the *flv4-2* operon-encoded proteins. Accelerated secondary charge separation kinetics was observed upon expression/overexpression of the *flv4-2* operon. This is likely induced by docking of the Flv2/Flv4 heterodimer in the vicinity of the Q_B pocket of PSII which, in turn, increases the Q_B redox potential and consequently stabilizes forward electron transfer. The alternative electron transfer route constituted by Flv2/Flv4 sequesters electrons from Q_B guaranteeing the dissipation of excess excitation energy in PSII under stressful conditions. In addition, we demonstrate that in the absence of the *flv4-2* operon-encoded proteins about 20% of the phycobilisome antenna becomes detached from the reaction centers, thus decreasing light harvesting. Phycobilisome detachment is a consequence of a decreased relative content of PSII dimers, a feature observed in the absence of the Sll0218 protein.

5.1 Introduction

Photosynthetic organisms use light as a primary source of energy but too much light can create excessive oxidative stress with lethal consequences for the cells. Also other environmental conditions that limit photosynthetic electron transport like inorganic carbon limitation expose cells to enhanced oxidative stress. The excess energy absorbed by antenna pigments, i.e. the energy that cannot be used for photochemical reactions (electron transport), is dissipated as heat in non-photochemical quenching processes (reviewed in (Bailey and Grossman, 2008; Niyogi, 1999)). Photosynthetic organisms use various strategies for (tuning of) the energy dissipation processes (see e.g. (Croce and van Amerongen, 2014)). Cyanobacteria, the ancestors of plant chloroplasts, and in particular the model organism *Synechocystis* sp. PCC6803 (hereafter *Synechocystis*), possess short-term regulation mechanisms which can dissipate the excess energy absorbed by the phycobilisome antenna (PBS) as heat with the help of the Orange Carotenoid Protein (OCP, (Wilson et al., 2006)) and via state

transitions (for a review, see (Mullineaux and Emlyn-Jones, 2005; van Thor et al., 1998)).

Other mechanisms of photoprotection involve the induction of alternative electron transfer routes which dissipate the excess of electrons in the photosynthetic chain, resulting in decreased photodamage of PSI and PSII. Only very recently, proteins encoded by the *flv* genes were discovered to play a central role in the dissipation of excess excitation energy of PSI (Allahverdiyeva et al., 2011; Allahverdiyeva et al., 2013) and PSII (Bersanini et al., 2014; Hakkila et al., 2013; Zhang et al., 2012; Zhang et al., 2009).

The *flv4-2* operon, specifically involved in photoprotection of PSII, is strongly induced at air level CO₂ concentration and/or high light irradiances (HL) (Zhang et al., 2009). These environmental conditions make PSII particularly sensitive to photodamage due to the fact that over-reduction of the terminal acceptors is limiting the photosynthetic electron flow. The operon encodes three proteins (Flv2, Flv4 and Sll0218) and it is conserved among β -cyanobacteria (Zhang et al. 2012). Flv2 and Flv4 form a heterodimer (Flv2/Flv4), which is localized in the cytoplasm but also has a high affinity for the membrane in the presence of cations (Zhang et al., 2012). Flv2/Flv4 constitutes an electron sink at the PSII acceptor side, which allows the PQ pool to be in the oxidized state, protects PSII against photodamage, and concomitantly reduces the production of singlet oxygen (Bersanini et al., 2014). Sll0218 is located in the thylakoid membrane. It forms a high molecular mass complex in association with unknown partners and stabilizes PSII dimers (Zhang et al., 2012). Flv2 and Flv4 are members of the flavodiiron protein (FDP) family. FDPs are electron transfer enzymes spread among strict and facultative anaerobic bacteria, where they are involved in O₂ and/or NO detoxification (Vicente et al., 2008). In oxygenic photosynthetic organisms (mainly cyanobacteria, green algae and lower plants as shown in Zhang et al., 2009), FDPs show a particular composition different from all other FDPs, with an extra C-terminal flavin reductase domain. Apart from Flv2 and Flv4, *Synechocystis* contains two more FDPs encoded by the *sll1521* (*flv1*) and *sll0550* (*flv3*) genes. Flv1 and Flv3 proteins form a very important electron sink which protects PSI from oxidative damage under fluctuating light conditions (Allahverdiyeva et al., 2013). *In vivo*, Flv1 and Flv3 acquire electrons at the acceptor side of PSI and deliver them to molecular oxygen (Allahverdiyeva et al., 2013), reducing it to water without the production of reactive oxygen species (ROS) (Helman et al., 2003), in a process called the “Mehler-like” reaction.

The question how the Flv2/Flv4 operon exactly influences the PSII kinetics has so far remained unanswered. The energy transfer and charge

[ROLE OF FLV4-2 OPERON IN CYANOBACTERIA]

separation kinetics in isolated PSII core particles and PSII cores *in vivo* have been well studied with time-resolved fluorescence and transient absorption measurements. Dominant lifetime components with open RCs (oxidized Q_A) were observed in the range from 35-40 ps (Miloslavina et al., 2006) to 60-80 ps (Schatz et al., 1987; Tian et al., 2013) and around ≈ 300 -500 ps. The first component reflects excitation trapping/primary charge separation in PSII core complexes containing only the antenna complexes CP43 and CP47, while the second has been assigned to secondary electron transfer to the quinone acceptor Q_A together with recombination (Tian et al., 2013; van der Weij-de Wit et al., 2011). The kinetics of PSII with closed RCs (Q_A reduced) in both isolated cores and intact organisms have been studied by a number of groups (Roelofs et al., 1992; Szczepaniak et al., 2009; Tian et al., 2013). One of the most pronounced effects of closing the RC in PSII both *in vivo* and *in vitro* is an increase of the fluorescence yield by a factor of 4–6, and a corresponding lengthening of the average fluorescence lifetime due to slowing down of the charge separation rate (Roelofs et al., 1992; Tian et al., 2013). Therefore, time-resolved fluorescence measurements constitute a valid tool to study if and how the Flv2/Flv4 proteins affect the ultrafast PSII kinetics.

The *flv4-2* operon provides the cells with an important photoprotective mechanism, and it is also important for effective energy transfer from PBSs to PSII in air level CO_2 conditions (Zhang et al., 2012, Bersanini et al., 2014). A high emission peak at 685 nm in the 77K fluorescence spectra, caused by uncoupled PBSs terminal emitters, suggested the occurrence of distorted energy transfer from the PBS terminal emitters to the PSII reaction centers in the *flv4-2* operon deletion mutants.

Both steady-state and time-resolved spectroscopy, at room temperature and at 77K, were applied here to investigate the effects of the *flv4-2* operon on excitation energy transfer (EET) from the PBS antenna and on PSII charge separation kinetics. A deletion ($\Delta flv4$) and an overexpression mutant (OE) of the whole *flv4-2* operon were compared with a wild type (WT) strain. It is demonstrated that deletion of the *flv4-2* operon results in the detachment of around 20% of the PBS antenna, and that the Flv2 and Flv4 proteins are not directly involved in EET from PBSs to PSII but instead the Sll0218 protein is important for this process. Furthermore, the Flv2/Flv4 heterodimer increases charge separation rates within reaction centers of PSII under air level CO_2 conditions by increasing the redox potential of a quinone acceptor.

5.2 Results

5.2.1 Steady-state fluorescence of the *flv4-2* operon mutants

As a first attempt to characterize energy flow from PBS to PSII, the steady-state fluorescence emission spectra were recorded for overexpression (OE) and deletion ($\Delta flv4$) mutants of the *flv4-2* operon, both at 77K and at room temperature (RT). The OE mutant had a 77K fluorescence emission spectrum (excitation light: 580 nm) more similar to the WT spectrum, showing a slightly

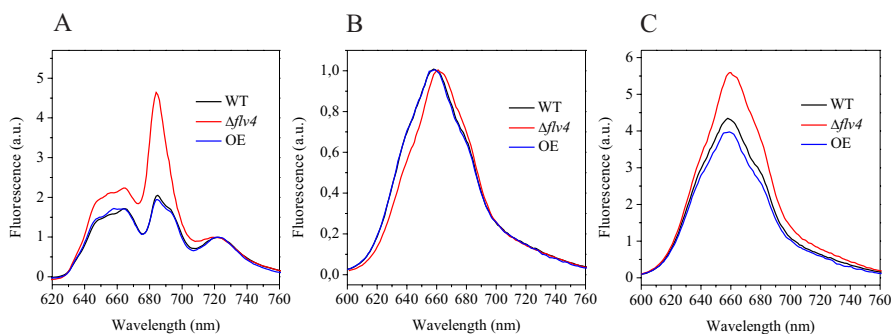


Figure 5.1. Fluorescence emission spectra recorded at 77K (A) and room temperature (B and C) from cultures excited at 580 nm. The cultures were adjusted to the same chlorophyll concentration. The spectra are averages of four different biological replicates. The fluorescence spectra were normalized to the PSI peak (723 nm) in A, and to the 660nm peak in B, while the spectra are not normalized in C.

lower peak at 685 nm as compared with WT (Figure 5.1 A). The lower F685 peak in the OE mutant was interpreted as a signal of enhanced efficiency of EET from PBSs to the PSII reaction centers (Bersanini et al. 2014).

The emission spectra recorded at 77K in the $\Delta flv4$ mutant, showed a higher peak at 685 nm (Figure 5.1 A) in accordance with Bersanini et al. (2014) and Zhang et al. (2012). Since the increase of the F685-nm band was not accompanied by enhancement of the F695-nm band, Zhang et al. concluded that the increase of the F685-nm band results from disturbed energy transfer from terminal emitters of PBSs to the PSII core. In our measurements F685 was always very high in $\Delta flv4$ when compared with the other strains, and F645 and F660,

[ROLE OF FLV4-2 OPERON IN CYANOBACTERIA]

corresponding to the emission of phycocyanin (C-PC) and allophycocyanin (APC) respectively, rose significantly in some of the measurements, resulting in the averaged spectra presented in Figure 5.1A.

To verify that the phenotype of $\Delta flv4$ was due to inactivation of the expression of the *flv4-2* operon a complementation strain was constructed. The expression of the *flv4-2* operon under the control of the *psbA2* promoter in $\Delta flv4$ strain (complementation mutant $\Delta flv4::flv4-2$) resulted in a WT-like phenotype (Supplemental Figure S1).

Fluorescence emission spectra recorded at RT showed a maximum at 660 nm, related to APC₆₆₀ emission. The $\Delta flv4$ mutant showed a decreased 645 nm shoulder and a slight increase of the 685 nm shoulder, when normalized at 660nm (Figure 1B). Non-normalized spectra showed increased F660 for $\Delta flv4$ and slightly decreased fluorescence for OE (Figure 5.1 C). The observed increase at 660 nm in the $\Delta flv4$ mutant indicates lower energy transfer from the PBSs to the reaction centers in agreement with the 77K fluorescence emission spectra.

5.2.2 Time-resolved fluorescence of the *flv4-2* operon mutants at 77K

The influence of the *flv4-2* operon on EET from PBSs towards PSII reaction centers is one of the main issues to be resolved. The time-resolved fluorescence results, obtained with the streak-camera setup at 77 K with 580 nm excitation, are compared in Figure 5.2. No large differences were observed between the WT, OE and $\Delta flv4$ strains in the “raw” streak-camera images (Figure 5.2 A, B, C). However, in agreement with steady-state fluorescence emission measurements (Bersanini et al., 2014; Zhang et al., 2012), the $\Delta flv4$ mutant appeared to have slightly higher and longer-lived emission in the 685 nm region. The time-resolved fluorescence data were fitted globally, and the decay-associated spectra (DAS) for WT, OE and $\Delta flv4$ are presented in Figure 5.2 D, 2 E and 2F, respectively. In all cases, the best fit was obtained with a sum of five exponential components.

The 1st DAS has two positive peaks at 630 and 690 nm and two negative peaks at 650 nm and 720 nm, thus representing energy equilibration in C-PC rods and within PSI, respectively. The 2nd DAS carries the typical signature of EET from C-PC towards APC trimers with maximum emission at 660 nm (APC₆₆₀) as concluded from the positive peak at 640 nm and the negative one at ~665 nm. The 3rd fluorescence decay component represents EET from APC₆₆₀ to APC₆₈₀ and Chls with 85 ps time constant (Tian et al., 2011). All three EET steps correspond to almost identical amplitudes and lifetimes for different strains indicating that EET

within PBSs does not differ for the three strains. The 4th fluorescence decay component represents the contribution from several complexes with corresponding spectra peaking at 665 nm, 682 nm, and 715 nm. The 665 nm peak is characteristic for PBSs (Liu et al., 2013). The 682 nm peak decaying with ~ 250 ps time constant was previously assigned to PSII, while the 715 nm peak is characteristic for PSI (Tian et al., 2013). The 5th DAS represents both PSII (~ 690 nm) and PSI (~ 725 nm), whereas a small contribution from detached PBSs results in the 650-660 nm band. The 360 ps and 1.3 ns lifetimes were reported previously for APC₆₈₀ in vivo (Scott et al., 2006), thus APC₆₈₀ emission might also contribute to the 4th and 5th DAS emission in the 680-685 nm region (Figure 5.3, D, E).

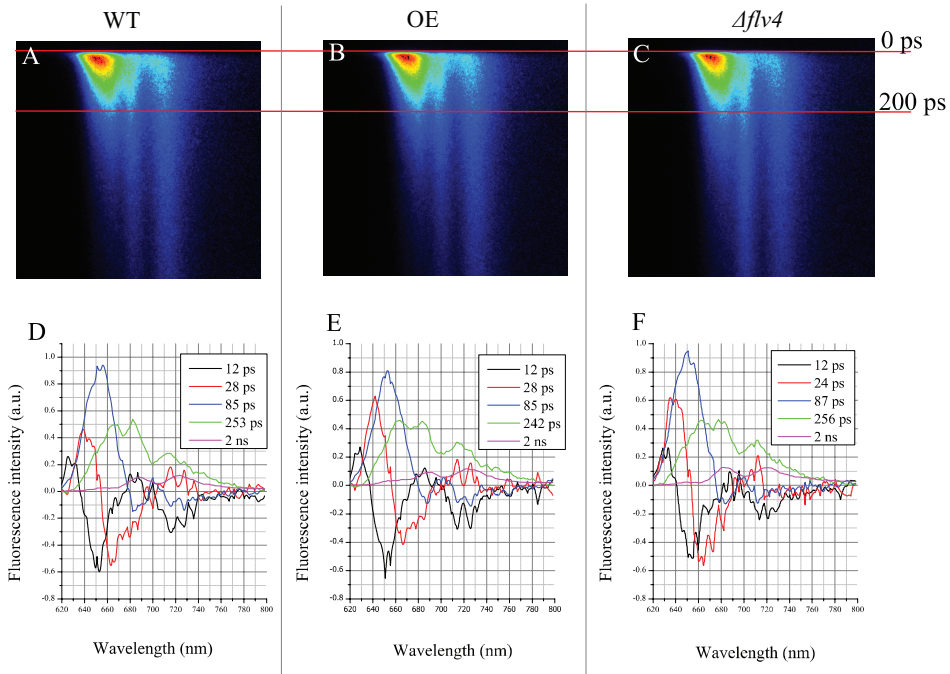


Figure 5.2. Representative streak-camera images (A, B, C) together with the resolved DAS and corresponding lifetimes (D, E, F) obtained for WT (A, D), OE (B, E) and $\Delta flv4$ (C, F) samples measured upon 580 nm excitation at 77K. The overall fluorescence spectra at $t = 0$ (which equals the sum of all DAS) for all three samples were normalized to each other and the DAS were scaled accordingly.

[ROLE OF FLV4-2 OPERON IN CYANOBACTERIA]

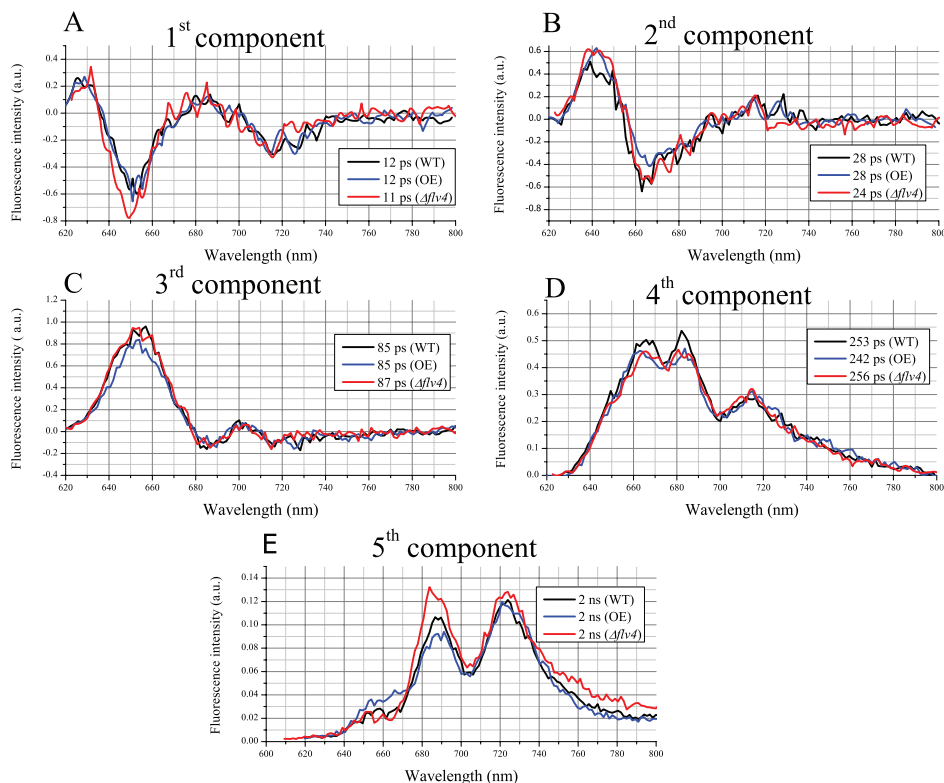


Figure 5.3. Comparison of individual DAS of WT (black lines), OE (blue lines) and $\Delta flv4$ (red lines) from Figure 5.2. To compare the fluorescence intensities of individual DAS, the overall fluorescence spectra at $t = 0$ for all three samples were normalized to each other.

Comparison of individual DAS showed only small differences between WT and OE samples. They were mostly observed in the 3rd -5th DAS and manifested by changes in the DAS amplitudes while the lifetimes of the components hardly differ. The $\Delta flv4$ strain showed some differences with WT in the 4th and 5th DAS. Yet the most pronounced difference between WT and $\Delta flv4$ concerns the higher amplitude of the ~ 685 nm peak of the 5th DAS for $\Delta flv4$ as compared with its counterpart in WT. Since the 5th DAS decays with 2 ns lifetime, its contribution to the total fluorescence yield is the biggest, and it results in the dominant contribution of the 685 nm peak for $\Delta flv4$ in steady-state measurements. This peak position is more

characteristic for APC₆₈₀ emitters than for CP47 of PSII (Liu et al., 2013; Scott et al., 2006). In the context of the lower emission of the 665 nm and 682 nm peaks in the 4th DAS of the $\Delta flv4$ strain, the results suggest some contribution of detached PBS in the sample. However, due to the very close proximity of the 685 nm peak with the PSII emission maxima, the data do not provide strong evidence for disturbed EET from PBSs to RCs in the $\Delta flv4$ mutant.

5.2.3 Time-resolved fluorescence of the *flv4-2* operon mutants at RT

The samples were also measured at their physiological state (RT) and the effect of the *flv4-2* operon-encoded proteins on EET from antenna to PSII RCs was studied.

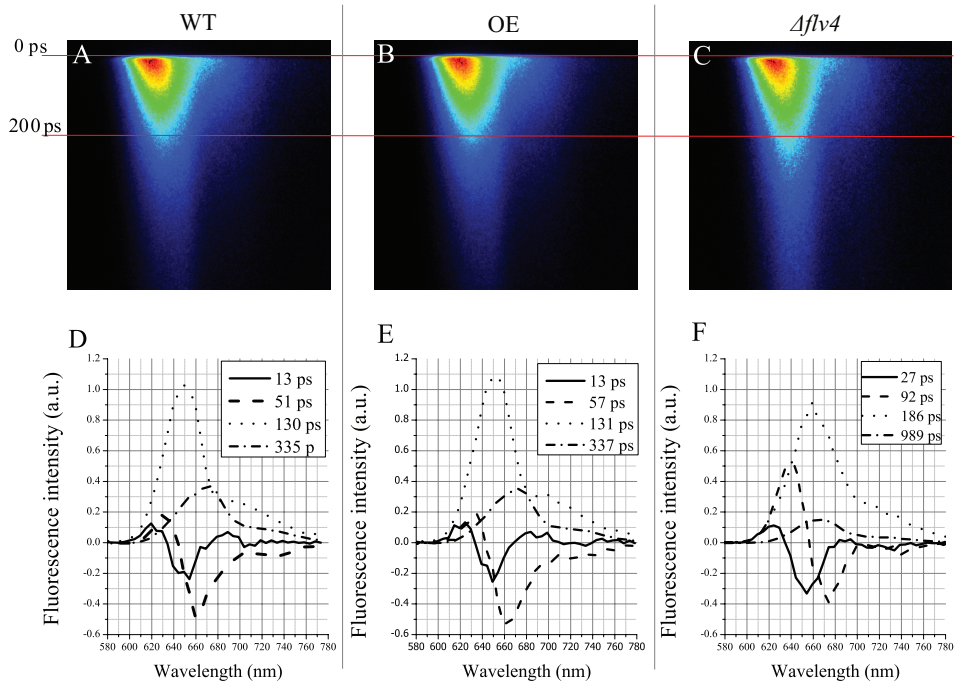


Figure 5.4. Representative streak-camera images (A, B, C) and DAS (D, E, F) obtained for WT (A, D), OE (B, E) and $\Delta flv4$ (C, F) samples upon 580 nm excitation, measured at RT. The overall fluorescence spectra at $t = 0$ for all three samples were normalized to each other and the DAS were scaled accordingly.

[ROLE OF FLV4-2 OPERON IN CYANOBACTERIA]

Differently from the 77K measurements, four components appeared to be enough to describe all streak-camera data at RT (see Supplemental Figure S2; Supplemental Figure S3). The WT and OE mutants showed very similar lifetimes and DAS shapes (Figure 5.4). The fastest component (13 ps) has a positive peak at 620 nm and negative peak at ~ 650 nm, thus representing EET within the C-PC rods at RT. The 2nd component having a positive peak at ~ 640 nm and a negative peak at ~ 660 nm represents EET from C-PC towards APC₆₆₀. The 3rd component with 130 ps lifetime, peaking at 650 nm, largely represents PBS decay. Since in WT and OE the 3rd DAS also shows a strong dip in the 680 nm region, EET to APC₆₈₀ and Chls should contribute to the DAS as well. According to the strongly positive characteristic of the DAS, PBS decay is the dominating process. The 4th DAS represents excitation trapping by PSII RCs.

The global analysis results of the $\Delta flv4$ mutant showed clear differences from those of WT and OE samples at RT. All four lifetimes were substantially longer in $\Delta flv4$. The EET spectrum disappearing with a 92 ps lifetime revealed a more positive amplitude for $\Delta flv4$ than for WT and OE cells, indicating that substantial excited-state decay already occurs on the time-scale of 90 ps, which is also characteristic for isolated PBSs (Tian et al., 2012). Detachment of PBSs in $\Delta flv4$ is also suggested by the fact that the increased lifetime of the 3rd DAS is not linked to a strong dip in the 680 nm region as observed for WT and OE, indicating that EET from APC₆₆₀ to APC₆₈₀ and Chls has also decreased. Most importantly, the 4th DAS changes its shape and instead of peaking at ~ 670 nm which is characteristic for PSII decay due to charge separation, it peaks at ~ 660 nm which reflects PBS emission. The lifetime of the 4th DAS has increased strongly (990 ps for $\Delta flv4$ instead of ~ 340 ps for WT, OE), suggesting distorted EET, which according to the spectral change should originate from detached PBSs.

Comparison of EET efficiency from PBSs towards PSII RCs in OE and WT

We next addressed the question whether OE shows an enhanced efficiency of EET from PBSs towards PSII reaction centers at RT as was suggested previously (Bersanini et al., 2014). The obtained OE and WT datasets of a representative measurement as well as the resolved DAS (Figure 5.4) did not show substantial differences between the two samples. Although some small differences between WT and OE were present, they were subject to variation between the measurements and could come from natural variations observed in different biological replicates. For proper comparison of WT and OE strains, their lifetimes

at four independent measuring days, were all linked together (the lifetimes were equalized for all measuring days, while the amplitudes were allowed to vary) and averaged. The averaged DAS were plotted together with estimated error margins (Figure 5.5).

In agreement with the 77K measurements, the comparison of averaged WT and OE DAS from streak-camera data showed no substantial differences (Figure 5.5), demonstrating that EET from PBS to RCs does not differ for OE and WT.

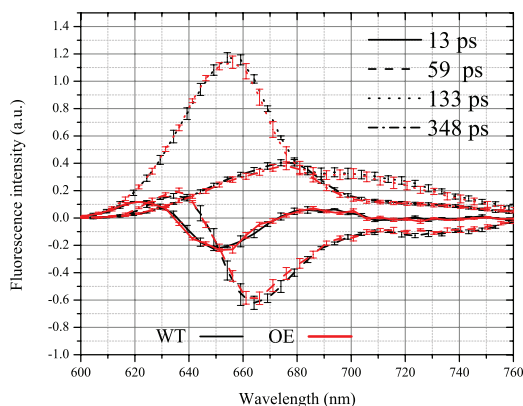


Figure 5.5. Comparison of averaged DAS together with their error margins for WT (black lines) and (red lines) OE cells upon 580 nm excitation, measured at RT. The overall fluorescence spectra at $t = 0$ for WT and OE samples were normalized to each other and the DAS were scaled accordingly. The lifetimes of the corresponding DAS are presented in the legend.

Comparison of EET the efficiency from PBSs towards PSII RCs in WT and $\Delta flv4$

From the streak-camera data presented in Figure 5.4, we can conclude that the $\Delta flv4$ fluorescence decays slower than the WT one. A linked analysis of representative WT and $\Delta flv4$ datasets was then performed in order to understand what is influencing the fluorescence decay behavior of the $\Delta flv4$ strain. The result is presented in Figure 5.6.

The two fastest components represent EET within PBSs. The amplitudes do not differ for WT and $\Delta flv4$, and this confirms again that EET steps within PBSs are not affected by the $flv4-2$ operon-encoded proteins. The main difference between WT and $\Delta flv4$ relates to the two slowest components with lifetimes 159 ps and 654 ps. The amplitude of the 159 ps DAS, which is mainly assigned to PBSs because of the spectral shape, decreases by around 16% in $\Delta flv4$. This decrease is accompanied by a similar increase of the amplitude of the 4th (654 ps) DAS in $\Delta flv4$

[ROLE OF FLV4-2 OPERON IN CYANOBACTERIA]

as compared to WT. The 4th DAS for $\Delta flv4$ peaks at ~ 665 nm instead of 680 nm for WT, which is strongly reminiscent of the spectrum of PBSs. This reflects some PBS detachment in $\Delta flv4$ which also leads to an increase of the fluorescence lifetime.

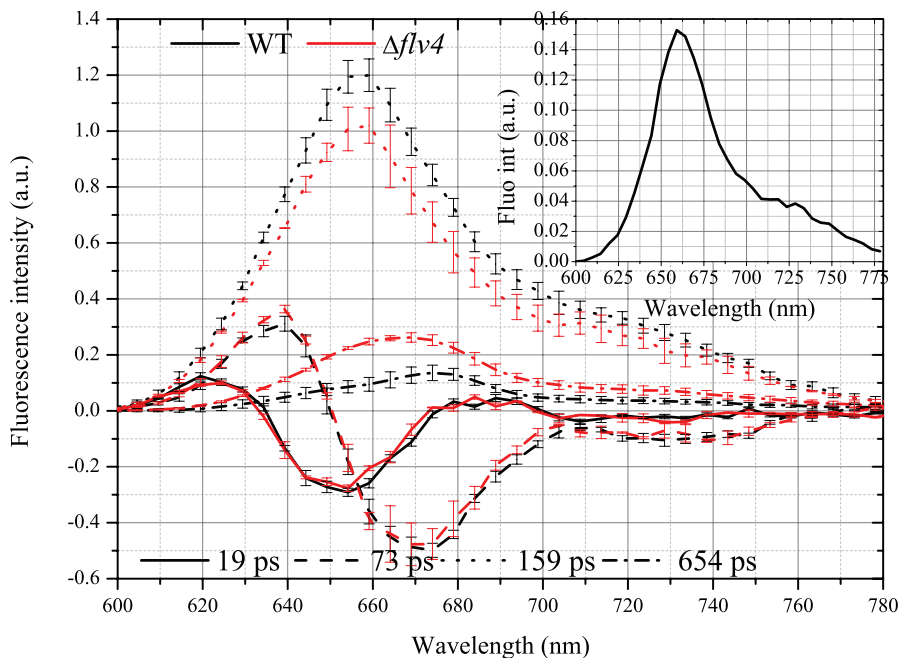


Figure 5.6. Comparison of averaged DAS together with their error margins for WT (black lines) and $\Delta flv4$ (red lines) cells upon 580 nm excitation, measured at RT. The overall fluorescence spectra at $t = 0$ for WT and $\Delta flv4$ were normalized to each other and the DAS were scaled accordingly. The insert represents the difference spectrum of the 4th DAS ($\Delta flv4$ minus WT spectra).

This is confirmed by the difference spectra for WT and $\Delta flv4$ mutant, calculated by subtraction of the fluorescence emission spectrum of the 4th DAS of WT from that of $\Delta flv4$ (Figure 5.6, insert). The difference spectrum does not have any shoulder or band in the 680 nm region but represents the PBS peak at 660 nm, thus confirming that the increase of fluorescence in the spectra indeed reflects detached PBSs and is not due to a higher contribution of closed RCs observed for $\Delta flv4$ (see section “Effect of *flv4-2* operon-encoded proteins on EET and charge separation in PSII”). This effect on the 4th fluorescence decay component of $\Delta flv4$ is

caused by the decoupling of around 16% of the PBSs, as calculated from the change in the amplitude of the 3rd component.

5.2.4 Organization of the PSII complexes in the *flv4-2* operon mutants

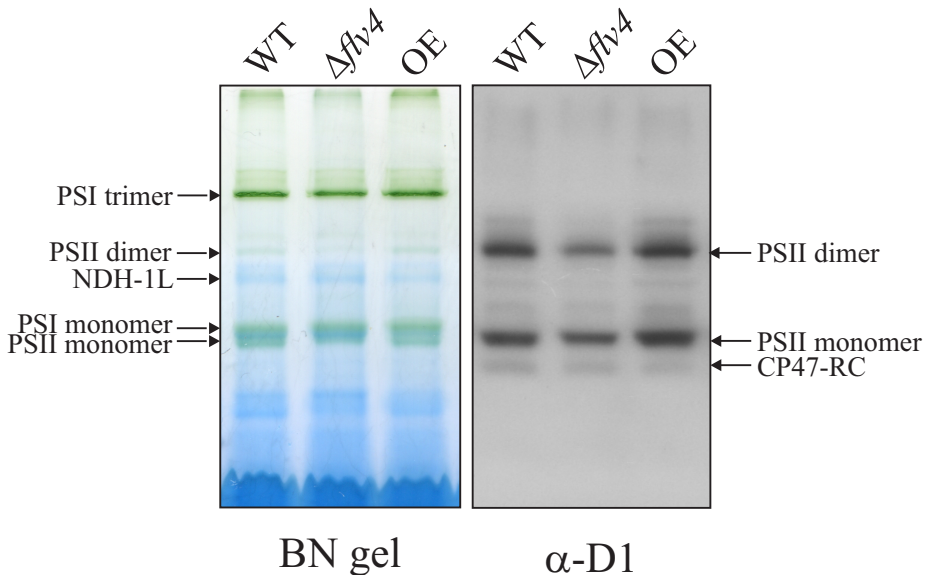


Figure 5.7. Different forms of the PSII complexes in the WT, $\Delta flv4$ and OE strains. Representative BN-PAGE gel and respective D1 protein immunoblot demonstrating the different PSII complexes. Thylakoid membranes were isolated from the cells grown at air level of CO₂ and subsequently applied to BN-PAGE. After electrotransfer, the polyvinylidene fluoride membranes were probed with the D1 antibody.

The thylakoid membranes of WT and *flv4-2* operon mutants were analyzed with blue native (BN)-PAGE gels (Figure 5.7). Three major forms of PSII complexes were identified after BN-PAGE: the dimer, the monomer, and the CP47-RC monomer, i.e. the PSII monomeric complex that lacks the CP43 protein. The PSII core protein D1 was quantified by immunoblotting the BN gel, in order to give an estimation of the amounts of the different PSII complexes (Table 1). The PSII total content and the PSII dimer to monomer ratio in the WT and OE strains were

[ROLE OF FLV4-2 OPERON IN CYANOBACTERIA]

comparable (Figure 5.7 and Table 1). Additionally, the OE strain showed a decreased content of CP47-RC and equal increase of relative content of both PSII dimer and monomer forms. As reported earlier by Zhang et al. (2012), the $\Delta flv4$ mutant had lower amounts of PSII than the WT. Further, a clear decrease of PSII dimer and a minor decrease of PSII monomer complexes were evident in the $\Delta flv4$ mutant, resulting in a decreased PSII dimer to monomer ratio. Previously, the PSII dimer/monomer ratio was suggested to be regulated by the Sll0218 protein (Zhang et al., 2012). Considering these results, we suggest a correlation between the reduction of the PSII dimer to monomer ratio and the antenna detachment, which is displayed by a consistent increase of PBS fluorescence in $\Delta flv4$.

Table 1. Quantification of the different forms of PSII complexes in the WT, OE and $\Delta flv4$ strains.

| Strain | Total (%) | Different forms of PSII (%) | | | dimer/monomer |
|---------------|-----------|-----------------------------|---------|---------|---------------|
| | | PSII dimer | monomer | CP47-RC | |
| WT | 100 | 44 ± 6 | 45 ± 3 | 11 ± 4 | 1,0 ± 0,2 |
| OE | 104 ± 2 | 48 ± 2 | 49 ± 3 | 3 ± 1 | 1,0 ± 0,1 |
| $\Delta flv4$ | 55 ± 2 | 35 ± 3 | 54 ± 4 | 11 ± 4 | 0,6 ± 0,1 |

The quantification was performed from immunoblots with the D1 antibody of four independent BN-PAGE gels. The values are the means of the D1 signals of the three PSII complexes ± SD.

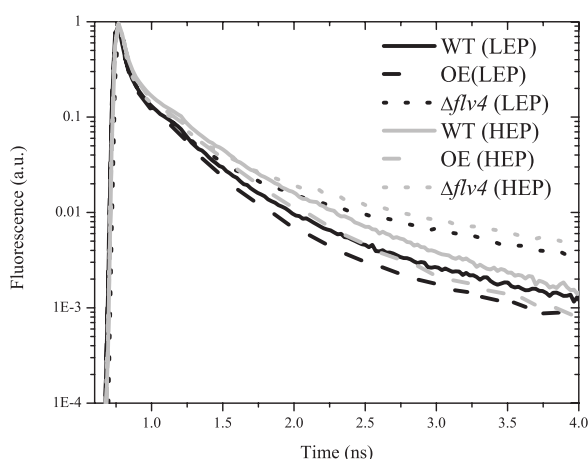


Figure 5.8. Comparison of individual fluorescence decay curves measured at room temperature ($\lambda_{exc}=440$ nm, $\lambda_{det}=679$ nm) for different cells when the samples were measured during low excitation pressure (LEP, black lines) and high excitation pressure (HEP, gray lines) conditions (see Materials and Methods for measuring details).

5.2.5 Effect of *flv4-2* operon-encoded proteins on EET and charge separation in PSII

In order to investigate further the effect of the expression of the *flv4-2* operon on PSII EET and charge separation rates, the fluorescence decay kinetics of WT, OE and $\Delta flv4$ were measured with the time-correlated single-photon counting setup (TCSPC). To maximize Chl *a* excitation and minimize PBS excitation, the cells were excited at 440 nm. In this case PBSs are hardly excited (<10 %) (Supplemental Figure S4, Supplemental Table S1) and the decay traces are dominated by the contribution of Chl *a* in PSI and PSII.

Representative decay curves measured at 679 nm are presented in Figure 5.8. OE traces were always faster than those of WT, when measured at both low and high excitation pressure conditions (LEP and HEP, respectively) whereas the decay for $\Delta flv4$ was always slower than in WT.

According to (Bersanini et al., 2014; Zhang et al., 2012), the Flv2/Flv4 heterodimer accepts electrons at the secondary electron-accepting PQ (Q_B) pocket of PSII. Considering this, it becomes important to assess whether charge separation times of OE and $\Delta flv4$ differ from those of WT. To obtain more quantitative information on the fluorescence decay kinetics, we fitted the decay curves to a multi-exponential decay function. To separate the PSI-related fluorescence decay components from PSII-related decay kinetics, the decay traces detected at three different wavelengths were globally analyzed (Table 2). In all cases, the data were well described by 4 decay components (Table 2). In LEP, the contribution of photochemistry is almost negligible, thus changes in PSII fluorescence lifetimes are related to charge separation kinetics, which almost does not affect redox state of PQ pool; in HEP more reduced Q_A and Q_B and sequentially lengthening of PSII lifetimes represent changes in both charge separation as well as PQ redox state (Tian et al., 2013).

The fastest decay component with ~ 25 ps lifetime is mostly attributed to PSI since its contribution increases from 81-86 % to 95-96 % going from 680 nm to 720 nm detection wavelengths (Table 2). The high amplitude is due to the fact that the Chl molecules are mainly localized in the core antenna of cyanobacteria: the Chl/P700 ratio in each PSI monomer complex is 96 (Jordan et al., 2001), whereas the Chl/P680 ratio in each PSII monomer complex is only 35 (Umena et al., 2011). So almost 90% of Chls in *Synechocystis* are localized in PSI (PSI/PSII = 4) (Stadnichuk et al., 2009). Some small contribution of PSII decay kinetics to the shortest component especially at 679 nm cannot be excluded. It should be mentioned that the amplitudes and lifetimes of the PSI-related component do not

[ROLE OF FLV4-2 OPERON IN CYANOBACTERIA]

vary in LEP or HEP conditions for any individual sample, excluding a role of spillover for adaptation to HEP conditions. The 2nd and 3rd fluorescence decay components are mostly attributed to PSII since their amplitudes had a peak at 679 nm where PSII has its highest contribution. Those components obtained for the WT/OE measurements in LEP conditions fall in the range of 140-170 ps and 360-400 ps. The latter was reported before and was attributed mostly to electron transfer to Q_A (secondary charge separation) in open RCs. On the other hand, the shortest PSII-related components (140 -170 ps) dominate the PSII fluorescence kinetics, just like the 40-80 ps DAS, resolved in previous time-resolved studies (Schatz et al., 1988; van der Weij-de Wit et al., 2011; Vassiliev et al., 2002), and it is influenced by excitation trapping within PSII and primary charge separation kinetics (van Oort et al., 2010). The relative contribution of the shortest PSII-

Table 2. Global fitting results of time-resolved fluorescence kinetics resolved upon 440 nm excitation.

| Low Excitation pressure (LEP) | | | | High excitation pressure (HEP) | | | |
|-------------------------------|--------------|-----------|-----------|--------------------------------|--------------|-----------|-----------|
| Lifetime, ps | Amplitude, % | | | Lifetime, ps | Amplitude, % | | |
| | 679 nm | 693 nm | 721 nm | | 679 nm | 693 nm | 721 nm |
| WT | | | | | | | |
| 21 | 81.7 | 90.5 | 94.9 | 28 | 80.8 | 88.3 | 95.1 |
| 138 | 13.4 | 6.9 | 4 | 191 | 14 | 9.2 | 4 |
| 402 | 4.6 | 2.3 | 0.9 | 529 | 4.8 | 2.3 | 0.8 |
| 1965 | 0.2 | 0.1 | 0.2 | 1823 | 0.3 | 0.2 | 0.1 |
| OE | | | | | | | |
| 21 | 82.3 | 91.5 | 95.2 | 26 | 81.6 | 87.2 | 94.7 |
| 140 | 12.2 | 6.0 | 3.7 | 169 | 14 | 10.2 | 4.7 |
| 359 | 5.3 | 2.4 | 1.0 | 464 | 4.2 | 2.2 | 0.6 |
| 2096 | 0.2 | <0.1 | <0.1 | 1780 | 0.2 | 0.1 | <0.1 |
| <i>Δflv4</i> | | | | | | | |
| 24 | 86.1 | 93.1 | 96 | 24 | 86.8 | 92.3 | 96 |
| 195 | 12.4 | 6.1 | 3.6 | 191 | 11.1 | 6.6 | 3.5 |
| 925 | 1.3 | 0.6 | 0.3 | 764 | 1.7 | 0.9 | 0.4 |
| 2454 | 0.3 | 0.2 | 0.1 | 2493 | 0.4 | 0.2 | 0.1 |

related components (140 -170 ps) to the total PSII amplitude is somewhat lower especially at 679 nm in LEP conditions than the relative amplitude of the 40-80 ps DAS reported before (WT: 70% (current work), 78-81% from (Schatz et al., 1988; van der Weij-de Wit et al., 2011; Vassiliev et al., 2002). The 8-11% decrease indicates that most probably the 21-28 ps component is also partly “contaminated” by PSII. That explains why our fastest PSII-related components are longer-lived than those previously reported, while the average fluorescence lifetime is of the same order ($\lambda_{\text{det}} = 680 \text{ nm}$: 60 ps (WT, current work), 75 ps (PBS-less mutant (PAL), from (Tian et al., 2013).

In the WT strain, both PSII-related lifetimes (2nd and 3rd components) became considerably longer-lived in HEP as compared with LEP conditions (by 50 ps and 130 ps, respectively), indicating an increase of closed RCs in HEP. In OE, the lifetime of the 2nd component did not change considerably both in LEP and HEP, while the lifetime of the 3rd one increased by 100 ps in HEP. The lifetime of the 3rd component was shorter in OE compared with WT already in LEP, demonstrating an increase of secondary charge separation and a concomitant decrease of back charge recombination (Schatz et al., 1988; Szczepaniak et al., 2009; Tian et al., 2013). The differences do not originate from changes in PQ pool redox state, since it hardly affects PSII fluorescence lifetimes in LEP, which mostly represent energy trapping and primary/secondary charge separation rates (van Oort et al., 2010). In general, the amount of closed RCs was higher for WT than for OE in both LEP and HEP. The resolved PSII components for $\Delta flv4$ were considerably longer than those obtained for WT and OE both in LEP and HEP measurements (Table 2). This indicates a significant build-up of RCs with reduced Q_A in $\Delta flv4$ already in LEP conditions when the probability of a PSII being excited is almost negligible due to low photon density. Thus, PSII lifetimes of $\Delta flv4$ in LEP are affected by decreased charge separation exclusively, while the longer PSII lifetimes in HEP are caused by Q_A reduction as well as concomitant reduction of the PQ pool. The higher amount of reduced Q_A in the $\Delta flv4$ samples can be partially caused by PSII monomerization, since a higher redox potential of Q_A/Q_A^- and inefficient forward electron transfer was suggested in one fraction of the PSII monomers isolated from the cyanobacterium *Thermosynechococcus elongates* (Mamedov et al., 2007). However, in our case the effect should be mostly Flv-related, since OE shows faster PSII lifetimes than WT, although both samples have the same PSII monomer/dimer ratios (Table 1).

The fluorescence decay component with the longest lifetime (2.0- 2.5 ns) in the samples most probably originated from closed RCs and/ or free Chl. Since its contribution was almost negligible and the variation of its relative amplitude in

different measuring conditions (LEP or HEP) was extremely small, if present at all ($\leq 0.1\%$), its origin could not be identified.

In summary, the *flv4-2* operon neither affects the PSI fluorescence lifetimes nor the PSII/PSI ratio. The deficiency of *flv4-2* operon-encoded proteins strongly slows down PSII fluorescence kinetics by reducing Q_A even when the measuring conditions minimize the chance of PSII being excited, indicating a strong decrease of charge separation with concomitant increase of backward charge recombination. This is in agreement with the model proposed by Zhang et al. (2012), where the Flv2/Flv4 heterodimer is supposed to intercept electrons from the Q_B pocket of PSII. But the reason for such pronounced differences in the reduction state of Q_A between different *flv4-2* operon mutants should be still further investigated.

5.2.6 Thermoluminescence characteristics of the *flv4-2* operon mutants

The changes in secondary charge separation kinetics of PSII in the *flv4-2* operon mutants might arise as a consequence of a different redox potential of Q_A and/or Q_B in the mutants. To resolve this issue, WT and *flv4-2* operon mutants were subjected to thermoluminescence (TL) characterization. The TL curves of WT showed a characteristic peak around 31-32°C, the so-called B band, which arises from $S_2Q_B^-$ recombination when a single saturating flash is applied (Demeter and Vass, 1984; Rutherford et al., 1982). A shift of the B band to higher temperature was observed in the OE mutant (33.6 °C), while in $\Delta flv4$ the TL peak moved to lower temperature (29.7 °C, see Figure 5.9 A). Another important TL band, the Q band, is obtained by the addition of DCMU, an electron transfer inhibitor of the Q_A to Q_B electron transfer. The Q band is characterized by a typical downshift of the position of the major TL peak to 23°C in the WT, and it arises from $S_2Q_A^-$ recombination (Droppa et al., 1981; Rutherford et al., 1982).

Nevertheless, the peak temperature values for the Q band were similar in the mutants and WT (Figure 5.9 B). Deconvolution analysis for the B and Q bands (Supplemental Figure S5 and Supplemental Table S2) support the data presented in Figure 5.9.

The amplitudes of the B and Q bands (Figure 5.9) were lower for $\Delta flv4$ in comparison to WT, due to a reduced PSII content (Zhang et al., 2009; Zhang et al., 2012), while the peak amplitudes were comparable for WT and OE strains.

These results indicate the absence of a shift of the redox potential of Q_A in the *flv4-2* operon mutants. On the contrary, the shifted position of the B band in the mutants as compared to WT suggests that the presence of the *flv4-2* operon-encoded proteins (WT and OE) could increase the redox potential of Q_B , thus expanding the redox gap between Q_A and Q_B and favoring forward electron transfer. In the absence of *flv4-2* operon-encoded proteins ($\Delta flv4$), the shift of the B band to lower temperature might indicate reduced redox potential of Q_B , thus favoring backward electron transfer towards Q_A .

To conclude, the presence of *flv4-2* operon-encoded proteins is likely to induce a modification of the Q_B redox potential to favor forward electron transfer, resulting in increased charge separation, as described in the previous paragraph.

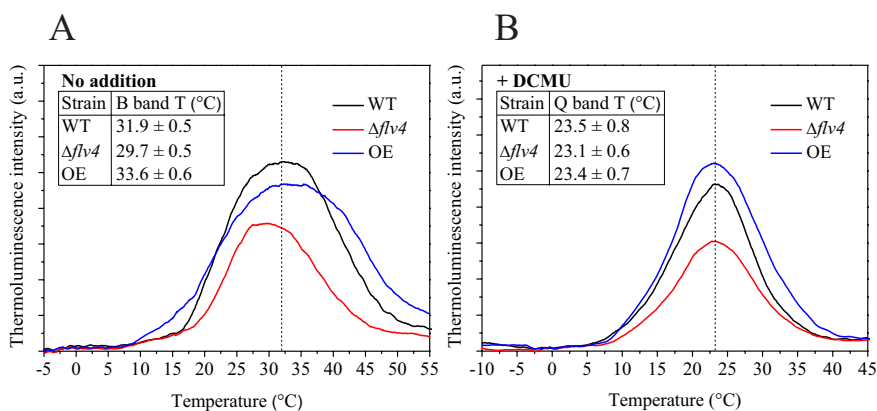


Figure 5.9. Thermoluminescence characteristics of the WT, OE and $\Delta flv4$ strains. Filter paper disks containing a quantity of 25 μg Chl of cells were excited with a single turnover saturating flash at $T = -20^\circ\text{C}$. The measurements were performed in the absence of electron transport inhibitors (A) and in the presence of 10 μM DCMU (B). Thermoluminescence was measured on at least four biological replicates by using 0.6°C s^{-1} heating rate. The tables in the graphs reports the peak temperature of thermoluminescence bands (B band with no addition and Q band with addition of DCMU) \pm SD. The dashed lines indicate the WT peak temperature for B band (A) and Q band (B).

5.3 Discussion

5.3.1 Deletion of the *flv4-2* operon results in antenna detachment

The *flv4-2* operon-encoded proteins were shown to be important for PSII stability, electron transfer properties, and also for EET from PBS to RCs (Zhang et al., 2012, Bersanini et al., 2014). In particular, an increased fluorescence emission at 685 nm in the 77K measurements of the $\Delta flv4$ mutant was indicative of distorted energy transfer between PBS and RCs (Figure 5.1 A, Zhang et al 2012), but the underlying mechanism has remained elusive. It is relevant to understand i) whether the excitation energy transfer is distorted within PBS or from PBSs towards the RCs; ii) if this is a secondary effect or it is related directly to structural association of the *flv4-2* operon-encoded proteins to PBS, and finally iii) whether the changes of the F685 intensity are related to a relative increase of PBS-PSII association rather than to PBS-PSI association.

In the current work, EET from PBSs towards RCs was closely studied using both steady-state and time-resolved fluorescence measurements performed at 77K and RT. At a first glance, the steady-state fluorescence measurements at RT suggested the presence of disconnected PBS in the $\Delta flv4$ mutant (Figure 5.1 C). Streak-camera measurements at 77K and RT revealed that the *flv4-2* operon encoded proteins do not affect EET steps within PBSs. Since at 77K the fluorescence yield of both PSII and PSI increase substantially as compared with RT, even small variations in PBS-PSII/PBS-PSI as well as PBS/RC ratios cause changes in the amplitude of steady-state fluorescence peaks making the latter technique unsuitable to draw conclusions about alterations in EET from PBSs towards RCs.

Time-resolved RT measurements provided strong evidence that deletion of the *flv4-2* operon affects EET from PBSs towards RCs and leads to decoupling of part of the PBSs (~16 %). This effect by far dominates the difference between WT and $\Delta flv4$ time-resolved data upon PBS excitation as compared to the higher amount of closed RCs in $\Delta flv4$ (observed by TCSPC upon Chl *a* excitation, Figure 8). In fact, PBS fluorescence contributed predominantly to the increase of amplitude in the 4th DAS (650 ps) of $\Delta flv4$ (see Figure 5.5 (insert)) instead of PSII emission (~670-680 nm). Based on our results, we conclude that the streak camera measurements at RT constitute a reliable way to quantify the amount of detached antenna from RCs in cyanobacteria.

Interestingly, the overexpression of the *flv4-2* operon (OE mutant) did not produce any significant alteration in the EET rate from PBS to RCs.

5.3.2 Antenna detachment is caused by destabilization of PSII dimers

BN-PAGE gel experiments (Figure 5.7) showed that the PSII dimer to monomer ratio is around 1 in WT and OE strains. However, the $\Delta flv4$ strain showed a strong decrease of PSII content in general, and in particular of PSII dimers (PSII dimer/PSII monomer ~ 0.6), with a relative decrease of PSII dimer content in relation to WT of around 20%. Importantly, we did not detect an increase of EET efficiency towards PSII in the OE mutant, but we clearly observed that almost 20% of PBSs are decoupled from the RCs in $\Delta flv4$. Further, the phycobilin to Chl *a* ratio is not significantly changed in these three strains (Supplemental Figure S6), suggesting that the amount of PBS is proportional to the Chl *a*-containing complexes in all the strains. In light of these results, we suggest that the detachment of PBS is a secondary effect related mainly to the instability of PSII dimer complexes in the $\Delta flv4$ mutant (Figure 5.10 A). The decrease of the PSII dimer content was shown to be related to the absence of the Sll0218 protein (Zhang et al., 2012). This suggests that the absence of the Flv2/Flv4 heterodimer does not play a role in antenna detachment, which is more likely related to the lack of the Sll0218 protein.

Other mutations resulting in an altered PSII dimer to monomer ratio have also been shown to affect EET from antennae to reaction centers, resulting in increased F685 in 77K fluorescence emission measurements. A few examples are the $\Delta pgsA$ mutant, lacking normal phosphatidylglycerol content (Sakurai et al., 2007), the iron-starved $\Delta IsiA$ mutant (Wilson et al., 2007), and $\Delta psbT$ (Bentley et al., 2008; Young, 2010). Many studies support the fact that PBSs attach well to PSII dimers but not to monomers (Arteni et al., 2009; Bald et al., 1996; Barber et al., 2003; Mörschel and Mühlethaler, 1983; Mörschel and Schatz, 1987). These observations support the interpretation that energy harvested by PBSs flows only or majorly to PSII dimers, and not to PSII monomers, explaining the distorted energy transfer observed in the *flv4-2* operon and other mutants with relatively decreased PSII dimer content.

The monomerization of PSII dimers under stressful conditions is a common process among photosynthetic organisms. In fact, it is considered to be a prerequisite for the PSII repair process, both in cyanobacteria and in higher plant thylakoids (for reviews see (Aro et al., 2005; Nixon et al., 2005)). Furthermore, PSII monomerization is accompanied by antenna dissociation, as demonstrated in the present work for cyanobacteria. In higher plants, the light-harvesting complex of PSII (LHCII) antenna detaches from photodamaged PSII in grana appressions.

[ROLE OF FLV4-2 OPERON IN CYANOBACTERIA]

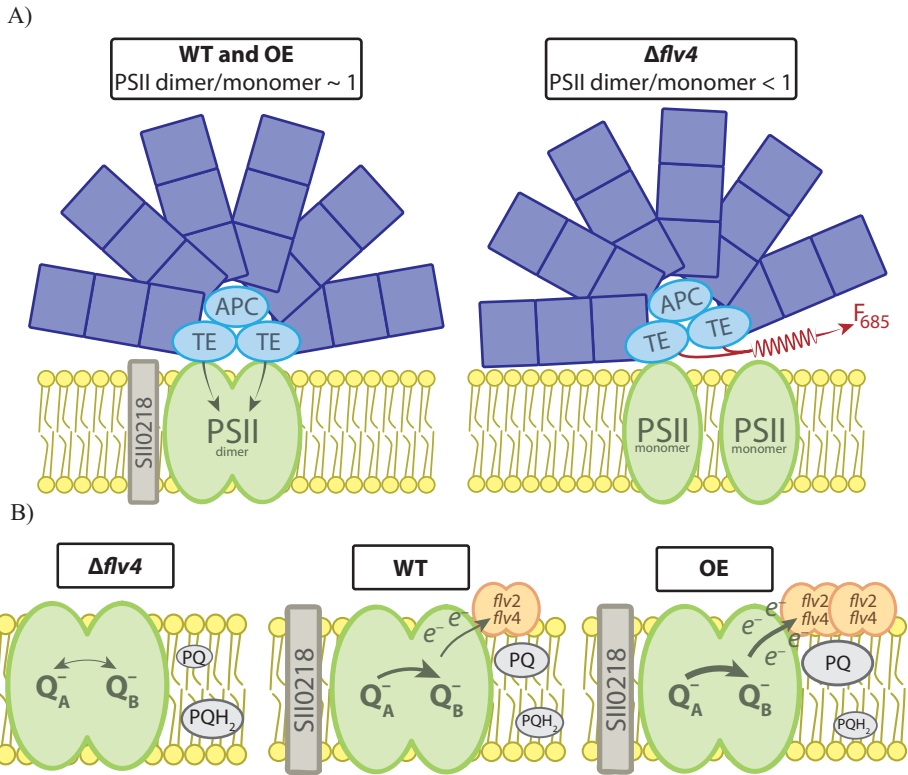


Figure 5.10. Hypothesis on the effect of *flv4-2* operon deletion on antenna connectivity (A) and PSII activity (B). A) In air level CO_2 conditions, PSII dimers are stabilized by the *Sll0218* protein, showing efficient EET from PBSs towards PSII RCs. In $\Delta flv4$, the lack of *Sll0218* protein destabilizes PSII dimers: the proportion of PSII dimers decreases by 20%, while the proportion of monomers increases, resulting in disturbed energy transfer from PBSs to PSII monomers (antenna detachment and subsequent increase of terminal emitter fluorescence at 685 nm). B) The electron transfer activity or the binding of the Flv2/Flv4 heterodimer closely to PSII increases the Q_B redox potential, thus stabilizing the forward electron transfer and accelerating the charge separation rates in PSII. In $\Delta flv4$ the increased probability of backward electron transfer from Q_B^- keeps Q_A more reduced. The activity of the Flv2/Flv4 heterodimer provides more oxidized state of the PQ pool (Bersanini et al. 2014). APC, allophycocyanin; TE, terminal emitters; PQ, plastoquinone; PQH₂, dihydroplastoquinone.

Subsequently, the damaged PSII dissociates into monomers and migrates to the grana margins and/or stroma thylakoids for repair (Aro et al., 2005; Herbstova et

al., 2012; Tikkanen et al., 2008). It is not yet known whether PBSs detach before PSII monomerization from photodamaged PSII dimers in cyanobacteria. In particular, here we provide evidence that PBS detachment is a secondary effect of PSII dimer destabilization observed in the absence of the Sll0218 protein (Zhang et al., 2012). Nevertheless, the antenna detachment mechanism seems to be beneficial under continuous stress conditions, when the photoprotective responses have been exhausted and the maintenance of efficient light harvesting and energy transfer would be both superfluous and harmful (Tamary et al., 2012).

5.3.3 *Flv2/Flv4 accelerates charge separation kinetics*

The unique function of the *flv4-2* operon-encoded proteins, Flv2, Flv4 and Sll0218, in photoprotection of PSII has remained mechanistically elusive, especially with respect to the function of each single protein of the operon. The results presented above provide evidence that the Sll0218 protein is the main player for correct PBS association with PSII dimers while previous results have suggested a role for the Flv2/Flv4 heterodimer in an alternative electron transfer route via PSII (Zhang et al., 2012; Bersanini et al., 2014).

In this work, TCSPC measurements clearly show that the absence of the *flv4-2* operon-encoded proteins strongly increases PSII fluorescence lifetimes by reducing Q_A , or by not oxidizing reduced Q_A/Q_B , even when the measuring conditions minimize the chance of a PSII being excited. In these conditions also the OE mutant shows some difference from WT. By increasing excitation pressure on PSII, simulating high light stress, the OE mutant was capable of keeping Q_A more oxidized than WT, while the $\Delta flv4$ mutant had more reduced Q_A compared to WT.

Importantly, from one hand, the reduction of the 2nd and 3rd fluorescence decay lifetimes in the TCSPC measurements in LEP indicate that the charge separation rates increase whereas backward charge recombination rates decrease in the presence of *flv4-2* operon-encoded proteins, thus supporting the decreased production of singlet oxygen as reported earlier (Bersanini et al., 2014). On the other hand, the TL data in Figure 5.9 show that the presence of the *flv4-2* operon-encoded proteins could induce an increase in the redox potential of Q_B , thus stabilizing forward electron transfer. In the absence of the *flv4-2* operon-encoded proteins the Q_B redox potential might decrease, leading to increased backward electron transfer to Q_A , with a higher probability to induce PSII photoinhibition (Vass et al., 1992). It has, in fact, been reported that the $\Delta flv4$ mutant is more sensitive to photoinhibitory conditions, due to an over-reduction of the PQ pool, while OE is more resistant (Zhang et al., 2009, Bersanini et al., 2014). However the

[ROLE OF FLV4-2 OPERON IN CYANOBACTERIA]

differences obtained in the TL curves could also be influenced by other factors. Previously it was shown that a specific D1 copy (D1:2 form) encoded by the *psbA3* gene in *Synechococcus elongatus* and *Thermosynechococcus elongatus* is responsible for a temperature downshift of the B and Q bands in TL curves (Sander et al., 2010; Sane et al., 2002; Sugiura et al., 2014). This functional difference is related to the presence of a glutamate residue instead of a glutamine at position 130 in the D1:2 protein sequence, which interacts with a key pheophytin co-factor (Nixon et al., 1991; Rappaport et al., 2002). Contrary to *Synechococcus*, the *psbA3* gene of *Synechocystis* does not encode this specific D1:2 form but both the *psbA2* and *psbA3* genes encode identical D1 proteins (for a review on D1 forms see Mulo et al., 2009; 2012), which do not possess a Q130E mutation. Thus, the differences in TL curves observed in Flv mutants are not related to changes in the expression of the *psbA* gene family.

Since CO₂ can affect charge accumulation in leaves (Garab and Rozsa, 1988), we cannot exclude the possibility that the differences in the TL data would relate to the stabilization of the bicarbonate binding site on the acceptor side of PSII by Flv2/Flv4 under air level CO₂ (for reviews about the “bicarbonate effect”, see McConnell et al., 2012; Shevela et al., 2012).

Previously, it was proposed that the Flv2/Flv4 heterodimer is accepting electrons from the Q_B pocket of PSII, allowing the PQ pool to be in a more oxidized state (Bersanini et al. 2014). However, our present results suggest that the probable binding of Flv2/Flv4 heterodimer in the vicinity of the Q_B pocket enhances charge separation in PSII by possibly increasing the redox potential of Q_B. Following our hypothesis, the electron transfer to Q_B is increased and the Flv2/Flv4-related alternative electron transfer route is likely to remove electrons from Q_B⁻ and keep the PQ pool in a more oxidized state, resulting in shorter PSII fluorescence lifetimes in HEP (see model in Figure 5.10 B).

In summary, new data concerning the function of the *flv4-2* operon encoded proteins in cyanobacterial photoprotection under ambient CO₂ conditions are provided. The deletion of the operon induces an antenna detachment effect, corresponding to the disconnection of around 20% of the PBSs. The reduced PSII dimer to monomer ratio, caused by the absence of the small Sll0218 protein, favors a relative decrease of the PSII dimer content of about 20%, showing a direct correlation between PSII dimer destabilization and PBS detachment from reaction centers. On the other hand, the binding of the Flv2/Flv4 heterodimer in close vicinity of the Q_B pocket of PSII might increase the Q_B redox potential, thus stabilizing forward electron transfer and increasing the charge separation rates in PSII.

Finally, the *flv4-2* operon-encoded proteins play an important role in the condition of excess excitation pressure on PSII: they stabilize the PSII dimer and the light-harvesting processes and enhance charge separation in PSII due to a higher redox potential of Q_B , allowing the alternative electron transfer route to sequester electrons from Q_B^- and to maintain the other electron acceptors of PSII, like PQ, in a more oxidized state (Figure 5.10 A, B).

5.4 Methods

5.4.1 Strains and Growth Conditions

The *Synechocystis* sp. PCC 6803 glucose-tolerant strain (Williams, 1988) was used as the wild type. The $\Delta flv4$ and OE strains were described previously by Zhang et al. (2012) and Bersanini et al. (2014), respectively. The $\Delta flv4::flv4-2$ complementation strain was obtained with the same procedure applied for the OE mutant (Bersanini et al., 2014), but the transformation host was the $\Delta flv4$ strain. The WT and mutant strains were grown at 30°C in BG-11 (Allen, 1968) buffered with 20 mM HEPES-NaOH (pH 7.5) and sodium carbonate was omitted from the culture ingredients. White light was used for illumination, with intensity of 50 $\mu\text{mol photons m}^{-2} \text{s}^{-1}$. The cultures were grown in flasks shaking at 100 rpm. For physiological experiments, the cells were harvested at the logarithmic phase (OD_{750} between 0.6 and 1.1), resuspended in fresh BG-11 medium, and adjusted to $OD_{670} = 0.25\text{-}0.3$, as measured by Cary 4000 spectrophotometer with integrating sphere.

5.4.2 Steady-State Fluorescence

Steady-state fluorescence spectra were recorded with a Fluorolog FL3-22 spectrofluorimeter (Horiba Jobin Yvon, Edison, NJ) and corrected for wavelength-dependent sensitivity of the detection and fluctuations in lamp output. The excitation wavelength was 580 nm; a band-pass of 3 nm was used for both the excitation and emission monochromator. Fluorescence emission and excitation spectra were recorded using an integration time of 0.4 s. Before performing the steady-state fluorescence measurements the optical density at 670 nm (chlorophyll) was adjusted to 0.25-0.3 for all samples. 77K measurements were performed with light-adapted cells frozen in liquid nitrogen in a 1 mm-optical path length cuvette to avoid reabsorption effect. Room-temperature measurements

[ROLE OF FLV4-2 OPERON IN CYANOBACTERIA]

were performed with a 3 mm-optical path length flow cuvette where samples were pumped from a reservoir of 5 ml with a speed of ~ 2.5 ml/s. Fluorescence emission spectra were recorded for cells excited with 580 nm wavelength light. Fluorescence excitation spectra were obtained for emission at 660 nm, 685 nm, 695 nm and 723 nm.

5.4.3 Streak-camera measurements

For the fluorescence measurements on the streak-camera setup samples were diluted to an optical density of 0.25/cm at 670 nm and a cuvette with 1 mm optical path was used. Time-resolved emission spectra were recorded using a synchroscan streak-camera system as described in (van Oort et al., 2009; van Stokkum et al., 2006). Measurements have been performed both at RT and 77K. Each experiment was repeated at least 4 times on different generations of the cells. An excitation wavelength of 580 nm was used to excite preferentially the PBSs. The laser power was 60 μ W, the spot size was 100 μ m, and the repetition rate 250 kHz. An average of 100 images, all measured for 10 s, was used for further analysis.

Before analysis the images were corrected for the background signal and detector sensitivity and sliced up into traces of 5 nm (RT) or 2 nm (77K). For RT measurements the sample was kept in a flow cuvette and a sample reservoir (5 ml). It was flowing from the reservoir to the cuvette and back, with a speed of ~ 2.5 ml/s. $\Delta flv4$ samples were measured using two time windows: 800 ps and 2 ns, for other samples only the 800-ps time window was used.

For 77K measurements, samples were collected in glass Pasteur pipettes with ~ 1 mm diameter and then frozen by immersion in liquid nitrogen. For all samples measured at 77K two time windows were used: 800 ps and 2 ns.

Streak-camera images were analyzed using the TIMP package for R language (Mullen and van Stokkum, 2007) and Glotaran, a graphical user interface for the R-package TIMP (Snellenburg et al., 2012). To get an equally good estimation of long (>700 ps) and short components of $\Delta flv4$ samples measured at RT, streak images obtained with two time windows were linked during the analysis. Linked fitting of two time ranges was also used for the 77K data to estimate the longest lifetime. The obtained ns component (~ 2 ns was obtained for all datasets) was used in a 5-component fit of 800 ps time-window data. A Gaussian-shaped instrument response function was used for the analysis and its width was a free fitting parameter. Typical FWHM values obtained from the fit were ~ 11 ps for the 800-ps time window and ~ 28 ps for the 2-ns time window.

The synchroscan period (13.17 ns) results in a back and forth sweeping of long-lived components and leads to some signal “before time zero” in the streak-camera images (van Stokkum et al., 2006). The fit quality was judged by singular value decomposition of the residuals matrix (Mullen and van Stokkum, 2007).

5.4.4 TCSPC measurements

Time-correlated single photon counting (TCSPC) measurements were performed at magic angle (54.7°) polarization as described previously (Somsen et al., 2005). Excitation was carried out by ~ 0.2 ps vertically polarized excitation pulses at a repetition rate of 3.8 MHz. The excitation wavelength was 440 nm. The sample was kept at 287 K in a flow cuvette and a sample reservoir (5 ml). The optical path length of the cuvette was 3 mm. The size of the excitation spot was 2 mm.

The cells were measured in two different states. First, to keep the reaction centers mostly open and minimize PSII excitation pressure (low excitation pressure conditions, LEP), the samples were flowing from the reservoir to the cuvette and back, with a speed of ~ 2.5 ml/s. Together with low laser powers (~ 7 μ W), this insures that multiple excitations of PSII complexes by laser pulses during the passage through the laser beam are avoided. The estimated probability of a PSII complex being excited in this case is <5 %. Subsequently the samples were measured with high excitation pressure (HEP). To achieve this, the flow speed was decreased to 0.2 ml/sec and the laser power was increased up to 50 μ W. In this case the probability of a PSII complex being excited by at least 1 photon during the passage through the laser beam rises up to 95%, which results in a substantial increase of closed RCs (RCs with reduced Q_A). For each run of measurements, the following interference filters were used for detection: 679, 693 and 724 nm (15 nm bandwidth) (Balzers, Liechtenstein model B40). To check the stability of the samples, the final experiment of a measuring series was always a repetition of the first one. The resulting decay curves were indistinguishable.

5.4.5 TCSPC data analysis

The full-width at half-maximum (FWHM) of the system response function was 35 ps when a resolution of 2.5 ps per channel was used, as obtained with the 6 ps decay of pinacyanol iodide in methanol (van Oort et al., 2008). Data analysis was performed using a home-built computer program (Digris et al., 1999). The data were fitted to multi-exponential decay functions with amplitudes α_i and

[ROLE OF FLV4-2 OPERON IN CYANOBACTERIA]

fluorescence decay times τ_i . The decay traces at different detection wavelengths were fitted globally, meaning that the decay lifetimes of a sample were forced to be equal at each detection wavelength but the amplitudes were allowed to differ. The fit quality was judged from the Poissonian maximum likelihood estimator, the residuals, and the autocorrelation of the residuals.

5.4.6 Electrophoresis and Immunoblotting

Protein complexes in the membrane fraction were analyzed by BN-PAGE, which was performed as described by Zhang et al. (2012). Gradient polyacrylamide gels (4.5-12%) were used in this study. After electrophoresis, the proteins were electro-transferred to a polyvinylidene fluoride membrane and detected by protein-specific antibodies.

5.4.7 Thermoluminescence measurements

TL was measured with a home-built apparatus as in (Tyystjärvi et al., 2009) on filter paper disks containing a quantity of 25 μg Chl of cells. Samples were dark adapted for 20 min at +30 °C. TL was induced by a single turnover saturating flash at -20 °C as indicated in the legend of Figure 5.9. The TL curves were analyzed by fitting with Gaussians as reported in Supplemental material.

Acknowledgements

This work was supported by the HARVEST Marie Curie Research Training Network (PITN-GA-2009-238017 to VUC, LB, EMA and HvA), the People Programme (Marie Curie Actions) of the European Union's Seventh Framework Programme FP7/2007-2013/ under REA grant agreement n° 317184 (EMA) and by the Academy of Finland Projects (N° 271832 to LB and EMA, and N° 273870 to EMA). This project was also carried out within the research program of BioSolar Cells, co-financed by the Dutch Ministry of Economic Affairs (to VUC and HvA), and by the FinSynBio2013 project (N° 272424 to LB and EMA). We thank R.B.M. Koehorst, Dr. A. Bader, Dr. E. Tyystjärvi and Dr. Arjun Tiwari for technical support with the measurements and data analysis

References

- Allahverdiyeva, Y., Ermakova, M., Eisenhut, M., Zhang, P.P., Richaud, P., Hagemann, M., Cournac, L., and Aro, E.M. (2011). Interplay between Flavodiiron Proteins and Photorespiration in *Synechocystis* sp. PCC 6803. *J Biol Chem* 286:24007-24014.
- Allahverdiyeva, Y., Mustila, H., Ermakova, M., Bersanini, L., Richaud, P., Ajlani, G., Battchikova, N., Cournac, L., and Aro, E.M. (2013). Flavodiiron proteins Flv1 and Flv3 enable cyanobacterial growth and photosynthesis under fluctuating light. *Proceedings of the National Academy of Sciences of the United States of America* 110:4111-4116.
- Allen, M.M. (1968). Simple Conditions for Growth of Unicellular Blue-Green Algae on Plates. *J Phycol* 4:1-4.
- Aro, E.M., Suorsa, M., Rokka, A., Allahverdiyeva, Y., Paakkarinen, V., Saleem, A., Battchikova, N., and Rintamaki, E. (2005). Dynamics of photosystem II: a proteomic approach to thylakoid protein complexes. *Journal of experimental botany* 56:347-356.
- Arteni, A.A., Ajlani, G., and Boekema, E.J. (2009). Structural organisation of phycobilisomes from *Synechocystis* sp strain PCC6803 and their interaction with the membrane. *Bba-Bioenergetics* 1787:272-279.
- Bailey, S., and Grossman, A. (2008). Photoprotection in cyanobacteria: regulation of light harvesting. *Photochem Photobiol* 84:1410-1420.
- Bald, D., Kruij, J., and Rogner, M. (1996). Supramolecular architecture of cyanobacterial thylakoid membranes: How is the phycobilisome connected with the photosystems? *Photosynth Res* 49:103-118.
- Barber, J., Morris, E.P., and da Fonseca, P.C.A. (2003). Interaction of the allophycocyanin core complex with photosystem II. *Photoch Photobio Sci* 2:536-541.
- Bentley, F.K., Luo, H., Dilbeck, P., Burnap, R.L., and Eaton-Rye, J.J. (2008). Effects of inactivating psbM and psbT on photodamage and assembly of photosystem II in *Synechocystis* sp. PCC 6803. *Biochemistry* 47:11637-11646.
- Bersanini, L., Battchikova, N., Jokel, M., Rehman, A., Vass, I., Allahverdiyeva, Y., and Aro, E.M. (2014). Flavodiiron Protein Flv2/Flv4-Related Photoprotective Mechanism Dissipates Excitation Pressure of PSII in Cooperation with Phycobilisomes in Cyanobacteria. *Plant physiology* 164:805-818.
- Croce, R., and van Amerongen, H. (2014). Natural strategies for photosynthetic light harvesting. *Nature chemical biology* 10:492-501.
- Demeter, S., and Vass, I. (1984). Charge accumulation and recombination in photosystem II studied by thermoluminescence. I. Participation of the primary acceptor Q and secondary acceptor B in the generation of thermoluminescence of chloroplasts. *Biochimica et Biophysica Acta (BBA)-Bioenergetics* 764:24-32.
- Digris, A.V., Skakoun, V.V., Novikov, E.G., van Hoek, A., Claiborne, A., and Visser, A.J.W.G. (1999). Thermal stability of a flavoprotein assessed from associative analysis of polarized time-resolved fluorescence spectroscopy. *Eur Biophys J Biophys* 28:526-531.
- Droppa, M., Horváth, G., Vass, I., and Demeter, S. (1981). Mode of action of Photosystem II herbicides studied by thermoluminescence. *Biochimica et Biophysica Acta (BBA)-Bioenergetics* 638:210-216.
- Garab, G., and Rozsa, Z. (1988). Carbon dioxide affects charge accumulation in leaves. *Naturwissenschaften* 75:517-519.

[ROLE OF FLV4-2 OPERON IN CYANOBACTERIA]

- Hakkila, K., Antal, T., Gunnelius, L., Kurkela, J., Matthijs, H.C.P., Tyystjarvi, E., and Tyystjarvi, T. (2013). Group 2 Sigma Factor Mutant DeltasigCDE of the Cyanobacterium *Synechocystis* sp. PCC 6803 Reveals Functionality of Both Carotenoids and Flavodiiron Proteins in Photoprotection of Photosystem II. *Plant Cell Physiol* 54:1780-1790.
- Helman, Y., Tchernov, D., Reinhold, L., Shibata, M., Ogawa, T., Schwarz, R., Ohad, I., and Kaplan, A. (2003). Genes encoding A-type flavoproteins are essential for photoreduction of O₂ in cyanobacteria. *Current biology* : CB 13:230-235.
- Herbstova, M., Tietz, S., Kinzel, C., Turkina, M.V., and Kirchhoff, H. (2012). Architectural switch in plant photosynthetic membranes induced by light stress. *Proceedings of the National Academy of Sciences of the United States of America* 109:20130-20135.
- Jordan, P., Fromme, P., Witt, H.T., Klukas, O., Saenger, W., and Krauss, N. (2001). Three-dimensional structure of cyanobacterial photosystem I at 2.5 Å resolution. *Nature* 411:909-917.
- Liu, H.J., Zhang, H., Niedzwiedzki, D.M., Prado, M., He, G.N., Gross, M.L., and Blankenship, R.E. (2013). Phycobilisomes Supply Excitations to Both Photosystems in a Megacomplex in Cyanobacteria. *Science* 342:1104-1107.
- Mamedov, F., Nowaczyk, M.M., Thapper, A., Rogner, M., and Styring, S. (2007). Functional characterization of monomeric photosystem II core preparations from *Thermosynechococcus elongatus* with or without the Psb27 protein. *Biochemistry* 46:5542-5551.
- McConnell, I.L., Eaton-Rye, J.J., and van Rensen, J.J. (2012). Regulation of photosystem II electron transport by bicarbonate. In: *Photosynthesis*: Springer. 475-500.
- Miloslavina, Y., Szczepaniak, M., Muller, M.G., Sander, J., Nowaczyk, M., Rogner, M., and Holzwarth, A.R. (2006). Charge separation kinetics in intact photosystem II core particles is trap-limited. A picosecond fluorescence study. *Biochemistry* 45:2436-2442.
- Mörschel, E., and Mühlethaler, K. (1983). On the linkage of exoplasmatic freeze-fracture particles to phycobilisomes. *Planta* 158:451-457.
- Mörschel, E., and Schatz, G.H. (1987). Correlation of photosystem-II complexes with exoplasmatic freeze-fracture particles of thylakoids of the cyanobacterium *Synechococcus* sp. *Planta* 172:145-154.
- Mullen, K.M., and van Stokkum, I.H. (2007). TIMP: an R package for modeling multi-way spectroscopic measurements. *Journal of Statistical Software* 18:1-46.
- Mullineaux, C.W., and Emlyn-Jones, D. (2005). State transitions: an example of acclimation to low-light stress. *Journal of experimental botany* 56:389-393.
- Mulo, P., Sakurai, I., and Aro, E.M. (2012). Strategies for psbA gene expression in cyanobacteria, green algae and higher plants: from transcription to PSII repair. *Biochimica et biophysica acta* 1817:247-257.
- Mulo, P., Sicora, C., and Aro, E.M. (2009). Cyanobacterial psbA gene family: optimization of oxygenic photosynthesis. *Cellular and molecular life sciences* : CMLS 66:3697-3710.
- Nixon, P.J., Barker, M., Boehm, M., de Vries, R., and Komenda, J. (2005). FtsH-mediated repair of the photosystem II complex in response to light stress. *Journal of experimental botany* 56:357-363.
- Nixon, P.J., Rogner, M., and Diner, B.A. (1991). Expression of a higher plant psbA gene in *Synechocystis* 6803 yields a functional hybrid photosystem II reaction center complex. *The Plant cell* 3:383-395.

[CHAPTER 5]

- Niyogi, K.K. (1999). Photoprotection revisited: Genetic and molecular approaches. *Annu Rev Plant Phys* 50:333-359.
- Rappaport, F., Guergova-Kuras, M., Nixon, P.J., Diner, B.A., and Lavergne, J. (2002). Kinetics and pathways of charge recombination in photosystem II. *Biochemistry* 41:8518-8527.
- Roelofs, T.A., Lee, C.H., and Holzwarth, A.R. (1992). Global Target Analysis of Picosecond Chlorophyll Fluorescence Kinetics from Pea-Chloroplasts - a New Approach to the Characterization of the Primary Processes in Photosystem-II Alpha-Units and Beta-Units. *Biophysical journal* 61:1147-1163.
- Rutherford, A., Crofts, A., and Inoue, Y. (1982). Thermoluminescence as a probe of photosystem II photochemistry. The origin of the flash-induced glow peaks. *Biochimica et Biophysica Acta (BBA)-Bioenergetics* 682:457-465.
- Sakurai, I., Mizusawa, N., Ohashi, S., Kobayashi, M., and Wada, H. (2007). Effects of the lack of phosphatidylglycerol on the donor side of photosystem II. *Plant physiology* 144:1336-1346.
- Sander, J., Nowaczyk, M., Buchta, J., Dau, H., Vass, I., Deák, Z., Dorogi, M., Iwai, M., and Rögner, M. (2010). Functional Characterization and Quantification of the Alternative PsbA Copies in *Thermosynechococcus elongatus* and Their Role in Photoprotection. *J Biol Chem* 285:29851-29856.
- Sane, P.V., Ivanov, A.G., Sveshnikov, D., Huner, N.P., and Oquist, G. (2002). A transient exchange of the photosystem II reaction center protein D1:1 with D1:2 during low temperature stress of *Synechococcus* sp. PCC 7942 in the light lowers the redox potential of QB. *J Biol Chem* 277:32739-32745.
- Schatz, G.H., Brock, H., and Holzwarth, A.R. (1987). Picosecond kinetics of fluorescence and absorbance changes in photosystem II particles excited at low photon density. *Proceedings of the National Academy of Sciences of the United States of America* 84:8414-8418.
- Schatz, G.H., Brock, H., and Holzwarth, A.R. (1988). Kinetic and Energetic Model for the Primary Processes in Photosystem II. *Biophysical journal* 54:397-405.
- Scott, M., McCollum, C., Vasil'ev, S., Crozier, C., Espie, G.S., Krol, M., Huner, N.P., and Bruce, D. (2006). Mechanism of the down regulation of photosynthesis by blue light in the Cyanobacterium *synechocystis* sp. PCC 6803. *Biochemistry* 45:8952-8958.
- Shevela, D., Eaton-Rye, J.J., Shen, J.R., and Govindjee. (2012). Photosystem II and the unique role of bicarbonate: a historical perspective. *Biochimica et biophysica acta* 1817:1134-1151.
- Snellenburg, J.J., Liptenok, S.P., Seger, R., Mullen, K.M., and van Stokkum, I.H.M. (2012). Glotaran: A Java-Based Graphical User Interface for the R Package TIMP. *Journal of Statistical Software* 49:1-22.
- Somsen, O.J., Keukens, L.B., de Keijzer, M.N., van Hoek, A., and van Amerongen, H. (2005). Structural Heterogeneity in DNA: Temperature Dependence of 2-Aminopurine Fluorescence in Dinucleotides. *ChemPhysChem* 6:1622-1627.
- Stadnichuk, I.N., Lukashev, E.P., and Elanskaya, I.V. (2009). Fluorescence changes accompanying short-term light adaptations in photosystem I and photosystem II of the cyanobacterium *Synechocystis* sp. PCC 6803 and phycobiliprotein-impaired mutants: State 1/State 2 transitions and carotenoid-induced quenching of phycobilisomes. *Photosynth Res* 99:227-241.
- Sugiura, M., Azami, C., Koyama, K., Rutherford, A.W., Rappaport, F., and Boussac, A. (2014). Modification of the pheophytin redox potential in *Thermosynechococcus*

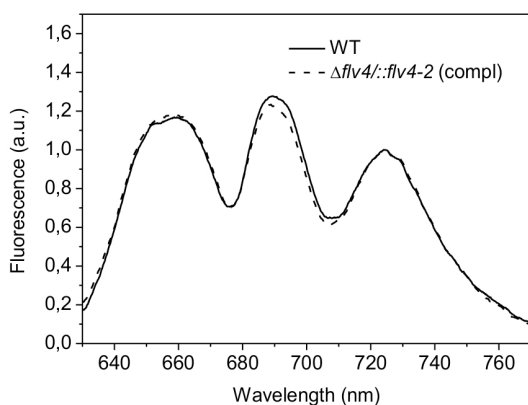
[ROLE OF FLV4-2 OPERON IN CYANOBACTERIA]

- elongatus Photosystem II with PsbA3 as D1. *Biochimica et biophysica acta* 1837:139-148.
- Szczepaniak, M., Sander, J., Nowaczyk, M., Muller, M.G., Rogner, M., and Holzwarth, A.R. (2009). Charge separation, stabilization, and protein relaxation in photosystem II core particles with closed reaction center. *Biophysical journal* 96:621-631.
- Tamary, E., Kiss, V., Nevo, R., Adam, Z., Bernat, G., Rexroth, S., Rogner, M., and Reich, Z. (2012). Structural and functional alterations of cyanobacterial phycobilisomes induced by high-light stress. *Biochimica et biophysica acta* 1817:319-327.
- Tian, L., Farooq, S., and van Amerongen, H. (2013). Probing the picosecond kinetics of the photosystem II core complex in vivo. *Phys Chem Chem Phys* 15:3146-3154.
- Tian, L., Gwizdala, M., van Stokkum, I.H., Koehorst, R., Kirilovsky, D., and van Amerongen, H. (2012). Picosecond Kinetics of Light Harvesting and Photoprotective Quenching in Wild-Type and Mutant Phycobilisomes Isolated from the Cyanobacterium *Synechocystis* PCC 6803. *Biophysical journal* 102:1692-1700.
- Tian, L., van Stokkum, I.H., Koehorst, R.B., Jongerius, A., Kirilovsky, D., and van Amerongen, H. (2011). Site, rate, and mechanism of photoprotective quenching in cyanobacteria. *Journal of the American Chemical Society* 133:18304-18311.
- Tikkanen, M., Nurmi, M., Kangasjarvi, S., and Aro, E.M. (2008). Core protein phosphorylation facilitates the repair of photodamaged photosystem II at high light. *Biochimica et biophysica acta* 1777:1432-1437.
- Tyystjarvi, E., Rantamaki, S., and Tyystjarvi, J. (2009). Connectivity of photosystem II is the physical basis of retrapping in photosynthetic thermoluminescence. *Biophysical journal* 96:3735-3743.
- Umena, Y., Kawakami, K., Shen, J.R., and Kamiya, N. (2011). Crystal structure of oxygen-evolving photosystem II at a resolution of 1.9 angstrom. *Nature* 473:55-U65.
- Van der Weij-de Wit, C.D., Dekker, J.P., van Grondelle, R., and van Stokkum, I.H. (2011). Charge separation is virtually irreversible in photosystem II core complexes with oxidized primary quinone acceptor. *The journal of physical chemistry. A* 115:3947-3956.
- Van Oort, B., Alberts, M., de Bianchi, S., Dall'Osto, L., Bassi, R., Trinkunas, G., Croce, R., and van Amerongen, H. (2010). Effect of antenna-depletion in Photosystem II on excitation energy transfer in *Arabidopsis thaliana*. *Biophys J* 98:922-931.
- Van Oort, B., Amunts, A., Borst, J.W., van Hoek, A., Nelson, N., van Amerongen, H., and Croce, R. (2008). Picosecond fluorescence of intact and dissolved PSI-LHCI crystals. *Biophysical journal* 95:5851-5861.
- Van Oort, B., Murali, S., Wientjes, E., Koehorst, R.B.M., Spruijt, R.B., van Hoek, A., Croce, R., and van Amerongen, H. (2009). Ultrafast resonance energy transfer from a site-specifically attached fluorescent chromophore reveals the folding of the N-terminal domain of CP29. *Chem Phys* 357:113-119.
- Van Stokkum, I.H.M., Gobets, B., Gensch, T., van Mourik, F., Hellingwerf, K.J., van Grondelle, R., and Kennis, J.T.M. (2006). (Sub)-picosecond spectral evolution of fluorescence in photoactive proteins studied with a synchroscan streak camera system. *Photochem Photobiol* 82:380-388.
- Van Thor, J.J., Mullineaux, C.W., Matthijs, H.C.P., and Hellingwerf, K.J. (1998). Light Harvesting and State Transitions in Cyanobacteria. *Botanica Acta* 111:430-443.
- Vass, I., Styring, S., Hundal, T., Koivuniemi, A., Aro, E., and Andersson, B. (1992). Reversible and irreversible intermediates during photoinhibition of photosystem II: stable reduced QA species promote chlorophyll triplet formation. *Proceedings of the National Academy of Sciences* 89:1408-1412.

[CHAPTER 5]

- Vassiliev, S., Lee, C.I., Brudvig, G.W., and Bruce, D. (2002). Structure-based kinetic modeling of excited-state transfer and trapping in histidine-tagged photosystem II core complexes from *synechocystis*. *Biochemistry* 41:12236-12243.
- Vicente, J.B., Justino, M.C., Goncalves, V.L., Saraiva, L.M., and Teixeira, M. (2008). Biochemical, spectroscopic, and thermodynamic properties of flavodiiron proteins. *Methods Enzymol* 437:21-45.
- Williams, J.G. (1988). Construction of specific mutations in photosystem II photosynthetic reaction center by genetic engineering methods in *Synechocystis* 6803. *Methods Enzymol* 167:766-778.
- Wilson, A., Ajlani, G., Verbavatz, J.M., Vass, I., Kerfeld, C.A., and Kirilovsky, D. (2006). A soluble carotenoid protein involved in phycobilisome-related energy dissipation in cyanobacteria. *The Plant cell* 18:992-1007.
- Wilson, A., Boulay, C., Wilde, A., Kerfeld, C.A., and Kirilovsky, D. (2007). Light-induced energy dissipation in iron-starved cyanobacteria: roles of OCP and IsiA proteins. *The Plant cell* 19:656-672.
- Young, R.D. (2010). Characterisation of the Role of the PsbT Subunit of Photosystem II in *Synechocystis* Sp. PCC 6803: A Thesis Submitted for the Degree of Master of Science at the University of Otago, Dunedin, New Zealand: University of Otago.
- Zhang, P., Eisenhut, M., Brandt, A.M., Carmel, D., Silen, H.M., Vass, I., Allahverdiyeva, Y., Salminen, T.A., and Aro, E.M. (2012). Operon *flv4-flv2* provides cyanobacterial photosystem II with flexibility of electron transfer. *The Plant cell* 24:1952-1971.
- Zhang, P.P., Allahverdiyeva, Y., Eisenhut, M., and Aro, E.M. (2009). Flavodiiron Proteins in Oxygenic Photosynthetic Organisms: Photoprotection of Photosystem II by Flv2 and Flv4 in *Synechocystis* sp PCC 6803. *Plos One* 4.

SUPPLEMENTARY MATERIAL

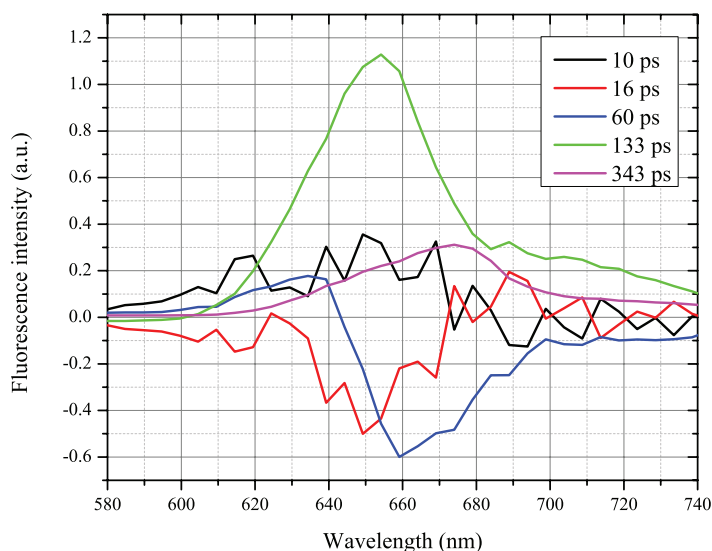
1. Complementation of $\Delta flv4$ resulted in WT-like phenotype in steady state 77K fluorescence measurements

Supplemental Figure S1. Fluorescence emission spectra recorded at 77K from cultures excited at 580 nm. The cultures were adjusted to the same chlorophyll concentration. The spectra are averages of three different biological replicates. The fluorescence spectra were normalized to the PSI peak (723 nm).

2. Determination of required number of components for global analysis: quality of the fit.

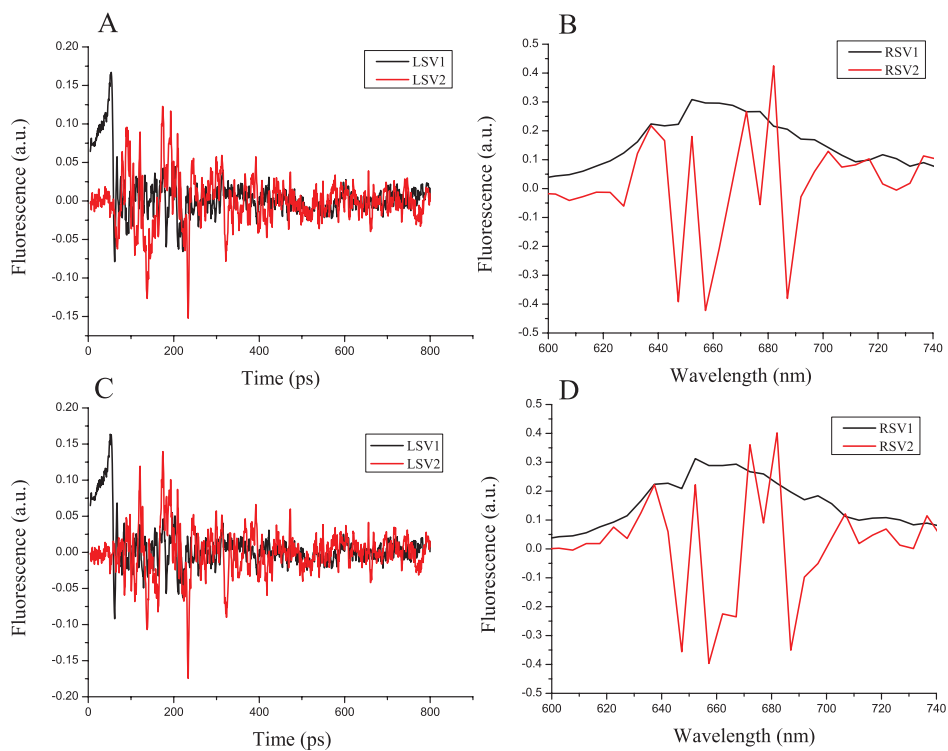
Previously, a 5-component global-analysis fit was reported for *Synechocystis sp.* PCC 6803, measured at RT (Tian et al., 2011). Two components were assigned to EET/equilibration steps within PBSs (8 ps, 36 ps). The 3rd DAS with the lifetime of 130 ps was assigned to EET from APC₆₆₀ to APC₆₈₀ and Chls. The 4th DAS with ~200 ps lifetime was assigned to excitation trapping by RCs while a small amplitude of the ~700 ps component to second charge separation event and recombination. Unlike (Tian et al., 2011), four components appeared to be enough to describe all our data measured at RT, although a 5-component fit was possible for several datasets. In order to check the real necessity of the additional 5th component for the datasets where it was possible to resolve from the global analysis of streak-camera data, the 5 and 4 components fits were compared. The DAS resulting from the 5-component fit of WT are given in Supplemental Figure S2. The quality of the fit was judged by singular value decomposition of the residual matrix: it should show no significant structure in the first two left and

right singular vectors (Supplemental Figure S3). We conclude from the Supplemental Figure S3 that the 5-component fit does not improve the structure of two first singular vectors. Furthermore the two fastest components (10 ps, 16 ps) are too noisy, justifying that a 5th component is redundant (Supplemental Figure S2). It looks like the difference between the time-resolved data presented in the current work from the results published earlier originates from a smaller contribution of closed RCs in the current data. So the excitations from PBSs are immediately trapped by PSII RCs so that the EET step from PBSs towards PSII RC cannot be resolved as a separate component but it only contributes to the DAS with a 130 ps lifetime as a dip in 680 nm region (Figure 5.4 A, Supplemental Figure S2). This is in agreement with the fact that the average fluorescence lifetime for PSII here is mostly presented by the 340 ps DAS which is shorter than was observed earlier.



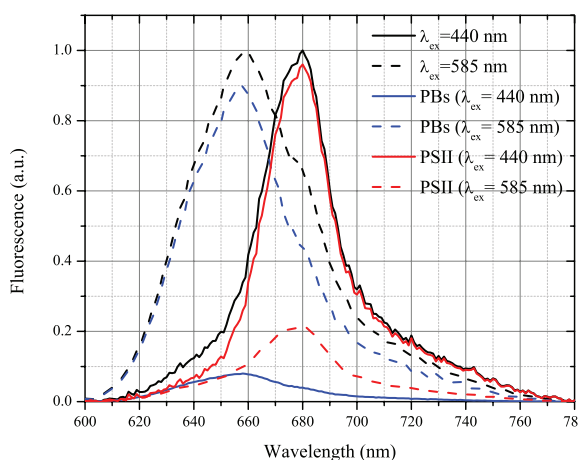
Supplemental Figure S2. DAS from the 5 - component fit obtained for WT cells from global analysis of streak-camera data upon 580 nm excitation at RT.

[ROLE OF FLV4-2 OPERON IN CYANOBACTERIA]



Supplemental Figure S3. The comparison of left (A, C), right (B, D) singular vectors obtained from a 4- (A, B) and 5- (C, D) component fit.

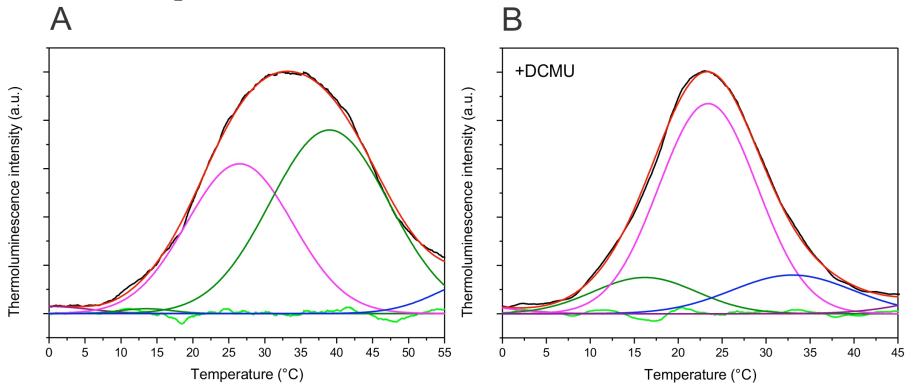
3. Estimation of PBS and PS spectral contributions for different excitation wavelengths



Supplemental Figure S4. Comparison of steady-state emission spectra measured with 440 nm (black solid line) and 585 nm excitation (black dashed line). Both steady-state spectra were decomposed into corresponding PS and PBS fluorescence contributions (presented by blue and red lines, respectively).

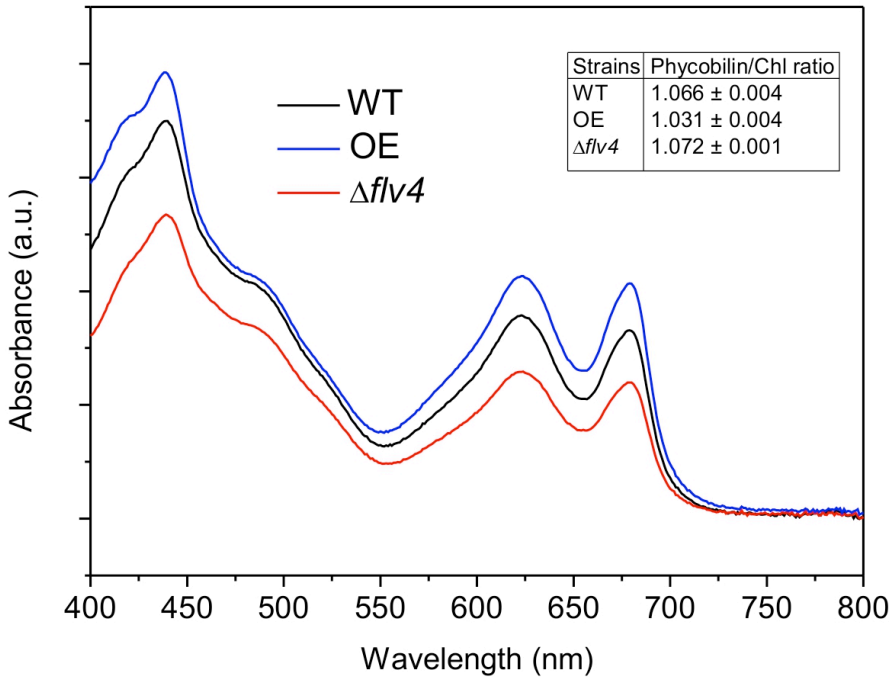
To judge how selectively PSs were excited at 440 nm, the corresponding steady-state emission spectrum was decomposed into its PBS and PS contributions (Supplemental Figure S4). Since PSs also get excitation energy from PBSs, the contribution of PS excitation would be overestimated via this method. That is why the results of 440 nm excitation data were compared with the results upon 585 nm excitation (PBSs are excited selectively). The maximal similarity of the obtained PBS spectra to the one reported was a criterion of the fit quality (Jallet et al., 2012). The estimation of PS and PBS contributions (fluorescence spectrum area) to the total steady-state emission spectra is reported below in Supplemental Table S1.

4. Decomposition of TL curves



Supplemental Figure S5. An example of the Gaussian sub-band deconvolution of the thermoluminescence curves presented in Figure 5.9 in the absence (A) and presence of DCMU (B). The black line shows the original curve, the red line shows the fitted curve using Gaussians and the green line represents the residual spectrum (original minus fitted curve). The other colored lines are the Gaussian deconvolution sub-bands from the original curve. The B band is decomposed into two main peaks (A), while the Q band can be approximated to a single peak (B).

5. Estimation of different pigment contents with absorption spectra



Supplemental Figure S6. Absorption spectra of WT, $\Delta flv4$ and OE strains. The cultures were grown in standard conditions and normalized to $OD_{750}=0.5$ before the measurements. The phycobilin peak at 625 nm and Chl a peak at 678 nm were measured, and the ratios of phycobilin to Chl were calculated (see table inside the graph).

The three strains possess similar Phycobilin/Chl ratios

[ROLE OF FLV4-2 OPERON IN CYANOBACTERIA]

Supplemental Table S1. Estimation of PS and PBS contributions (fluorescence spectrum area) to the total steady-state emission spectra obtained from the Supplemental Figure S5.

| | | |
|-------------------|-----------|-----------|
| Contributions (%) | 440 nm ex | 585 nm ex |
| PSs | 90 | 18 |
| PBSs | 10 | 82 |

Supplemental Table S2. Peak temperatures of the main decomposed bands obtained from thermoluminescence curves.

| Strains | B band decomposed peaks (°C) | | Q band decomposed peak (°C) |
|---------------|------------------------------|------------|-----------------------------|
| WT | 27.0 ± 1.0 | 37.0 ± 0.8 | 23.2 ± 0.8 |
| OE | 26.5 ± 1.0 | 38.8 ± 0.7 | 23.4 ± 0.7 |
| $\Delta flv4$ | 26.9 ± 0.9 | 34.9 ± 0.8 | 23.9 ± 0.8 |

Jallet, D., Gwizdala, M., and Kirilovsky, D. (2012). ApcD, ApcF and ApcE are not required for the Orange Carotenoid Protein related phycobilisome fluorescence quenching in the cyanobacterium *Synechocystis* PCC 6803. *Bba-Bioenergetics* 1817:1418-1427.

Tian, L., van Stokkum, I.H., Koehorst, R.B., Jongerius, A., Kirilovsky, D., and van Amerongen, H. (2011). Site, rate, and mechanism of photoprotective quenching in cyanobacteria. *Journal of the American Chemical Society* 133:18304-18311.

Chapter 6

General discussion

Introduction

Photosynthesis is the natural process of harvesting, converting, and storing the energy of sunlight in chemical form. It sustains virtually all life on Earth, by providing chemical energy for plants, algae and bacteria, while essentially all non-photosynthetic organisms rely on these species as their energy source. Photosynthetic solar energy harvesting occurs on an immense scale, dramatically impacting our biosphere (Carpenter et al., 2011; Melillo et al., 1993; Ware and Thomson, 2005). Photosynthesis produces 100 billion tons of biomass annually (Barber, 2009). Around half of this biomass is accounted for by oceanic light-harvesting organisms. Because aquatic photosynthetic organisms are exposed and successively adapted to extreme light changes, they could serve as a source of inspiration for scientists for effectively collecting and storing solar energy.

Many light-harvesting strategies of aquatic photosynthesis, such as light acclimation, photoprotection, and state transitions are still not completely understood. In this thesis, various time-resolved spectroscopy techniques are applied to diatoms and cyanobacteria, preferentially *in vivo*, to obtain essential information how aquatic organisms adapt to changing light conditions.

6.1 Fluorescence kinetics of diatom *C. meneghiniana in vivo*

In spite of their ecological importance, diatoms remain one of the most poorly studied taxonomic groups of photosynthetic organisms. The main bottleneck is that none of the molecular structures of their photosynthetic complexes has been resolved. Detailed studies on diatom photosystems are hampered by the difficulty of isolating photoactive thylakoid membranes from diatom cells, since the cells are enveloped by silicate shells that are hard to break (Martinson et al., 1998). This problem leads us towards *in vivo* studies, but results obtained *in vivo* are often more difficult to explain. In chapter 2, we demonstrate for the first time the variation of fluorescence kinetics of *C. meneghiniana in vivo* upon excitation with various wavelengths. In this way we managed to resolve fluorescence kinetics of both photosystems as well as to describe excitation energy transfer from the antennas towards RCs.

Both antennas and RCs are excited by *Chl a* excitation. Excitation trapping of low-light grown cultures in PSI corresponds to a 75 ps lifetime, which is close to the lifetime of PSI in higher plants (Van Oort et al., 2008; Wientjes et al., 2009; Wientjes et al., 2011) and green algae (Melkozernov et al., 2004; Ünlü et al., 2014). In higher plants and green algae, PSI forms a supercomplex called PSI light-harvesting complex I (PSI-LHCI). This supercomplex in plants binds approximately 170 Chls in total and

[GENERAL DISCUSSION]

consists of a core complex and four LHCI (Amunts et al., 2010; Ben-Shem et al., 2003; Jordan et al., 2001). In green algae, the antenna size is about two times larger than in plants and the LHCI-PSI supercomplex binds ~380 Chls in total, which is substantially more than observed in plants (Bassi et al., 1992). However, the average lifetimes for LHCI-PSI in plants and green algae are comparable. The reason is the presence of a smaller number of “red” Chls in the antenna of green algae as compared to plants: “Red” Chls absorb at longer wavelengths than the primary electron donor and have a large effect on excitation trapping time in PSI (Ihalainen et al., 2005). Only 28% of the PSI antenna in the green alga *Chlamydomonas reinhardtii* is constituted by Lhca proteins harboring “red” Chls as compared to almost 50% found in the plant *Arabidopsis thaliana* (Stauber et al., 2009).

FCP-PSI complexes have been isolated from the diatoms *Chaetoceros gracilis* (Ikeda et al., 2008) and *Phaeodactylum tricornutum* (Veith and Büchel, 2007), which bind 220 and 200 Chls, respectively. These values are closer to the values reported for plants. Unlike in plants, however, no “red” Chls were observed in the PSI RCs or antennas in FCP-PSI complexes of these diatoms. However, our 77K data on whole *C. meneghiniana* cells demonstrate some contribution of “red” FCP forms, emitting in the 690-730 nm region (chapter 3).

To summarize, although a combination of biochemical data and time-resolved measurements suggests that PSI complexes in diatoms bind a roughly similar amount of pigments as in higher plants, one should realize that the antenna composition and PSI complex organization of diatoms differs from those in plants and green algae and are still not completely resolved. If, for example, PSI would bind less antennas (generally leading to faster fluorescence kinetics) that are loosely attached to the reaction center or with more red forms (slowing down the kinetics), the observed fluorescence lifetimes might be similar.

The average lifetime for PSII for low-light grown *C. meneghiniana* cells *in vivo* (chapter 2) is substantially (~at least 100 ps) longer than the average lifetime of PSII from thylakoid membranes of *Arabidopsis thaliana* grown in similar light conditions (Wientjes et al., 2013). The longer lifetime of PSII in *C. meneghiniana* may be due to a larger antenna size (*Arabidopsis* thylakoids contain ~300 pigments/RC (Croce and van Amerongen, 2011; Sandonà et al., 1998; Van Oort et al., 2010; Wientjes et al., 2013)).

Miloslavina and coworkers were the first to report *in vivo* time-resolved fluorescence measurements of diatoms. They obtained similar spectral shapes and peak positions for time-resolved PSII and PSI spectral components (Miloslavina et al., 2009). A rough estimation of the average lifetime from their results leads to lifetimes of ~51 ps for PSI and ~395 ps for PSII (*C. meneghiniana*). These values are slightly

[GENERAL DISCUSSION]

shorter than in our case. We conclude that the antenna sizes in the samples used by Miloslavina et al. were smaller, probably as a result of higher illumination conditions used during growth. The reported light intensity was $40 \mu\text{mol photons m}^{-2}\text{s}^{-1}$, where we used $20 \mu\text{mol photons m}^{-2}\text{s}^{-1}$ for our low-light-grown cultures. This conclusion is further supported by our results obtained for cells grown in higher light conditions.

In chapter 2 we show that most of the diatom light-harvesting complexes in *C. meneghiniana* transfer their energy to PSII. Light-harvesting complexes comprise several antenna proteins (fucoxanthin-chlorophyll proteins, FCPs). The PSII-related lifetime upon antenna excitation is slightly longer than the average PSII lifetime upon Chl *a* excitation, when both antennas and cores are excited. This can be explained by an increase of the migration time (the average time that excitation created in PSII complex takes to reach the RC) when there are relatively more excitations in the outer antenna. In plants, the difference in lifetime between Chl *b* (LHCII accessory pigment) and Chl *a* excitation scales with the migration time in PSII (Broess et al., 2008; Van Oort et al., 2010). Several studies on the low-light-grown plants showed a lifetime difference of ~ 15 ps, which was shown to correspond to a migration time of ~ 150 ps (Van Oort et al., 2010; Wientjes et al., 2013).

In our case, however, we cannot estimate the migration time, because, without having time-resolved spectra of PSI, we cannot completely exclude the PSI kinetics from our data. To obtain these spectra, the PSI complex of *C. meneghiniana* should be isolated and described with time-resolved measurements. Moreover, calculation of the migration time also requires knowledge of the amount of excitations in PSII core and antennas upon Chl *a* or *fx* excitation.

In chapter 2 we also contributed to the discussion about the question whether certain light-harvesting complexes bind preferably to either photosystem. Two different major light-harvesting complexes can be isolated from *C. meneghiniana*: trimeric FCPa and oligomeric FCPb. The FCPa and FCPb light-harvesting complexes constitute different FCPs and have slightly different spectroscopic properties. Oligomeric FCPb shows slightly less absorption around 490 nm and increased values around FCPa trimers (Beer et al., 2006; Gildenhoff et al., 2010; Premvardhan et al., 2010), implying that trimers might bind more blue-shifted *fx* as compared to FCPb. This marker gives opportunity to assign fluorescence signals *in vivo* to either FCPa or FCPb. We separated the PSI and PSII excitation spectra of diatoms *in vivo* and found the antennas of PSI and PSII to have different spectroscopic properties. The enrichment of the PSII antenna with fx_{red} points at FCPb association with PSII. FCPb is thus not only connected to PSI, as shown by (Veith et al., 2009), but also to PSII.

The Fcp6 antenna protein, one of the FCPa antenna complexes is known to be involved in photoprotection (Bailleul et al., 2010). In agreement with that, we

conclude in chapter 3 that only FCPa complexes participate in PSII photoprotection *in vivo*. This means that both FCPa and FCPb bind to PSII in *C. meneghiniana*, where FCPa serves both light-harvesting and photoprotective roles, while FCPb only harvests light.

6.2 Effect of light acclimation

Although the general responses of diatoms to changes in the light intensity are comparable to the responses of green algae and plants, some differences in the underlying mechanisms have been observed, yielding clear evidence that the regulatory network in diatoms has unique traits that might explain their ecological success (Lepetit et al., 2012; Strzepek and Harrison, 2004). In chapter 2 we contributed to the topic of light acclimation in diatoms by comparing variation in fluorescence kinetics between the cultures grown in three different light conditions—low light, medium light and high light to disentangle what happens to photosystems and antenna during the acclimation to light.

The reduction of the number of antenna complexes per photosystem is a common mechanism during the high-light acclimation of higher plants and green algae (Caffarri et al., 2011; Croce and van Amerongen, 2011; Durnford et al., 2003; Kurasova et al., 2002). On the other hand, in diatoms no significant difference in the antenna size under different light regimes was observed in *C. meneghiniana*, as could be judged based on the $f_x/\text{Chl } a$ ratio (Lepetit et al., 2010). In other diatoms significant changes in $f_x/\text{Chl } a$ ratios are observed (Smith and Melis, 1988; Van De Poll et al., 2005).

Time-resolved fluorescence is a common method to study antenna sizes in various photosynthetic organisms. For plant membranes that contain 2.0-2.5 LHCII trimers per PSII RC, the fluorescence lifetime was reported to be around 160 ps upon antenna excitation (Broess et al., 2006; Broess et al., 2008) whereas for thylakoid membranes with 4.0 trimers per PSII RC, the lifetime goes up to around 340 ps (Caffarri et al., 2011; Croce and van Amerongen, 2011; Van Oort et al., 2010).

Upon selective antenna excitation of *C. meneghiniana*, the average lifetime decreased from 460 ps for low-light-grown cultures to 363 ps in the case of high-light-grown cultures. The ~100 ps shortening reflects a decrease of the FCP antenna size connected to the RC of PSII.

Although the antenna composition and organization differ for diatoms and higher plants, substantial sequence similarity exists between FCP and LHCII proteins and we tentatively assume that losing one FCP complex from the PSII antenna might be responsible for the 100 ps decrease in PSII lifetime between low-light and high-

light-grown cells. Such a decrease in PSII antenna size would not result in a detectable change in the Chl *a*/f_x ratio, meaning that this value is not a good indicator for the change in antenna size in contrast to what was assumed in (Lepetit et al., 2010).

Thus we conclude that diatoms, like plants and green algae, co-regulate the number of antennae per photosystem core complexes to fine-tune the amount of absorbed light energy with the biochemical capacity of the cell.

Furthermore, the increase of growth light intensity for *C. meneghiniana* leads to a decrease of the relative amount of PSI as compared to PSII. Interestingly, an alternative energy sink like the one provided by cyclic electron flow around PSII, presumably via cytochrome b559, has been suggested for several diatom species (Lavaud et al., 2002; Onno Feikema et al., 2006). That is why the electron transfer cycle around PSII might release excess electrons produced, making high amounts of PSII beneficial for the cells in high light conditions.

In chapter 2 we also conclude that the samples grown in medium-light- and high-light-conditions experience photoinhibition as compared with *C. meneghiniana*, grown in low light. The photoinhibition effect increases with light intensity and manifests itself by a substantial increase of the contribution of long-lifetime components to the PSII fluorescence kinetics and by lower values of PSII quantum efficiency (F_v/F_m). A drop of PSII quantum efficiency was always observed in high-light-grown diatom cultures, not only of *C. meneghiniana* but other types as well (Beer et al., 2011; Strzepek and Harrison, 2004; Van De Poll et al., 2005). Strzepek and Harrison demonstrated that oceanic species are more prone to photoinhibition than coastal species. However, in high-light conditions diatoms are still capable of maintaining similar photosynthetic capacities (Friedman and Alberte, 1986; Strzepek and Harrison, 2004) due to increased compensatory increase of electron transfer through the PSII centers that remain functional (Strzepek and Harrison, 2004). It is still an open question whether photoinhibition in diatoms is induced by certain light quality. Costa et al demonstrated that light acclimation of *Phaeodactylum tricornutum* diatom requires blue light (Costa et al., 2013). On the contrary Wu et al. showed that blue light does induce higher photoinhibition as compared to white light (Wu et al., 2011).

6.3 Photoprotection in *C. meneghiniana* diatoms

The process of non-photochemical quenching (NPQ) is another characteristic type of diatom light response. NPQ is a mechanism of enhanced thermal dissipation of excessively absorbed energy responding to a fast increase in light intensity. Diatoms are able to apply the NPQ mechanism to maintain high growth rates and a high

[GENERAL DISCUSSION]

photosynthetic efficiency over a wide range of light intensities (Falkowski and Laroche, 1991). Moreover, they are capable of showing an extremely high NPQ capacity, up to five times higher than that of green algae and higher plants (Ruban et al., 2004). This observation is quite intriguing since the mechanism of NPQ in diatoms has some similarities to that in vascular plants and green algae: they are modulated by the conversion of xanthophyll cycle (XC) pigments. In diatoms, XC pigments are diadinoxanthin (Ddx) and diatoxanthin (Dtx). However, the reason for such strong NPQ is still not completely understood. One of the explanations might be a significantly larger XC pigment pool in diatoms, especially when cells are grown in high light, as compared to higher plants and green algae (Goss et al., 2006; Lepetit et al., 2010). Furthermore, Dtx, once accumulated during light-driven Ddx de-epoxidation (Lavaud and Kroth, 2006; Goss and Jakob, 2010), is able to maintain NPQ in the absence of a proton gradient (Goss et al., 2006a). Grouneva et al. demonstrated that in darkness that follows strong light, the Dtx that has been accumulated during a period of strong light, is not converted to the “light-harvesting” Ddx form, and the Dtx-related part of NPQ persists in the cells. A comparable NPQ component that solely relies on the presence of the diatoxanthin analogue in plants, zeaxanthin (Z), has also been found in higher plants (Demmig-Adams and Adams, 2006). In contrast to diatoms, where the stable Dt-dependent NPQ has a substantial contribution to the main component (Goss et al., 2006; Grouneva et al., 2009), Z-related NPQ only plays a substantial role in plants that have been exposed to severe light stress. However, Z is only able to enhance NPQ in the presence of the proton gradient. This is also seen during the relaxation of NPQ after an illumination period, and shows kinetics identical to the breakdown of the lumen acidification (ΔpH) (Goss et al., 2006). Grouneva and coworkers demonstrated that a substantial part of NPQ in diatoms is, like in plants, ΔpH -related and relaxes/disappears relatively fast upon switching from high light to darkness (Grouneva et al., 2008). It was suggested more recently that in *C. meneghiniana* the FCPa antenna might aggregate upon pH gradient build-up (Gundermann and Büchel, 2012), thereby leading to excited-state quenching (Van Oort et al., 2007). Interestingly, it was shown that the fluorescence yield of FCPa depends on the Dtx content *in vitro*, which is not the case for FCPb (Gundermann and Büchel, 2008). That is why it is still not clear whether antenna-related NPQ, if present *in vivo*, persists in the absence of a ΔpH across the thylakoid membrane. In the scope of these findings it becomes of primary importance to disentangle and describe ΔpH and XC contributions to NPQ in diatoms. In chapter 3 we initiated research in this direction using time-resolved fluorescence measurements for the first time, using three instead of two characteristic states of the cells: Besides using conventional unquenched and quenched states of the cells (in the absence and presence of the total

[GENERAL DISCUSSION]

NPQ component, respectively), we also performed measurements on the dark-adapted state that followed NPQ. In this state, Dtx, accumulated during the NPQ period, stays in the cells while the ΔpH -related NPQ relaxes (Grouneva et al., 2009). By comparing time-resolved fluorescence of the samples in these three states, a sequence of Dtx- and ΔpH -relaxed NPQ components build up can be reconstructed (chapter 3). Upon the induction of NPQ, at first a substantial amount of FCPa aggregates and becomes quenched, after FCPa detaches from the PSII cores while the quenching persists. Then the continued formation of Dtx leads to the additional quenching of isolated PSII cores and to a minor extent of aggregated FCPa complexes that detach from these cores. Quenching of PSII cores as a substantial part of NPQ was already suggested previously both in diatoms and plants (Eisenstadt et al., 2008; Finazzi et al., 2004). However, our results show for the first time that this mechanism might be Dtx-related. Although the amount of quenching during Dtx-related NPQ is smaller than during ΔpH , as can be observed during our 77K measurements, at room temperature it should show a substantial contribution (chapter 3, Fig. 1, (Grouneva et al., 2009)). FCPb antenna complexes on the other hand remain unquenched during the whole illumination period. The quenching of FCPa aggregates should be the ΔpH -related quenching as proposed earlier (Miloslavina et al., 2009) for low-light grown cells. However, its amplitude might decrease substantially in high-light-grown cells that contain smaller antenna complexes but a bigger XC pool. In those cells I would expect the Dtx-related quenching sites to be more pronounced due to a bigger XC pool, so Dtx-related quenching of PSII cores and FCPa complexes might dominate. Therefore, I suggest that both a large XC pool size and unique FCP antenna characteristics are responsible for the high values of NPQ in *C. meneghiniana* (chapter 3) and, presumably in other centric diatom species (Lavaud and Lepetit, 2013). In pennate diatoms like *Phaeodactylum tricornutum* no differentiation of FCP complexes into FCPa and FCPb forms could be observed so far, and the native state of the *P. tricornutum* antenna complex (trimeric, oligomeric or both (Grouneva et al., 2011; Gundermann et al., 2012; Lepetit et al., 2007)) is still not known. However, the antennas seem to contribute substantially to 710–720 nm emission and the amplitude of the 710–720 nm emission increases with the increase of NPQ capacity in pennate diatom cells: the *P. tricornutum* cells grown in intermittent light show 2.7 times higher NPQ values and approximately 2.5 times higher amplitude of the “red” emission band than the cells grown in continuous light (Lavaud and Lepetit, 2013). This effect is accompanied by a 1.6-fold increase of the Dtx pool in the cells grown in intermittent light, so it looks like antenna-related high NPQ values of *P. tricornutum* are, at least partially, Dtx related. On the other hand, in *C. meneghiniana* the quenching of FCPs during NPQ seems to be

mainly ΔpH related (chapter 3). That is why, interspecies variations in NPQ between centric and pennate diatoms cannot be excluded.

6.7 State transitions in cyanobacteria

Unlike diatoms, plants, green algae and cyanobacteria can optimize their light-harvesting capacity by redistributing absorbed light energy between the PSs by state transitions (Croce and van Amerongen, 2014; Kirilovsky, 2014; Minagawa, 2011; Mullineaux and Emlyn-Jones, 2005). State transitions are a response of photosynthetic organisms to a change of the redox status of intersystem electron carriers. Two states were classically defined: State 1 is induced by oxidation of intersystem electron carriers, usually upon excess excitation of PSI relative to PSII; State 2 is induced by reduction of intersystem electron carriers, either through excess excitation of PSII or by dark respiratory pathways (Mullineaux and Allen, 1990).

For a long time, it was accepted that state transitions in green algae mainly involve phosphorylation/dephosphorylation of LHCII and its relocation between the two PSs (Delosme et al., 1996; Iwai et al., 2008), until NPQ of LHCII during state transitions was visualized (Iwai et al., 2010). Using chlorophyll fluorescence lifetime imaging microscopy, Iwai demonstrated that transitions from state 1 to state 2 in the green alga *Chlamydomonas reinhardtii* are followed by the appearance of a 250-ps lifetime component, which was interpreted as the formation of energy-dissipative aggregates of phosphorylated LHCII detached from PSII in live cells (Iwai et al., 2010). This finding raised a question about the primary role of state transitions in the cell; namely, does it serve to modulate the absorption cross-section of (1) only PSII, (2) only PSI, or (3) of both PSII and PSI? Recently, several studies on green algae argue in favor of the first hypothesis. Contrary to the notion that almost all LHCII leave the PSII complexes and re-associate with PSI during state transitions in *Chlamydomonas*, Ünlü et al. demonstrated that during the state 1 to state 2-transition, only a very small fraction of LHCII released from PSII binds to PSI in state 2, while the majority adopts an energy-dissipative state (Ünlü et al., 2014). Furthermore, Nagy et al. showed that PSII-LHCII macrodomains are largely preserved in state 2: Only about 20% of LHCII (located at the periphery of PSII –LHCII supercomplexes) has migrated to PSI, while a large part of LHCII is in an energetically quenched state either bound or unbound to PSII (Nagy et al., 2014).

In cyanobacteria, the restricted mobility of PSs in the internal thylakoid membrane contrasts with the relatively mobile PBSs (Mullineaux et al., 1997; Sarcina and Mullineaux, 2004). The latter are attached to the surface of the thylakoid membrane (Arteni et al., 2009). Joshua and Mullineaux were the first to correlate the

[GENERAL DISCUSSION]

presence of PBS mobility in cyanobacteria with state transitions. They fixed cyanobacteria in either state 1 or 2 by immersing the cells in a buffer of high osmotic strength, which strongly inhibited PBS diffusion (Joshua and Mullineaux, 2004). The common notion that PBSs detach from PSI and attach to PSII during the transition from state 2 to state 1 was based on enhanced fluorescence emission from PSII in the 680-695 nm spectral region at 77K (Joshua and Mullineaux, 2004; Kana et al., 2014). However, PBS movement between PSs during state transitions has never been explicitly demonstrated.

In chapter 4, we show that during dark-to light transition, which can be approximated as state 2 to state 1-transition there is mainly detachment of PBSs from PSI, which is hardly followed by their attachment to PSII: only 15 % of the PBSs that detach from PSI actually move to PSII, while the major part remains detached from both PSs. These findings are intriguing. It suggests that in cyanobacteria, unlike in green algae, the main role of state transitions is to change the absorption cross-section of PSI, rather than that of PSII. Because in cyanobacteria 1) the number of Chls in PSI is almost three times higher than in PSII (Jordan et al., 2001; Umena et al., 2011) and 2) the PSI/PSII ratio is 4 (Stadnichuk et al., 2009), which is substantially higher than in green algae and diatoms where it is around 1 or less (Melis et al., 1996; Strzepak and Harrison, 2004), illumination with light, mainly absorbed by Chl (substantial part of visible spectrum), in cyanobacteria results in a higher activity of PSI as compared to that of PSII. We suggest that PBS attachment to PSI in darkness might be beneficial (chapter 4): The PQ pool is reduced in the dark due to respiration and residual cyclic electron transport (Mullineaux, 2014; Mullineaux and Allen, 1986), and, once light is introduced again, the primary task of the cell is to rapidly achieve a redox balance. In this situation a larger PSI antenna will increase PQ re-oxidation rate by PSI. Sufficient oxidation power is achieved faster, and a fraction of PBSs detaches from PSI.

Interestingly, spectral properties of the antenna pool, consisting of PBSs detached from PSI, differ from the spectrum of conventional hemidiscoidal PBSs: The 640-660 nm emission is higher than for a conventional PBS spectrum, suggesting that the former contains more PC (Figure 4.7, chapter 4). Our findings suggest that the pool of antennas detached from PSI mainly constitutes 'alternative' PBSs consisting of only PC rods, which were described by Kondo et al. (Kondo et al., 2007). NPQ in cyanobacteria is OCP-related. Recently, Tian et al. demonstrated that NPQ occurs at the level of the PBS core (APC₆₆₀) (Tian et al., 2011), so PC rods alone, if not attached to the APC core, cannot safely dissipate excess light energy as heat. PSI antenna, if mainly constituted by 'alternative' PBSs, cannot decrease the PSI absorption cross-section through OCP-related NPQ in strong light. That is why detachment of such PBSs

from PSI might play not only a regulatory but also a photoprotective role in certain conditions.

6.8 Alternative photoprotective mechanisms: role of *flv4-2* operon-encoded proteins

Other mechanisms of photoprotection involve “electron valves”: alternative electron transfer routes, which dissipate the excess of electrons in the photosynthetic chain and result in decreased photodamage of PSs. Their contribution becomes vital for the cells in conditions where the photosynthetic electron transport chain is over-reduced (for example if NADPH is generated faster than it can be used in the Calvin cycle or in low CO₂ conditions for cyanobacteria). Flv1 and Flv3 heterodimers are an example of such a cyanobacterial electron valve, which sequesters electrons from the acceptor side of PSI and uses them to reduce oxygen, protecting PSI especially in natural occurring fluctuating light conditions (Allahverdiyeva et al., 2013). Only recently *flv4-2* operon-encoded proteins were found to play a central role in safeguarding PSII activity in a number of cyanobacteria in high light and in air-level CO₂ conditions (Zhang et al., 2012; Zhang et al., 2009). Three genes found in the operon are arranged in a tandem orientation (Flv4, Sll0218, and Flv2), suggesting that they have a functional relationship. However, the individual role of the proteins remains illusive.

Flv4 and Flv2 were found to function as a heterodimer, capable of rapid electron transfer between the flavin mononucleotide moiety of Flv2 and the diiron center of Flv4 (Zhang et al., 2012). Previously, it was proposed that the Flv2/Flv4 heterodimer is accepting electrons from the Q_B pocket of PSII, allowing the PQ pool to be in a more oxidized state (Bersanini et al., 2014). The results presented in chapter 5 suggest that the binding or docking of a Flv2/Flv4 heterodimer in the vicinity of the Q_B pocket enhances charge separation in PSII by increasing the redox potential of Q_B. Accelerated electron transfer to Q_B results in shorter PSII fluorescence lifetimes (chapter 5). The fast oxidation of Q_B is maintained by the Flv2/Flv4-related alternative electron transfer route, which likely removes electrons from Q_B⁻, keeping the PQ pool in a more oxidized state.

Interestingly, unlike Flv4 and Flv2, Sll0218 is associated with the thylakoid membrane independently of the cation concentration (Zhang et al., 2012). The absence of the small Sll0218 protein favors a relative decrease of the PSII dimer content of about 20% (chapter 5). On top of that, in the absence of Sll0218 protein, 20% of the PBSs becomes detached from the PSs. Such a direct correlation between PSII dimer destabilization and PBS detachment from PSII demonstrates that dimer

[GENERAL DISCUSSION]

destabilization causes PBS detachment. It is in agreement with multiple studies showing that PBSs attach well to PSII dimers but not to monomers (Arteni et al., 2009; Barber et al., 2003; Young, 2010). To summarize, the *flv4-2* operon-encoded proteins act as a booster of photosynthesis upon excess excitation pressure on PSII: they stabilize PSII dimers, their light-harvesting and enhance charge separation in PSII, allowing the alternative electron transfer route to sequester electrons from Q_B and to maintain the other electron acceptors of PSII, like PQ, in a more oxidized state. However, several questions still remain unanswered, namely, which molecule or complex accepts electrons from Flv4/Flv2 heterodimer, and how is Sll0218 exactly involved in PSII dimer stabilization.

References

- Allahverdiyeva, Y., Mustila, H., Ermakova, M., Bersanini, L., Richaud, P., Ajlani, G., Battchikova, N., Cournac, L., and Aro, E.M. (2013). Flavodiiron proteins Flv1 and Flv3 enable cyanobacterial growth and photosynthesis under fluctuating light. *Proc Natl Acad Sci U S A* 110:4111-4116.
- Amunts, A., Toporik, H., Borovikova, A., and Nelson, N. (2010). Structure determination and improved model of plant photosystem I. *The Journal of biological chemistry* 285:3478-3486.
- Arteni, A.A., Ajlani, G., and Boekema, E.J. (2009). Structural organisation of phycobilisomes from *Synechocystis* sp strain PCC6803 and their interaction with the membrane. *Bba-Bioenergetics* 1787:272-279.
- Bailleul, B., Rogato, A., de Martino, A., Coesel, S., Cardol, P., Bowler, C., Falcatore, A., and Finazzi, G. (2010). An atypical member of the light-harvesting complex stress-related protein family modulates diatom responses to light. *P Natl Acad Sci USA* 107:18214-18219.
- Barber, J. (2009). Photosynthetic energy conversion: natural and artificial. *Chemical Society Reviews* 38:185-196.
- Barber, J., Morris, E.P., and da Fonseca, P.C.A. (2003). Interaction of the allophycocyanin core complex with photosystem II. *Photoch Photobio Sci* 2:536-541.
- Bassi, R., Soen, S.Y., Frank, G., Zuber, H., and Rochaix, J.D. (1992). Characterization of chlorophyll a/b proteins of photosystem I from *Chlamydomonas reinhardtii*. *The Journal of biological chemistry* 267:25714-25721.
- Beer, A., Gundermann, K., Beckmann, J., and Büchel, C. (2006). Subunit composition and pigmentation of fucoxanthin-chlorophyll proteins in diatoms: evidence for a subunit involved in diadinoxanthin and diatoxanthin binding. *Biochemistry* 45:13046-13053.
- Beer, A., Juhas, M., and Büchel, C. (2011). Influence of Different Light Intensities and Different Iron Nutrition on the Photosynthetic Apparatus in the Diatom *Cyclotella meneghiniana* (Bacillariophyceae). *Journal of Phycology* 47:1266-1273.
- Ben-Shem, A., Frolow, F., and Nelson, N. (2003). Crystal structure of plant photosystem I. *Nature* 426:630-635.

[GENERAL DISCUSSION]

- Bersanini, L., Battchikova, N., Jokel, M., Rehman, A., Vass, I., Allahverdiyeva, Y., and Aro, E.M. (2014). Flavodiiron Protein Flv2/Flv4-Related Photoprotective Mechanism Dissipates Excitation Pressure of PSII in Cooperation with Phycobilisomes in Cyanobacteria. *Plant physiology* 164:805-818.
- Broess, K., Trinkunas, G., van der Weij-de Wit, C.D., Dekker, J.P., van Hoek, A., and van Amerongen, H. (2006). Excitation energy transfer and charge separation in photosystem II membranes revisited. *Biophysical journal* 91:3776-3786.
- Broess, K., Trinkunas, G., van Hoek, A., Croce, R., and van Amerongen, H. (2008). Determination of the excitation migration time in Photosystem II consequences for the membrane organization and charge separation parameters. *Biochimica et biophysica acta* 1777:404-409.
- Caffarri, S., Broess, K., Croce, R., and van Amerongen, H. (2011). Excitation energy transfer and trapping in higher plant Photosystem II complexes with different antenna sizes. *Biophys J* 100:2094-2103.
- Carpenter, S.R., Cole, J.J., Pace, M.L., Batt, R., Brock, W.A., Cline, T., Coloso, J., Hodgson, J.R., Kitchell, J.F., Seekell, D.A., et al. (2011). Early Warnings of Regime Shifts: A Whole-Ecosystem Experiment. *Science* 332:1079-1082.
- Costa, B.S., Jungandreas, A., Jakob, T., Weisheit, W., Mittag, M., and Wilhelm, C. (2013). Blue light is essential for high light acclimation and photoprotection in the diatom *Phaeodactylum tricornutum*. *Journal of experimental botany* 64:483-493.
- Croce, R., and van Amerongen, H. (2011). Light-harvesting and structural organization of Photosystem II: from individual complexes to thylakoid membrane. *J Photochem Photobiol B* 104:142-153.
- Croce, R., and van Amerongen, H. (2014). Natural strategies for photosynthetic light harvesting. *Nature chemical biology* 10:492-501.
- Delosme, R., Olive, J., and Wollman, F.-A. (1996). Changes in light energy distribution upon state transitions: an in vivo photoacoustic study of the wild type and photosynthesis mutants from *Chlamydomonas reinhardtii*. *Biochimica et Biophysica Acta (BBA)-Bioenergetics* 1273:150-158.
- Durnford, D.G., Price, J.A., McKim, S.M., and Sarchfield, M.L. (2003). Light-harvesting complex gene expression is controlled by both transcriptional and post-transcriptional mechanisms during photoacclimation in *Chlamydomonas reinhardtii*. *Physiologia Plantarum* 118:193-205.
- Eisenstadt, D., Ohad, I., Keren, N., and Kaplan, A. (2008). Changes in the photosynthetic reaction centre II in the diatom *Phaeodactylum tricornutum* result in non-photochemical fluorescence quenching. *Environmental microbiology* 10:1997-2007.
- Falkowski, P.G., and Laroche, J. (1991). Acclimation to Spectral Irradiance in Algae. *Journal of Phycology* 27:8-14.
- Finazzi, G., Johnson, G.N., Dall'Osto, L., Joliot, P., Wollman, F.A., and Bassi, R. (2004). A zeaxanthin-independent nonphotochemical quenching mechanism localized in the photosystem II core complex. *Proc Natl Acad Sci U S A* 101:12375-12380.

[GENERAL DISCUSSION]

- Friedman, A.L., and Alberte, R.S. (1986). Biogenesis and light regulation of the major light harvesting chlorophyll-protein of diatoms. *Plant physiology* 80:43-51.
- Gildenhoff, N., Amarie, S., Gundermann, K., Beer, A., Büchel, C., and Wachtveitl, J. (2010). Oligomerization and pigmentation dependent excitation energy transfer in fucoxanthin-chlorophyll proteins. *Biochimica et biophysica acta* 1797:543-549.
- Goss, R., Ann Pinto, E., Wilhelm, C., and Richter, M. (2006). The importance of a highly active and DeltapH-regulated diatoxanthin epoxidase for the regulation of the PS II antenna function in diadinoxanthin cycle containing algae. *Journal of plant physiology* 163:1008-1021.
- Grouneva, I., Jakob, T., Wilhelm, C., and Goss, R. (2008). A new multicomponent NPQ mechanism in the diatom *Cyclotella meneghiniana*. *Plant & cell physiology* 49:1217-1225.
- Grouneva, I., Jakob, T., Wilhelm, C., and Goss, R. (2009). The regulation of xanthophyll cycle activity and of non-photochemical fluorescence quenching by two alternative electron flows in the diatoms *Phaeodactylum tricornutum* and *Cyclotella meneghiniana*. *Biochimica et biophysica acta* 1787:929-938.
- Grouneva, I., Rokka, A., and Aro, E.M. (2011). The Thylakoid Membrane Proteome of Two Marine Diatoms Outlines Both Diatom-Specific and Species-Specific Features of the Photosynthetic Machinery. *J Proteome Res* 10:5338-5353.
- Gundermann, K., and Büchel, C. (2008). The fluorescence yield of the trimeric fucoxanthin-chlorophyll-protein FCPa in the diatom *Cyclotella meneghiniana* is dependent on the amount of bound diatoxanthin. *Photosynthesis research* 95:229-235.
- Gundermann, K., and Büchel, C. (2012). Factors determining the fluorescence yield of fucoxanthin-chlorophyll complexes (FCP) involved in non-photochemical quenching in diatoms. *Bba-Bioenergetics* 1817:1044-1052.
- Gundermann, K., Schmidt, M., Weisheit, W., Mittag, M., and Büchel, C. (2012). Identification of several sub-populations in the pool of light harvesting proteins in the pennate diatom *Phaeodactylum tricornutum*. *Biochimica et biophysica acta* 1827:303-310.
- Ihalainen, J.A., van Stokkum, I.H.M., Gibasiewicz, K., Germano, M., van Grondelle, R., and Dekker, J.P. (2005). Kinetics of excitation trapping in intact Photosystem I of *Chlamydomonas reinhardtii* and *Arabidopsis thaliana*. *Biochimica et Biophysica Acta (BBA) - Bioenergetics* 1706:267-275.
- Ikeda, Y., Komura, M., Watanabe, M., Minami, C., Koike, H., Itoh, S., Kashino, Y., and Satoh, K. (2008). Photosystem I complexes associated with fucoxanthin-chlorophyll-binding proteins from a marine centric diatom, *Chaetoceros gracilis*. *Biochimica et biophysica acta* 1777:351-361.
- Iwai, M., Takahashi, Y., and Minagawa, J. (2008). Molecular remodeling of photosystem II during state transitions in *Chlamydomonas reinhardtii*. *The Plant cell* 20:2177-2189.
- Iwai, M., Yokono, M., Inada, N., and Minagawa, J. (2010). Live-cell imaging of photosystem II antenna dissociation during state transitions. *Proc Natl Acad Sci U S A* 107:2337-2342.
- Jordan, P., Fromme, P., Witt, H.T., Klukas, O., Saenger, W., and Krauss, N. (2001). Three-dimensional structure of cyanobacterial photosystem I at 2.5 Å resolution. *Nature* 411:909-917.

[GENERAL DISCUSSION]

- Joshua, S., and Mullineaux, C.W. (2004). Phycobilisome diffusion is required for light-state transitions in cyanobacteria. *Plant physiology* 135:2112-2119.
- Kana, R., Kotabova, E., Lukes, M., Papacek, S., Matono, C., Liu, L.N., Prasil, O., and Mullineaux, C.W. (2014). Phycobilisome Mobility and Its Role in the Regulation of Light Harvesting in Red Algae. *Plant physiology* 165:1618-1631.
- Kirilovsky, D. (2014). Modulating energy arriving at photochemical reaction centers: orange carotenoid protein-related photoprotection and state transitions. *Photosynthesis research*.
- Kondo, K., Ochiai, Y., Katayama, M., and Ikeuchi, M. (2007). The membrane-associated CpcG2-phycobilisome in *Synechocystis*: a new photosystem I antenna. *Plant physiology* 144:1200-1210.
- Kurasova, I., Cajanek, M., Kalina, J., Urban, O., and Spunda, V. (2002). Characterization of acclimation of *Hordeum vulgare* to high irradiation based on different responses of photosynthetic activity and pigment composition. *Photosynthesis research* 72:71-83.
- Lavaud, J., and Lepetit, B. (2013). An explanation for the inter-species variability of the photoprotective non-photochemical chlorophyll fluorescence quenching in diatoms. *Biochimica et biophysica acta* 1827:294-302.
- Lavaud, J., van Gorkom, H., and Etienne, A.-L. (2002). Photosystem II electron transfer cycle and chlororespiration in planktonic diatoms. *Photosynthesis research* 74:51-59.
- Lepetit, B., Goss, R., Jakob, T., and Wilhelm, C. (2012). Molecular dynamics of the diatom thylakoid membrane under different light conditions. *Photosynthesis research* 111:245-257.
- Lepetit, B., Volke, D., Gilbert, M., Wilhelm, C., and Goss, R. (2010). Evidence for the Existence of One Antenna-Associated, Lipid-Dissolved and Two Protein-Bound Pools of Diadinoxanthin Cycle Pigments in Diatoms. *Plant physiology* 154:1905-1920.
- Lepetit, B., Volke, D., Szabó, M., Hoffmann, R., Garab, G., Wilhelm, C., and Goss, R. (2007). Spectroscopic and molecular characterization of the oligomeric antenna of the diatom *Phaeodactylum tricorutum*. *Biochemistry* 46:9813-9822.
- Martinson, T.A., Ikeuchi, M., and Plumley, F.G. (1998). Oxygen-evolving diatom thylakoid membranes. *Biochimica et biophysica acta* 1409:72-86.
- Melillo, J.M., Mcguire, A.D., Kicklighter, D.W., Moore, B., Vorosmarty, C.J., and Schloss, A.L. (1993). Global Climate-Change and Terrestrial Net Primary Production. *Nature* 363:234-240.
- Melis, A., Murakami, A., Nemson, J.A., Aizawa, K., Ohki, K., and Fujita, Y. (1996). Chromatic regulation in *Chlamydomonas reinhardtii* alters photosystem stoichiometry and improves the quantum efficiency of photosynthesis. *Photosynthesis research* 47:253-265.
- Melkozernov, A.N., Kargul, J., Lin, S., Barber, J., and Blankenship, R.E. (2004). Energy Coupling in the PSI-LHCI Supercomplex from the Green Alga *Chlamydomonas reinhardtii*. *The Journal of Physical Chemistry B* 108:10547-10555.

[GENERAL DISCUSSION]

- Miloslavina, Y., Grouneva, I., Lambrev, P.H., Lepetit, B., Goss, R., Wilhelm, C., and Holzwarth, A.R. (2009). Ultrafast fluorescence study on the location and mechanism of non-photochemical quenching in diatoms. *Biochimica et biophysica acta* 1787:1189-1197.
- Minagawa, J. (2011). State transitions—The molecular remodeling of photosynthetic supercomplexes that controls energy flow in the chloroplast. *Biochimica et Biophysica Acta (BBA) - Bioenergetics* 1807:897-905.
- Mullineaux, C.W. (2014). Co-existence of photosynthetic and respiratory activities in cyanobacterial thylakoid membranes. *Biochimica et biophysica acta* 1837:503-511.
- Mullineaux, C.W., and Allen, J.F. (1986). The State-2 Transition in the Cyanobacterium *Synechococcus*-6301 Can Be Driven by Respiratory Electron Flow into the Plastoquinone Pool. *Febs Lett* 205:155-160.
- Mullineaux, C.W., and Allen, J.F. (1990). State-1-State-2 Transitions in the Cyanobacterium *Synechococcus* 6301 Are Controlled by the Redox State of Electron Carriers between Photosystem-I and Photosystem-II. *Photosynthesis research* 23:297-311.
- Mullineaux, C.W., and Emlyn-Jones, D. (2005). State transitions: an example of acclimation to low-light stress. *J Exp Bot* 56:389-393.
- Mullineaux, C.W., Tobin, M.J., and Jones, G.R. (1997). Mobility of photosynthetic complexes in thylakoid membranes. *Nature* 390:421-424.
- Nagy, G., Ünneper, R., Zsiros, O., Tokutsu, R., Takizawa, K., Porcar, L., Moyet, L., Petroustos, D., Garab, G., and Finazzi, G. (2014). Chloroplast remodeling during state transitions in *Chlamydomonas reinhardtii* as revealed by noninvasive techniques in vivo. *Proceedings of the National Academy of Sciences* 111:5042-5047.
- Onno Feikema, W., Marosvölgyi, M.A., Lavaud, J., and van Gorkom, H.J. (2006). Cyclic electron transfer in photosystem II in the marine diatom *Phaeodactylum tricorutum*. *Biochimica et Biophysica Acta (BBA) - Bioenergetics* 1757:829-834.
- Premvardhan, L., Robert, B., Beer, A., and Büchel, C. (2010). Pigment organization in fucoxanthin chlorophyll a/c(2) proteins (FCP) based on resonance Raman spectroscopy and sequence analysis. *Biochimica et biophysica acta* 1797:1647-1656.
- Ruban, A.V., Lavaud, J., Rousseau, B., Guglielmi, G., Horton, P., and Etienne, A.L. (2004). The super-excess energy dissipation in diatom algae: comparative analysis with higher plants. *Photosynthesis research* 82:165-175.
- Sandonà, D., Croce, R., Pagano, A., Crimi, M., and Bassi, R. (1998). Higher plants light harvesting proteins. Structure and function as revealed by mutation analysis of either protein or chromophore moieties. *Biochimica et Biophysica Acta (BBA) - Bioenergetics* 1365:207-214.
- Sarcina, M., and Mullineaux, C.W. (2004). Mobility of the IsiA chlorophyll-binding protein in cyanobacterial thylakoid membranes. *The Journal of biological chemistry* 279:36514-36518.
- Smith, B.M., and Melis, A. (1988). Photochemical apparatus organization in the diatom *Cylindrotheca fusiformis*: photosystem stoichiometry and excitation distribution in cells grown under high and low irradiance. *Plant and cell physiology* 29:761-769.

[GENERAL DISCUSSION]

- Stadnichuk, I.N., Lukashev, E.P., and Elanskaya, I.V. (2009). Fluorescence changes accompanying short-term light adaptations in photosystem I and photosystem II of the cyanobacterium *Synechocystis* sp. PCC 6803 and phycobiliprotein-impaired mutants: State 1/State 2 transitions and carotenoid-induced quenching of phycobilisomes. *Photosynthesis research* 99:227-241.
- Stauber, E.J., Busch, A., Naumann, B., Svatoš, A., and Hippler, M. (2009). Proteotypic profiling of LHCI from *Chlamydomonas reinhardtii* provides new insights into structure and function of the complex. *Proteomics* 9:398-408.
- Strzeppek, R.F., and Harrison, P.J. (2004). Photosynthetic architecture differs in coastal and oceanic diatoms. *Nature* 431:689-692.
- Tian, L., van Stokkum, I.H., Koehorst, R.B., Jongerius, A., Kirilovsky, D., and van Amerongen, H. (2011). Site, rate, and mechanism of photoprotective quenching in cyanobacteria. *J Am Chem Soc* 133:18304-18311.
- Umena, Y., Kawakami, K., Shen, J.R., and Kamiya, N. (2011). Crystal structure of oxygen-evolving photosystem II at a resolution of 1.9 angstrom. *Nature* 473:55-U65.
- Ünlü, C., Drop, B., Croce, R., and van Amerongen, H. (2014). State transitions in *Chlamydomonas reinhardtii* strongly modulate the functional size of photosystem II but not of photosystem I. *Proc Natl Acad Sci U S A* 111:3460-3465.
- Van De Poll, W.H., Van Leeuwe, M.A., Roggevel, J., and Buma, A.G. (2005). Nutrient limitation and high irradiance acclimation reduce PAR and UV-induced viability loss in the Antarctic diatom *Chaetoceros brevis* (Bacillariophyceae). *Journal of Phycology* 41:840-850.
- Van Oort, B., Alberts, M., de Bianchi, S., Dall'Osto, L., Bassi, R., Trinkunas, G., Croce, R., and van Amerongen, H. (2010). Effect of antenna-depletion in Photosystem II on excitation energy transfer in *Arabidopsis thaliana*. *Biophysical journal* 98:922-931.
- Van Oort, B., Amunts, A., Borst, J.W., van Hoek, A., Nelson, N., van Amerongen, H., and Croce, R. (2008). Picosecond fluorescence of intact and dissolved PSI-LHCI crystals. *Biophys J* 95:5851-5861.
- Van Oort, B., van Hoek, A., Ruban, A.V., and van Amerongen, H. (2007). Aggregation of Light-Harvesting Complex II leads to formation of efficient excitation energy traps in monomeric and trimeric complexes. *Febs Lett* 581:3528-3532.
- Veith, T., Brauns, J., Weisheit, W., Mittag, M., and Büchel, C. (2009). Identification of a specific fucoxanthin-chlorophyll protein in the light harvesting complex of photosystem I in the diatom *Cyclotella meneghiniana*. *Biochimica Et Biophysica Acta-Bioenergetics* 1787:905-912.
- Veith, T., and Büchel, C. (2007). The monomeric photosystem I-complex of the diatom *Phaeodactylum tricornutum* binds specific fucoxanthin chlorophyll proteins (FCPs) as light-harvesting complexes. *Bba-Bioenergetics* 1767:1428-1435.
- Ware, D.M., and Thomson, R.E. (2005). Bottom-up ecosystem trophic dynamics determine fish production in the northeast Pacific. *Science* 308:1280-1284.

[GENERAL DISCUSSION]

- Wientjes, E., Oostergetel, G.T., Jansson, S., Boekema, E.J., and Croce, R. (2009). The role of Lhca complexes in the supramolecular organization of higher plant photosystem I. *J Biol Chem* 284:7803-7810.
- Wientjes, E., van Amerongen, H., and Croce, R. (2013). Quantum yield of charge separation in photosystem II: functional effect of changes in the antenna size upon light acclimation. *The journal of physical chemistry. B* 117:11200-11208.
- Wientjes, E., van Stokkum, I.H., van Amerongen, H., and Croce, R. (2011). The role of the individual Lhcas in photosystem I excitation energy trapping. *Biophys J* 101:745-754.
- Wu, H., Cockshutt, A.M., McCarthy, A., and Campbell, D.A. (2011). Distinctive photosystem II photoinactivation and protein dynamics in marine diatoms. *Plant Physiol* 156:2184-2195.
- Young, R.D. (2010). Characterisation of the Role of the PsbT Subunit of Photosystem II in *Synechocystis* Sp. PCC 6803: A Thesis Submitted for the Degree of Master of Science at the University of Otago, Dunedin, New Zealand: University of Otago.
- Zhang, P., Eisenhut, M., Brandt, A.M., Carmel, D., Silen, H.M., Vass, I., Allahverdiyeva, Y., Salminen, T.A., and Aro, E.M. (2012). Operon flv4-flv2 provides cyanobacterial photosystem II with flexibility of electron transfer. *The Plant cell* 24:1952-1971.
- Zhang, P.P., Allahverdiyeva, Y., Eisenhut, M., and Aro, E.M. (2009). Flavodiiron Proteins in Oxygenic Photosynthetic Organisms: Photoprotection of Photosystem II by Flv2 and Flv4 in *Synechocystis* sp PCC 6803. *Plos One* 4.

Summary

Aquatic photosynthetic organisms unavoidably experience light fluctuations that vary in amplitude, duration and origin, compromising their photosynthetic efficiency. Weather conditions and underwater flow cause continuous changes in irradiance to which the organisms have to adapt. Many light-adaptation strategies of photosynthetic organisms, such as light acclimation, photoprotection and state transitions are still not well understood. In this thesis, time-resolved fluorescence spectroscopy is used to obtain insight into the response of diatoms and cyanobacteria, both aquatic photosynthetic organisms, to changing light conditions.

In chapter 2, photoacclimation (long-term acclimation to irradiance conditions) of the diatom *Cyclotella meneghiniana* is discussed. It is shown that the diatom cells fine-tune the amount of absorbed light energy by modifying their antenna size: cells grown in high light intensity have smaller antennas than those grown in low light. At the same time, the increase of growth light intensity leads to a decrease of the relative amount of photosystem I (PSI) as compared to PSII. Such a strategy might be beneficial for diatoms, since they are known to have an electron transfer cycle around PS II to release excess electrons produced in high light intensities. Besides discussing photoacclimation, we give a detailed description the fluorescence kinetics in *C. meneghiniana*. It is concluded that the diatom antenna, represented by light-harvesting fucoxanthin chlorophyll proteins (FCPs), transfer their excitation energy predominantly to PSII. FCPs associated with PSII are slightly richer in red-absorbing fucoxanthin than the FCPs associated with PSI, suggesting that PSII antennas (partly) constitute the antenna form FCPb (i.e. oligomeric antenna complexes).

In chapter 3 the process of non-photochemical quenching (NPQ, thermal dissipation of excess absorbed light energy) of chlorophyll *a* fluorescence was studied in the same diatom species. Diatoms can rapidly switch on/off NPQ to respond to fast light-intensity changes in moving waters. They are capable to induce higher NPQ values than plants or other photosynthetic organisms. The reason for such high NPQ values, however, is not clear. We performed picosecond fluorescence measurements at 77K on cells locked in three different states: Besides using conventional unquenched and quenched states of the cells (in the absence and presence of the total NPQ component, respectively), we also performed measurements on the dark-adapted state directly following NPQ. In this state, diatoxantin (Dtx, a carotenoid related to NPQ), accumulated during the NPQ period and Dtx-related NPQ persists, while ΔpH -related NPQ has relaxed. In this way we revealed the following sequence of

[SUMMARY]

events during full development of NPQ. First, the pH gradient across the thylakoid membrane induces quenching of FCP trimers (FCPa complexes), while they are still part of PSII. This is followed by (partial) detachment of FCPa from PSII after which quenching persists. The pH gradient also causes the formation of Dtx, which leads to further quenching of isolated PSII cores and some aggregated FCPa. To summarize, quenching of PSII -both cores and complexes- and FCPa substantially contribute to NPQ in diatoms. The FCPb antenna form on the other hand does not contribute to the NPQ process.

Certain aquatic photosynthetic organisms, such as cyanobacteria and green algae, can also cope with changing light conditions by dynamically varying the relative antenna size of PSI and of PSII. Consequently, a redistribution of light energy between the PSs is achieved. This phenomenon is called “state transitions”. It is known to be driven via a change in the redox status of electron carriers between PSII and PSI. In cyanobacteria, this redox change can be achieved via dark-light transitions. However, the cascade of microscopic events that lead to subsequent energy redistribution in cyanobacteria is still not completely clear. In chapter 4, a study on dark-light transitions using the cyanobacterium *Synechocystis* sp. PCC 6803 as a model organism is described. It is demonstrated that during dark to light transitions, there is mainly detachment of phycobilisomes (PBSs) (cyanobacterial antennas) from PSI, generally not followed by their attachment to PSII: only 15 % of the PBSs that detach from PSI actually move to PSII, while the major part remains detached from both PSs. We conclude that PSI-PSII-PBS megacomplexes, which were recently isolated using chemical cross-linking, are not involved in dark/light state transitions, suggesting that, if present, they are only transiently formed in cyanobacteria. To summarize, the findings presented in chapter 4 suggest that in cyanobacteria, unlike in green algae or higher plants, the main role of state transitions is to change the absorption cross-section of PSI, rather than that of PSII.

In chapter 5, a study of the role of flv4-2 operon-encoded proteins in *Synechocystis* is described. Three genes are found in the operon: Flv4, Sll0218, and Flv2. Only recently flv4-2 operon-encoded proteins were found to constitute an additional photoprotective mechanism in a number of cyanobacteria by safeguarding PSII activity via an alternative electron chain. Its contribution becomes vital for the cells in high light and in air-level CO₂, when the photosynthetic electron transport chain is over-reduced. It is demonstrated that deletion of the operon induces 20% PBS detachment. The reduced PSII dimer to monomer ratio, as a result of the absence of the small Sll0218 protein, favors a relative decrease of the PSII dimer content of about 20%, showing a direct correlation between PSII dimer destabilization and PBS detachment from reaction centers. On the other hand, the suggested binding of the

[SUMMARY]

Flv2/Flv4 heterodimer closely to the quinone B (Q_B) pocket in PSII increases the Q_B redox potential, thereby promoting forward electron transfer and increasing the charge separation rates in PSII. This activity of the Flv2/Flv4 heterodimer in combination with its earlier reported role as an electron acceptor in alternative electron chain provides more oxidized state of the PQ pool in high light and in air-level CO_2 .

Samenvatting

Fotosynthetische aquatische organismen staan bloot aan fluctuaties in licht, die variëren in amplitude, duur en oorzaak. Deze fluctuaties verlagen de efficiëntie van het fotosyntheseproces. Weersomstandigheden en stroming veroorzaken niet-aflatende veranderingen in bestralingssterkte, waaraan de organismen zich moeten aanpassen. Vele licht-aanpassingsstrategieën, zoals fotoacclimatie, fotoprotectie en “state transitions” worden nog steeds niet volledig begrepen. In dit proefschrift wordt de reactie van diatomeeën en cyanobacteriën, beiden aquatische fotosynthetische organismen, op veranderende lichtomstandigheden beschreven, waarvoor gebruik is gemaakt van tijdsopgeloste fluorescentiespectroscopie.

In hoofdstuk 2 wordt fotoacclimatie (lange-termijn-acclimatie aan bestralingsomstandigheden) van *Cyclotella meneghiniana*, een soort diatomeeën, behandeld. Aangetoond wordt dat de cellen waaruit zij bestaan de hoeveelheid geabsorbeerd licht nauwkeurig kunnen afregelen door de grootte van hun antennes te veranderen: Cellen die gekweekt zijn onder hoge lichtintensiteit hebben kleinere antennes dan cellen die gekweekt zijn onder een lage lichtintensiteit. Tegelijkertijd leidt een toename van de lichtintensiteit tot een afname van de relatieve hoeveelheid fotosysteem I (PSI) in vergelijking met fotosysteem II (PSII). Een dergelijke aanpassingsstrategie zou voordelig kunnen zijn voor diatomeeën, omdat het bekend is dat zij een elektrontransportcyclus hebben rond PSII waarmee overtollige elektronen, geproduceerd onder hoge lichtintensiteit, afgevoerd kunnen worden. Naast de bespreking van fotoacclimatie wordt er een uitgebreide beschrijving gegeven van de fluorescentiekinetiek in *C. meneghiniana*. De conclusie is dat antennes in diatomeeën, vertegenwoordigd door lichtinvangende fucoxanthine-chlorofyl-eiwitten (FCP's), hun excitatie-energie voornamelijk overdragen aan PSII. FCP's die geassocieerd zijn met PSII zijn een klein beetje rijker aan rood-absorberende fucoxanthines dan de FCP's die met PSI zijn geassocieerd, hetgeen suggereert dat PSII-antennes (gedeeltelijk) de FCPb-antennevariant (d.w.z. oligomere antennecomplexen) bevatten.

Hoofdstuk 3 omvat een studie naar ‘niet-fotochemische quenching of doving’ (NPQ, warmtedissipatie van overmatig geabsorbeerde lichtenergie) van chlorofyl-*a* fluorescentie, wederom in *C. meneghiniana*. Diatomeeën kunnen NPQ snel aan en uit schakelen als reactie op snelle veranderingen in lichtintensiteit in stromend water. Ze kunnen hogere NPQ-waardes induceren dan planten of andere fotosynthetische organismen. De onderliggende reden voor zulke hoge NPQ-waardes is echter onduidelijk. We hebben picoseconde-fluorescentiemetingen uitgevoerd bij 77K aan

[SAMENVATTING]

cellen die werden geblokkeerd in drie verschillende toestanden: Naast de gebruikelijke niet-gedoofde en gedoofde celtoestanden (respectievelijk in afwezigheid en aanwezigheid van de totale NPQ-component) hebben we ook metingen verricht aan de toestand aangepast aan duisternis onmiddellijk na NPQ. In deze toestand accumuleert diatoxantine (Dtx, een carotenoïde gerelateerd aan NPQ) gedurende de NPQ-periode, en blijft Dtx-gerelateerde NPQ bestaan, terwijl Δ pH-gerelateerde NPQ relaxeert. Zodanig komen we tot deze volgorde van gebeurtenissen tijdens de volledige ontwikkeling van NPQ: Eerst induceert de pH-gradient over het thylakoidmembraan doving van FCP trimeren (FCPa-complexen) die nog steeds onderdeel zijn van PSII. Dit wordt gevolgd door (gedeeltelijke) loslating van FCPa van PSII, waarna de doving aanhoudt. De pH-gradient veroorzaakt ook de vorming van Dtx, hetgeen leidt tot verdere doving van geïsoleerde PSII- core complexen en enkele FCPa-aggregaten. Samenvattend, de doving van PSII en FCPa dragen substantieel bij aan NPQ in diatomeeën. De FCPb-antennevariant draagt echter niet bij aan het dovingproces.

Bepaalde fotosynthetische aquatische organismen, zoals cyanobacteriën en groene algen, kunnen ook omgaan met veranderende licht-omstandigheden door op dynamische wijze de relatieve antennegrootte van PSI en PSII te variëren. Als gevolg daarvan wordt een herverdeling van lichtenergie tussen beide fotosystemen gerealiseerd. Dit fenomeen wordt aangeduid met de term “state transition” ofwel toestandsverandering. Het is bekend dat het wordt gedreven vanwege een verandering in de redox-status van de elektronendragers tussen PSII en PSI. In cyanobacteriën kan deze redoxverandering worden bereikt via donker-naar-lichtovergangen. De opeenvolging van microscopische gebeurtenissen die leiden tot de herverdeling van energie in cyanobacteriën is echter nog niet volledig opgehelderd. Hoofdstuk 4 beschrijft een studie naar donker-naar-lichtovergangen met als modelorganisme de cyanobacterie *Synechocystis* sp. PCC 6803. Daarin wordt aangetoond dat gedurende donker-naar-lichtovergangen voornamelijk loskoppeling van fycobilisomen (PBS, antennes van cyanobacteriën) van PSI optreedt, in het algemeen niet gevolgd door hun aankoppeling aan PSII: slechts 15% van de PBS die loskoppelen van PSI gaan naar PSII, terwijl het overgrote deel niet meer aan één van beide fotosystemen verbonden is. De conclusie is, dat PSI-PSII-PBS megacomplexen, die recentelijk werden geïsoleerd door middel van chemische crosslinking, geen rol spelen gedurende donker-naar-lichtovergangen. Dit suggereert dat deze megacomplexen, indien zij al aanwezig zijn, in cyanobacteriën alleen transiënt worden gevormd. Samenvattend, de bevindingen van hoofdstuk 4 suggereren dat in cyanobacteriën, anders dan in groene algen of hogere planten, de voornaamste rol van

[SAMENVATTING]

toestandsveranderingen is om de absorptiedoorsnede van in het bijzonder PSI te veranderen, meer dan die van PSII.

In hoofdstuk 5 wordt de rol van *flv4-2* operon-geëncodeerde eiwitten in *Synechocystis* beschreven. Het operon bevat drie genen: *Flv4*, *Sll0218* en *Flv2*. Pas recentelijk is ontdekt dat, in een aantal cyanobacteriën, *flv4-2* operon-geëncodeerde eiwitten een eigen fotoprotectie-mechanisme vormen, door PSII-activiteit te consolideren via een alternatieve elektronenketen. De bijdrage van dit mechanisme wordt essentieel voor de cellen in hoge lichtintensiteit en in CO₂-concentraties vergelijkbaar met die in lucht, wanneer de fotosynthetische elektrontransportketen over-gereduceerd is. Aangetoond wordt dat deletie van het operon een loskoppeling van PBS van 20% induceert. De gereduceerd-PSII dimeer-tot-monomeer verhouding die veroorzaakt wordt door het *Sll0218*-eiwit zorgt voor een relatieve afname van PSII-dimeren van ongeveer 20%, hetgeen wijst op een directe correlatie tussen PSII-dimeer destabilisatie en PBS-ontkoppeling van de reactiecentra. Anderzijds veroorzaakt de gesuggereerde binding van het *Flv2/Flv4* heterodimeer nabij de chinon-B (Q_B) pocket in PSII een toename in de Q_B-redoxpotential, hetgeen voorwaartse elektronenoverdracht stimuleert en de snelheid van ladingsscheiding in PSII doet toenemen. Deze activiteit van het *Flv2/Flv4* heterodimeer in combinatie met de eerder gerapporteerde rol als elektronenacceptor in een alternatieve elektronketen verschaft een meer geoxideerde status van het plastochinonreservoir in hoge lichtintensiteit en CO₂-concentraties vergelijkbaar met die in lucht.

Acknowledgements

First and foremost I would like to express my gratitude towards my advisor, prof. Herbert van Amerongen, for his patience, comments, suggestions and corrections. His encouragement and constructive feedback have been the basis of all progress during the writing of this thesis.

My pathway through science began at the Belarusian State University in Minsk, more specifically at the department of Statistical Analysis. I would like to express my gratitude towards prof. Vladimir Apanasovich, Peter Nazarov and Nikolay Yatskov not only for their help and support during my bachelor and master studies but also for encouraging me to pursue a PhD. This decision I have never regretted!

During the course of my project I had the pleasure of working with many people from all over the continent. I would like to thank all of them for a pleasant and fruitful collaboration: Luca Bersanini and prof. Eva-Mari Aro (Turku), prof. Claudia Büchel (Frankfurt am Main), and Tünde Tóth and prof. Győző Garab (Szeged). The scientific results presented in this thesis would not have been there without them. I would like to thank all ESRs and ERs of the Harvest network for the lovely atmosphere during our meetings. It was wonderful to be part of this group.

None of my measurements would have been successful without excellent technical support, for which I would like to thank Arie, Arjen and Rob. Thanks to Rob for helping me to move around Wageningen three consecutive times, and for being extremely helpful in any emergency situation. Arie is acknowledged for his continued support relating to TCSPC. Gratitude goes to Netty for all her help and her unique talent to solve any problem with a single phone call. I'm grateful to Sergey and Joris for swift answers to all my questions. Thanks go to Daan for all support, the least of which was his Dutch translation. I would like to express my gratitude also towards the other students and members of the Biophysics group for their support and the friendly atmosphere in the lab, during meetings and "lab biertjes".

Last but not least: I wouldn't have survived the last four years in the Netherlands without moral support from my Belarusian team: Nadya, Alena, Olga and my family, Andrei, Svetlana, Vladimir and Tamara.

**Education Statement of the Graduate School
Experimental Plant Sciences**



Issued to: Volha Chukhutsina
Date: 25 February 2015
Group: Laboratory of Biophysics
University: Wageningen University & Research Centre

| | <u>date</u> |
|--|--------------|
| 1) Start-up phase | |
| ▶ First presentation of your project Modeling of Photosystem I in vivo | Mar 01, 2011 |
| ▶ Writing or rewriting a project proposal Studying nonphotochemical quenching in photosynthetic organisms with the use of time-resolved fluorescence spectroscopy and modeling thereof | Dec 2010 |
| ▶ Writing a review or book chapter | |
| ▶ MSC courses | |
| ▶ Laboratory use of isotopes | |

Subtotal Start-up Phase **4.5 credits***

| | <u>date</u> |
|---|--|
| 2) Scientific Exposure | |
| ▶ EPS PhD student days EPS PHD Student day, Wageningen University EPS PHD Student day, Leiden University | May 20, 2011 Nov 29, 2013 |
| ▶ EPS theme symposia EPS Theme 3 'Metabolism and Adaptation', Wageningen University EPS Theme 3 'Metabolism and Adaptation', Wageningen University | Mar 22, 2013 Mar 03, 2014 |
| ▶ NWO Lunteren days and other National Platforms NWO CW Study group meeting Chemistry in relation to Physics and Materials Sciences, Veldhoven Annual Dutch meeting on Molecular and Cellular Biophysics, Veldhoven Annual Dutch meeting on Molecular and Cellular Biophysics, Veldhoven Annual Dutch meeting on Molecular and Cellular Biophysics, Veldhoven BiosolarCell Theme 3 cluster meeting, Amsterdam BiosolarCell Theme 3 cluster meeting, Wageningen | Mar 04-05, 2013 Oct 03-04, 2011 Oct 01-02, 2012 Sep 30-Oct 01, 2013 Nov 28, 2013 Jun 23-24, 2014 |
| ▶ Seminars (series), workshops and symposia Biophysica colloquium series, WUR, Laboratory of Biophysics International Workshop "Mechanisms of Non-photochemical Quenching" EU Marie Curie Network "HARVEST", Passau, Germany International workshop "Photosynthesis: from Science to Industry", Noordwijkerhout, the Netherlands "Photons for Fuel" Symposium, Amsterdam, the Netherlands The Tünde Toth State Transitions Symposium Mini-symposium "How to Write a World-class Paper", Wageningen UR Library, Wageningen | Feb 2010-2014 Apr 06-10, 2011 Oct 08-12, 2012 Dec 07, 2012 Sep 02, 2014 Oct 17, 2013 |
| ▶ Seminar plus | |
| ▶ International symposia and congresses Marie Curie ITN, Harvest network meeting, Venice, Italy Midterm Review Meeting HARVEST, Clare College, Cambridge, UK Harvest Network meeting, Kronlund, Sweden Internal Meeting of HARVEST Young Researchers, Sevilla, Spain HARVEST final meeting, Chania, Greece International Conference on the Biophysics of Photosynthesis, Rome, Italy Gordon Research Seminar, Mount Snow Resort in West Dover VT United States Gordon Research Congress, Mount Snow Resort in West Dover VT United States | Sep 22-24, 2010 Sep 15-16, 2011 Jun 05-06, 2012 Mar 15-18, 2012 Sep 18-21, 2013 Oct 28-30, 2013 Aug 9-10, 2014 Aug 10-15, 2014 |
| ▶ Presentations Oral: Marie Curie ITN, Harvest network meeting, Venice, Italy Poster: Intern. Workshop "Mechanisms of Non-photochemical Quenching" EU Marie Curie Network "HARVEST" Oral: Midterm Review Meeting HARVEST, Clare College, Cambridge, UK Oral: Internal Meeting of HARVEST Young Researchers, Sevilla, Spain Oral: Harvest Network meeting, Kronlund, Sweden Poster: Intern. Workshop "Photosynthesis: from Science to Industry", Noordwijkerhout, the Netherlands Poster: Annual Dutch meeting on Molecular and Cellular Biophysics, Veldhoven Oral: HARVEST final meeting, Chania, Greece Oral: BiosolarCell Theme 3 cluster meeting, Amsterdam Oral: BiosolarCell Theme 3 cluster meeting, Wageningen Poster: Gordon Research Seminar, Mount Snow Resort in West Dover VT United States Poster: Gordon Research Congress, Mount Snow Resort in West Dover VT United States Oral: The Tünde Toth State Transitions Symposium, BIP WUR, Wageningen | Sep 23, 2010 Apr 06-10, 2011 Sep 16, 2011 Mar 16, 2012 Jun 05, 2012 Oct 08-12, 2012 Oct 01, 2013 Sep 20, 2013 Nov 28, 2013 Jun 24, 2014 Aug 10, 2014 Aug 12, 2014 Sep 02, 2014 |
| ▶ IAB interview | |
| ▶ Excursions | |

Subtotal Scientific Exposure **30.5 credits***

| | <u>date</u> |
|---|--|
| 3) In-Depth Studies | |
| ▶ EPS courses or other PhD courses Systems Biology of Photosynthesis & Innovation Strategies, Brno, CZ, Harvest Network Course Harvest Network course in "Agricultural photosynthesis", Nottingham, UK 9th Course on "Time-Resolved Fluorescence Spectroscopy", Berlin, Adlershof, Germany NetBeans Platform course, Wageningen, NetBeans Platform Certified Associate certification | Apr 03-06, 2011 Sep 11-14, 2011 Oct 31-Nov 03, 2011 Apr 23-25, 2012 |
| ▶ Journal club | |
| ▶ Individual research training | |

Subtotal In-Depth Studies **4.5 credits***

| | <u>date</u> |
|---|---|
| 4) Personal development | |
| ▶ Skill training courses Training Course English Scientific Writing, Venice, Italy Course "Licensing Agreements for Commercial Purposes" Brno, CZ, Harvest Network Course Intellectual Property rights, Harvest Network Course, Nottingham Grant writing course, Harvest Network Course, Sweden Career development course, Harvest Network Course, Sweden Voice matters, EPS course Social Dutch, Wageningen into Languages | Sep 24-26, 2010 Apr 02, 2011 Sep 13, 2011 Jun 03-04, 2012 Jun 05, 2012 Nov 13, 2012 Oct 27, 2013-Jan 2014 |
| ▶ Organisation of PhD students day, course or conference Time-resolved spectroscopy in the life sciences, Harvest Network Course, Wageningen University, the Netherlands | Oct 16-19, 2012 |
| ▶ Membership of Board, Committee or PhD council | |

Subtotal Personal Development **7.1 credits***

| | |
|---|-------------|
| TOTAL NUMBER OF CREDIT POINTS* | 46.6 |
| Herewith the Graduate School declares that the PhD candidate has complied with the educational requirements set by the Educational Committee of EPS which comprises of a minimum total of 30 ECTS credits | |
| * A credit represents a normative study load of 28 hours of study. | |